FLUOROUS OXIDANTS FOR RADIOCHEMISTRY AND TETRAZINE SYNTHESIS

FLUOROUS SUPPORTS AND OXIDANTS FOR RADIOCHEMISTRY, TETRAZINE SYNTHESIS, AND HYDROGEN SULFIDE PROCESSING

By

JAMES PATRICK K. DZANDZI, B.Sc., M.Sc.

A Thesis

Submitted to the School of Graduate Studies

In Partial Fulfillment of the Requirements

For the Degree

Doctor of Philosophy

McMaster University

DOCTOR OF PHILOSOPHY (2015) McMASTER UNIVERSITY

Chemical Biology Hamilton, Ontario

TITLE: Fluorous Supports and Oxidants for Radiochemistry, Tetrazine Synthesis, and Hydrogen Sulfide Processing

AUTHOR: James Patrick K. Dzandzi, B.Sc. (KNUST, Kumasi), M.Sc. (UMD, Duluth)

SUPERVISOR: Professor John Fitzmaurice Valliant

NUMBER OF PAGES: xix, 265

Abstract

A new class of fluorous materials was developed to create a hybrid solid-solution phase strategy for the expedient preparation of ^{125}I-labelled compounds, without the need of HPLC purification. The system is referred to as a hybrid platform in that it combines solution phase labelling and fluorous solid-phase purification in one step as opposed to two separate individual processes. Initial success was achieved by treating fluorous stannanes, coated on fluorous silica, with [^{125}I]NaI and chloramine-T (CAT) as the oxidant, where the desired nonfluorous radiolabelled products were isolated in minutes in biocompatible solutions in high purity (>98%) free from excess starting material and unreacted radioiodine. This platform was initially developed through a model system based on a fluorous benzoic acid derivative. The platform was then validated with simple aryl and heterocyclic derivatives, known radiopharmaceuticals including *meta*-iodobenzylguanidine (MIBG) and iododeoxyuridine (IUdR), and a new agent with high affinity for prostate-specific membrane antigen (PSMA).

The limitation of the platform was the presence of non-radioactive UV impurities which came from the oxidants employed. To resolve this issue a new class of fluorous oxidants based on chloramine-T (CAT, F-CAT) were prepared. F-CAT, was prepared in 87% overall synthesis yield from commercially available starting materials and found to be effective in labelling arylstannanes and proteins with [^{125}I]NaI. The utility of the oxidant was further demonstrated in successfully preparing a radioiodinated tetrazine (^{125}I-Tz) through a concomitant oxidation-

halodemetallation reaction. ^{125}I-Tz can be used to label biomolecules through bioorthogonal coupling reactions with prosthetic groups containing strained alkenes including norbornene and *trans*-cyclooctene (TCO). The reported hybrid platform labelling approach is readily accessible and requires minimal radiochemistry expertise and should therefore find widespread use.

It is also noteworthy that a second generation of the fluorous oxidant, F-CAT2, was also prepared with the aim of obtaining an oxidant which has a higher solubility in perfluorinated solvents. Application of F-CAT2 for oxidation of hydrogen sulfide to elemental sulphur in a fluorous-aqueous biphasic system was demonstrated. This approach offers a new metal-free approach to scrubbing sour gas wells and demonstrates that the fluorous oxidants developed here have utility beyond radiochemistry.

Acknowledgements

If it had not been for the Lord God Almighty on my side, I could not have made it. To Him am forever grateful. “Thus far the LORD has helped us” (1 Samuel 7:12). Many are the people that the Lord has used to help me accomplish this feat. I would like to express my gratitude, first and foremost, to my supervisor Prof. John Valliant, for granting me the opportunity to work on such a challenging and rewarding research project. I am thankful that he continuously challenged me and asked me to always critique my own work. This has made me a better researcher and scientist.

I would also like to thank my committee members, Profs. Capretta, Britz-McKibbin, and McCurry (the late) for all of their input to my work. They have challenged me in all areas of chemistry and with their combined expertise have enriched my knowledge greatly.

I will also like to thank my many colleagues whose support, friendship and encouragement has sustained me every inch on my journey. To the Valliant research group members over the years, I know that my daily interactions with you have enriched my life both scientifically and personally and I carry with me countless cherished memories.

I would also like to thank the NMR and the mass-spec facilities staff for all their hard work dealing with my “awkward” fluorous compounds. Special thanks to Drs. Kirk Green, Steve Kornic and Hilary Jenkins for being very generous with both their time and vast wealth of knowledge. I am also grateful to

all departmental administrative staff (past and present members), for their administrative support and genuinely caring attitudes; special thanks to Mrs. Tammy Feher.

I will also like to acknowledge the friendship and encouragement of my church-family; All Nations Full Gospel Church, Hamilton-ON. My special thanks to Dr. Uche Anumba and family, and other church members who have been there every step of the way since my wife and I moved to Hamilton.

I am forever grateful to my family for their love and patience throughout my entire academic experience. I appreciate knowing that they were in the trenches with me every step of the way; regardless of whether or not they fully understood. Finally, to my wife- Esinam, and my children (Edem and Eyram), I owe so much. Thanks for all of your encouragement through the years. It has been a long haul and I know I probably wouldn't be here if not for your unending support. I look forward to experiencing life's many adventures with you.

Dedication

"I can do all things through Him who gives me strength." Phillipians 4:13

This dissertation is dedicated to my parents, Raphael Atsu and Rose Adzoa Kwasitse (deceased), my wife, Esinam, my children: Edem and Eyram, and to my siblings: Michael Yankson, Dr. Kennedy T. C. Brightson, Comfort Dede Barkeh, Olivia Afi Atsu and Florence Akpene Atsu, who have all provided unwavering support and patience in the pursuit of this doctoral work. I am forever grateful to you all for your sacrifice and encouragement throughout this endeavor.

Table of Contents

List of Figures

List of Tables

List of Schemes

List of Abbreviations and Symbols

A

AcOH	Acetic acid
CH_3CN	Acetonitrile
α	Alpha particles
Å	Angstrom
aq	Aqueous
^{211}At	Astatine-211
$(NH_4)_2SO_4$	Ammonium sulfate

B

β	Beta
β^-	Beta particle
^{212}Bi	Bismuth-212
^{76}Br	Bromine-76
^{80m}Br	Bromine-80 metastable

C

ca	*circa*
calc	calculated
^{11}C	Carbon-11
^{13}C	Carbon-13
^{13}C NMR	Carbon-13 NMR
cm	Centimeter(s)
δ	Chemical shift (NMR)
CAT	Chloramine-T
$CHCl_3$	Chloroform
CT	Computed tomography
CPM	Counts per minute
^{64}Cu	Copper-64
^{67}Cu	Copper-67
COSY	Correlated spectroscopy
J	Coupling constant (NMR)
Ci	Curie

D

Da	Daltons
d	day
°C	Degrees Celcius
DNA	Deoxyribonuclieic acid
$CDCl_3$	Deuterated chloroform
CD_3OD	Deuterated methanol

DCM	Dichloromethane
Et_2O	Diethyl ether
d	Doublets
dd	Doublet of doublets

E

ESA	Effective specific activity
EC	Electron capture
ESI	Electrospray ionization
EtOH	Ethanol
EtOAc	Ethyl acetate
^{169}Er	Erbium-169
EtOH	Ethanol

F

^{18}F	Fluorine-18
FLS	Fluorous labelling strategy
FBC	Fluorous biphasic catalysis
FS	Fluorous silica
FSPE	Fluorous solid-phase extraction
FDA	Food and Drug Administration
FTIR	Fourier transformed infrared spectroscopy

G

^{67}Ga	Gallium-67
^{68}Ga	Gallium-68
γ	Gamma ray
GBq	Giga-Becquerel
g	Gram

H

$t_{1/2}$	Half-life
Hz	Hertz
HMBC	Heteronuclear multiple bond correlation
HSQC	Heteronuclear single quantum coherence
Hex	Hexanes
HPLC	High-performance liquid chromatography
HRMS	High-resolution mass spectrometry
h	Hour(s)

I

ICPMS	Inductively coupled plasma mass spectrometry
IR	Infrared spectroscopy
IT	Isomeric transition

I	Iodine
^{123}I	Iodine-123
^{124}I	Iodine-124
^{125}I	Iodine-125
^{128}I	Iodine-128
^{131}I	Iodine-131
ICl	Iodine monochloride
^{111}In	Indium-111

K

K	Kelvin
keV	kiloelectron volt(s)
kJ	kilojoule(s)

L

LET	Linear energy transfer

M

MS	Mass spectrometry
m/z	Mass-to-charge ratio
MHz	Megahertz
MIBG	*Meta*-iodobenzylguanidine
MeOH	Methanol
μL	Microliter(s)
μm	Micrometer(s)
mCi	Millicurie(s)
mg	Milligram(s)
mL	Milliliter(s)
mm	Millimeter(s)
mmol	Millimole(s)
min	Minute(s)
MBq	Mega-Becquerel(s)
MeV	Megaelectron volt(s)
^{99}Mo	Molybdenum-99

N

nm	nanometer(s)
DMF	*N*,*N*-Dimethylformamide
^{14}N	Nitrogen-14
NCA	No-carrier-added
NMR	Nuclear magnetic resonance

O

ORTEP	Oak Ridge thermal ellipsoid plot

ON	Ontario
^{15}O	Oxygen-15

P

ppb	parts per billion
ppm	parts per million
FC-72	Perfluorohexane (or tetradecafluorohexane)
PFBME	Perfluorobutyl methyl ether
PBS	Phosphate buffered saline
H_3PO_4	Phosphoric acid
pg	picogram
β^+	Positron
PET	Positron emission tomography
^{32}P	Phosphorus-32
pH	Potential of hydrogen
PSMA	Prostate specific membrane antigen
^{1}H NMR	Proton NMR

Q

q	Quartet (NMR)

R

RCP	Radiochemical purity
RCY	Radiochemical yield
R_f	Retention factor
R_t	Retention time
^{186}Re	Rhenium-186
$^{223}RaCl_2$	Radium-223 dichloride

S

^{153}Sm	Samarium-153
s	second(s)
s	singlet (NMR)
SPECT	Single photon emission computed tomography
$NaHCO_3$	Sodium bicarbonate
Na_2CO_3	Sodium carbonate
NaOH	Sodium hydroxide
NaI	Sodium iodide
$Na_2S_2O_5$	Sodium metabisulfite
Na_2SO_4	Sodium sulfate
SPE	Solid-phase extraction
^{89}Sr	Strontium-89

T

^{99m}Tc	Technetium-99 metastable
THF	Tetrahydrofuran
TFP	Tetrafluorophenol
θ	Theta (x-ray)
TLC	Thin layer chromatography
3D	Three-dimensional
Sn	Tin
t	triplet(s)
2D	Two-dimensional
^{201}Tl	Thallium-201
TAAG	Triazole appending agent
TFA	Trifluoroacetic acid

U

UV	Ultraviolet
UV-Vis	Ultraviolet-visible
USP	United States Pharmacopeia

V

v/v	volume by volume

W

H_2O	Water
λ	Wavelength
w/v	weight by volume

X

^{133}Xe	Xenon-133

Y

^{90}Y	Yittrium-90

Z

^{89}Zr	Zirconium-89

Chapter 1 - Introduction

1.1 Iodine and the History and Growth of Nuclear Medicine

The first preclinical use of a radioisotope of iodine (^{128}I) which was shown to concentrate in the thyroid of rabbits, was reported in 1938.[1] This was later followed by the administration of radioiodine to patients once a longer live radioisotope of iodine (^{131}I) was discovered.[2] Patients with overactive thyroid glands took up more than ten times the amount of radioiodine than was the case for healthy individuals. This work formed the foundation for the widespread use of ^{131}I for the treatment of hyperthyroidism.[3]

The United States Atomic Energy Commission (AEC) harnessed the power of isotopes and subsequently started providing ^{131}I for clinical use shortly after the end of the World War II.[3] This significantly expanded the field of nuclear medicine in the 1950s. In 1971 the American Medical Association officially recognized nuclear medicine as a medical specialty,[4] which was based on examining the regional chemistry of the living body through the use of radioactive isotopes.[5]

In the periods following the official inception of nuclear medicine, the field assumed an increasingly important role in diagnostic medicine and disease treatment, growing to such an extent that over 16 million procedures are now conducted throughout the United States each year. According to the Society of Nuclear Medicine and Molecular Imaging (SNMMI) there are nearly 100 different nuclear medicine imaging procedures available today. In Canada, Great

Britain and Japan, 39-48 procedures per 1000 people are carried out annually, with an average annual increase of 7-14 % worldwide.[6]

Nuclear medicine has evolved as a multidisciplinary field combining fundamental aspects of chemistry, physics and clinical medicine.[7] The field is rapidly evolving through improvements in medical visualization methods, the production of target specific radiopharmaceuticals, and the introduction of highly sensitive diagnostic equipment. The ability to design agents which can target new biochemical pathways of diseases as they are uncovered allows nuclear medicine techniques to continually address unmet medical needs.

1.2 Molecular imaging

Modern non-invasive diagnostic imaging modalities are used routinely to identify diseases and injuries. Examples include computed tomography (CT), magnetic resonance imaging (MRI), optical, ultrasound (US), and nuclear imaging, along with various combinations of these techniques. Nuclear imaging methods stand apart because of their unparalleled sensitivity and ability to visualize and characterize biochemical processes and targets, not just structure or macroscopic physical processes (blood flow, oxygenation etc.).[8] This type of "molecular" imaging enables the early detection and characterization of disease before major anatomical changes are evident.[9,10] Identification of disease through monitoring biochemical markers has the added advantage that it can be used to select the ideal treatment option, particularly for targeted biological agents, and to monitor early response. This can eliminate potentially unnecessary biopsies or

ineffective interventions.[8]

1.3 Radionuclides for imaging

In molecular imaging, advantage is taken of the large signal (in this case the emitted radiation) produced by the relatively small mass of radiopharmaceutical (typically nanograms) employed for a given study. The minute mass allows for non-invasive observation of biological processes without disturbing the system under study. The tracer principle states that a very small (i.e. trace) amount of biologically active drug can be introduced into a subject and the distribution is representative of the (much larger amount) of naturally occurring compound.[11] This principle makes it possible to study specific systems and avoid any pharmacological or toxicological effects.

The choice of a radionuclide to be used in a non-invasive imaging specific study is influenced by a number of factors including:[12]

- The half-life, which should be commensurate with the duration of the imaging study
- Decay mode, where the radionuclide should emit gamma or X-rays and there should be no, or minimal, charged particle emissions (except for Positron Emission Tomography (PET))
- The energy of the gamma rays should be between 50 and 300 keV or 511 keV
- The radionuclide or radionuclide-prosthetic group derivative should be suitable for incorporating into a targeting vector without altering its

biological behavior

- The radionuclide should be readily available

Examples of radionuclides used for imaging and their key nuclear properties are shown in Table 1-1.

Table 1-1. Characteristics of commonly used radionuclides.[12]

Radionuclide	Type of decay[a]	Principal photon emissions (keV)	Half-life
^{18}F	β^+	511	110 min
^{67}Ga	EC	92, 182, 300, 390	78 h
^{123}I	EC	160	13 h
^{131}I	β^-	280, 360, 640	8 days
^{111}In	EC	173, 247	2.8 days
^{99m}Tc	IT	140	6 h
^{201}Tl	EC	60-80	73.5 h
^{133}Xe	β^-	81	5.3 days

[a]EC, electron capture; IT, isomeric transition.

1.4 Radionuclide therapy

Radionuclides can also be used to treat disease. Therapeutic medical isotopes typically decay by emission of three types of particles: β-particles, α-particles and Auger electrons. Examples of radionuclides emitting these particles are shown in Table 1-2. β-Particle emitters release high energy electrons and are the most common therapeutic radionuclides used clinically and provide a highly homogeneous radiation dose even though their deposition may be heterogeneously distributed in target tissues.[13] High energy β^- emitters are generally effective at treating larger tumors whiles those with lower energy

emissions are considered better at treating single cancer cells and metastases between 1 and 12 mm owing to their shorter path length.[13]

Radionuclides that emit α-particles are attractive in settings where it is more advantageous to use particulate radiation with a range of only a few cell diameters.[14] Alpha emitters typically have monoenergetic emissions deposit their energy over short ranges (i.e., usually between 40 and 100 μm). Because of their relatively short penetration range and high linear energy transfer (LET), α-particles have the capability for producing a high degree of tumoricidal activity while sparing the surrounding normal tissues making α-particles more effective in killing cancer cells that are in a hypoxic environment.[13]

The third class are Auger electrons, which produce highly localized energy density in the immediate vicinity of the decay site. They have very short path-lengths (~0.06-17 μm), and if localized close to chromosomal DNA, their biological effectiveness is close to that for high LET radionuclides.[15] Thus Auger-emitting radiopharmaceuticals must concentrate in the nuclei of diseased cells to be effective.

Table 1-2. Physical characteristics of radionuclides used for therapy.[16,17]

Radionuclide	Half-life	Emission	$E_{\alpha, max}$ (MeV)	$E_{\beta, max}$ (MeV)	Max. range
^{80m}Br	4.42 h	Auger	-	-	<10 nm
^{125}I	60.0 d	Auger	-	-	10 nm
^{211}At	7.2 h	α	6.8	-	65 μm
^{212}Bi	1.0 h	α	7.8	-	70 μm
^{169}Er	9.5 d	β	-	0.34	1.0 mm
^{67}Cu	2.6 d	β, γ	-	0.58	2.2 mm

^{131}I	8.0 d	β, γ	-	0.61/0.20	2.4 mm
^{153}Sm	1.9 d	β, γ	-	0.81/0.225	3.0 mm
^{198}Au	2.7 d	β, γ	-	0.96/0.31	4.4 mm
^{186}Re	3.8 d	β, γ	-	1.08/0.35	5.0 mm
^{165}Dy	2.3 h	β, γ	-	1.29/0.44	6.4 mm
^{89}Sr	50.5 d	β	-	1.49/0.58	8.0 mm
^{32}P	14.3 d	β	-	1.71/0.695	8.7 mm
^{90}Y	2.7 d	β	-	2.28/0.935	12.0 mm

Development of radionuclide therapy requires achieving a balance between the specific *in vivo* targeting of the diseased site and the clearance of radioactivity from non-target tissues,[13] in order to maximize the radiation dose to diseased cells. This is achieved by considering both the radioactive decay properties of the radionuclide and the characteristics of the diseased tissues/cells targeted, since the energy and half-lives of particles from different radioisotopes as well as their range in tissue vary. As a general guideline, the half-life of the isotope must be long enough for the agent to clear the blood and bind the target of interest and the energy of the particle must be high enough to induce apoptosis or related mechanism of cell death.[18] The most appropriate isotope will vary depending on the application, the disease, the nature of the targeting construct and the accessibility of the diseased tissue.

^{131}I-Sodium iodide, [^{131}I]NaI, administered as a liquid or capsule, has been employed in the treatment of benign thyrotoxicosis, which does not respond to medical treatment.[19,20] There is extensive data that shows that the incidence of induction of hypothyroidism (by radioiodine therapy) ranges from 7% to 25% in the first year.[19] ^{131}I-Sodium iodide has also been an integral part of the treatment

of differentiated (papillary and follicular) thyroid carcinoma. In most cases, after total or near-total thyroidectomy, an ablative dose of 1.85–3.7 GBq (50–100 mCi) is administered to clear the neck of any remaining thyroid tissue and to treat metastases.[19]

Another example of a beta therapy is [^{131}I]-*m*-iodobenzylguanidine (^{131}I-MIBG) therapy, which has been employed for the treatment of malignant phaeochromocytoma. Clinical data showed tumour regression or tumour control resulting in the reduction of the tumour's metabolic function and palliation of symptoms (such as hypertension, palpitations, sweats and bone pain).[19] It has also been applied in malignant paraganglioma, with reported remission, pain relief and improved quality of life.

Radium-223 dichloride, ($^{223}RaCl_2$) also known as Xofigo®, is an α-emitting radiotherapeutic that was recently approved by the US FDA for symptomatic late-stage (metastatic) castration-resistant prostate cancer that has reached bones but not other organs. Radium-223 mimics calcium and forms complexes with the bone mineral hydroxyapatite at areas of increased bone turnover, such as bone metastases.[21] Xofigo® not only increases patients' life expectancies by an average of about three months, but also improves their quality of life by offering pain relief.

1.5 Radiopharmaceuticals

A radiopharmaceutical is a chemical entity derived from a medical isotope that has regulatory approval for use for imaging or treatment of human diseases.

In nuclear medicine nearly 95% of radiopharmaceuticals are used for diagnostic purposes, however the utility of therapeutic radiopharmaceuticals is growing rapidly.[22] A typical radiopharmaceutical has two components: a radionuclide to generate the signal or induce a therapeutic response and a non-radioactive component that is designed to impart the desired targeting and clearance properties.

Radiopharmaceuticals accumulate via many different mechanisms. These include simple perfusion and targeted uptake. The most frequently used radiopharmaceuticals are perfusions agents, which are employed for the assessment of cardiac, renal, pulmonary and other functions, related to the diagnosis of disease or injuries.[23] Generally, uptake of perfusion agents into diseased site is *via* physical process and not a molecular mechanism. Processes of this nature include bone adsorption, hepatocyte clearance, blood circulation, and changes in brain perfusion associated with disease or trauma.[24]

Targeted radiopharmaceuticals used for imaging or therapy, can be considered as having three components: (*i*) the targeting vector, (*ii*) the radionuclide and (*iii*) a means of linking the two together that may, or may not, include a pharmacokinetic modifier (Figure 1-1).[25] These agents are designed as indicators of specific metabolic or biochemical dysfunction that are characteristic of a disease state or injury.[26] For example, biochemical targets that are present at increased levels in cancer cells can be visualized using radiolabelled inhibitors of those targets. The advantage here is that molecular changes tend to occur before

structural and bulk physical process changes that can be detected using perfusion agents or by conventional anatomical imaging methods. Imaging targeted agents provides a sensitive way to identify and characterize diseases at an early stage and to aid in treatment selection and monitoring response to therapy.

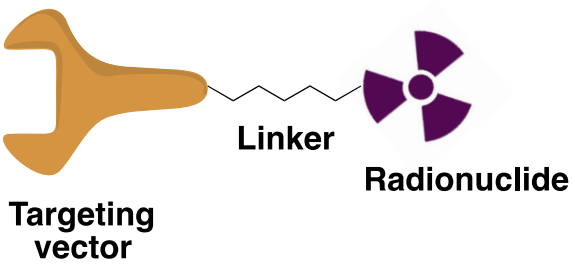

Figure 1-1. Schematic of a targeted radiopharmaceutical. Targeting vectors are typically connected to the radionuclide via linker and prosthetic group whose structure depends upon the nature of the radionuclide used.

Radiopharmaceuticals used for treatment are designed to deliver therapeutic doses of ionizing radiation.[13] Ideally, therapeutic radiopharmaceuticals localize with high specificity at the disease site while clearing from non-target tissues so as to minimize unwanted radiation damage, as was mentioned previously.[17] Radiotherapy is attractive because it is minimally invasive. It can be used to target multiple metastases, circumvents classical drug resistance mechanisms and in many cases it lacks drug related toxicity effects in comparison with chemotherapy.[17] The latter is a result of the fact that small mass doses (typically in the microgram range) are administered when using radionuclide therapies.[27]

1.6 Nuclear imaging modalities: PET and SPECT

Nuclear medicine imaging procedures require highly penetrating radiation such as γ-photons or X-rays (exceeding 100 keV) that can pass through overlying body tissues and be detected by suitable instruments outside the body. Both positron emission tomography (PET) and single photon emission computed tomography (SPECT) detect the emission of radiation from an administered medical isotope. PET uses a circular array of detectors to reconstruct images from coincidence detection of gamma emissions arising from positron decay.[28] Positrons are produced from proton-rich nuclei and travel a short distance before colliding with an electron, leading to annihilation. Two gamma rays with 511 keV are then emitted in opposite directions (180º) which are detected in coincidence by the ring of detectors which encircle the subject. Positron emitting radionuclides include halogens (^{18}F, ^{76}Br, or ^{124}I), transition metals (^{64}Cu, or ^{89}Zr), and main group elements (^{11}C, ^{15}O, ^{13}N or ^{68}Ga).[29]

SPECT is similar to PET in that images are generated based on the detection of gamma emission however there is no coincident emission of 511 keV gamma rays where each SPECT isotope has a unique gamma energy that is emitted in a random direction. Data is collected in two-dimensional (2D) projections (giving planar images at each projection angle) which is then converted into three-dimensional (3D) reconstructions. This is achieved by rotating one or more gamma cameras around the patient and recording multiple projections at different angles and subsequently calculating where the gamma rays

originated. For gamma cameras, collimators, which are devices designed to confine a beam of radiation within a specific field of view, are attached to the detectors to block gamma radiation from outside the field of view from interacting with the camera. Some examples of clinically relevant gamma emitting isotopes include ^{123}I, ^{99m}Tc, ^{67}Ga and ^{111}In.[28]

Because PET scanners do not require collimation, and therefore use a greater proportion of the emitted signal, the technique is more sensitive than SPECT. It also has a higher practical resolution, and images can be readily quantified. The main advantage of SPECT imaging over PET is that SPECT isotopes are typically lower cost and generally have longer half-lives than commonly used PET isotopes. This fact, coupled with the low cost of conventional gamma cameras and SPECT radiopharmaceuticals has made SPECT imaging more prevalent than PET for routine clinical studies.[8]

Currently, there are over 50 different radiopharmaceuticals incorporating single photon emitters in clinical use.[11] Their half-life periods range from 6 hours to 8 days and their γ-photon energy between 70-511 keV. [28] The most widely used agents are based on ^{99m}Tc, accounting for about 80% of the scans conducted in the clinic.[30] One of the advantages of this isotope is its commercial availability at low cost from a ^{99}Mo:^{99m}Tc generator, which allows for widespread distribution and accessibility. Furthermore, ^{99m}Tc has nearly ideal nuclear properties for SPECT imaging and imparts a low dose to the patient which adds to its desirability.

The widespread use of ^{99m}Tc radiopharmaceuticals is also partly due to the

availability of instant kits that can be used to prepare ^{99m}Tc radiopharmaceuticals. These kits contain freeze-dried components, in a sterile vial, to which ^{99m}Tc is added and heated at an appropriate temperature for a given time yielding the desired ^{99m}Tc radiopharmaceutical. The freeze-dried components include a ligand to be complexed to ^{99m}Tc, an optimum amount of reducing agent, buffer to adjust the pH, stabilizing agents and excipients. The produced radiopharmaceutical is used without further purification consequently the agents can be generated with minimal expertise and infrastructure. Similar strategies for other SPECT isotopes is much sought after, where high costs and the lack of kit type production methods has hindered their clinical use.

1.7 Radioisotopes of iodine

The use of radiohalogenated radiopharmaceuticals continues to be an important and growing area of nuclear medicine for both imaging and radiotherapy.[31] While about 30 radioisotopes of iodine have been reported, only one stable isotope, ^{127}I, is found in nature. Three of the radioisotopes (^{123}I, ^{125}I and ^{131}I) have found practical utility in nuclear medicine and have been used widely for labelling small and large molecules. Three other positron-emitting isotopes (^{120}I, ^{122}I and ^{124}I) have recently been examined as potential candidates for tracer development.[32–34]

The attractive decay characteristics of iodine radioisotopes (Table 1-3) and ease of incorporation into targeting molecules lead to their use in biochemical and pharmaceutical research, which included radioimmunoassays for biochemical

research and drug development as well as in clinical trials. Iodine-123 is perhaps the most useful diagnostic iodine isotope because of its relatively long half-life (13.3 h) and nearly ideal γ-ray energy for SPECT. Iodine-124 has gained popularity as a PET isotope for imaging of molecules with slow pharmacokinetics such as antibodies because of the isotope's long half-life (4.2 d). Iodine-125 emits γ-rays, but of insufficient energy to be adequately imaged outside of the human body. However, its long half-life and relatively low energy x-ray emission makes it useful for *in vitro* assays and quantitative biodistribution studies.[35,36] Iodine-125 in higher concentrations is also used in brachytherapy; a treatment for primary prostate cancer that involves implanting seeds loaded with ^{125}I. Iodine-131 has decay properties (γ-ray and β^- emitter) that make it a suitable radionuclide for both imaging and therapeutic applications and is the most widely used of the iodine isotopes in the clinic driven mainly by the aforementioned use in treating thyroid disorders.

Table 1-3. Radioisotopes of iodine used in nuclear medicine.

Isotope	Half-life ($t_{1/2}$)	Type of Emission	Applications
^{120}I	1.4 h	β^+	PET
^{122}I	3.6 min	β^+	PET (blood flow)
^{123}I	13.3 h	γ	SPECT
^{124}I	4.2 d	β^+	PET
^{125}I	60.0 d	X-ray	Therapy / small animal SPECT
^{131}I	8.0 d	β^- / γ	Therapy / SPECT

Iodine represents a versatile starting point to create radiopharmaceuticals because altering the isotope can change the utility of the agent. One successful agent can potentially be used for imaging (PET or SPECT) and targeted radiotherapy. When developing a new iodine radiopharmaceutical, ^{125}I can be used for method development and *in vitro* testing. Once a lead is found, preclinical and clinical studies can be completed using ^{124}I (PET), ^{123}I or ^{131}I (SPECT). A labelling procedure developed for one isotope of iodine should be adaptable to another, provided the time required by the procedure, the half-lives of the isotopes, and the chemical form and specific activity in which the radioiodine are supplied are taken into account.[36] In addition, similar labelling reactions can be used to incorporate other halogens (Br, I and At), which expands the potential scope of imaging and therapeutic applications for a radiohalogen based agent.

1.8 Radioiodination methods

In general, classical iodination methods used in organic chemistry can be employed in radiochemistry. However, these methods have to be adapted taking into account several parameters such as the half-life of the radionuclide and the low reaction concentrations used.[32] The main classes for radiolabelling with iodine are nucleophilic and electrophilic substitution reactions. The specific choice of method and desired labelling site is determined by biological, chemical and structural considerations where particular attention must be paid to the stability of the C-I bond and the influence of the isotope on target binding.

Regioselective labelling reactions are therefore critical in order to prevent tedious separation and purification procedures.[32] Because of the high cost and hazard, when working with radionuclides a strong emphasis is also placed on reducing reaction times and minimizing handling requirements.

1.8.1 Nucleophilic substitution reactions

Radioiodination reactions employing nucleophilic substitution occur by the attack of an iodide anion on an electrophile to form a new C-I bond. The mechanism, like in classical organic chemistry, depends on the substrate, the leaving group and the reaction conditions (solvent, temperature, etc.). Radioiodination via nucleophilic substitution is most often performed with aromatic compounds through halogen exchange type reactions.[32] This involves the direct substitution of radioactive iodine as I^- for a non-radioactive iodine atom, or other halogen, present in the precursor molecule.[37] For successfully performing a nucleophilic substitution reaction on an aromatic substrate the reaction must be either activated by electron-withdrawing groups, or the process performed in the presence of a catalyst. An alternative method is to perform the isotopic exchange in a melt or under solid-state conditions in which the exchange between no-carrier-added (NCA) radioiodide and unactivated aryl iodide under mildly acidic conditions (Scheme 1-1) is possible.[38,39]

Scheme 1-1. Isotope exchange labelling. *I represents radioiodine.

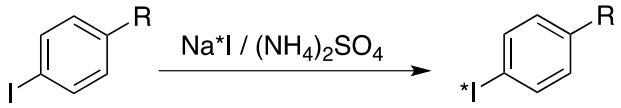

The main disadvantage of halogen exchange is that products are obtained as a mixture of radiolabelled and stable products. For iodine exchange reactions, since both the starting material and radiolabelled product are structurally identical, they cannot be separated chromatographically.[32] In a typical radiolabelling experiment, the non-radioactive starting material is in excess of the amount of radioactive sodium iodide by several orders of magnitude. This issue can be addressed by using bromine at the cost of lower reaction yields and the need to employ higher reaction temperatures (Scheme 1-2) (temperatures in excess of 100 ^{o}C) which can lead to the degradation of thermally unstable compounds.[40]

Scheme 1-2. Iodine for bromine halogen exchange radiolabelling methodology

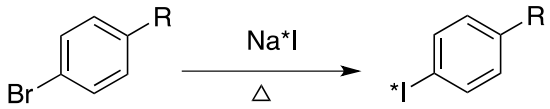

1.8.2 Electrophilic substitutions

Halogen exchange has fallen out of favour because it requires harsh conditions and generally gives poor radiolabelling yields and low specific activity products. Electrophilic labelling with radioiodine in contrast is the preferred synthetic route because it uses mild reaction conditions and reactions are generally regioselective. Iodide can be oxidized *in situ* to an electropositive form of iodine, postulated to be H_2OI^+ at low pH and ICl at higher pH with chlorine based oxidants.[36] Electrophilic reactions are performed by simply adding sodium iodide and an oxidant into a solution containing the appropriate precursor.[31] Reactions, which are described in more detail below, are typically completed in

mere minutes at room temperature.

1.8.2.1 Direct electrophilic radioiodination reactions

Electron rich aromatic compounds including phenols, aryl ethers, and anilines, are strongly activated toward electrophilic substitution. These compounds react rapidly with electrophilic halogens, which is particularly useful in radiochemical reactions which use dilute solutions of radioiodine.[41] This approach has been exploited for labelling proteins where *in situ* generated electrophilic iodine reacts with tyrosine residues and, to a lesser extent, histidine residues producing covalent bonds *ortho* to the activating group (Scheme 1-3).[42]

Scheme 1-3. Labelling of tyrosine using the direct-radioiodination method

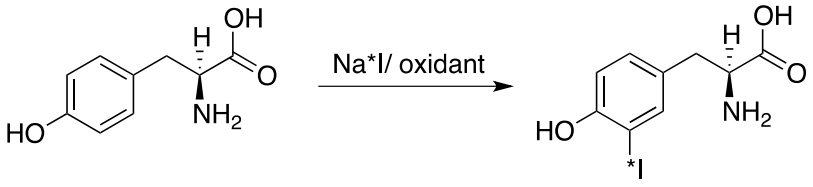

The main limitations of this method is that radioiodinated proteins frequently undergo deiodination *in vivo*, resulting in a large accumulation of radioactivity in the thyroid.[31] This results from destabilization of the iodine by the adjacent hydroxyl group on the phenyl ring and the action of deiodinases.[43]

1.8.2.2 Iododemetallation

Iododemetallation reactions involve replacement of an organometallic group such as trialkylstannyl, trialkylsilyl or trialkylgermyl derivatives by

iodine.[32,44] It represents a milder alternative to halogen exchange and can also produce radiotracers in high effective specific activity (ESA). ESA is the amount of activity per mole of radiotracer (typically reported in Ci/mmol) and is important for molecular imaging applications. The high ESA requirement is because of the low population of receptors expressed on the cell surface, whereby the tracer with low specific activity may saturate the receptor, disobey the tracer principle, and change the pharmacokinetics *in vivo*, causing poor image quality and misleading results.[45]

Although a number of organometallic compounds can be used for this class of reactions, group IV arene derivatives have been the most widely studied. Arylstannanes are favoured[31,32,46,47] over trialkylsilyl and trialkylgermanyl analogues because the metal-carbon bonds in germanium and silicon are stronger than the corresponding carbon-tin bond,[32] so while the tin reagents are inherently less thermally stable, they display significantly higher reactivity and thus higher radiolabelling yields as compared to silicon and germanium analogues.[32,47,48]

Mechanistically, electrophilic substitution reactions involving aromatic trialkylstannyl compounds are considered to occur as a two-step process, beginning with nucleophilic addition to the electropositive carbon atom, which is quickly followed by electrophilic substitution at the *ipso* carbon atom (Scheme 1-4).[32] These reactions are generally carried out at room temperature which limits the amount of thermal decomposition of the molecule being labelled.[47] A comparison of isotopic exchange labelling reaction with iododemetallation

reaction showed that the specific activity of the latter method was at least two orders of magnitude greater than the former.[49]

Scheme 1-4. General scheme of the iodo-destanyllation reaction

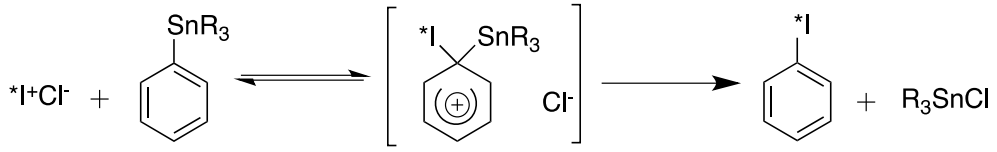

Demetallation strategies typically require HPLC purification of the radiolabelled product both to achieve the necessary ESA and to completely remove the potentially toxic stannyl-precursor from the radiopharmaceutical formulation.[32,40] The recommended parenteral limit for tin that can be administered to a patient is 300 ppm.[50] However, the use of HPLC, which is the most common technique employed to remove unreacted starting material and impurities, is time consuming and challenging for products destined for routine clinical use, particularly when using radioisotopes with short half-lives.[51] Furthermore, the risk of radiation exposure during the routine production of radiotracers is increased when using preparative HPLC protocols.

1.8.2.3 Polymer-supported iododestannylation

To eliminate the need for HPLC purification as a means of preparing radiotracers in high ESA, solid-phase analogues of the iododestannylation reaction have been developed.[51–54] In solid-phase radiolabelling the substrate is covalently bound to an insoluble polymer. Treatment of the polymer-bound

substrate with electrophilic radioiodine results in the selective release of the radioiodinated compound into solution *via* cleavage of the aryl-tin bond (Scheme 1-5). The unreacted polymer-bound substrate and polymer-bound side products are insoluble and thus are easily removed by filtration[52,53]

Scheme 1-5. Schematic of a solid-phase radiolabelling platform.

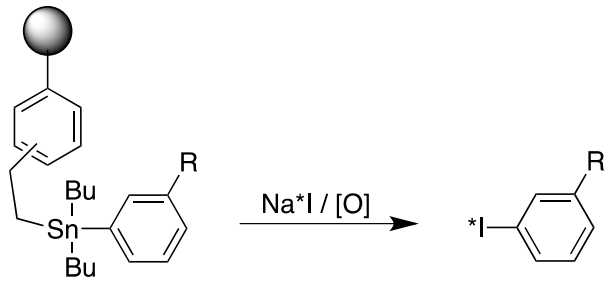

This radiolabelling strategy has advantages over solution-phase techniques in that it affords ease of product isolation via simple filtration, and it is amenable to automation. However, it has a number of limitations that arise from using insoluble polymer supports. Purity analysis and characterization are not nearly as straightforward for cross-linked insoluble polymers as they are for small molecules.[55] There is also no way to purify resin-bound material so all polymer loading reactions and subsequent transformations done prior to labelling must take place in quantitative yield. If impurities are present, iodination can result in the release of a mixture of products, which negates any inherent advantage of using the solid-phase approach. An additional concern is that because resin-bound precursors are prepared using polymers that can vary in composition, resins may have variable amounts of precursor loaded. This can lead to inconsistent

radiochemical yields.[51] These issues motivated the search for new HPLC free labelling methods.

1.9 Fluorous Chemistry

1.9.1 Scope and Concept

Fluorous chemistry is the study of the structure, composition, properties, and reactions of highly fluorinated molecules, molecular fragments, materials, and media.[56] Developed nearly two decades ago, fluorous chemistry has emerged as a complementary type of liquid-phase synthetic tool that is similar to solid-phase synthesis in concept but very different in practice. The term "fluorous" refers to highly perfluorinated molecules which display unique intermolecular interactions akin to the term aqueous.[55] Fluorous compounds are both hydrophobic and oleophobic while displaying a high affinity for other fluorine rich compounds.

Perfluoroalkyl solvents are immiscible with most organic solvents at room temperature and are extremely hydrophobic and lipophobic.[57] Highly fluorinated solvents, and compounds that partition into them, form a separate, orthogonal liquid phase called the “fluorous” phase into which organic and inorganic compounds have little or no tendency to dissolve.[55] The solubility of fluorous compounds in these solvents is dependent on the percentage weight of fluorine. Compounds containing 60% or more fluorines by weight (heavy fluorous molecules) will preferentially partition into a fluorous solvent instead of an aqueous or organic solvent.

Curran and coworkers did extensive work in the use of fluorous chemistry in the field of organic synthesis.[55,58] In fluorous synthesis, a fluorous molecule is created by attaching a fluorous tag to an organic substrate. The resulting fluorous molecule has two domains: a fluorous domain that controls the solubility of the molecule and an organic domain that directs the reactivity of the compound.[55] Fluorous tags are usually fluorinated alkyl chains ranging from C_3F_{11} to $C_{10}F_{21}$.[56,59] These tags are generally stable under normal reaction conditions and are compatible with typical organic chemical reactions. Thus, fluorous tags are chemically inert and have minimal effect on the reactivity of the organic component; hence, the organic substrate undergoes chemical transformation without interference from the fluorous tag. When the desired chemical transformation has been achieved, the organic product is obtained by the detachment of the fluorous tag, as illustrated in Figure 1-2.[60,61]

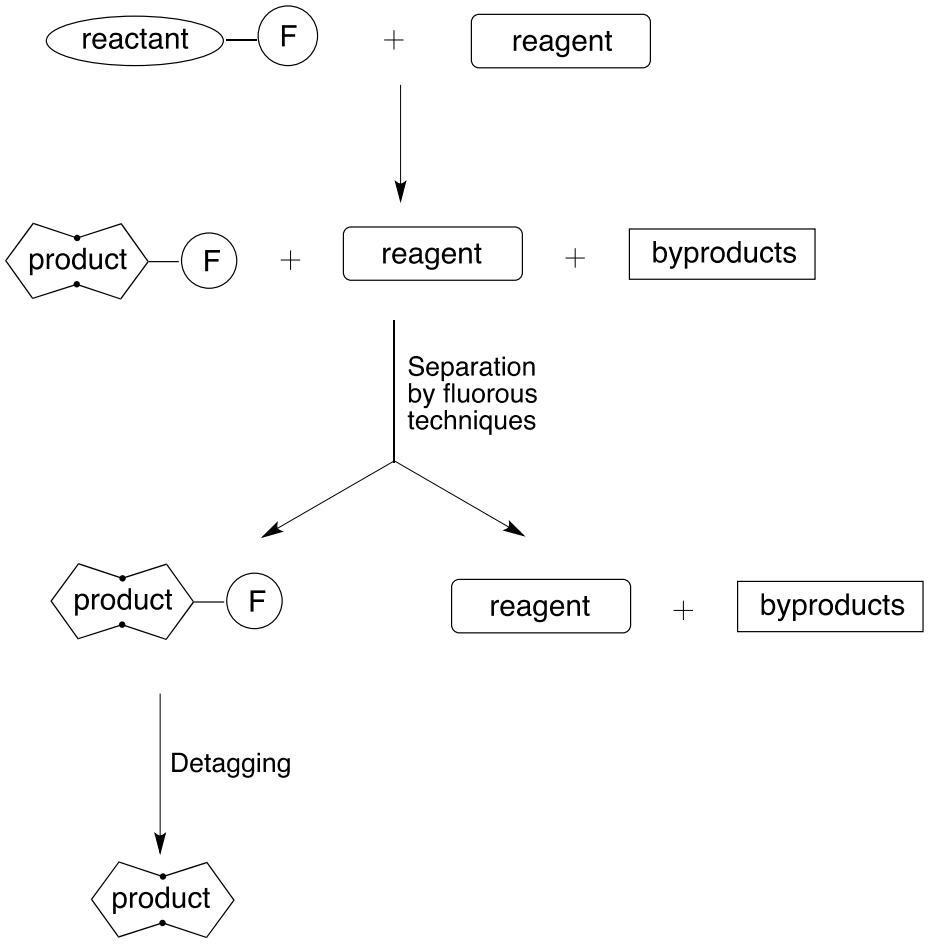

Figure 1-2. General schematic showing the fluorous tagging and detagging strategy. F represents the fluorous tag.

1.9.2 Fluorous Separation Techniques

Fluorous chemistry offers the advantage of easy separation based on differential affinities of organic and fluorous molecules. These differences have been exploited to create several techniques for isolating fluorous-tagged substrates from purely organic molecules.[61] These methods include liquid-liquid extraction, fluorous solid-phase extraction (F-SPE) and fluorous HPLC (F-HPLC). These are not influenced by polarity, or other molecular features that govern traditional chromatography, but depend solely on the presence (or absence) of a fluorous

tag.[55,59,61] Liquid-liquid extraction is the method of choice for purification of "heavy fluorous" compounds. These compounds can be extracted efficiently into perfluorinated solvents such as perfluorohexanes (C_6F_{14}, commonly referred to as FC-72®) and perfluorobutyl methyl ether (PFBME), which are immiscible with water and common organic solvents such as ether and dichloromethane.[59,61]

"Light fluorous" compounds can be separated from non-fluorous compounds using fluorous solid-phase extraction (F-SPE) on silica gel that has been modified with fluorous groups such as -$SiMe_2(CH_2)_2C_8F_{17}$.[59,61] In a typical separation procedure, a reaction mixture is loaded onto an F-SPE cartridge with a minimum amount of solvent (less than 20% of silica gel volume). The cartridge is subsequently washed with a 'fluorophobic solvent' such as 80:20 (v/v) MeOH/H_2O to selectively remove non-fluorous compounds. Washing with a 'fluorophilic solvent' such as MeOH, acetonitrile, or THF elutes fluorous-tagged compounds.[61] One of the major advantages of this method is the fact that costly and potentially environmentally harmful perfluorinated solvents are not needed. Furthermore, the F-SPE cartridges can be regenerated for further use by flushing with warm THF.[62]

Silica gel that has a bonded phase of fluorous groups packed in an HPLC column can be used for separation of mixtures of fluorous compounds based on the differences in fluorine content.[63,64] Molecules with longer fluorine chains have longer retention times on the column. A gradient of MeOH/H_2O with increasing MeOH content is the most common mobile phase similar to that for reversed

phase HPLC.

One of the major advantages of fluorous chemistry over solid-phase synthesis is that the products can be characterized by a variety of standard techniques. These include TLC, HPLC, MS, IR spectroscopy, NMR spectroscopy, and X-ray crystallography. The added gain is that if an impurity is detected the compounds can be re-purified using one of the methods described previously.

1.10 Application of Fluorous Chemistry to Radiolabelling

The facile purification protocols offered by fluorous media have been exploited to afford HPLC-free methods for preparing radiolabelled compounds. Zhang *et al.* developed a method for scavenging excess amines in sulfur-35-labelled radioligand preparations using fluorous scavengers in an effort to simplify the purification.[65] They effectively applied fluorous scavenging and F-SPE purification to obtain a high specific activity [^{35}S]sulfonamide radioligand. Compared to the use of a solid-phase-isocyanate resin, their method provided a more complete and faster removal of undesired reaction components due to the homogenous nature of the fluorous reaction. More recently, Bejot *et al.* have demonstrated that ^{18}F-radiolabelled material can be prepared by nucleophilic fluorination using fluorous-tagged precursors and the products isolated by FSPE.[66]

The fluorous approach was also adapted by our group for radioiodination where fluorous-aryl tin precursors where treated with radioiodine in the presence of an oxidant. The fluorous starting materials were separated from the desired

non-fluorous radioiodinated compound by passing the reaction mixture through an F-SPE cartridge (Scheme 1-6) The isolated products were obtained in high radiochemical yield and purity.[67–69]

Scheme 1-6. General representation of the fluorous radiolabelling strategy applied to a halodestanylation reaction.

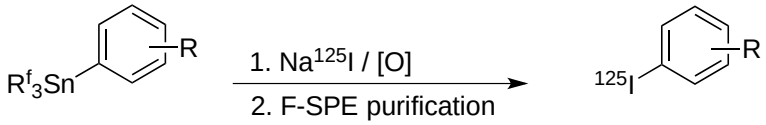

$R^f = CH_2CH_2(CF_2)_5CF_3$

When comparing fluorous and solid-phase labelling methods one obvious advantage is that fluorous compounds can be purified by conventional means while cross-linked polymer derivatives cannot.[51] Furthermore, the radiochemical yields are typically reduced in heterogeneous solid-phase reactions due to the biphasic nature of reactions. Solid-phase labelling can also require heating and/or use of organic solvents.[70] It is important to note however that solid phase labelling is simpler in that purification requires only filtration as opposed to more involved handling of solutions associated with F-SPE.

One way to combine the advantages of both methods is to create a "hybrid" fluorous-solid-phase system. Fluorous-tagged precursors can feasibly be loaded onto a fluorous solid support by physisorption to create a non-covalent fluorous-chemistry based solid-phase analogue. The desired radiolabelled product would still be released from the support upon labelling since it is rendered "non-fluorous". The advantage of loading the material onto the fluorous support, as

opposed to labelling and then passing the mixture through a FSPE cartridge, is that the combined system could be used to create a single step "instant kit" which would minimize handling of the radioactive solutions and facilitate clinical translation. Finding an instant kit system that works for iodine has, as was mentioned previously, been a longstanding goal in the field of radiopharmaceutical chemistry.

1.11 Objectives and summary of research goals

The objective of this thesis was to develop, optimize and evaluate the utility of a novel hybrid solid-fluorous phase radioiodination and purification platform for the production of radiopharmaceuticals for imaging and therapy based on the principles of fluorous chemistry. Initially work focused on a known fluorous-benzoic acid derivative[67] as the model compound to develop the platform using iodogen and chloramine-T as oxidants. This construct was expanded to include a series of fluorous-aryl tin precursors to further evaluate the platform (Chapter 2). When increasing amounts of the oxidant, particularly chloramine-T, were employed to increase radiochemical yields, there was co-elution of the non-fluorous oxidant and the radiolabelled product. This reduced the radiochemical yield and introduced unwanted UV impurities. To address this issue a fluorous oxidant was developed such that the only non-fluorous component to be eluted was the desired product (Chapter 3).

Following the successful preparation and testing of the iodine instant kit using the fluorous oxidant with a model compound (fluorous-benzoic acid), the

platform was used to prepare a series of radioiodinated compounds including well-known radiopharmaceuticals and emerging tools that can be used in pretargeting strategies that employ new bioorthogonal coupling reactions (Chapter 4). Given the ease with which the oxidant and resulting byproducts can be removed from reaction mixtures, the utility of the fluorous oxidant for applications beyond radiolabelling, notably hydrogen sulfide processing, were investigated (Chapter 5).

1.12 References

(1) Hertz, S.; Roberts, A.; Evans, R. D. *P. Soc. Exp. Biol. Med.* **1938**, *38*, 510–513.

(2) Becker, D. V.; Sawin, C. T. *Semin. Nucl. Med.* **1996**, *XXVI*, 155–164.

(3) Creager, A. N. H. *J. Hist. Biol.* **2006**, *39*, 649–684.

(4) Welch, M. J.; Redvanly, C. S. *Handbook of Radiopharmaceuticals: Radiochemistry and Applications.*; John Wiley & Sons Ltd.: Chichester, 2003.

(5) Elgazzar, A. H. *The Pathophysiologic Basis of Nuclear Medicine.*; 2nd ed.; Springer-Verlag: New York, 2006.

(6) Makeyev, S. S. In *Radiation Detectors for Medical Applications*; Tavernier, S.; Gektin, A.; Grinyov, B.; Moses, W. W., Eds.; Springer: Dordrecht, 2006.

(7) Valliant, J. F. *J. Nucl. Med.* **2010**, *51*, 1258–1268.

(8) Pomper, M. G. *Acad. Radiol.* **2001**, *8*, 1141–1153.

(9) Hoffman, J. M.; Gambhir, S. S. *Radiology* **2007**, *244*, 39–47.

(10) Weissleder, R. *Radiology* **1999**, *212*, 609–614.

(11) Moses, W. W.; Gayshan, V.; Gektin, A. In *Radiation Detectors for Medical Applications*; Tavernier, S.; Gektin, A.; Grinyov, B.; Moses, W. W., Eds.; Springer: Dordretcht, 2006; pp. 1–12.

(12) *Practical Nuclear Medicine*; Sharp, P. F.; Gemmell, H. G.; Murray, A. D., Eds.; Springer–Verlag London Limited: London, 2005.

(13) Volkert, W. A.; Hoffman, T. J. *Chem. Rev.* **1999**, *99*, 2269–2292.

(14) Humm, J. L.; Cobb, L. M. *J. Nucl. Med.* **1990**, *31*, 75–83.

(15) Behr, T. M.; Béhé, M.; Löhr, M.; Sgouros, G.; Angerstein, C.; Wehrmann, E.; Nebendahl, K.; Becker, W. *Eur. J. Nucl. Med.* **2000**, *27*, 753–765.

(16) Troutner, D. E. *Nucl. Med. Biol.* **1987**, *14*, 171–176.

(17) Hoefnagel, C. A. *Anticancer Drug.* **1991**, *2*, 107–132.

(18) Liu, S. *Adv. Drug Deliver. Rev.* **2008**, *60*, 1347–1370.

(19) Chatal, J. F.; Hoefnagel, C. A. *Lancet* **1999**, *354*, 931–935.

(20) Ross, D. S. *N. Engl. J. Med.* **2011**, *364*, 542–550.

(21) Shirley, M.; McCormack, P. L. *Drugs* **2014**, *74*, 579–586.

(22) Saha, G. B. *Fundamentals of Nuclear Pharmacy*; 6th ed.; Springe: New York, 2010., 2010.

(23) Baggish, A. L.; Boucher, C. A. *Circulation* **2008**, *118*, 1668-1674.

(24) Eckelman, W. C. *Eur. J. Nucl. Med.* **1995**, *22*, 249–263.

(25) Mather, S. J. *Mol. Biosyst.* **2007**, *3*, 30–35.

(26) Chua, S. S. C.; Cook, G. J. R. *Surgery* **2008**, *26*, 261–268.

(27) Orlova, A. Indirect Radiohalogenation of Targeting Proteins: Labelling Chemistry and Biological Characterization, University of Uppsala, 2003.

(28) Phelps, M. E.; Hoffman, E. J.; Mullani, N. A.; Ter-Pogossian, M. M. *J. Nucl. Med.* **1975**, *16*, 210–224.

(29) Saha, G. B. *Physics and Radiobilogy of Nuclear Medicine*; 3rd ed.; Springer: New York, 2006.

(30) Jurisson, S. S.; Lydon, J. D. *Chem. Rev.* **1999**, *99*, 2205–2218.

(31) Adam, M. J.; Wilbur, S. D. *Chem. Soc. Rev.* **2005**, *34*, 153–163.

(32) Coenen, H. H.; Mertens, J.; Maziere, B. *Radioiodination Reactions for Radiopharmaceuticals*; Springer: Dordretch, 2006; pp. 1–98.

(33) Jones, T. *Eur. J. Nucl. Med.* **1996**, *23*, 207–211.

(34) Holland, J. P.; Williamson, M. J.; Lewis, J. S. *Mol. Imaging* **2010**, *9*, 1–20.

(35) Mathis, C. A.; Shulgin, A. T.; Sargent, T. *J. Labelled Compd. Rad.* **1986**, *XXIII*, 115–125.

(36) Seevers, R. H.; Counsell, R. E. *Chem. Rev.* **1982**, *82*, 575–590.

(37) Eersels, J. L. H.; Mertens, J.; Herscheid, J. D. M. *J. Labelled Compd. Rad.* **2012**, *55*, 135–139.

(38) Mangner, T. J.; Wu, J.; Wieland, D. M. *J. Org. Chem.* **1982**, *47*, 1484–1488.

(39) Davarpanah, M. R.; Attar Nosrati, S.; Khoshhosn, H. A.; Fazlali, M.; Kazemi Boudani, M. *J. Labelled Compd. Rad.* **2013**, *56*, 686–688.

(40) Eersels, J. L. H.; Travis, M. J.; Herscheid, J. D. M. *J. Labelled Compd. Rad.* **2005**, *48*, 241–257.

(41) Wilbur, S. D. *Bioconjugate Chem.* **1992**, *3*, 433–470.

(42) Krummeich, C.; Holschbach, M.; Stocklin, G. *Appl. Radiat. Isotopes* **1994**, *45*, 929–935.

(43) Wroblewski, V. J. *Biochem. Pharmacol.* **1991**, *42*, 889–897.

(44) Moerlein, S. M. *J. Chem. Soc. Perk. T. 1* **1985**, 1687–1692.

(45) Hume, S. P.; Gunn, R. N.; Jones, T. *Eur. J. Nucl. Med.* **1998**, *25*, 173–176.

(46) Bolton, R. *J. Labelled Compd. Rad.* **2002**, *45*, 485–528.

(47) Moerlein, S. M.; Mathis, C. A.; Yano, Y. *Appl. Radiat. Isotopes* **1987**, *38*, 85–90.

(48) Moerlein, S. M.; Coenen, H. H. *J. Chem. Soc. Perk. T. I* **1985**, 1941–1947.

(49) Mairs, R. J.; Gaze, M. N.; Watson, D. G.; Skellern, G. G.; Constable, P.; McKellar, K.; Owens, J.; Vaidyanathan, G.; Zalutsky, M. R. *Nucl. Med. Commun.* **1994**, *15*, 268–274.

(50) United-States Pharmacopeia. General Chapter on Inorganic Impurities.

(51) Vaidyanathan, G.; Affleck, D. J.; Alston, K. L.; Zhao, X.-G.; Hens, M.; Hunter, D. H.; Babich, J.; Zalutsky, M. R. *Bioorgan. Med. Chem.* **2007**, *15*, 3430–3436.

(52) Hunter, D. H.; Zhu, X. *J. Labelled Compd. Rad.* **1999**, *42*, 653–661.

(53) Gifford, A. N.; Kuschel, S.; Shea, C.; Fowler, J. S. *Bioconjugate Chem.* **2011**, *22*, 406–412.

(54) Janabi, M.; Pollock, C. M.; Chacko, A.; Hunter, D. H. *Can. J. Chem.* **2015**, *93*, 1–11. doi: 10.1139/cjc – 2014–0265.

(55) Gladysz, J. A.; Curran, D. P.; Horváth, I. T. *Handbook of Fluorous Chemistry*; Wiley-VCH: Weinheim, 2004.

(56) Gladysz, J. A.; Curran, D. P. *Tetrahedron* **2002**, *58*, 3823–3825.

(57) Sandford, G. *Tetrahedron* **2003**, *59*, 437–454.

(58) Curran, D. P. *Angew. Chem. Int. Ed.* **1998**, *37*, 1174–1196.

(59) Zhang, W.; Curran, D. P.; Chen, C. H.-T. *Tetrahedron* **2002**, *58*, 3871–3875.

(60) Ubeda, M. A.; Dembinski, R. *J. Chem. Educ.* **2006**, *83*, 84–92.

(61) Zhang, W. *Tetrahedron* **2003**, *59*, 4475–4489.

(62) Dobbs, A. P.; Penny, M. J.; Jones, P. *Tetrahedron Lett.* **2008**, *49*, 6955–6958.

(63) Curran, D. P.; Luo, Z. *J. Am. Chem. Soc.* **1999**, *121*, 9069–9072.

(64) Curran, D. P.; Oderaotoshi, Y. *Tetrahedron* **2001**, *57*, 5243–5253.

(65) Zhang, A. S.; Elmore, C. S.; Egan, M. A.; Melillo, D. G.; Dean, D. C. *J. Labelled Compd. Rad.* **2005**, *48*, 203–208.

(66) Bejot, R.; Fowler, T.; Carroll, L.; Boldon, S.; Moore, J. E.; Declerck, J.; Gouverneur, V. *Angew. Chem. Int. Ed.* **2009**, *48*, 586–589.

(67) Donovan, A. C.; Forbes, J.; Dorff, P.; Schaffer, P.; Babich, J.; Valliant, J. F. *J. Am. Chem. Soc.* **2006**, *128*, 3536–3537.

(68) Donovan, A. C.; Valliant, J. F. *Nucl. Med. Biol.* **2008**, *35*, 741–746.

(69) McIntee, J. W.; Sundararajan, C.; Donovan, A. C.; Kovacs, M. S.; Capretta, A.; Valliant, J. F. *J. Org. Chem.* **2008**, *73*, 8236–8243.

(70) Yong, L.; Yao, M.-L.; Green, J. F.; Kelly, H.; Kabalka, G. W. *Chem. Commun.* **2010**, *46*, 2623–2625.

Chapter 2 - A Hybrid Solid-Fluorous Phase Radioiodination and Purification Platform

The following chapter was published in the Journal of Labelled Compounds and Radiopharmaceuticals, under the citation:

James P. K. Dzandzi, Denis R. Beckford Vera and John F. Valliant. A hybrid solid-fluorous phase radioiodination and purification platform. *J. Labelled Compd. Rad.*, **2014**, 57, 551-557.

I was responsible for the synthesis and characterizations of all precursor compounds used, development of the platform and all related experiments, while contributing to the manuscript text and complete experimental write-up of the work described in this chapter. Dr. Beckford Vera was responsible and acknowledged for help with optimization of the radiolabelling experiments and contribution to manuscript write-up. Prof. Valliant was responsible for the overall structure of the manuscript and project, along with key scientific input and editorial reviews.

A Hybrid Solid-Fluorous Phase Radioiodination and Purification Platform

2.1 Abstract

A new class of fluorous materials was developed to create a hybrid solid-solution phase strategy for the expedient preparation and HPLC-free purification of ^{125}I-labelled compounds. The system is referred to as a hybrid platform in that it combines solution phase labelling and fluorous solid-phase purification in one step as opposed to two separate individual processes. Treatment of fluorous arylstannanes coated on fluorous silica with [^{125}I]NaI and the appropriate oxidant made it possible to produce and selectively isolate the non-fluorous radiolabelled products in high purity (>98%) free from excess starting material and unreacted radioiodine. Examples included simple aryl and heterocyclic (click) derivatives, known radiopharmaceuticals including *meta*-iodobenzylguanidine (MIBG) and iododeoxyuridine (IUdR), and a new agent with high affinity for prostate specific membrane antigen. The coated fluorous silica kits are simple to prepare and reactions can be performed at room temperature using different oxidants generating products in minutes in biocompatible solutions.

Keywords: Labelling methods; ^{125}I; instant kits; fluorous; MIBG; IUdR.

2.2 Introduction

Radiopharmaceuticals are typically produced using "just-in-time" manufacturing methods where radioactive decay necessitates expedient and efficient synthesis and purification methods. For many targeted small molecule radiopharmaceuticals, unlike for more traditional perfusion-type agents, HPLC is necessary to separate the desired product from impurities and the large excess of unlabelled precursor that is often used in radiolabelling reactions. HPLC purification has a number of limitations particularly for routine production of radiopharmaceuticals in that it is time-consuming, requires extensive validation efforts for agents being translated to clinical use, and HPLC adds the risk of instrument failure during production runs.

To eliminate the need for HPLC, alternative labelling and purification methods employing solid-phase synthesis and solid-phase extraction (SPE) have been developed for a variety of medical isotopes. These include systems based on polymer-supported precursors[1–7] and fluorous-tagged molecules.[8-11] In solid-phase labelling, compounds are linked to insoluble supports via covalent bonds or ionic interactions in a way that the desired product is released upon labelling and isolated by simple filtration. For the fluorous labelling strategy (FLS)[8-12], fluorous-tagged precursors, which are prepared and purified using traditional synthetic methods,[13,14] are converted to non-fluorous analogues upon labelling. The fluorous precursor is separated from the desired radiolabelled compound by passing the reaction mixture through a fluorous SPE (FSPE) cartridge.[10,15-17]

The advantage of the solid-phase system is that labelling and purification is carried out in a single step. Unfortunately the inability to purify cross-linked polymer derivatives limits this method to the small number of loading reactions that proceed in quantitative yield. Groups developing solid-phase labelling systems have in certain instances also reported reduced radiochemical yields compared with solution phase methods, which is associated with the heterogeneous nature of the reaction mixture and non-specific binding of the product and isotope to the support. Solid-phase labelling can also require heating and/or use of organic solvents.[4]

One approach to addressing these limitations is to combine fluorous and solid-phase labelling methods. Fluorous precursors can be prepared, purified and fully characterized using traditional solution-phase methods and then the material loaded onto a solid support by physisorption (taking advantage of the fluorine-fluorine interactions) to create a hybrid fluorous-solid-phase system. The product would be released from the support upon labelling because it is rendered "non-fluorous". The advantage of loading the material onto the fluorous support, as opposed to labelling and then passing the mixture through a FSPE cartridge, is that the combined system could be used to create a single step "instant kit" which would minimize handling of the radioactive solutions and facilitate clinical translation. Such a system, including the preparation of the fluorous coated materials, was developed here for labelling and purifying a range of different molecules with ^{125}I.

2.3 Results and Discussion

Previous work on the FLS involved labelling fluorous tin derivatives in solution and then isolation of the products subsequently using a FSPE cartridge. Here the goal was to develop a different paradigm where labelling takes place directly on a hybrid fluorous-solid-phase material such that the product, free from residual starting materials and impurities, can be eluted directly and selectively.

The initial focus was to determine the range of loadings that can be achieved on fluorous silica (FS), which was carried out using a simple fluorous-tin benzoic acid (FBA) derivative **1a** (Figure 2-1), which can be prepared using a commercially available fluorous tin bromide[18] following a minor modification of a previously published method.[8] To prepare silica coated with tin precursor, varying quantities of **1a** as a 500 mg/mL solution in $CHCl_3$ were added to FS. The resulting chloroform-silica slurry was agitated periodically and the solvent allowed to evaporate to give loading ranges of 100-500 mg/g of coated FS in 50 mg/g increments. The hybrid fluorous-solid-phase labelling and purification cartridges were prepared by first loading normal (uncoated) FS (500 mg) that had been preconditioned with DMF, H_2O and 80:20 (v/v) MeOH/H_2O into a polypropylene SPE tube (3 mL) followed by a sample (50 mg) of coated FS. Each cartridge was capped with a polyethylene frit and washed with H_2O followed by 80:20 MeOH/H_2O where fractions (1 mL) were collected and analyzed by HPLC to determine if any **1a** leached from the support.

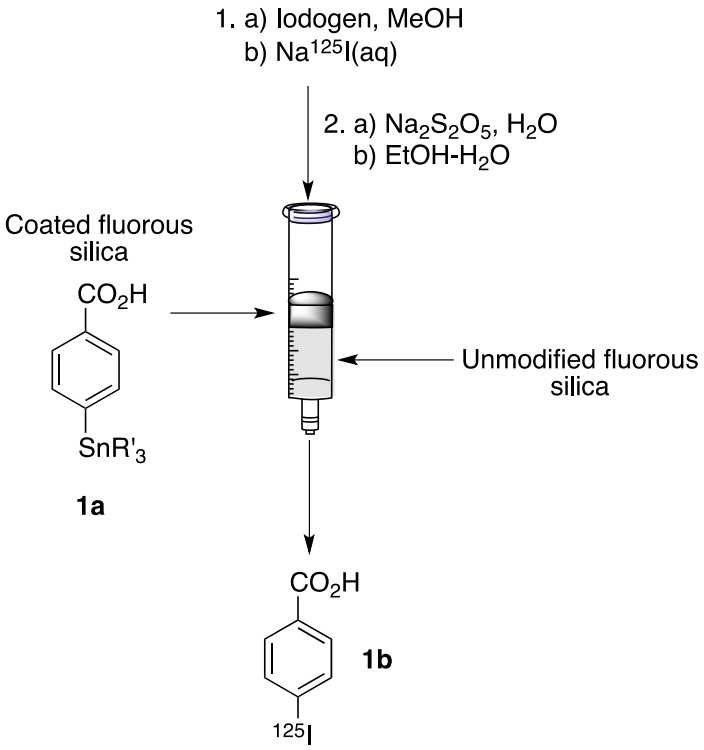

Figure 2-1. Schematic representation of the hybrid solid-fluorous phase radioiodination and purification system. R' = $(CH_2)_2(CF_2)_5CF_3$. Additional examples of compounds tested are shown in Scheme 2-2.

Based on HPLC analysis there was no elution of the tin precursor in the 100-300 mg/g samples of FS-**1a**.[19] However, the tin compound was detected in samples containing higher loadings (400-500 mg/g). Initial experiments were therefore performed with the 200 mg/g (FS(200)-**1a**) material. To identify the optimal elution conditions, a 50 mg sample of FS(200)-**1a** that also contained *para*-iodobenzoic acid (10 mg) was loaded onto a sample of preconditioned unmodified FS (500 mg). This combination of materials was washed with water followed by different alcohol-water mixtures. The aqueous fractions did not contain any *para*-iodobenzoic acid whereas the desired product was eluted

quantitatively using an 80:20 (v/v) MeOH/H_2O mixture. None of the fractions contained any detectable amount of **1a**.

One of the concerns raised over using arylstannanes is their potential toxicity, where the recommended parenteral limit for tin is 300 ppm.[20] To further demonstrate the FS is able to effectively retain the tin precursors, a fluorous-tin derivative of fluorescein was prepared and loaded onto FS. This provided a convenient tool to visualize the distribution of the fluorous precursor on the silica after loading and washing. Compound **3a** (Scheme 2-1) was prepared by coupling the fluorous-tin benzylamine **2a** to fluorescein 5(6)-isothiocyanate which was achieved in 71% yield. FS(300)-**3a** was prepared as previously described for **1a** where visually the precoated fluorous-tin dye was clearly retained on the top portion of the FS. There was little change after washing with water and 80:20 alcohol/H_2O (Figure 2-2) and the precursor remained bound to the FS and was not detected spectroscopically in any fraction where the detection limit for **3a** was 6 μg/mL (6 ppm) which is well below (50×) the USP recommended limit. Inductively coupled plasma mass spectrometry analysis was also performed on the product and showed that there was no tin present above the detection limit of the instrument (1 ppb).

Scheme 2-1. Synthesis of the fluorous-tin fluorescein derivative **3a**.

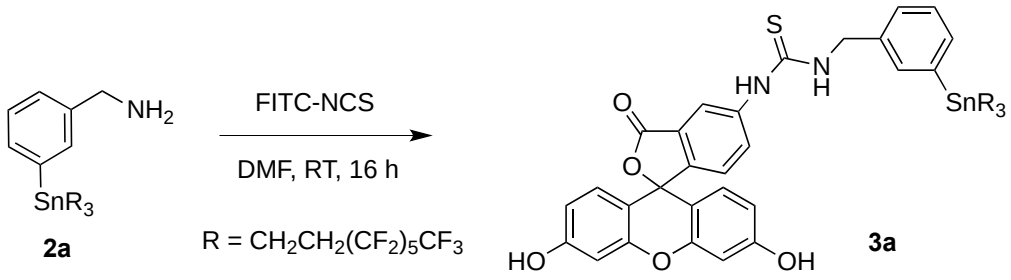

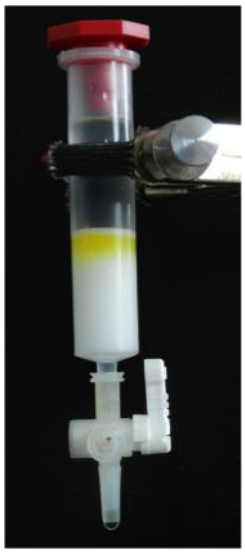

Figure 2-2. Fluorescein derivative **3a** (yellow color) loaded on unmodified fluorous silica gel. The picture shows the cartridge after loading and elution with water and 80:20 EtOH/H2O.

Radiochemical experiments were performed subsequently using $Na^{125}I$ and a range of fluorous compounds to test the general utility of the approach and to allow for comparison to previously reported solution phase work. For the initial tests a cartridge containing 50 mg of FS(200)-**1a** and preconditioned FS (500 mg) giving a ratio of loaded material to FS of 1:10 w/w was prepared. EtOH/H_2O (80:20, pH adjusted to 3-4 with AcOH) was added followed by iodogen and

$Na^{125}I$ (3.7-7.4 MBq). The reaction was allowed to proceed for 20 min. and then quenched with aqueous $Na_2S_2O_5$ followed by a water wash to remove any residual salts and unreacted $Na^{125}I$. The desired product was obtained by elution with 80:20 EtOH/H_2O (5 mL) which was used in place of MeOH/H_2O to ensure biocompatibility upon dilution of the product with isotonic saline or buffer.[21] HPLC analysis revealed no evidence of **1a** in the ultraviolet (UV)-trace and a single peak in the γ-trace. The identity of the peak was confirmed by comparing its retention time to that for an authentic sample of *para*-iodobenzoic acid (Figure 2-3). The product was obtained in 97% radiochemical purity and 49±3% (n=3) isolated radiochemical yield. There was some small amount of residual activity on the FSPE cartridge and the three-way-valve attached to the polypropylene SPE tube. The remainder of the activity was unreacted $Na^{125}I$, which was detected in the initial aqueous fractions.

Following the successful proof of concept experiment with FS(200)-**1a**, the general utility of the method was evaluated using other previously reported fluorous-precursors. The fluorous-tin compounds spanned simple aryl derivatives to known and emerging radiopharmaceuticals (Scheme 2-2). The FS-coated materials (200 mg/g) were prepared and labelled as previously described, and all reactions were performed in head-to-head comparisons with solution phase (two step) FLS reactions.

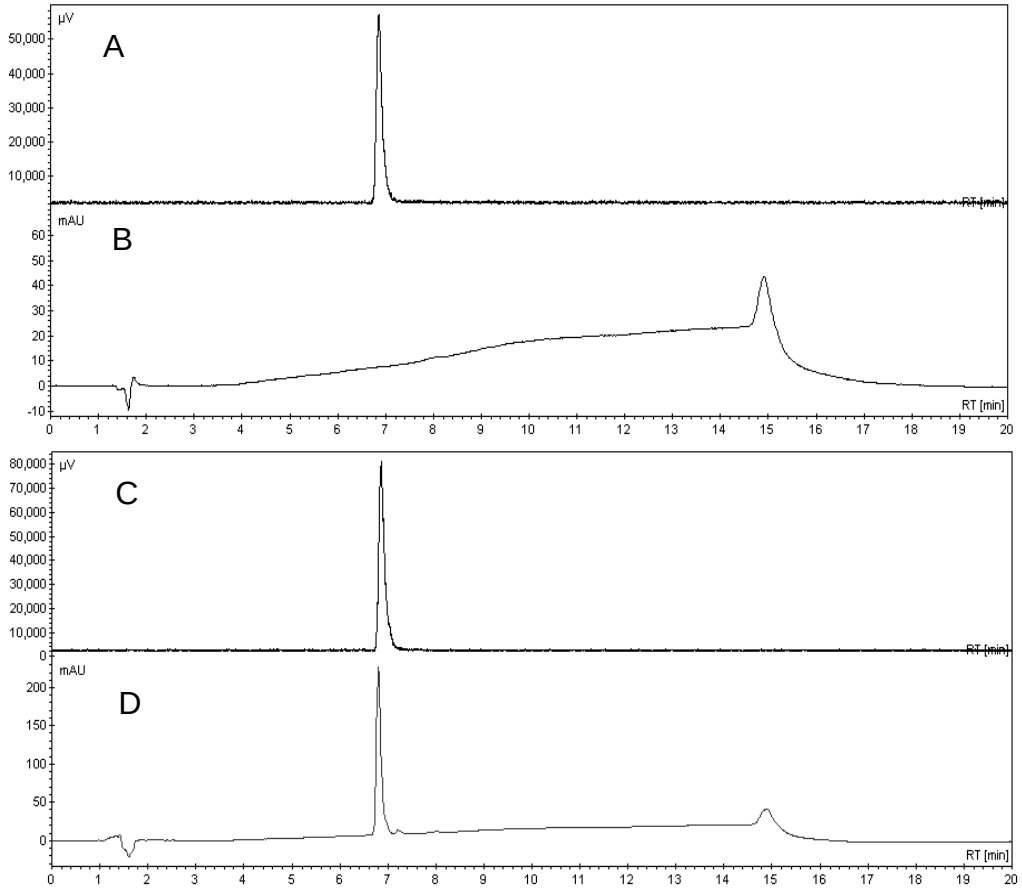

Figure 2-3. A) γ-HPLC chromatogram of **1b** B) UV-HPLC chromatogram of the same sample C) γ-HPLC chromatogram of **1b** co-injected with a cold reference standard D) UV-HPLC chromatogram of the same sample. The small difference in the retention times between the UV and the corresponding γ-trace is due to the time lag between the detectors which are connected in series (elution method A). The peak and change in the baseline between 14.5-15.5 min is a result of a rapid change in the gradient.

Scheme 2-2. Basic radioiodination reaction, fluorous precursors and radioiodinated products.

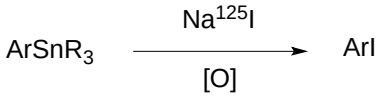

R = $CH_2CH_2(CF_2)_5CF_3$

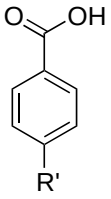

R' = SnR_3, **1a**
R' = ^{125}I, **1b**

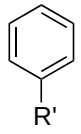

R' = SnR_3, **4a**
R' = ^{125}I, **4b**

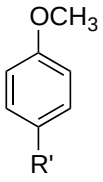

R' = SnR_3, **5a**
R' = ^{125}I, **5b**

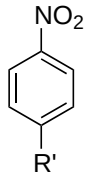

R' = SnR_3, **6a**
R' = ^{125}I, **6b**

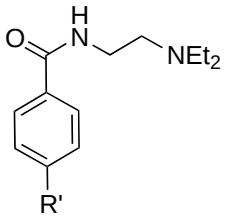

R' = SnR_3, **7a**
R' = ^{125}I, **7b**

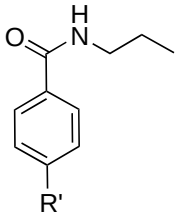

R' = SnR_3, **8a**
R' = ^{125}I, **8b**

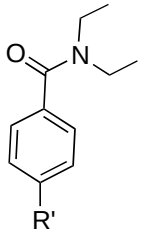

R' = SnR_3, **9a**
R' = ^{125}I, **9b**

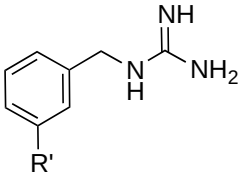

R' = SnR_3, **10a**
R' = ^{125}I, **10b**

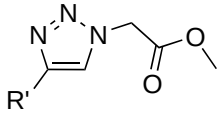

R' = SnR_3, **11a**
R' = ^{125}I, **11b**

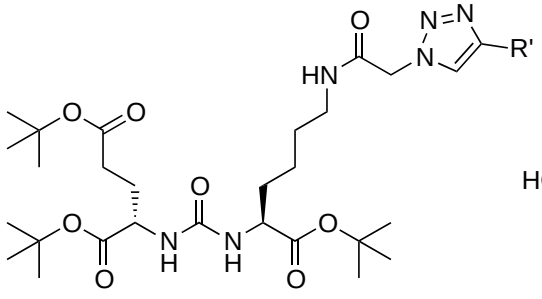

R' = SnR_3, **12a**
R' = ^{125}I, **12b**

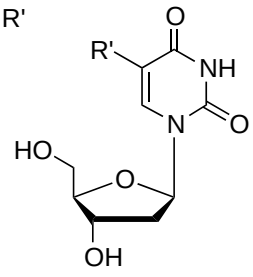

R' = SnR_3, **13a**
R' = ^{125}I, **13b**

In all cases radiochemical purities were greater than 95% while isolated radiochemical yields ranged from 30% to 49%, except for the nitrobenzene derivative where the isolated yield was less than 5% (Table 2-1). For the anisole derivative **5b** the yields were higher than for the phenyl (**4b**) and nitro (**6b**) derivatives, which is expected given the electrophilic nature of the starting material. The yields reported are lower than for the traditional FLS reactions but were comparable with yields reported for polymer supported aryltrifluoroborates.[4]

Table 2-1. Radiochemical yields for solution (fluorous) and hybrid fluorous solid-phase (coated) radioiodination reactions with different oxidants.

Precursor	Iodogen		Chloramine-T
	Solution	Coated	Coated
4a	83 ± 2	49 ± 3	75 ± 6
8a	80 ± 2	30 ± 4	47 ± 8
9a	81 ± 2	43 ± 6	—
10a	70 ± 3	36 ± 2	83 ± 6
11a	78 ± 5	42 ± 4	72 ± 12
12a	80 ± 3	40 ± 6	63 ± 10
13a	13 ± 5	≤ 5	—
14a	86 ± 3	45 ± 5	73 ± 3
15a	78 ± 5	45 ± 3	—
16a	81 ± 3	48 ± 6	67 ± 2
17a	—	—	57 ± 3

The coated FS system was also evaluated using a series of simple benzamides including an analogue of *N*-(2-(diethylamino)ethyl)-4-iodobenzamide (BZA); an agent that has been evaluated as a SPECT agent for imaging melanoma.[22] The fluorous precursors **7a-9a** were prepared via the tetrafluorophenol (TFP) active ester of **1a**.[8] The purified products were coated onto FS using the chloroform evaporation method to give FS(200)-**7a**, FS(200)-**8a**

and FS(200)-**9a**, which were loaded onto FS (1:10 w/w). Upon labelling, the yields for **7b**, **8b** and **9b** were 42 ± 4%, 43 ± 6%, and 36 ± 2% respectively, with radiochemical purities greater than 98% in all cases. The yields were again lower than the corresponding solution phase method, which were 78 ± 5%, 81 ± 2%, and 70 ± 3% respectively. Elution of **7b** was not successful with 80:20 EtOH/H_2O as the majority of the product was retained on the FSPE cartridge. Because of the basicity of the tertiary amine, a small amount of acid (0.1% TFA) was needed to elute the product.

The system was also effective in producing *meta*-iodobenzylguanidine (MIBG, **10b**); a radiopharmaceutical which is used for imaging and treating neuroendocrine tumors.[23] The yield obtained with the one-step radioiodination was 40 ± 6% which is a twofold and 1.5 fold reduction in yield compared with the solution phase FLS labelling and an existing polymer supported MIBG labelling method, respectively.[2] However, the radiochemical purity of the product was greater than 98% and loading the material onto FS was simple and optimized in a couple of hours whereas developing a method to produce polymer supported MIBG quantitatively was non-trivial.[2]

One of the potential limitations of the fluorous system is in using FSPE to purify polar molecules which could co-elute with unreacted iodide. To test this, a new and polar heterocyclic iodine prosthetic group known as the triazole-appending agent (TAAG)[24] was investigated as a substrate. The fluorous TAAG precursor **11a** could be effectively loaded onto FS to give FS(200)-**11a** which

when loaded onto FS (1:10 w/w) showed no evidence of breakthrough when using 80:20 EtOH/H_2O. Upon radioiodination however, some of the desired product, **11b**, eluted in the 100% aqueous wash along with free [^{125}I]NaI. To address this, a C-18 SPE cartridge was connected in series to the FSPE cartridge so that after elution with water the radioiodinated product was retained and subsequently selective eluted in 45 ± 3% radiochemical yield using 80:20 EtOH/H_2O.

The utility of the hybrid labelling system was tested further using a novel TAAG derivative that can bind to prostate specific membrane antigen;[24] a protein that is over expressed on prostate cancers and associated metastases.[25,26] Compound **12a** was loaded onto F-silica to give FS(200)-**12a** (1:10 w/w) and labelled with Na^{125}I. The desired product **12b** was eluted with 80:20 EtOH/H_2O in 48 ± 6% radiochemical yield (n=3) with a radiochemical purity that was greater than 98%, which is comparable with that for the solution phase method. To test whether or not the cartridges can be used multiple times, following the elution of the product, the labelling of FS(200)-**12a** was repeated using the same cartridge which was washed with water followed by 80:20 EtOH/H_2O. The yield for the subsequent labelling was 30 ± 6% and the product isolated in 90% radiochemical purity. A third labelling was performed where the yield and radiochemical purity decreased to 12 ± 7 and 75% respectively indicating that the cartridges are best suited for single use applications.

Not all molecules can be iodinated effectively with iodogen consequently the general utility of the system with other oxidants was also explored.

Preliminary experiments using peracetic acid were found to give inconsistent radiochemical yields. Chloramine-T in contrast showed that comparable or superior yields compared with iodogen could be obtained using less precursor. Isolated yields of 65 ± 5%, 71 ± 3% and 70 ± 2% (n=3) were obtained using 30 mg of FS(30)-**1a**, FS(50)-**1a**, and FS(100)-**1a**. With chloramine-T it was advantageous to connect the FSPE cartridge to a C18 SPE cartridge and to acidify the 80:20 EtOH/H_2O eluent with dilute phosphoric acid. This eliminated the need to collect fractions and resulted in selective separation of the desired product from free iodide. For example, using this system isolated radiochemical yields of 75 ± 6% (n=5) and radiochemical purity greater than 95% were obtained for **1b**. To demonstrate the elution conditions did not cause protodestannylation, compound **5a** was incubated in the acidified 80:20 EtOH/H_2O solution and samples analyzed by HPLC at 5 and 40 min, where there was no evidence of anisole at either time point. The system remains biocompatible as the eluted product when added to PBS was isotonic and within a pH and radioactivity concentration range suitable for injection.

As a result of the increased yield with chloramine-T at reduced ligand loading levels several of the fluorous derivatives previously labelled using iodogen were radioiodinated using chloramine-T. Yields ranged from 47% to 83% (Table 2-1) where the radiochemical purity was greater than 95% for all products. In terms of specific activity, the limit of detection for **1b** was determined and the value was greater than 240 Ci/mmol (average of three experiments). As an

additional test of the labelling method, 5-iodo-2'-deoxyuridine (IUdR)-**13b** an agent currently undergoing investigation as therapeutic radiopharmaceutical[27] was also produced using the chloramine-T approach where the isolated yield was 57% ± 3%. In general the isolated yields obtained using chloramine-T are comparable or higher than those previously reported for other solid-phase radioiodination methods.[2,4, 28-30] It should also be noted that the coated material was evaluated over 2 months after storage at 4 °C where there was no significant change in radiochemical yield or purity.

2.4 Conclusion

The reported hybrid fluorous-solid phase labelling material is a convenient platform for producing radioiodinated compounds in high purity and effective specific activity (i.e. free from any residual precursor) without the need to use HPLC. An advantage of the hybrid system over covalent polymer modification is that the precursor compounds can be prepared and fully characterized prior to immobilization which is convenient and can be carried out using a wide range of compounds. Reactions were performed at room temperature using either iodogen or chloramine-T and reached completion within 20 minutes and the system did not require the use of organic solvents (other than ethanol). All products can be isolated in biocompatible solvents ready for injection by simple dilution with isotonic saline or PBS.

2.5 Experimental

2.5.1 Reagents and general procedures

Unless otherwise stated, all chemicals reagents were purchased and used as received from Sigma-Aldrich without further purification. Toluene, dichloromethane and tetrahydrofuran (THF) were distilled using a PURE SOLV distillation system. FC-72 was purchased from 3M, $(CF_3(CF_2)_5(CH_2)_2)_3SnPh$ and $(CF_3(CF_2)_5(CH_2)_2)_3SnH$ were purchased from Fluorous Technologies Inc. SiliaFlash® P60 Silica gel from SiliCycle was used for silica gel chromatography. Analytical thin-layer chromatograms (Merck F254 silicagel on aluminum plates) were visualized using ultraviolet (UV) light. Compounds **1a**, **2a**, and **4a-12a** were prepared according to literature methods.[8,9,12,24] 1,3,5,7-Tetramethyl-2,4,8-trioxa-(2,4-dimethoxyphenyl)-6-phosphaadamantane ligand for cross coupling reactions was generously provided by Prof. Alfredo Capretta (McMaster University, Hamilton, Ontario).[31] KF/silica stationary phase contained 10% w/w of KF and 90% w/w SiliaFlash® P60 silica gel (finely ground together) loaded in a disposable glass pipette plugged with glass wool. Empty fritted polypropylene solid-phase-extraction (SPE) tubes were purchased from Sigma-Aldrich. SepPak® Plus C18 cartridges were purchased from Waters Corporation. Sodium [^{125}I]iodide with a specific activity of ~17 Ci/mg was provided by the McMaster Nuclear Reactor (Hamilton, ON, Canada).

Caution: ^{125}I is radioactive and should only be handled in an appropriately equipped and licensed facility.

2.5.2 Instrumentation

Nuclear magnetic resonance (NMR) spectra were recorded using a Bruker DRX-500 and 600 spectrometers with chemical shifts reported in parts per million relative to the residual proton signal of the deuterated solvent (^{1}H NMR) or the carbon signal of the solvent (^{13}C NMR). Reactions requiring microwave heating were performed using a Biotage Initiator 60 instrument. Infrared (IR) spectra were acquired using a BioRad FTS-40 FT-IR spectrometer. ESI mass spectrometry experiments were performed on a Waters/Micromass Quattro Ultima instrument where samples were first dissolved in methanol. High resolution mass spectral data were obtained using a Waters-Micromass Q-TOF (quadrupole/time-of-flight) Ultima Global spectrometer. High pressure liquid chromatography (HPLC) was performed using a Varian ProStar Model 230 instrument, fitted with a Varian ProStar model 330 PDA detector, an IN/US γ-RAM gamma detector, a Star 800 analog interface module and a Phenomenex Gemini-C18 column (4.6×100 mm, 110 Å, 5 μm). The wavelength for UV detection was set at 254 nm, and the dwell time in the gamma detector was 5 sec in a 10 μl loop. The mobile phase was composed of solvent A = H_2O (0.1% TFA), and solvent B = CH_3CN (0.1% TFA). Method A: 0-10 min, 40-100% B; 10-14 min, 100% B; 14-15 min, 100-40% B; 15-20 min, 40% B. Method B: 0-10 min, 2-100% B; 10-14 min, 100% B; 14-15 min 100-2% B; 15-18 min 2% B. Method C: 0-1 min, 40 % B; 1-7 min, 40-100 % B, 7-12 min, 100 % B; 12-13 min, 100-40 % B, 13-18 min 40 % B. Method D: 0-1 min, 20 % B; 1-7 min, 20-100 % B, 7-12 min, 100 % B; 12-13 min, 100-20 %

B, 13-18 min 20 % B. Method E: 0-5 min, 5 % B; 5-12 min, 5-100 % B; 12-13 min 100-5 % B, 13-18 min 5 % B. For the anisole stability test, HPLC was performed using a Waters 1525 Binary HPLC system fitted with a 2998 photodiode array detector and a Bioscan γ detector. A Phenomenex Gemini column (5 μm, 4.6 Å 250 mm, C18) at a flow rate of 1.0 mL/min and monitoring at 215 and 254 nm was employed. The mobile phase was composed of: solvent A = H_2O (0.1% TFA), and solvent B = CH_3CN (0.1% TFA). Method F: 0−15 min, 20-100% B; 15-25 min, 100% B. For calibration curves, each calibration solution was evaluated in triplicate and the data analyzed by the least-squares method. The limit of quantitation and the limit of detection were calculated using the standard deviation method.

2.5.3 Synthesis of Compounds

1-(3',6'-Dihydroxy-3-oxo-3*H*-spiro[isobenzofuran-1,9'-xanthen]-6-yl)-3-(3-(tris(2-perfluorohexylethyl)stannyl)benzyl)thiourea (3a)

To a solution of compound **2a** (50 mg, 0.039 mmol) in DMF (5 mL) was added fluorescein 5(6)-isothiocyanate (41 mg, 0.11 mmol), and the reaction mixture stirred at room temperature overnight. The solution was subsequently concentrated to dryness, FC-72® was added (10 mL) and the solution extracted with DCM (3 × mL). FC-72® was removed by rotary evaporation and the desired product isolated using column chromatography eluting with methanol/DCM (1:9, v/v) yielding **3a** as an orange solid. Yield (46 mg, 71%). ^{1}H NMR (600 MHz, MeOD-d_4) δ 8.13 (s, 1H), 7.78-7.76 (m, 1H), 7.59 (s, 1H), 7.42-7.39 (s, 3H), 7.14-

7.12 (m, 1H), 6.68-6.66 (m, 4H), 6.53-6.52 (m, 2H), 4.88 (s, 2H), 2.47-2.38 (m, 6H), 1.42-1.29 (m, 6H); HRMS (ESI^+) *m*/*z* calcd for $C_{52}H_{32}F_{39}N_2O_5SnS$ $[M+H]^+$ 1657.0431, found: 1657.0454; FTIR (KBr, cm^{-1}): 2922, 1699, 1592, 1206; HPLC (method B) t_R = 12.8 min.

1-(4-Hydroxy-5-(hydroxymethyl)tetrahydrofuran-2-yl)-5-(tris(2-perfluorohexyl-ethyl)stannyl)pyrimidine-2,4(1*H*,3*H*)-dione (13a)

A solution of diacetoxypalladium (4 mg, 0.02 mmol) in THF (0.5 mL) was added to 1,3,5,7-tetramethyl-2,4,8-trioxa-(2,4-dimethoxyphenyl)-6-phosphaadamantane (8 mg, 0.03 mmol) in THF (0.5 mL).[12] The resulting solution was stirred for 10 min. and tris-(2-perfluorohexylethyl)stannane (650 mg, 0.56mmol) in THF (0.5 mL) was added. After 10 min., 1-(4-hydroxy-5-(hydroxymethyl)tetrahydrofuran-2-yl)-5-iodopyrimidine-2,4(1*H*,3*H*)-dione (92 mg, 0.26 mmol) in THF (0.5 mL) was added and the resulting mixture was heated in a Biotage microwave reactor at 160 $^{\circ}$C for 15 min. The reaction mixture was filtered through KF/silica and the solvent removed by rotary evaporation. The desired product was isolated using column chromatography eluting with methanol/DCM (1:9, v/v) yielding **13a** as a colourless oil. Yield (126 mg, 35%). ^{1}H NMR (600 MHz, MeOD-d_4) δ 7.92 (s, 1H), 6.31 (m, 1H), 4.41 (m, 1H), 3.95 (m, 1H), 3.78-3.72 (m, 2H), 2.47-2.41 (m, 6H), 2.32-2.21 (m, 2H), 1.35-1.23 (m, 6H); ^{13}C NMR (150 MHz, MeOD-d_4) δ 169.3, 152.7, 147.7, 110.8, 89.4, 87.0, 72.6, 62.9, 41.7, 28.7, 0.0; HRMS (ESI^+) *m*/*z* calcd for $C_{33}H_{23}F_{39}N_2O_5Sn$ $[M+H]^-$ 1389.0061, found: 1389.0084; FTIR (KBr, cm^{-1}): 3410, 3043, 2944, 1691, 1238, 1144.

2.5.4 General procedure for preparing coated fluorous silica

Fluorous silica was added to the required concentration of the fluorous precursor in chloroform and the mixture agitated by hand until a slurry was formed. After sitting at room temperature overnight, the resulting powder was added to a polypropylene SPE tube that contained 500 mg of unmodified FS previously washed with DMF (1 mL), H_2O (5 mL) and 80:20 EtOH/H_2O (5 mL).

2.5.5 General procedure for solid-phase radioiodination with iodogen

80% (v/v) EtOH/H_2O (100 μL) (pH adjusted between 3 and 4 with conc. AcOH) was added to the SPE cartridge containing the coated FS. Iodogen (5 μL, 0.4 mg/mL in MeOH) was added followed by $Na^{125}I$ (10 μL, 3.7-7.4 MBq) in 0.1 M NaOH. After 20 min. the reaction was quenched with 0.1 M $Na_2S_2O_{5(aq)}$ (50 μL) and the cartridge was washed with water (5 mL) followed by 80% EtOH/H_2O (5 mL), where (0.5 mL) fractions were collected. HPLC retention times for all products were compared with that for authentic non-radioactive standards.

2.5.6 General procedure for solution phase (FLS) labelling with iodogen

Iodogen (5 μL, 0.4 g/mL in MeOH) followed by $Na^{125}I$ (10 μL, 3.7-7.4 MBq in 0.1 M NaOH) was added to the fluorous-tin precursor (100 μL, 5 mg/mL in 5% AcOH/MeOH). After 5 min. $Na_2S_2O_{5(aq)}$ (50 μL, 0.1 M) was added, and the mixture diluted to 1 mL with water. The solution was then transferred to a 2 g preconditioned FSPE cartridge. This was washed with water (3 mL) followed by 80:20 EtOH/H_2O (8 mL), and 1 mL fractions were collected.

2.5.7 General procedure for solid-phase radioiodination with chloramine-T

An SPE cartridge containing the coated fluorous silica was connected to a SepPak® plus C18 cartridge. Ten percent acetic acid in EtOH (50 µL) was added, followed by chloramine-T (50 µL, 4 mg/mL in water) and $Na^{125}I$ (10 µL, 1.85 GBq/mL in 0.1 M NaOH). After 20 min. $Na_2S_2O_{5(aq)}$ (50 µL, 0.2 M) was added, and the system washed with water (5 mL) followed by 1.5:200:50 (v/v/v) H_3PO_4/EtOH/H_2O (5 mL) to elute the desired product. HPLC retention times were compared to those of non-radioactive authentic standards.

2.5.8 Stability Study

Compound **5a** (20 µL of a 6.9 mg/mL solution in MeOH) was added to 1.5:200:50 (v/v/v) H_3PO_4/EtOH/H_2O (160 µL). Samples were taken at 5 and 40 min. and analyzed by reverse-phase HPLC (method C).

2.6 Supporting information

HPLC chromatograms for labelled compounds, ^{1}H and ^{13}C NMR spectra, FTIR spectra and HRMS of all fluorous precursor compounds. This material is available online at http://onlinelibrary.wiley.com/doi/10.1002/jlcr.3214/suppinfo.

2.7 Acknowledgements

This work was supported by the Natural Sciences and Engineering Research Council (NSERC) of Canada and the Ontario Institute for Cancer Research (OICR) through funding provided by the Government of Ontario.

2.7.1 Conflict of Interest

The authors did not report any conflict of interest.

2.8 References

(1) P. A. Culbert, D. H. Hunter, *React. Polym.* **1993**, *19*, 247–253.

(2) D. H. Hunter, X. Zhu, *J. Labelled Compd. Rad.* **1999**, *42*, 653–661.

(3) R. Dunn-Dufault, A. Pollak, J. Fitzgerald, J. R. Thornback, J. R. Ballinger, *Nucl. Med. Biol.* **200**, *27*, 803–807.

(4) L. Yong, M. -L. Yao, J. F. Green, H. Kelly, G. W. Kabalka, *Chem. Commun.* **2010**, *46*, 2623–2625.

(5) A. N. Gifford, S. Kuschel, C. Shea, J. S. Fowler, *Bioconjugate Chem.* **2011**, *22*, 406–412.

(6) S. Mundwiler, L. Candreia, P. Hafliger, K. Ortner, R. Alberto, *Bioconjugate Chem*. **2004**, *15*, 195−202.

(7) R. W. Riddoch, P. Schaffer, J. F. Valliant, *Bioconjugate Chem.* **2006**, *17*, 226–235.

(8) A. Donovan, F. Forbes, P. Dorff, P. Schaffer, J. Babich, J. F. Valliant, *J. Am. Chem. Soc.* **2006**, *128*, 3536–3537.

(9) A. C. Donovan, J. F. Valliant, *Nucl. Med. Biol.* **2008**, *35*, 741–746.

(10) R. Bejot, T. Fowler, L. Carroll, S. Boldon, J. E. Moore, J. Declerck, V. Gouverneur, *Angew. Chem. Int. Ed.* **2009**, *48*, 586 –589.

(11) A. S. Zhang, C. S. Elmore, M. A. Egan, D. G. Melillo, D. C. Dean, *J. Labelled Compd. Rad.* **2005**, *48*, 203–208.

(12) J. W. McIntee, C. Sundararajan, A. C. Donovan, M. S. Kovacs, A. Capretta, J. F. Valliant, *J. Org. Chem.* **2008**, *73*, 8236–8243.

(13) W. Zhang, *Tetrahedron* **2003**, *59*, 4475–4489.

(14) W. Zhang, *Chem. Rev.* **2004**, *104*, 2531–2556.

(15) D. P. Curran, *Handbook of Fluorous Chemistry*. Wiley-VCH, Weinheim, **2004**, pp. 101–127.

(16) D. P. Curran, S. Hadida, M. He, *J. Org. Chem.* **1997**, *62*, 6714-6715.

(17) J. -M. Vincent, *Top. Curr. Chem.* **2012**, *308*, 153–174.

(18) M. Hoshino, P. Degenkolb, D. P. Curran, *J. Org. Chem.* **1997**, *62*, 8341–8349.

(19) C. C. Chan, H. Lam, Y. C. Lee, X. -M. Zhang, *Analytical Method Validation and Instrument Performance Verification*, 1st ed.; John Wiley & Sons, Inc., Hoboken, New Jersey, **2004**, pp 37–40.

(20) General chapter on inorganic impurities, United States pharmacopeia, USP ad hoc advisory panel on inorganic impurities. http://www.usp.org/sites/default/files/usp_pdf/EN/USPNF/2008-04-10InorganicImpuritiesStim.pdf. [24 May 2013].

(21) A. Vale, *Medicine* **2007**, *35*, 633–634.

(22) J. M. Michelot, M. F. C. Moreau, A. J. Veyre, F. J. Bonafous, F. J. Bacin, J. C. Madelmont, F. Bussiere, P. A. Souteyrand, L. P. Mauclaire, F. M. Chossat, J. M. Papon, P. G. Labarre, P. Kauffmann, R. J. Plagne, *J. Nucl. Med.* **1993**, *34*, 1260–1266.

(23) G. Prabhakar, A. Mathur, G. Shunmugam, Y. D. Teje, S. S. Sachdev, N. Sivaprasad, *Appl. Radiat. Isot.* **2011**, *69*, 63–67.

(24) A. Darwish, M. Blacker, N. Janzen, S. M. Rathmann, S. Czorny, S. M. Hillier, J. L. Joyal, J. W. Babich, J. F. Valliant, *Med. Chem. Lett.* **2012**, *3*, 313–316.

(25) K. P. Maresca, S. M. Hillier, F. J. Femia, D. Keith, C. Barone, J. L. Joyal, C. N. Zimmerman, A. P. Kozikowski, J. A. Barrett, W. C. Eckelman, J. W. Babich, *J. Med. Chem.* **2009**, *52*, 347–357.

(26) B. Youngjoo, M. Pullambhatla, H. Wang, R. C. Mease, M. G. Pomper, *Macromol. Res.* **2013**, *21*, 565-573.

(27) S. Lehnert, Y. Li, E. Bump, B. Riddoch, A. Chenite, M. Shive, M. *Open Nucl. Med. J.* **2011**, *3*, 19–24.

(28) T. J. Mangner, J. L. Wu, D. M. Wieland, *J. Org. Chem.* **1982**, *47*, 1484–1488.

(29) G. W. Kabalka, V. Namboodiri, M. R. Akula, *J. Labelled Compd. Rad.* **2001**, *44*, 921–929.

(30) L. Yong, M. -L. Yao, H. Kelly, F. F. Green, G. W. Kabalka, *J. Labeled Compd. Rad.* **2011**, *54*, 173–174.

(31) T. Brenstrum, D. A. Gerristma, G. M. Adjabeng, C. S. Frampton, J. Britten, A. J. Robertson, J. McNulty, A. Capretta, *J. Org. Chem.* **2004**, *69*, 7635-7639.

Chapter 3 - A Fluorous Analogue of Chloramine-T: Preparation, X-Ray Structure Determination and Use as an Oxidant for Radioiodination and s-Tetrazine Synthesis

The following chapter has been accepted as a full article for publication in The Journal of Organic Chemistry (DOI: 10.1021/acs.joc.5b00988) under the authorship: James P. K. Dzandzi, Denis R. Beckford Vera, Afaf R. Genady, Silvia A. Albu, Louise J. Eltringham-Smith, Alfredo Capretta, William P. Sheffield, and John F. Valliant.

I was responsible for the preparation and characterization (including crystal growth) of the fluorous oxidant, fluorous precursor compounds, development of the platform and completing radioiodination reactions on small molecules and proteins. I contributed to drafting the manuscript including the entire experimental section. Dr. Beckford Vera was responsible and acknowledged for help with optimization of the radiolabelling experiments and contribution to manuscript. Dr. Genady prepared the bifunctional hydrotetrazine while the tetrazine work was initiated through collaboration with Drs. Albu and Capretta. Louise Eltringham-Smith performed the protein assays. Prof. William Sheffield designed the protein assay experiments and provided editorial input. Prof. John Valliant was responsible for the overall structure of the manuscript and project, along with key scientific input and editorial reviews.

A Fluorous Analogue of Chloramine-T: Preparation, X-Ray Structure Determination and Use as an Oxidant for Radioiodination and s-Tetrazine Synthesis

3.1 Abstract

A fluorous oxidant that can be used to introduce radioiodine into small molecules and proteins and generate iodinated tetrazines for bioorthogonal chemistry was developed. The oxidant was prepared in 87% overall yield by combining a fluorous amine with tosyl chloride, followed by chlorination using aqueous sodium hypochlorite. A crystal structure of the oxidant, a fluorous analogue of chloramine-T, was obtained, and the compound was shown to be stable for 7 days in EtOH and greater than three months as a solid. The oxidant was effective at promoting the labeling of arylstannanes using [^{125}I]NaI, where products were isolated in high specific activity in yields ranging from 46% to 86%. Similarly, iodinated biologically active proteins (e.g. thrombin) were successfully produced, as well as a radioiodinated tetrazine, through a concomitant oxidation-halodemetallation reaction. Because of its fluorous nature, unreacted oxidant and associated reaction byproducts can be removed quantitatively from reaction mixtures, by passing solutions through fluorous solid phase extraction cartridges. This feature enables rapid and facile purification, which is critical when working with radionuclides and similarly beneficial for general synthetic applications.

3.2 Introduction

Iodine is one of the only elements that has commercially available isotopes that can be used for single photon emission computed tomography (SPECT, ^{123}I)[1,2] and positron emission tomography (PET, ^{124}I) imaging,[3] targeted radionuclide therapy (^{131}I)[4,5] and pharmacokinetic, pharmacodynamic[6] and *in vitro* assay experiments (^{125}I). For drug development, particularly for biologics, radiotracer techniques based on isotopes like ^{125}I have a number of advantages over newer mass spectrometry and fluorescence-based methods particularly with respect to avoiding matrix effects and the need for extensive method development.[7]

Synthetic strategies used to introduce radioactive isotopes of iodine must be rapid, high yielding and require minimal purification and handling. For small molecules the predominant synthetic method involves oxidative demetallation, whereas for proteins, oxidative labelling of tyrosine residues or the use of prosthetic groups such as the Bolton-Hunter reagent[8,9] or *N*-succinimidyl-3-iodobenzoate (SIB)[10,11] for labelling lysine residues are the principal methods of choice. Although generally effective, these procedures typically require HPLC or a comparable bio-purification technique to remove unreacted starting materials, including excess oxidant and impurities, which increase contamination and exposure risks and reduces overall yields.

To address these issues, new synthetic methods for rapid introduction of iodine and *in situ* purification have been reported recently. These include

polymer-supported[12–16] and fluorous labelling[17–20] methods that allow for expedited "HPLC-free" preparation of iodine-based radiopharmaceuticals. Although a great deal of emphasis has been placed on creating new labelling constructs, the nature of the oxidants used for iodination reactions has remained unchanged for some time.[21] Peroxide and peracids are regarded as the ideal choice since they ultimately form benign reaction side products. However, they often give inconsistent yields and can degrade proteins.[22] Iodogen, chloramine-T (CAT) and iodobeads have been shown to be effective reagents for labelling proteins[9] and small molecules,[23] but difficulties associated with the removal of excess oxidant, formation of unwanted byproducts or slow reaction rates due to the heterogeneous nature of certain reactions reduces their effectiveness and can obviate any advantages gained using polymer, fluorous or other newer labelling methods.[12,24]

We sought to develop a new oxidant capable of introducing iodine into both small molecules and proteins that can be conveniently removed from reaction mixtures without the need to use HPLC. This lead to the preparation and characterization of a new high fluorine content (fluorous) oxidant that can be selectively separated from labelled materials by passing the reaction solution through a fluorous solid-phase extraction cartridge. While fluorous chemistry has not become a routine method for general synthetic chemistry and drug development, it is well-suited for radiochemistry, given the small scale of reactions that typically take place at micromolar to nanomolar concentrations, and

the need for rapid and facile purification methods. Not only can the fluorous oxidant reported here be used to label arylstannanes and proteins, it was also shown to be very effective for producing functionalized tetrazines, which are emerging as highly effective synthons for bioorthogonal labelling reactions.[25–28]

3.3 Results and Discussion

3.3.1 Preparation and characterization

A review of the literature revealed a limited number of fluorous oxidants have been reported and that these are not suitable for iodination reactions which must be rapid, selective and high yielding.[29–35] We therefore opted to prepare a fluorous analogue of chloramine-T (F-CAT), since the oxidant has been used effectively with a wide range of substrates. The first step involved treating *p*-toluenesulfonyl chloride with an excess of a commercially available fluorous amine **2** in ethanol (Scheme 3-1).[36] After 30 min the desired product was isolated by silica gel chromatography in 89% yield. The NMR and HRMS data were consistent with the formation of the sulfonamide **3**, which was obtained as a crystalline solid. *N*-chlorination was achieved by the treatment of a chloroform solution of **3** with aqueous sodium hypochlorite (6%, w/v). The *N*-chloro fluorous-sulfonamide **4** was isolated by simple extraction and the desired product obtained in quantitative yield. ^{1}H NMR revealed that the signal corresponding to the NH group in **3** (4.51 ppm) was absent following chlorination and the IR spectrum lacked the NH stretch (3263 cm^{-1}) observed in the sulfonamide **3,** as reported previously for similar *N*-alkyl sulfonamides.[37,38] In the ^{13}C NMR

spectrum, the signal corresponding to the methylene carbon adjacent to the N-Cl group shifted downfield compared to that in **3**, which is consistent with NMR data for chlorination of non-fluorous sulfonamides.[39,40]

Scheme 3-1. Synthesis of *N*-chloro-*N*-(4,4,5,5,6,6,7,7,8,8,9,9,10,10,11,11,11-heptadecafluoroundecyl)-4-methylbenzenesulfonamide (F-CAT) **4**.

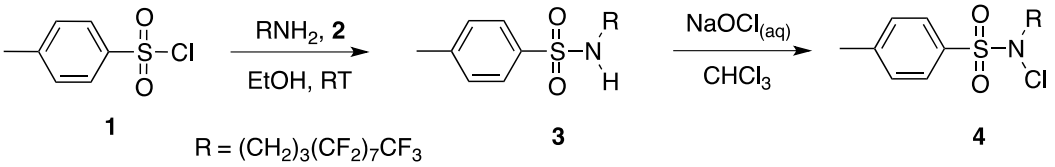

Single crystals of compounds **3** and **4** were obtained by slow evaporation of saturated chloroform solutions, and the associated X-ray structures determined (Figure 3-1). The data for **3** can be found in the supporting information, and key bond lengths and angles for **4** are presented in Tables 3-1 and 3-2 in comparison to the corresponding data reported for CAT.[41] The previous published crystal structure of CAT revealed a salt which formed an aquo-bridged dimer[41] whereas **4** is neutral and monomeric with S-O bond distances being similar (1.424(3) and 1.428(3) Å). The S-N bond length (1.677(3) Å) was longer than in CAT (1.590(2) Å), whereas the N-Cl bond distance in **4** (1.733(3) Å) was shorter. The differences are in part due to the ionic nature of CAT, which is also evident in the melting points (167-170 °C versus 77-79 °C) for the two compounds.

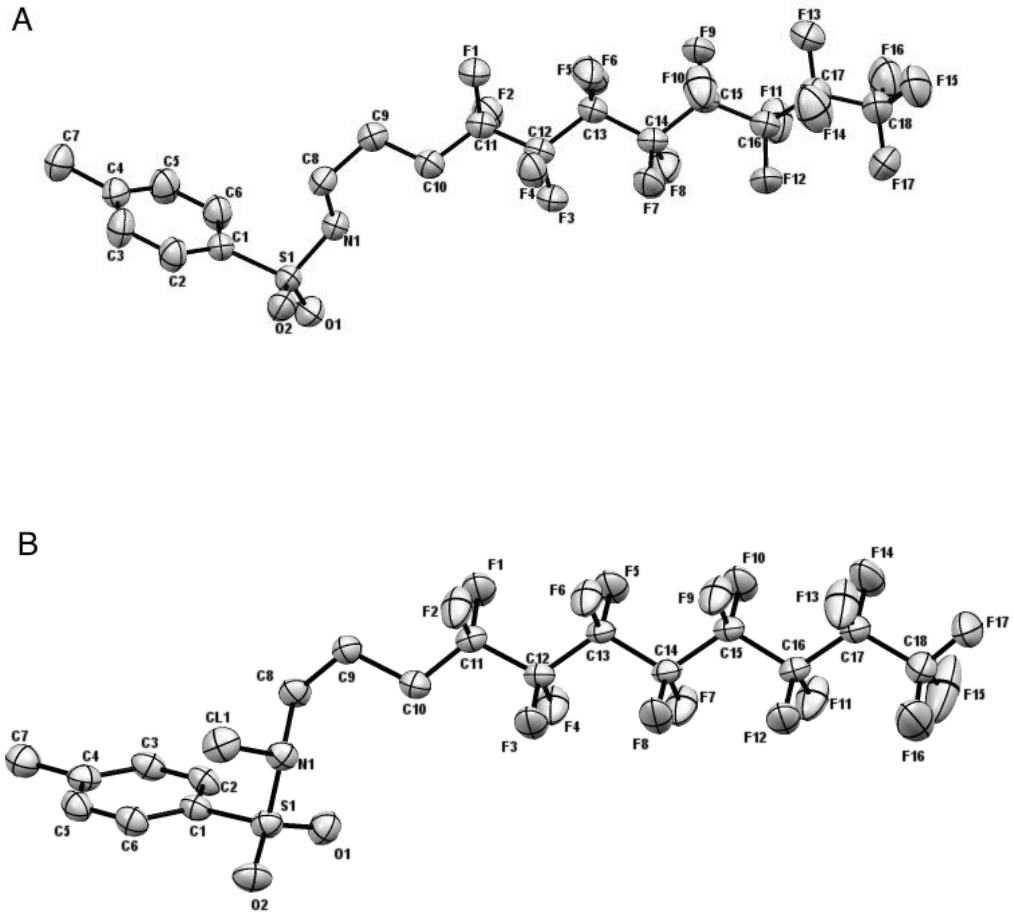

Figure 3-1. ORTEP drawings of the crystallographically determined structures of (A) **3** and (B) **4**. Thermal probability ellipsoids are shown at the 50% probability level. Hydrogen atoms are omitted for clarity.

Table 3-1. Comparison of select bond lengths (Å) for CAT[41] and **4** (F-CAT).

CAT		**F-CAT (4)**	
Bond	Length (Å)	Bond	Length (Å)
S-O(1)	1.455(2)	S-O(1)	1.428(3)
S-O(2)	1.439(2)	S-O(2)	1.424(3)
S-N	1.590(2)	S-N	1.677(3)
N-Cl	1.750(2)	N-Cl	1.733(3)

Table 3-2. Comparison of select bond angles (deg) for CAT[41] and **4** (F-CAT)

CAT		**F-CAT (4)**	
Bond	Angles (deg)	Bond	Angles (deg)
S-N-Cl	110.9(1)	S-N-Cl	111.9 (3)
O(2)-S-O(1)	116.1(1)	O(2)-S-O(1)	120.23 (18)
O(2)-S-N	103.6(1)	O(2)-S-N	106.48 (17)
O(2)-S-C(1)	103.3(1)	O(2)-S-C(1)	109.36 (18)
O(1)-S-C(1)	105.8(1)	O(1)-S-C(1)	108.50 (18)
N-S-C(1)	109.6(1)	N-S-C(1)	107.94 (17)

With respect to stability, HPLC analysis of an ethanol solution of **4** after 24 hours (Figure 3-2A) showed no significant decomposition. After 7 days in solution, a new peak at 8.4 min (Figure 3-2B) did appear which corresponded to approximately 10% of **3**. Notwithstanding, F-CAT is stable for more than three months when stored as a solid at room temperature.

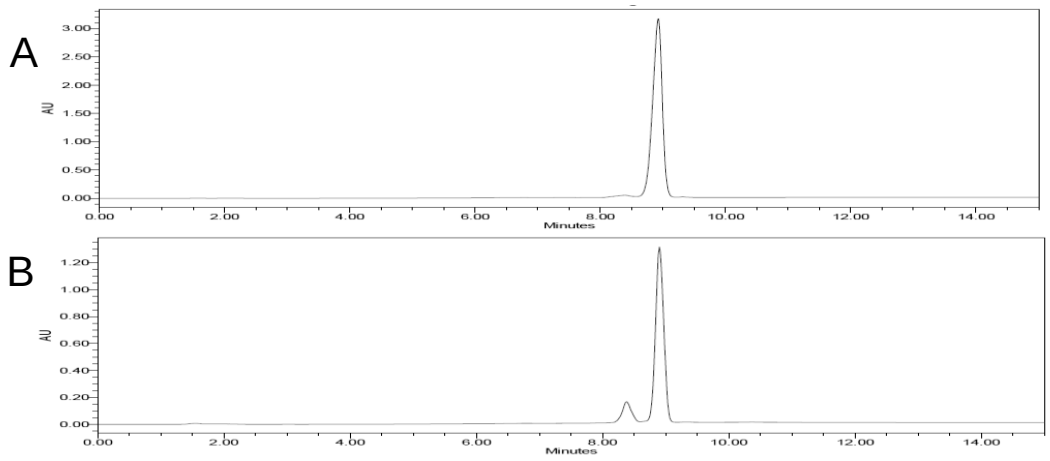

Figure 3-2. UV-HPLC chromatograms of a solution of compound **4** in ethanol after A) 24 hours and B) 7 days. The peaks at t_R = 8.4 and 8.9 min correspond to compounds **3** and **4** respectively.

3.3.2 Radiochemistry

To evaluate the ability of the oxidant to promote labelling of small molecules, a series of fluorous stannanes were used. The advantage of fluorous

stannanes over simple trialkyl tin derivatives is that the excess starting stannane and the oxidant can be removed selectively by passing the reaction mixture through a fluorous solid-phase extraction (FSPE) cartridge. The specific approach employed minimized sample handling, and involved loading the fluorous tin derivative on fluorous silica, prior to addition of the oxidant and iodide. After a set period of time, the desired product was eluted using a fluorophobic solvent ($EtOH/H_2O$).

As an initial test of the reactivity of F-CAT, the radioiodination of fluorous-tin benzoic acid (FBA) **5a** loaded onto fluorous silica was performed (Scheme 3-2). Using parallel reaction mixtures, HPLC analysis of the eluent (80:20 v/v $EtOH/H_2O$) was performed at different time points following the addition of [^{125}I]NaI and oxidant. After 30 minutes HPLC (Figure 3-3) showed complete consumption of the iodide, a single peak in the gamma chromatogram and no detectable amount of fluorous oxidant in the corresponding UV-HPLC chromatogram, where the limit of detection was 2 μg/mL. When the amount of oxidant used was doubled (100 versus 200 μg of **4**), the isolated yield of **5b** increased from 69 ± 5% to 82 ± 4%. Further increases in the amount of F-CAT did not improve the isolated yield. In all experiments, **5b** was obtained in greater than 98% radiochemical purity and high specific activity (> 240 Ci/mmol).

Scheme 3-2. Model reaction used to test F-CAT as an oxidant.

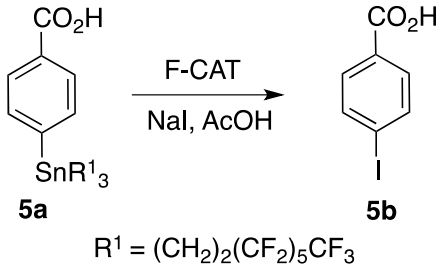

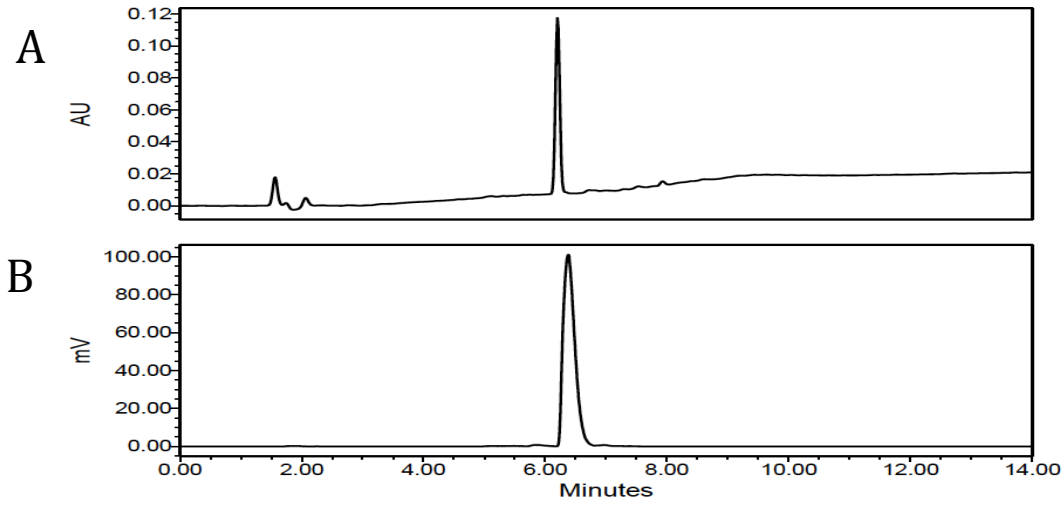

Figure 3-3. HPLC traces of ^{125}I-iodobenzoic acid **5b** co-injected with an authentic sample of 4-iodobenzoic acid (elution method B). A) UV-HPLC chromatogram. B) γ-HPLC chromatogram. Note that the precursor **5a** elutes at 12.5 min and that the γ- and UV detectors are connected in series.

The fluorous oxidant **4** was used subsequently to label a range of different arylstannanes whose synthesis we reported previously,[20] including precursors of known radiopharmaceuticals such as *meta*-iodobenzylguanidine (MIBG). All experiments were performed in triplicate and the products analyzed by gamma- and UV-HPLC to determine radiochemical purity and detect the presence of any residual oxidant. Isolated radiochemical yields ranged from 46% to 86% (Figure

3-4), with radiochemical purities greater than 97%. In no case was there evidence of any oxidant or precursor in the final product and the radiolabelling yields were generally higher than those reported using CAT as the oxidant.[20] This is largely due to the fact that a larger quantity of the fluorous oxidant can be used compared to CAT without being concerned about breakthrough during SPE purification, which would lead to contamination of the product.

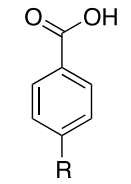

R = SnR'_3, **5a**
R = ^{125}I, **5b**
RCY = 82±4%

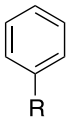

R = SnR'_3, **6a**
R = ^{125}I, **6b**
RCY = 46±4%

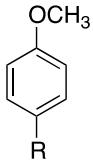

R = SnR'_3, **7a**
R = ^{125}I, **7b**
RCY = 73±5%

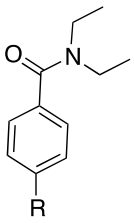

R = SnR'_3, **8a**
R = ^{125}I, **8b**
RCY = 79±5%

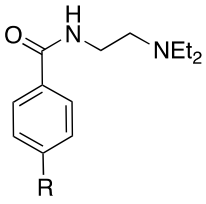

R = SnR'_3, **9a**
R = ^{125}I, **9b**
RCY = 55±10%

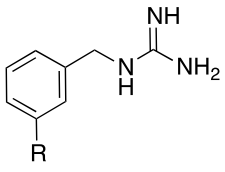

R = SnR'_3, **10a**
R = ^{125}I, **10b**
RCY = 65±8%

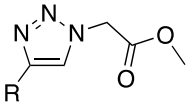

R = SnR'_3, **11a**
R = ^{125}I, **11b**
RCY = 57±3%

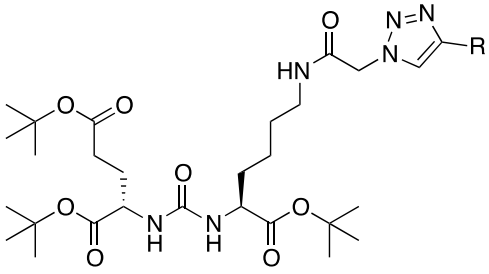

R = SnR'_3, **12a**
R = ^{125}I, **12b**
RCY =73±3%

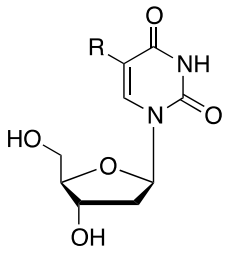

R = SnR'_3, **13a**
R = ^{125}I, **13b**
RCY = 61±11%

Figure 3-4. Structures of the fluorous precursors and corresponding radioiodinated compounds prepared using F-CAT **4**. RCY = Isolated radiochemical yield (n = 3). R' = $CH_2CH_2(CF_2)_5CF_3$.

3.3.3 Protein Labelling

The use of CAT as an oxidant for iodination of biomolecules has been widely reported.[10,42,43] However, there is concern about direct exposure of proteins to the oxidant, which is soluble in aqueous reaction media.[43,44] Consequently the water-insoluble oxidant iodogen is often used[45] since it can be employed as a thin film coated onto the wall of the reaction vial which minimizes direct interaction with the biomolecule being labelled. Given the insoluble nature of fluorous compounds in media typically employed for biomolecule iodination reactions, the ability of **4** to effectively label proteins was investigated.

Two proteins were selected as model candidates: thrombin and a fusion protein of human serum albumin fused to the C-terminus of hirudin variant 3 protein (HSACHV3).[46,47] Thrombin is the final effector enzyme generated by the coagulation cascade, and it activates platelets and converts fibrinogen into active fibrin.[48] It is tightly regulated by protease inhibitors of the serpin protein family, which trap thrombin in covalent complexes, whose formation can be monitored via SDS-PAGE and autoradiography.[47] HSACHV3 is a fusion protein under investigation as a fully latent, plasmin activatable, long-lasting hirudin, of potential benefit in thrombotic disorders resistant to natural or pharmacological clot lysis.[46,49] Many fusion proteins based on albumin or on the Fc portion of immunoglobulin G are either in clinical development or have reached the clinic.[50–52]

Thrombin and HSACHV3 were labelled separately using equivalent amounts of **4** and iodogen under identical reaction conditions. The labelled proteins were purified and concentrated using centrifugal filters (Amicon®) and the activity in both the protein concentrates and supernatant solutions measured using a calibrated NaI(Tl) well counter. SDS-page and *in vitro* assays were performed to compare the purity and function of the products produced using the two different oxidants.

Thrombin activity following labelling was quantified by assessing the rate of cleavage of a chromogenic substrate S-2238 using labelled thrombin concentrations of 14, 7 and 3.5 nM produced using both F-CAT and iodogen. The rates were compared to unmodified thrombin as a positive control and buffer as the negative control. At all concentrations of labelled thrombin produced using either oxidant, there was no significant difference among the mean rates of substrate cleavage (Supporting Information, Figure S3-22). For analysis of labelled HSACHV3, the isolated products from F-CAT or iodogen labelling were first incubated with plasmin. The fusion protein was designed to be cleaved by plasmin, releasing the active hirudin (HV3) molecule.[46] Following incubation of labelled HSACHV3 with plasmin, the resulting reaction mixture was analyzed by SDS-PAGE and autoradiography (Figure 3-5). The results showed that ^{125}I-HSACHV3 produced using F-CAT **4** was indistinguishable from that made using iodogen. What was also evident was a reduction in lower molecular weight impurities.

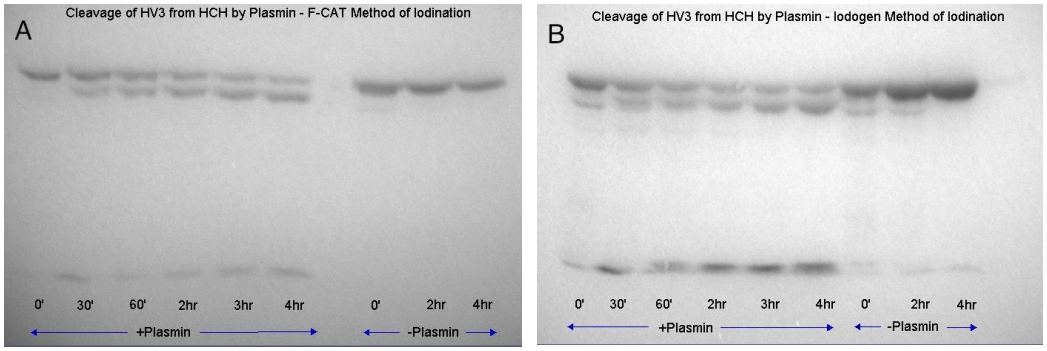

Figure 3-5. SDS-PAGE gel showing the products produced as a function of time by cleavage (+plasmin) of HV3 from ^{125}I-HSACHV3 prepared using A) F-CAT and B) Iodogen. Controls run in the absence of plasmin (-Plasmin) are also shown. HV3 = hirudin, HSA = human serum albumin and C is the plasmin cleavage site.

3.3.4 Tetrazine labelling

As an alternative to direct protein labelling, pre-targeting strategies that employ bioorthogonal coupling reactions are being used increasingly to develop molecular imaging probes and to study the distribution of new biological agents.[53–55] Of the many reactions being evaluated, the *trans*-cyclooctene (TCO) and tetrazine (Tz) coupling strategy has been shown to be particularly effective.[25,27,56–65] Here a TCO labelled targeting vector is administered and allowed to bind to its target *in vivo* and clear from non-target tissues, prior to administration of a radiolabelled tetrazine. The two components undergo a rapid inverse electron demand Diels-Alder reaction, thereby forming a covalent bond between the radiolabelled tetrazine and the TCO-modified targeting vector. This approach has a number of advantages over conventional targeting approaches for molecular imaging and has produced impressive results using a range of different isotopes.[59–66]

An iodinated tetrazine could be used as a convenient synthon to label biomolecules for *in vitro* assays and pharmacokinetic and pharmacodynamics studies. One critical advantage of the approach is that a non-radioactive TCO-labelled biomolecule could be prepared, purified and stored until needed. Leveraging the rapid kinetics, high yields and bioorthogonal nature of the TCO-tetrazine reaction, the labelled form can be generated as needed by simply adding the iodinated tetrazine. To determine if iodination using F-CAT would provide a convenient method to produce and purify an ^{125}I-labelled tetrazine, we synthesized 3-(pyridin-2-yl)-6-(5-(trisperfluorostannyl)pyridin-2-yl)-1,2-dihydro-1,2,4,5-tetrazine **14a** (fluorous-dihydrotetrazine), and loaded it onto a fluorous silica support. F-CAT was then employed to simultaneously oxidize **14a** to the tetrazine and promote the halodemetallation reaction with [^{125}I]NaI (Scheme 3-3). This approach was used, as opposed to labelling a tin-tetrazine derivative directly, because the fluorous-dihydrotetrazine is stable for extended periods of time when stored at -10 °C. The reaction was allowed to proceed for 30 min after which the desired product was eluted using an EtOH-water solution, in 69±4% (n=4) radiochemical yield in greater than 98% radiochemical purity, without the need to employ purification by HPLC. The HPLC retention time of the product matched that of the authentic non-radioactive standard (Figure 3-6), and there was no evidence of any oxidant or precursor in the final product.

Scheme 3-3. F-CAT-mediated, simultaneous oxidation and labelling reaction to produce an iodinated tetrazine for use in bioorthogonal coupling reactions.

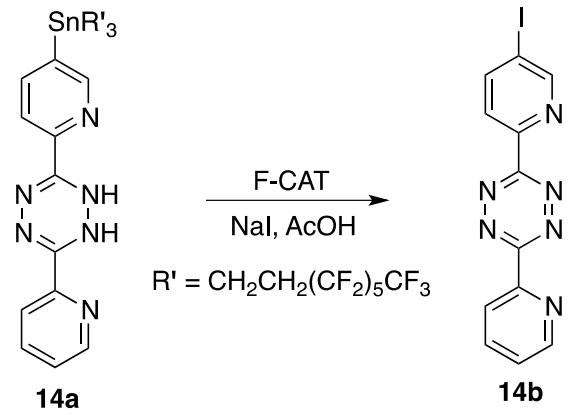

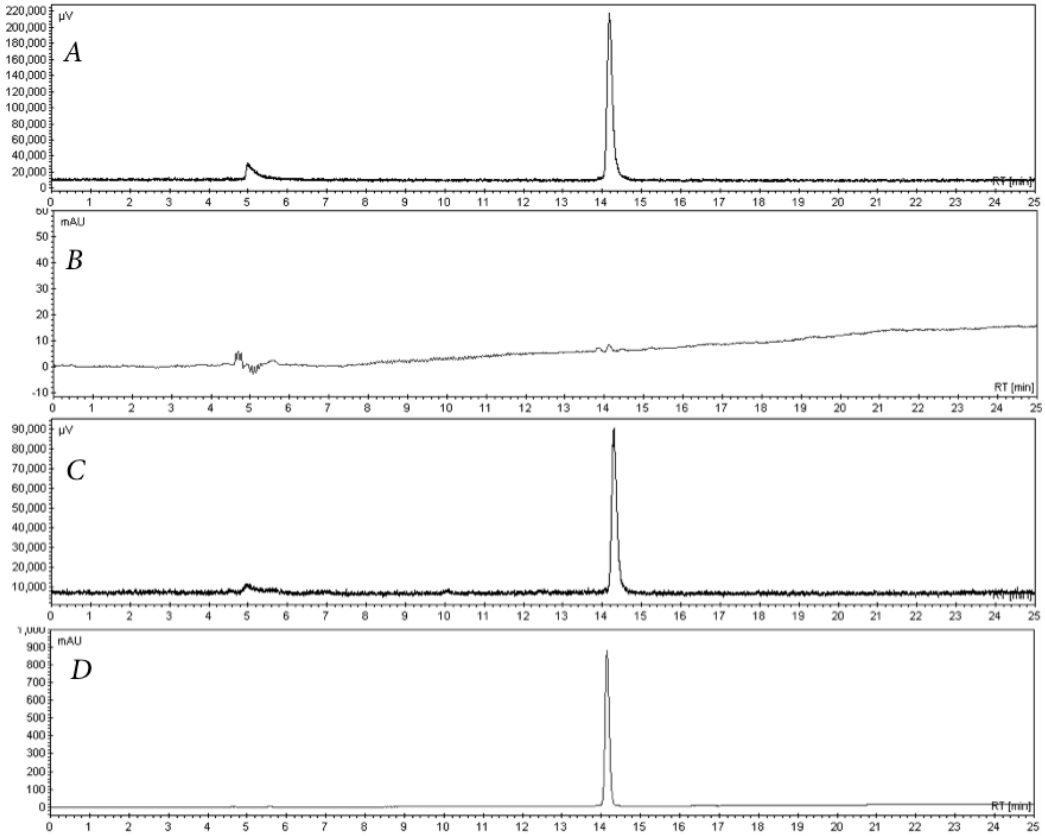

Figure 3-6. A) γ-HPLC chromatogram of [^{125}I]iodotetrazine **14b** (R_t = 14.2 min.). B) UV-HPLC chromatogram of the same reaction mixture. C) γ-HPLC and D) UV-HPLC chromatograms of 14b spiked with the non-radioactive reference standard.

To verify that the iodinated tetrazine was suitably reactive, **14b** was treated with (E)-cyclooct-4-enol (TCO-OH) in MeOH/H_2O for 15-20 sec. Analytical HPLC analysis of the reaction mixture revealed no evidence of residual **14b** and the formation of multiple peaks associated with the different Diels-Alder adducts and subsequent oxidation products, consistent with literature reports on comparable tetrazine reactions (Figure 3-7A).[25,65,67] The reaction was also repeated in the presence of a small amount of the non-radioactive analogue of **14b**

and the mixture analyzed by HPLC (Figure 3-7B) where there was good concordance between the gamma and UV chromatograms.

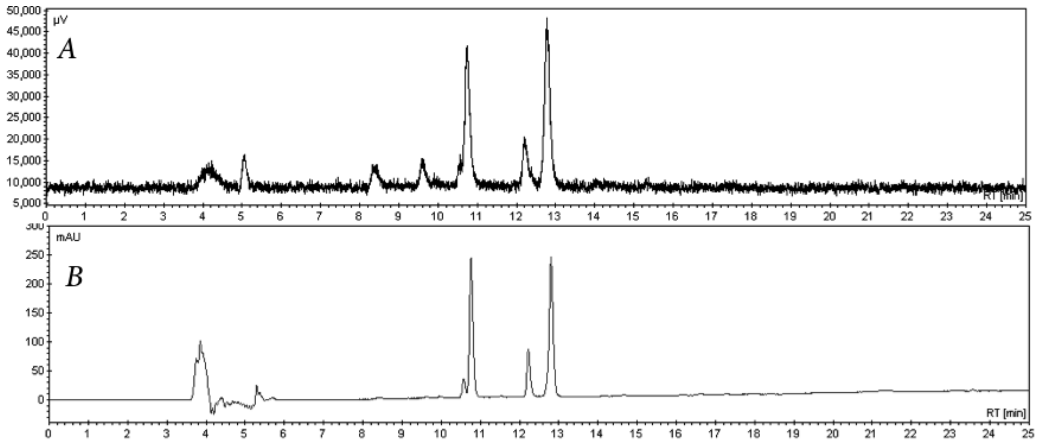

Figure 3-7. A) γ-HPLC chromatogram of the reaction mixture containing **14b**, its non-radioactive analogue, and (E)-cyclooct-4-enol. B) UV-HPLC chromatogram of the same reaction mixture.

The chemistry used to prepare **14b** suggested that the fluorous oxidant would also be useful for the synthesis of tetrazines themselves. Tetrazines are typically prepared by combining nitriles with hydrazine to form the corresponding 1,4-dihydro-*s*-tetrazine that is then oxidized. A range of oxidants can be used for the final step including sodium nitrite.[25,68,69] For the widely used bifunctional tetrazine **16**, the preparation (Scheme 3-4) reported by Fox and coworkers[25] involved the use of DDQ since nitrite can oxidize the amino group. While successful, we and others found the method produced a number of byproducts that complicated purification.[70] When **15** was treated with F-CAT the reaction was free from any unexpected impurities and the desired product, which was easily

separated from the fluorous oxidant, was isolated in 86% yield from the dihydrotetrazine.

Scheme 3-4. Preparation of 6-(6-(pyridin-2-yl)-1,2,4,5-tetrazin-3-yl)pyridin-3-amine using DDQ or F-CAT.

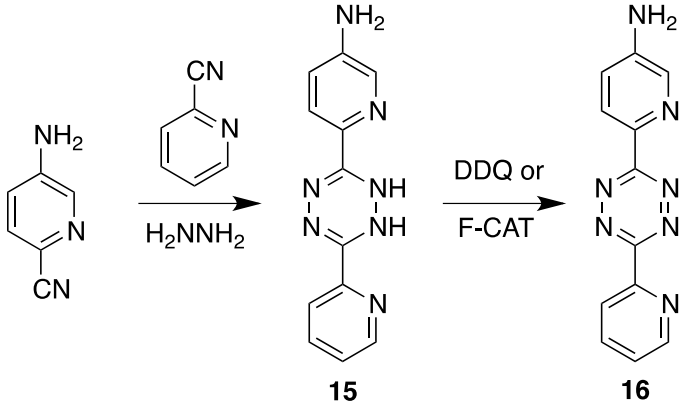

3.4 Conclusion

A new fluorous oxidant that is an analogue of chloramine-T was synthesized and shown to be an effective reagent for labelling small molecules and proteins with ^{125}I. In the case of biomolecules, F-CAT can be used as a water insoluble analogue of chloramine-T and a substitute for iodogen. The fluorous chloramine-T derivative **4** is stable as a solid for months and in solution for up to seven days and can be prepared in large quantities in two steps from commercially available starting materials. The fluorous nature of the oxidant is such that high purity radioiodinated compounds, including labelled tetrazines for use in bioorthogonal chemistry, can be prepared without HPLC purification in high effective specific activity, and free from any residual precursor and oxidant.

3.5 Experimental

3.5.1 Reagents and general procedures

Unless otherwise stated, all chemical reagents were purchased and used as received from Sigma-Aldrich, without further purification. Compounds **5a** to **14a** and **15** were prepared as previously described.[20,25,67] FC-72 was purchased from 3M, while 4,4,5,5,6,6,7,7,8,8,9,9,10,10,11,11,11-heptadecafluoroundecan-1-amine **2** was purchased from Fluorous Technologies Inc. SiliaFlash® P60 Silica gel from SiliCycle was used for silica gel chromatography. Analytical thin-layer chromatograms (Merck F254 silicagel on aluminum plates) were visualized using ultraviolet (UV) light. Polypropylene solid-phase-extraction (SPE) tubes were purchased from Sigma-Aldrich. Sep-Pak® C18 Plus cartridges were purchased from Waters Corporation. Amicon® Ultra-4 centrifugal filter units were purchased from EMD Millipore. Sodium [^{125}I]iodide with a specific activity of ~17 Ci/mg was purchased from the McMaster Nuclear Reactor (Hamilton, ON, Canada). *Caution: ^{125}I is radioactive and should only be handled in an appropriately equipped and licensed facility.*

3.5.2 Instrumentation

Nuclear magnetic resonance (NMR) spectra were recorded using a Bruker DRX-600 spectrometer with chemical shifts reported as δ values in parts per million (ppm) relative to the residual proton signal of the deuterated solvent or the carbon signal of the solvent. Infrared (IR) spectra were acquired using a Nicolet 6700 FT-IR spectrometer. Low-resolution mass spectra were obtained on an Agilent 630

ion trap electron spray ionization (ESI) instrument, using a Waters 1200 series LC system, H_2O/MeOH (1:1). High-resolution mass spectra (HRMS) were obtained using a Waters Micromass Global Ultima Q-TOF in ESI mode. A Capintec CR-25R dose calibrator was used for measuring the amount of radioactivity employed during the radiosynthesis protocols. Analytical (Method A and B) high-performance liquid chromatography (HPLC) was performed using a Waters 1525 Binary HPLC system fitted with a 2998 PDA detector (254 nm), a Bioscan γ detector (dwell time of 5 sec in a 10 µl loop) and a Phenomenex Gemini-C18 column (4.6 × 100 mm, 110 Å, 5 µm) at a flow rate of 1.0 mL/min. Analytical HPLC (Method C) was performed using a Varian ProStar Model 230 instrument, fitted with a Varian ProStar model 330 PDA detector, an IN/US γ-RAM gamma detector, a Star 800 analog interface module and a Phenomenex Gemini-C18 column (4.6 × 100 mm, 110 Å, 5 µm). The wavelength for UV detection was set at 254 nm, and the dwell time in the gamma detector was 5 sec in a 10 µl loop. The mobile phase was composed of solvent A = H_2O (0.1% TFA), and solvent B = CH_3CN (0.1% TFA). Method A: 0-7 min, 20-100% B; 7-15 min, 100% B. Method B: 0-7 min, 20-100 % B, 7-14 min, 100% B. Method C: 0-5 min, 20-100 % B, 5-14 min, 100% B. For calibration curves, each calibration solution was evaluated in triplicate and the data analyzed by the least-squares method. The limit of quantitation and the limit of detection were calculated using the standard deviation method.[71]

3.5.3 Synthesis of Primary Compounds 3, 4

***N*-(4,4,5,5,6,6,7,7,8,8,9,9,10,10,11,11,11-Heptadecafluoroundecyl)-4-methylbenzenesulfonamide (3).** *p*-Toluenesulfonyl chloride **1** (0.095 g, 0.5 mmol) was weighed into a 10 mL round bottom flask equipped with a stir bar. Ethanol (95%, 2 mL) was added and the solution stirred until **1** was completely dissolved. 4,4,5,5,6,6,7,7,8,8,9,9,10,10,11,11,11-Heptadecafluoroundecan-1-amine **2** (0.477 g, 1 mmol) was added to the solution with stirring at room temperature. The initial colorless reaction mixture became heterogenous after a few minutes. Stirring was continued until the reaction was complete (monitored by TLC in n-hexane:EtOAc, 3:1 v/v). The mixture was subsequently concentrated under reduced pressure and the product isolated by silica gel column chromatography using a gradient of 10-30% n-hexane:EtOAc. The fractions containing the product were combined and the solvent was removed to afford **3** as a white crystalline solid. Yield (0.281 g, 89%); mp 108-111 °C; FTIR (KBr) 3263, 2957, 1959, 1600 cm^{-1}; ^{1}H NMR (600 MHz, $CDCl_3$) δ 7.75 (d, *J* = 8.3 Hz, 2H, Ar-H), 7.32 (d, *J* = 8.2 Hz, 2H, Ar-H), 4.51 (t, *J* = 6.4 Hz, 1H, NH), 3.05 (q, *J* = 6.7 Hz, 2H, NCH_2), 2.43 (s, 3H, Ar-CH_3), 2.15-2.06 (m, 2H, CH_2CF_2), 1.82-1.77 (m, 2H, CH_2); ^{13}C NMR (150 MHz, $CDCl_3$) δ 143.9, 136.9, 130.0, 127.2, 42.4, 28.2 (m), 21.6, 21.1; HRMS (ESI^+) *m/z* calcd for $C_{18}H_{15}NO_2SF_{17}$ $[M+H]^+$ 632.0552, found: 632.0541.

***N*-Chloro-*N*-(4,4,5,5,6,6,7,7,8,8,9,9,10,10,11,11,11-heptadecafluoroundecyl)-4-methylbenzenesulfonamide (4).** The sulfonamide **3** (0.252 g, 0.4 mmol) was

dissolved in $CHCl_3$ (10 mL) in a 50 mL round bottom flask equipped with a stir bar. Aqueous NaOCl (6% w/v, 10 mL) was added and the biphasic reaction mixture stirred vigorously at room temperature. Stirring was continued until the reaction was complete (monitored by TLC using 3:1 v/v hexane:EtOAc). The reaction mixture was transferred into a separatory funnel and the $CHCl_3$ layer separated and the aqueous layer extracted with $CHCl_3$ (3 × 5 mL). The combined organic layers were dried over anhydrous Na_2SO_4 and concentrated by rotary evaporation to afford a white solid. Yield (0.260 g, 98%); mp 77-79 °C; FTIR (KBr) 2930, 1958, 1595 cm^{-1}; ^1H NMR (600 MHz, $CDCl_3$) δ 7.82 (m, 2H, Ar-H), 7.40 (d, *J* = 8.0 Hz, 2H, Ar-H), 3.33 (t, *J* = 6.3 Hz, 2H, NCH_2), 2.48 (s, 3H, Ar-CH_3), 2.27-2.18 (m, 2H, CH_2CF_2), 2.03-1.98 (m, 2H, CH_2); ^{13}C NMR (150 MHz, CDCl3) δ 145.7, 129.8, 129.6, 55.6, 27.8 (m), 21.7, 18.3; HRMS (ESI^+) *m/z* calcd for $C_{18}H_{17}N_2O_2SF_{17}Cl$ $[M+NH_4]^+$ 683.0428, found: 683.0439.

3-(5-Aminopyridin-2-yl)-6-(pyridin-2-yl)-1,2,4,5-tetrazine (16). To a solution of 3-(5-aminopyridin-2-yl)-6-(pyridin-2-yl)-1,4-dihydro-s-tetrazine **15** (50 mg, 0.20 mmol) in acetonitrile (5 mL) was added F-CAT **4** (146 mg, 0.22 mmol) and the reaction mixture allowed to stir at 40 °C. After 12 hours the solvent was evaporated under reduced pressure, the residue dissolved in methanol (300 µL) and the product (43 mg, 86%) isolated as a red coloured solid using a FluoroFlash® Cartridge and eluting with MeOH/H_2O (1:10, v/v). Characterization data matched that reported in the literature.[25]

3.5.4 General procedures

Preparation of coated fluorous silica. Fluorous silica (200 mg) was added to a solution of fluorous precursor in chloroform (1 mL, 10 mg/mL) and the mixture agitated by hand until a slurry was formed. After sitting at room temperature overnight, the resulting powder (30 mg) was added to a polypropylene SPE tube that contained 500 mg of unmodified fluorous silica previously washed with DMF (1 mL), H_2O (5 mL) and 80:20 (v/v) EtOH/H_2O (5 mL).

Small molecule radiolabelling. To an SPE cartridge containing the coated fluorous silica, connected to a Sep-Pak® C18 Plus cartridge (820 mg sorbent/cartridge), 10% acetic acid in EtOH (50 μL) was added followed by F-CAT **4** (100 μL, 2 mg/mL in ethanol) and [^{125}I]NaI (10 μL, 1.85 GBq/mL in 0.1 M NaOH). After 30 min at room temperature, $Na_2S_2O_{5(aq)}$ (50 μL, 0.2 M) was added and the system washed with water (5 mL) and a 0.09 M H_3PO_4 solution of EtOH/H_2O (200 mL EtOH, 50 mL water, 1.5 mL conc. H_3PO_4) and 1 mL fractions collected and counted. HPLC retention times were compared to those for non-radioactive authentic standards.

Protein radiolabelling. Eppendorf tubes were treated with 10 μL of oxidant solution (2.0 mg/mL of iodogen in $CHCl_3$ or 7.7 mg/mL of F-CAT **4** in $CHCl_3$) and the solution allowed to evaporate. A magnetic stir bar was added followed by protein (10 μL, 107 μg) in ice-cold phosphate buffered saline (PBS) (280 μL) and [^{125}I]NaI (10 μL, 37 MBq) and the mixture stirred slowly for 10 min. The reaction was quenched by the addition of $Na_2S_2O_5$ (0.1 M, 100 μL) and diluted to a final

volume of 1 mL with PBS. The content of the eppendorf tube was transferred to an Amicon® Ultra-4 centrifugal filter unit and the eppendorf tube rinsed twice with ice-cold PBS, which was added to the centrifugal filter unit, and the total volume made up to 4 mL. The sample was centrifuged at 5000 × g for 10 min in an Eppendorf 5473 centrifuge. The filtrate was transferred into a scintillation vial, and the protein residue in the sample reservoir diluted with ice-cold PBS (4 mL) and the centrifugation process repeated twice. After the final centrifugation the residual protein was reconstituted in ice-cold PBS (1 mL) and transferred to an eppendorf tube for analysis.

Thrombin Assay. Chromogenic substrate S2238 (Chromogenix, Instrumentation Laboratory Company, Lexington, MA 02421-3125, USA) was diluted to 100 µM in PPNE kinetics buffer (20 mM sodium phosphate pH 7.4, 100 mM NaCl, 0.1 mM EDTA and 0.1% w/vol polyethylene glycol). Samples (14 nM, 7 nM and 3.5 nM) of thrombin, and labelled thrombin prepared using iodogen and F-CAT were prepared in PPNE kinetics buffer. Samples (30 µL) and buffer control (30 µL) were added to microtitre wells. Diluted substrate S2238 (270 µL) portions were added to each well and the optical density at 405 nm read immediately and at 15 seconds intervals for 5 min on the plate reader. Blank measurements of 300 µL PPNE buffer only were also made.

HSACHV3 Cleavage and SDS-PAGE. Samples (10 µM) of HSACHV3, iodogen labelled HSACHV3 and F-CAT labelled HSACHV3 were prepared in PPNE buffer and then diluted to a final concentration of 376 nM with the total

volume in each eppendorf vial being 200 µL. Plasmin (Enzyme Research Laboratories Inc., South Bend, IN 46628, USA) was diluted to 12 µM in PPNE buffer and added to each vial at a final concentration of 600 nM. Immediately upon adding plasmin, at t_0, a 20 µL aliquot was removed from the reaction vial and add to a tube containing 20 µL PPNE and 13 µL 4 × SDS gel sample buffer and the vial placed in a 37 °C water bath. At 30 min, 1, 2, 3 and 4 hours, the reaction vial was agitated before a 20 µL aliquot was removed and treated as the aliquot obtained at t_0. A previously prepared 8% acrylamide gel was loaded with the 20 µL samples. After staining, destaining and drying, the gel was exposed to film overnight.

3.5.5 X-ray Structure Determination of 3 and 4

A crystal for each compound suitable for data collection was selected and mounted in paratone oil on a MiTeGen head, then placed in the cold stream of the diffractometer. Data were collected at 173 K using omega scans on a Bruker APEX2 platform with a SMART 6000 area detector, and rotating anode generating Cu Kα radiation (λ= 1.54178 Å). Data were processed using SAINT,[72] corrected for absorption using redundant data (SADABS) and then solved using direct methods with the SHELXTL[73] program suite in the space group P2(1)/n. All non-hydrogen atoms were refined anisotropically; hydrogen atoms were placed in idealized positions riding on their constituent atoms, and updated after each cycle of refinement. In the last stages of refinement, the largest residual peak (0.49 eÅ-3) was associated with F15.

3.6 Supporting Information

X-ray crystallographic data for **3** and **4**; HRMS, ^{1}H and ^{13}C NMR spectra and HPLC chromatograms. This material can be found in **APPENDIX 1**.

3.7 Acknowledgements

The authors gratefully acknowledge funding support from the Natural Science and Engineering Research Council (NSERC) of Canada, and the Ontario Institute for Cancer Research (OICR). In addition, we wish to acknowledge Dr. Hilary Jenkins of the McMaster Analytical X-Ray Diffraction Facility (MAX) for her support in obtaining the X-ray data, and Dr. Denis Snider of the Centre for Probe Development and Commercialization, McMaster University, for scientific/medical document editing.

3.8 References

(1) Orimo, S.; Ozawa, E.; Nakade, S.; Sugimoto, T.; Mizusawa, H. *J. Neurol. Neurosurg. Psychiatry* **1999**, *67*, 189–194.

(2) Eerola, J.; Tienari, P. J.; Kaakkola, S.; Nikkinen, P.; Launes, J. *J. Neurol. Neurosurg. Psychiatry* **2005**, *76*, 1211–1216.

(3) Koehler, L.; Gagnon, K.; McQuarrie, S.; Wuest, F. *Molecules* **2010**, *15*, 2686–2718.

(4) Volkert, W. A.; Hoffman, T. J. *Chem. Rev.* **1999**, *99*, 2269–2292.

(5) Chatal, J. F.; Hoefnagel, C. A. *Lancet* **1999**, *354*, 931–935.

(6) Owens, D. R.; Coates, P. A.; Luzio, S. D.; Tinbergen, J. P.; Kurzhals, R. *Diabetes Care* **2000**, *23*, 813–819.

(7) Chen, J.; Wang, M.; Joyce, A.; DeFranco, D.; Kavosi, M.; Xu, X.; O'Hara, D. M. *Pharm. Res.* **2014**, *31*, 2810–2821.

(8) Bolton, A. E.; Hunter, W. M. *Biochem. J.* **1973**, *133*, 529–539.

(9) Wilbur, S. D. *Bioconjugate Chem.* **1992**, *3*, 433–470.

(10) Lindegren, S.; Skarnemark, G.; Jacobsson, L.; Karlsson, B. *Nucl. Med. Biol.* **1998**, *25*, 659–665.

(11) Choi, J.; Vaidyanathan, G.; Koumarianou, E.; McDougald, D.; Pruszynski, M.; Osada, T.; Lahoutte, T.; Lyerly, K. H.; Zalutsky, M. R. *Nucl. Med. Biol.* **2014**, *41*, 802–812.

(12) Hunter, D. H.; Zhu, X. *J. Labelled Compd. Rad.* **1999**, *42*, 653–661.

(13) Mundwiler, S.; Candreia, L.; Häfliger, P.; Ortner, K.; Alberto, R. *Bioconjugate Chem.* **2004**, *15*, 195–202.

(14) Yong, L.; Yao, M.-L.; Kelly, H.; Green, J. F.; Kabalka, G. W. *J. Labelled Compd. Rad.* **2011**, *54*, 173–174.

(15) Janabi, M.; Pollock, C. M.; Chacko, A.; Hunter, D. H. *Can. J. Chem.* **2015**, *93*, 207–217.

(16) Yong, L.; Yao, M.-L.; Green, J. F.; Kelly, H.; Kabalka, G. W. *Chem. Commun.* **2010**, *46*, 2623–2625.

(17) Donovan, A. C.; Forbes, J.; Dorff, P.; Schaffer, P.; Babich, J.; Valliant, J. F. *J. Am. Chem. Soc.* **2006**, *128*, 3536–3537.

(18) Bejot, R.; Fowler, T.; Carroll, L.; Boldon, S.; Moore, J. E.; Declerck, J.; Gouverneur, V. *Angew. Chem. Int. Ed.* **2009**, *48*, 586–589.

(19) Donovan, A. C.; Valliant, J. F. *Nucl. Med. Biol.* **2008**, *35*, 741–746.

(20) Dzandzi, J. P. K.; Vera, D. R. B.; Valliant, J. F. *J. Labelled Compd. Rad.* **2014**, *57*, 551–557.

(21) Wager, K. M.; Jones, G. B. *Curr. Radiopharm.* **2010**, *3*, 37–45.

(22) Eersels, J. L. H.; Travis, M. J.; Herscheid, J. D. M. *J. Labelled Compd. Rad.* **2005**, *48*, 241–257.

(23) Seevers, R. H.; Counsell, R. E. *Chem. Rev.* **1982**, *82*, 575–590.

(24) Vaidyanathan, G.; Affleck, D. J.; Alston, K. L.; Zhao, X.-G.; Hens, M.; Hunter, D. H.; Babich, J.; Zalutsky, M. R. *Bioorg. Med. Chem.* **2007**, *15*, 3430–3436.

(25) Blackman, M. L.; Royzen, M.; Fox, J. M. *J. Am. Chem. Soc.* **2008**, *130*, 13518–13519.

(26) Rossin, R.; Verkerk, P. R.; van den Bosch, S. M.; Vulders, R. C. M.; Verel, I.; Lub, J.; Robillard, M. S. *Angew. Chem. Int. Ed.* **2010**, *49*, 3375–3378.

(27) Devaraj, N. K.; Weissleder, R. *Acc. Chem. Res.* **2011**, *44*, 816–827.

(28) Wu, H.; Yang, J.; Šečkutė, J.; Devaraj, N. K. *Angew. Chem. Int. Ed.* **2014**, *53*, 5805–5809.

(29) Miura, T.; Nakashima, K.; Tada, N.; Itoh, A. *Chem. Commun.* **2011**, *47*, 1875–1877.

(30) Holczknecht, O.; Pozzi, G.; Quici, S. *QSAR Comb. Sci.* **2006**, *25*, 736–741.

(31) Maayan, G.; Fish, R. H.; Neumann, R. *Org. Lett.* **2003**, *5*, 3547–3550.

(32) Huang, Y.-B.; Yi, W.-B.; Cai, C. *J. Fluor. Chem.* **2011**, *132*, 554–557.

(33) Matsubara, H.; Maegawa, T.; Kita, Y.; Yokoji, T.; Nomoto, A. *Org. Biomol. Chem.* **2014**, *12*, 5442–5447.

(34) Tada, N.; Cui, L.; Ishigami, T.; Ban, K.; Miura, T.; Uno, B.; Itoh, A. *Green Chem.* **2012**, *14*, 3007.

(35) Ang, W. J.; Lam, Y. *Org. Biomol. Chem.* **2014**.

(36) Jafarpour, M.; Rezaeifard, A.; Golshani, T. *Phosphorus, Sulfur Silicon Relat. Elem.* **2010**, *186*, 140–148.

(37) Aubineau, T.; Cossy, J. *Chem. Commun.* **2013**, *49*, 3303–3305.

(38) Topacli, C.; Topacli, A. *Spectrosc. Lett.* **2002**, *35*, 207–217.

(39) Larionov, O. V.; Kozhushkov, S. I.; de Meijere, A. *Synthesis* **2003**, *66*, 1916–1919.

(40) Shiri, A.; Khoramabadi-zad, A. *Synthesis* **2009**, *2009*, 2797–2801.

(41) Olmstead, M. M.; Power, P. P. *Inorg. Chem.* **1986**, *25*, 4057–4058.

(42) Pillai, M. R. A.; Gupte, J. H.; Jyotsna, T.; Mani, R. S. *J. Radioanal. Nucl. Chem.* **1987**, *116*, 193–202.

(43) Yamada, A.; Traboulsi, A.; Dittert, L. W.; Hussain, A. A. *Anal. Biochem.* **2000**, *277*, 232–235.

(44) Lane, D. J. R.; Richardson, D. R. *Biochem. J.* **2011**, *33*, 34–38.

(45) Saha, G. B.; Whitten, J.; Go, R. T. *Nucl. Med. Biol.* **1989**, *16*, 431–433.

(46) Sheffield, W. P.; Eltringham-Smith, L. J.; Gataiance, S.; Bhakta, V. *Thromb. Haemostasis* **2009**, *101*, 867–877.

(47) Filion, M. L.; Bhakta, V.; Nguyen, L. H.; Liaw, P. S.; Sheffield, W. P. *Biochemistry* **2004**, *43*, 14864–14872.

(48) Huntington, J. A. *J. Thromb. Haemost.* **2005**, *3*, 1861–1872.

(49) Roddick, L. A.; Bhakta, V.; Sheffield, W. P. *BMC Biochem.* **2013**, *14*, 31.

(50) Powell, J. S.; Pasi, K. J.; Ragni, M. V.; Ozelo, M. C.; Valentino, L. A.; Mahlangu, J. N.; Josephson, N. C.; Perry, D.; Manco-Johnson, M. J.; Apte, S.; Baker, R. I.; Chan, G. C.; Novitzky, N.; Wong, R. S.; Krassova, S.; Allen, G.; Jiang, H.; Innes, A.; Li, S.; Cristiano, L. M.; Goyal, J.; Sommer, J. M.; Dumont, J. A.; Nugent, K.; Vigliani, G.; Brennan, A.; Luk, A.; Pierce, G. F. *N. Engl. J. Med.* **2013**, *369*, 2313–2323.

(51) Santagostino, E.; Negrier, C.; Klamroth, R.; Tiede, A.; Pabinger-Fasching, I.; Voigt, C.; Jacobs, I.; Morfini, M. *Blood* **2012**, *120*, 2405–2411.

(52) Yousefpour, P.; Chilkoti, A. *Biotechnol. Bioeng.* **2014**, *111*, 1699–1716.

(53) Devaraj, N. K.; Weissleder, R.; Hilderbrand, S. A. *Bioconjugate Chem.* **2008**, *19*, 2297–2299.

(54) Devaraj, N. K.; Upadhyay, R.; Haun, J. B.; Hilderbrand, S. A.; Weissleder, R. *Angew. Chem. Int. Ed.* **2009**, *48*, 7013–7016.

(55) Carroll, L.; Evans, H. L.; Aboagye, E. O.; Spivey, A. C. *Org. Biomol. Chem.* **2013**, *11*, 5772–5781.

(56) Knall, A.-C.; Slugovc, C. *Chem. Soc. Rev.* **2013**, *42*, 5131–5142.

(57) Debets, M. F.; van Berkel, S. S.; Dommerholt, J.; Dirks, a T. J.; Rutjes, F. P. J. T.; van Delft, F. L. *Acc. Chem. Res.* **2011**, *44*, 805–815.

(58) Patterson, D. M.; Nazarova, L. A.; Prescher, J. A. *ACS Chem. Biol.* **2014**, *9*, 592–605.

(59) Rossin, R.; Robillard, M. S. *Curr. Opin. Chem. Biol.* **2014**, *21*, 161–169.

(60) Rossin, R.; Duijnhoven, S. M. J. van; Läppchen, T.; Bosch, S. M. van den; Robillard, M. S. *Mol. Pharm.* **2014**, *11*, 3090–3096.

(61) Rossin, R.; Läppchen, T.; van den Bosch, S. M.; Laforest, R.; Robillard, M. S. *J. Nucl. Med.* **2013**, *54*, 1989–1995.

(62) Denk, C.; Svatunek, D.; Filip, T.; Wanek, T.; Lumpi, D.; Fröhlich, J.; Kuntner, C.; Mikula, H. *Angew. Chem. Int. Ed.* **2014**, *53*, 9655–9659.

(63) Nichols, B.; Qin, Z.; Yang, J.; Vera, D. R.; Devaraj, N. K. *Chem. Commun.* **2014**, *50*, 5215–5217.

(64) Zeglis, B. M.; Sevak, K. K.; Reiner, T.; Mohindra, P.; Carlin, S. D.; Zanzonico, P.; Weissleder, R.; Lewis, J. S. *J. Nucl. Med.* **2013**, *54*, 1389–1396.

(65) Li, Z.; Cai, H.; Hassink, M.; Blackman, M. L.; Brown, R. C. D.; Conti, P. S.; Fox, J. M. *Chem. Commun.* **2010**, *46*, 8043–8045.

(66) Valliant, J. F.; Patel, R.; Vito, A. *Nucl. Med. Biol.* **2014**, *41*, 614–615.

(67) Albu, S. A.; Al-Karmi, S. A.; Dzandzi, J. P. K.; Zlitni, A.; Beckford-Vera, D.; Blacker, M.; Patel, R. M.; Capretta, A.; Valliant, J. F. *Submitted for publication in the Journal of Bioconjugate Chemistry*.

(68) Ding, J.; Song, N.; Li, Z. *Chem. Commun.* **2010**, *46*, 8668–8670.

(69) Clavier, G.; Audebert, P. *Chem. Rev.* **2010**, *110*, 3299–3314.

(70) Selvaraj, R.; Fox, J. M. *Tetrahedron Lett.* **2014**, *55*, 4795–4797.

(71) Chan, C. C.; Lam, H.; Lee, Y. C.; Zhang, X.-M. *Analytical Method Validation and Instrument Performance Verification*; 1st ed.; John Wiley & Sons, Inc.: Hoboken, New Jersey., 2004.

(72) SAINT and SADABS: APEX2, v.2010.3 software suite; Bruker AXS Inc.: Madison, WI.

(73) SHELXTL, as part of the APEX2 v.2010.3 software suite; Bruker AXS Inc.: Madison, WI.

Chapter 4 - ^{125}I-Tetrazine and Inverse-Electron-Demand Diels-Alder Chemistry: A Convenient Radioiodination Strategy for Biomolecule Labelling, Screening, and Biodistribution Studies.

The following chapter has been submitted as an article for publication in Bioconjugate Chemistry under the authorship: Silvia A. Albu, Salma A. Al-Karmi James P. K. Dzandzi, Aimen Zlitni, Denis Beckford-Vera, Alyssa Vito, Megan Blacker, Nancy Janzen, Ramesh M. Patel, Alfredo Capretta and John F. Valliant. I am responsible for the growing the iodo-tetrazine (I-Tz) crystal and interpretation of the x-ray data, and performing the reported kinetic studies. I am also responsible, in collaboration with Denis Beckford-Vera, for the experiments involving the insulin derivative and ^{125}I-Tz, and preparing the lead compound for biodistribution studies. I also contributed to writing the manuscript. Dr. Silvia Albu, in collaboration with Salma Al-Karmi, initiated the tetrazine work as part of her PhD work, where she was the first to prepare and fully characterize I-Tz, and developed the method of preparing the ^{125}I-Tz. Optimization of the reaction conditions as well as synthesis of *trans*-cyclooctene, measurement of log P of ^{125}I-Tz and its stability testing was performed by Salma Al-Karmi, Alyssa Vito, and Dr. Ramesh M. Patel. Aimen Zlitni prepared the TCO-modified antibody, antibody labelling, Western Blot analysis and developed the Flow Chamber assay.

Megan Blacker and Nancy Janzen performed the insulin receptor binding assay and biodistribution studies. Dr. Beckford Vera is responsible synthesis of insulin derivatives. Profs. Alfredo Capretta and John Valliant were responsible for the overall structure of the manuscript and project, along with key scientific input and editorial reviews.

^{125}I-Tetrazine and Inverse-Electron-Demand Diels-Alder Chemistry: A Convenient Radioiodination Strategy for Biomolecule Labelling, Screening, and Biodistribution Studies.

4.1 Abstract

A convenient method to prepare radioiodinated tetrazines was developed, such that a bioorthogonal inverse electron demand Diels-Alder reaction can be used to label biomolecules with ^{125}I for *in vitro* screening and *in vivo* biodistribution studies. The tetrazine was prepared by employing a high-yielding oxidative halo destannylation reaction that concomitantly oxidized the dihydrotetrazine precursor. The product reacts quickly and efficiently with *trans*-cyclooctene derivatives. Utility was demonstrated through antibody and hormone labelling experiments and by evaluating products using standard analytical methods, *in vitro* assays and quantitative biodistribution studies. The approach described provides a convenient and accessible alternative to conventional protein iodination methods that can expedite preclinical development and evaluation of biotherapeutics.

4.2 Introduction

The radiolabelling of biomolecules with long-lived isotopes such as ^{125}I remains a fundamentally important method in drug development. Radiolabelled biomolecules can be used in receptor binding assays and for assessing kinetics

and quantification of tissue concentrations in biodistribution studies, of particular importance for new biotherapeutics that include monoclonal antibodies, fusion or recombinant proteins and related structures.[1-6] Quantitative biodistribution data is critical to understanding dose-response relationships, where radioactive counting methods are generally faster and more economical than ligand binding assays or mass spectrometry based methods, which often require extensive method development to accurately quantify protein concentrations.[7] Radioisotope based methods based on ^{125}I exhibit high sensitivity and have minimal sample matrix interference and there is no need for extensive sample processing to extract the labelled biomolecule. Rather, simple radioactive counting of the low energy gamma emission (35 keV) is sufficient.

Labelling of proteins with ^{125}I has traditionally been accomplished by direct iodination of tyrosine residues in the presence of oxidants like iodogen or chloramine-T, or through coupling to lysine residues using a prosthetic group such as the Bolton-Hunter reagent.[8-10] An alternative approach that has not been described for ^{125}I is to utilize newer bioorthogonal coupling strategies (BCS) to conjugate the isotope to proteins. BCS involve highly efficient and selective reactions between functional groups that are not influenced by the presence of molecules found in biological systems.[11-14] They have been used widely for cellular fluorescence and *in vivo* imaging applications using both fluorescent dyes and radiotracers derived from radionuclides such as ^{11}C, ^{18}F, ^{64}Cu, ^{68}Ga, ^{89}Zr, and

^{111}In.[15-22] Pretargeting applications *in vivo*, using BCS have produced images with exquisite specificity and good target-to-non-target ratios.[13,15,19,22]

One particularly effective BCS involves the inverse electron demand Diels-Alder reaction between derivatized tetrazines and *trans*-cyclooctene (TCO).[16,17,19,22,23] This system offers a number of advantages including biocompatibility, rapid and typically quantitative coupling yields, and the ease with which TCO groups can be linked to biomolecules. Given the significant number of biotherapeutics being developed, particularly antibodies and antibody drug conjugates, access to an efficient ^{125}I labelling methodology would greatly assist the evaluation of these new constructs. In this regard, we sought to develop a convenient method to prepare an iodinated tetrazine and to demonstrate its utility as a tool to radiolabel TCO-derived biomolecules, providing constructs that can be used for *in vitro* assays and quantitative biodistribution studies.

4.3 Results and Discussion

Given the commercial availability of TCO derivatives for tagging biovectors, which include succinimidyl carbonate functionalized cyclooct-4-enol, our approach focused on the development of a convenient method to produce an iodinated tetrazine. The target was an iodine derivative of a bispyridyl tetrazine reported by Fox and coworkers, which was shown to couple to TCO derivatives with a second order rate constant of 1140 ± 40 M^{-1} s^{-1} in methanol.[24] A DOTA derivative of a related tetrazine was used to great success by Rossin, Robillard and coworkers for *in vivo* tumor imaging studies.[14]

The iodinated dihydrotetrazine **3** (Scheme 4-1) was prepared by taking advantage of the differential reaction rates between 2-cyanopyridine **1** and the iodinated pyridine-nitrile **2**.[17] The highest yield of **3** (37%) was realized when a 4-fold excess of **1** was coupled with 5-iodopicolinonitrile in the presence of ethanolic hydrazine. Oxidation of **3** using $NaNO_2$ in acetic acid gave the desired tetrazine **4a** in 90% yield. This compound served as the reference standard for the radiochemical work.

Scheme 4-1. Synthesis of iodotetrazine **4a**.

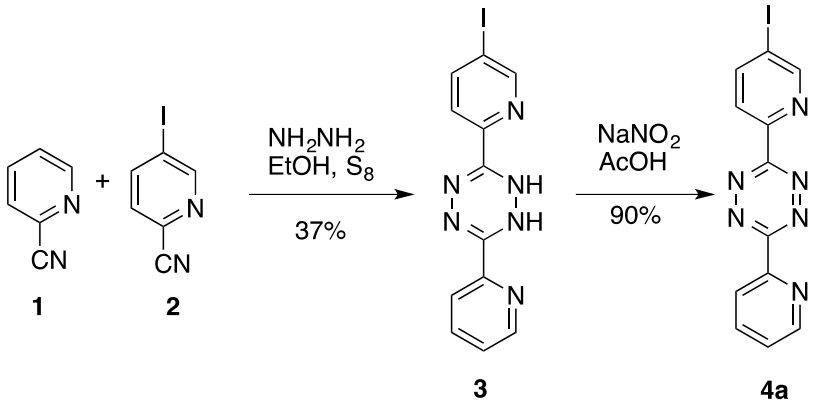

Single crystals of **4a** were obtained by slow evaporation of a saturated chloroform solution over multiple days. The structure (Figure 4-1) revealed the compound contained a single iodine atom, which as expected was located *para* to the tetrazine ring. The C-I bond was 2.089 Å, which is similar to the C-I bond distance in 4-iodopyridine (2.100(5) Å),[25] while the bond distances between the tetrazine and the two pyridine rings were similar (1.485(6) and 1.476(5) Å) (Table 4-1). The pyridine ring containing the iodine substituent was effectively coplanar with the tetrazine (dihedral angles = 4.2°), while the unsubstituted pyridine ring

had a dihedral angle of 8.2°. In the structure of 3,6-bis(2-pyridyl)-1,2,4,5-tetrazine, the pyridyl groups were twisted from the central tetrazine with a dihedral angle of 19.1^{o} as previously described,[26] while for the phenyl analogue the angle was 1^{o}.[27] For 3-phenyl-6-(2-pyridyl)-1,2,4,5-tetrazine containing one aryl group and one pyridine ring, the structure was also coplanar, which is unusual for aromatic rings with N-atoms in adjacent *ortho* positions.

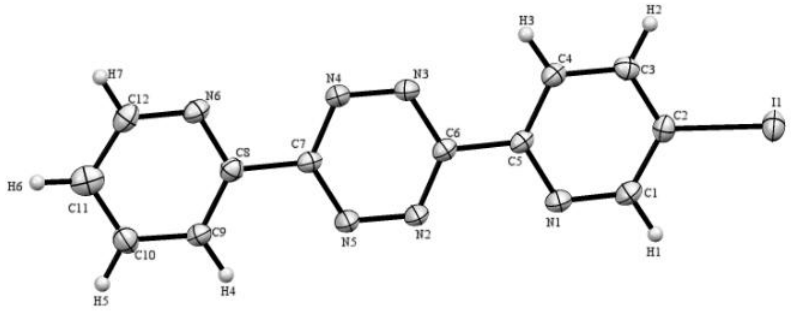

Figure 4-1. ORTEP drawing of **4a**. Thermal probability ellipsoids are shown at 50%.

Table 4-1. Bond distances, angles and torsional angles for **4a**.

Bond Lengths (Å)

I1-C2	2.089(4)	N1-C1	1.341(5)
N1-C5	1.351(5)	N2-N5	1.324(5)
N2-C6	1.337(5)	N3-N4	1.316(5)
N3-C6	1.349(5)	N4-C7	1.351(5)
N5-C7	1.341(6)	N6-C12	1.336(5)
N6-C8	1.352(5)	C1-C2	1.387(6)
C3-C4	1.391(6)	C2-C3	1.381(6)
C4-C5	1.394(6)	C7-C8	1.485(6)
C5-C6	1.476(5)	C9-C10	1.393(6)
C8-C9	1.388(6)	C10-C11	1.392(6)
C11-C12	1.402(7)		

Bond Angles (^{o})

C1-N1-C5	116.6(3)	N5-N2-C6	117.6(4)
N4-N3-C6	118.6(3)	N3-N4-C7	117.3(3)
N2-N5-C7	118.4(4)	C12-N6-C8	116.4(4)
C3-C2-I1	121.6(3)	C1-C2-I1	118.8(3)
C4-C5-C6	120.2(3)	N1-C5-C6	116.8(3)

N2-C6-C5	118.7(4)	N2-C6-N3	124.1(4)
N5-C7-N4	124.0(4)	N3-C6-C5	117.2(3)
N4-C7-C8	118.4(4)	N5-C7-C8	117.6(4)
N6-C8-C7	116.6(4)	C9-C8-C7	119.8(4)

Torsional Angles (^{o})

N1-C5-C6-N2	4.2(6)
N5-C7-C8-C9	-8.2(6)

The UV spectrum of **4a** in MeOH **(**Figure 4-2**)** shows a low energy n-π* transition between approximately 475 and 600 nm with a maximum at 535 nm.[28] Additional bands associated with the tetrazine π -π* were also observed at higher energy. The kinetics of the reaction between **4a** and (E)-cyclooct-4-enol (TCO-OH) was examined using UV spectroscopy by monitoring the disappearance of the absorbance at 535 nm as a function of time, which was complete in seconds (Figure 4-3). The second order rate constant k_2 was 229 ± 20 $M^{-1}s^{-1}$, which is slower than the parent bispyridyl tetrazine in the same solvent.[24] While not optimal for pretargeting strategies and *in vivo* coupling reactions, it is more than adequate for *in vitro* biomolecule labelling.

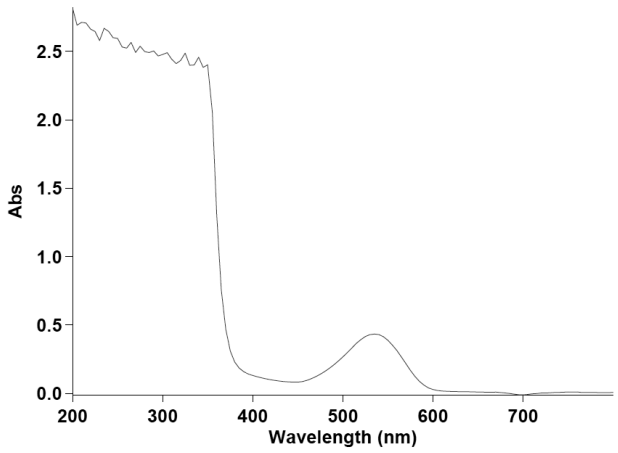

Figure 4-2. Absorption spectrum of **4a** (800 μM) in MeOH.

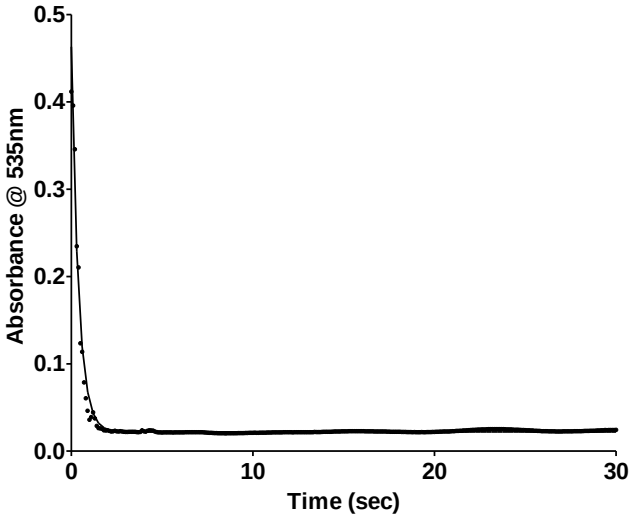

Figure 4-3. UV absorbance intensity at 535 nm versus time following the addition of TCO-OH (8.7 mM) to **4a** (0.8 mM) in MeOH.

For radiolabelling, conversion of **4a** to the trialkylstannane, the obvious precursor for introducing ^{125}I, was unsuccessful and gave a complex mixture of products. As a result, compound **5** was prepared in 76% yield by treating **3** with hexamethyldistannane (Scheme 4-2) in the presence of palladium acetate and 1,3,5,7-tetramethyl-2,4,8-trioxa-6-phenyl-6-phospha-adamantane (PA-Ph).[29] This

alternative approach is feasible since iodination reactions are done in the presence of excess oxidant, which would not only promote the substitution of tin but would also generate the desired tetrazine concomitantly. One practical advantage of this strategy is that compound **5** was found to be stable as a solid in the freezer for several months.

Scheme 4-2. Synthesis of ^{125}I-tetrazine **4b** from **3** using a concomitant-oxidation labelling strategy.

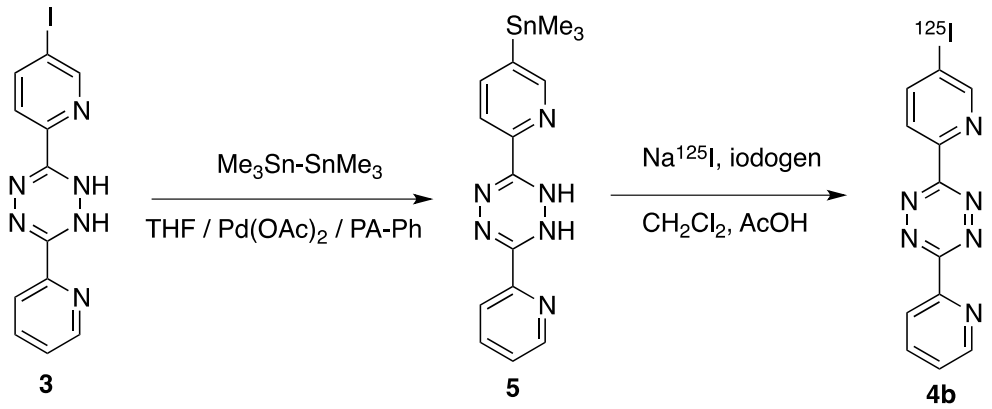

Radiolabelling was performed by treating **5** with [^{125}I]NaI and iodogen and allowing the reaction to proceed for 15 min at room temperature. Overall compound **4b** could be synthesized and isolated by semi-preparative HPLC (elution Method B) in 80% radiochemical yield, and the retention time of **4b** matched that for the non-radioactive **4a** by analytic HPLC (Figure 4-4). The iodotetrazine has a log P of 1.29,[30] and was stable for at least 24 hours in PBS. The latter feature provides the opportunity to use **4b** for multiple biomolecule labelling experiments from a single batch of ^{125}I-tetrazine.

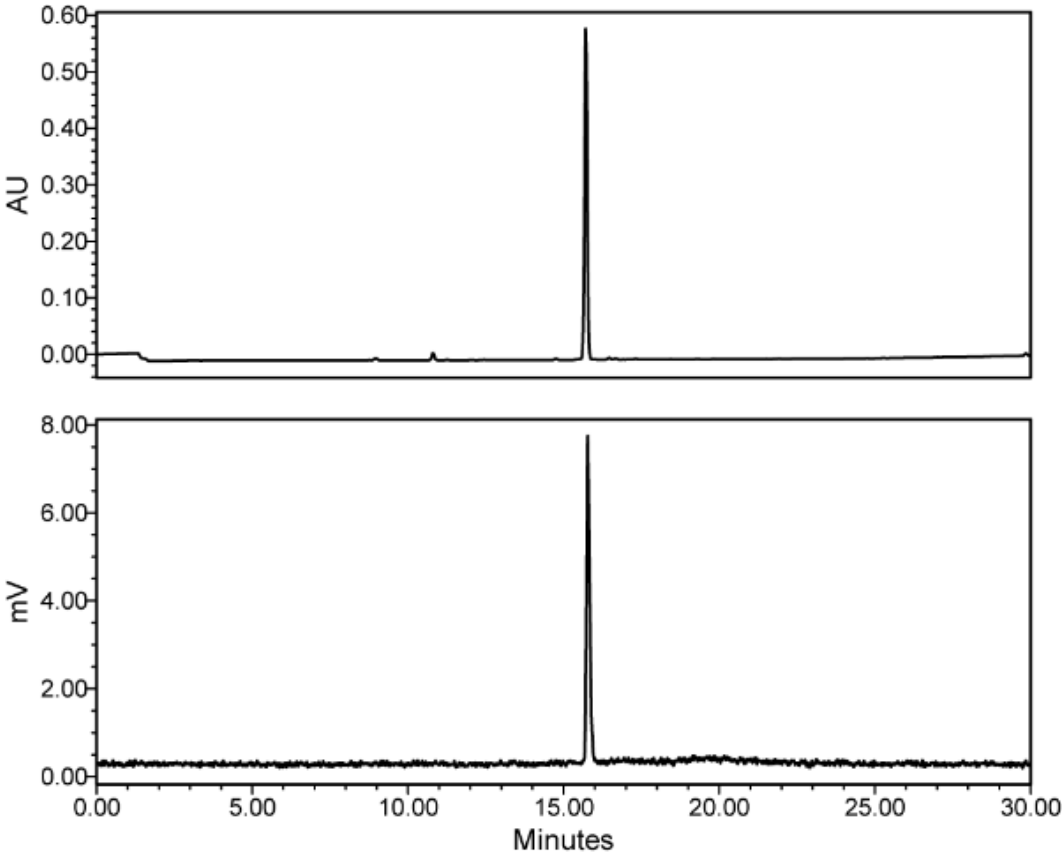

Figure 4-4. UV-HPLC-chromatogram of a mixture of **4a**/**4b** (top). γ-HPLC trace of the same sample (bottom).

Initial studies of the Diels-Alder ligation reaction were carried out with the non-radioactive tetrazine **4a** and TCO (Scheme 4-3) in ethanol and PBS buffer.[24,31] The reaction mixture showed an immediate change from purple to colorless. Analytical HPLC evaluation of the crude reaction mixture revealed three major peaks and no evidence of residual starting materials, which is consistent with literature reports on other analogous TCO-Tz reactions. HRMS followed by 2-D NMR studies of the isolated products allowed us to assign the peaks observed in the HPLC. The peak eluting at *ca.* 20 min was a mixture of **7a** and **8a** while the peak at 24 min was the oxidized product **9a**. We were unable to

isolate sufficient quantities of the early eluting product **6a** for NMR analysis as it rearranged to the other products during purification. This peak did show an *m/z* value comparable to **7a** and **8a** suggesting that it is a related isomer. In addition, the relative amounts of the different products was sensitive to the reaction conditions and times, as has been observed by others.[16] After 2 hours under the reaction conditions reported, ^{1}H NMR indicated the relative ratios of **7a**:**8a** was 88:12 while after 12 hours the ratio was 65:35.

Scheme 4-3. Scheme 4-3. Reaction products formed following the combination of **4a**/**4b** with TCO.

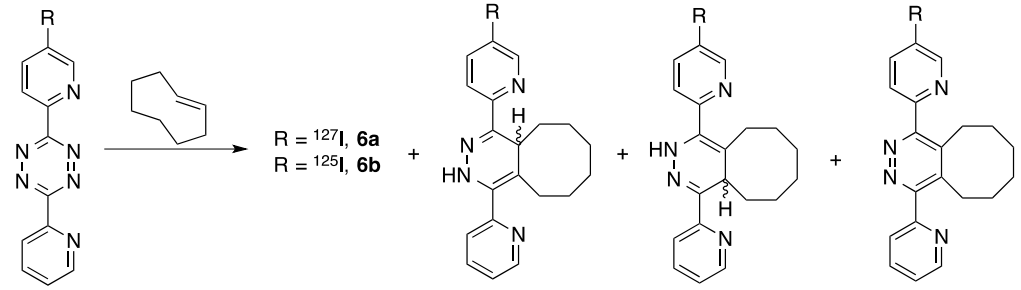

For the tracer level reaction, 3.7 MBq of **4b** was added to TCO which proceeded to completion quickly (<1 min) in ethanol and PBS buffer. To ensure consistency and generate reference standards, a reaction with **4a** was run in parallel. HPLC of the mixture after 4 min (Figure 4-5) revealed complete consumption of the tetrazine and 3 peaks in both the UV (panel a) and gamma (panel b) traces corresponding to the retention times for compounds **6a**/**b**, **7a**/**b** and **8a**/**b**, and **9a**/**b**. After an additional 45 min compounds **6a** and **6b** underwent

similar rearrangement to generate **7a/b**, **8a/b** and **9a/9b**. These experiments demonstrate that the tracer level work matches that of the reference standards and that **4b** can feasibly be used to label TCO-derived targeting vectors.

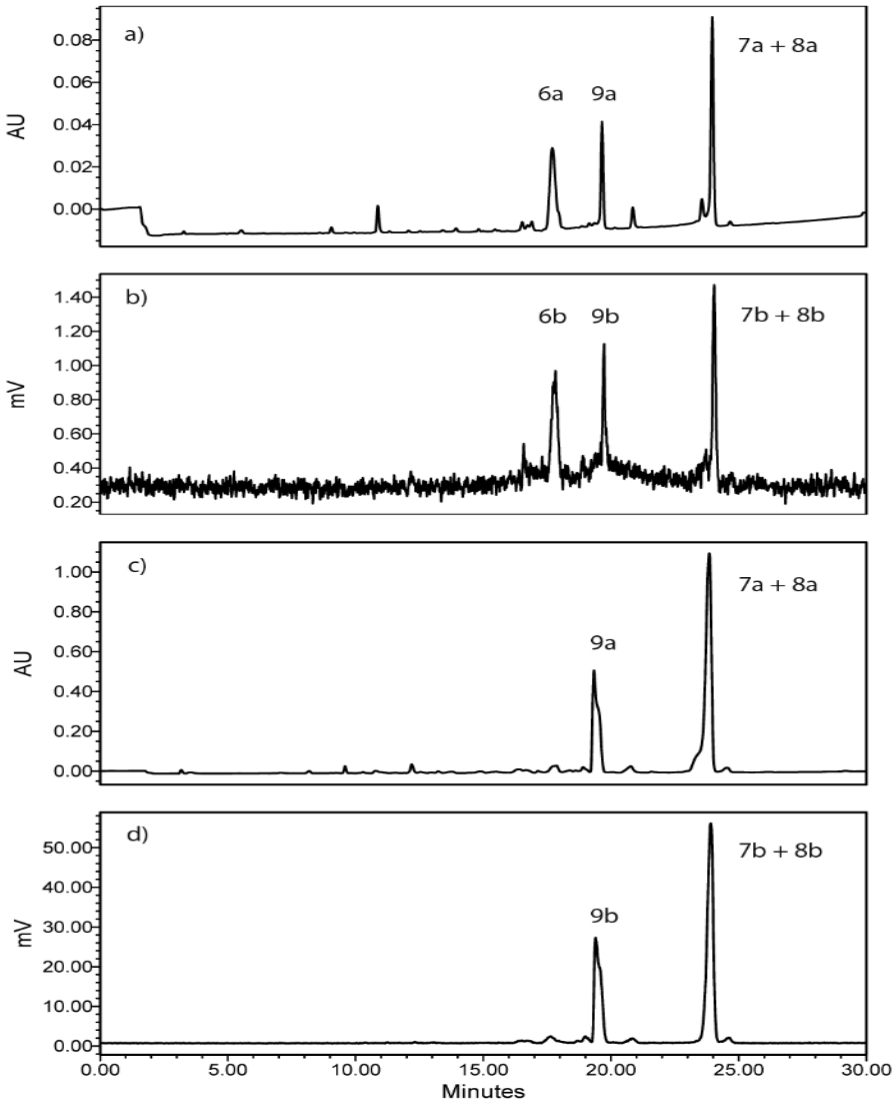

Figure 4-5. a) UV-HPLC chromatogram of the reaction mixture containing **4a**/**4b** and TCO. b) γ-HPLC traces of the same reaction mixture. c) UV-HPLC chromatogram of the reaction mixture after an additional 45 min. d) γ-HPLC chromatogram corresponding to c). (Elution Method A).

To evaluate the reaction of **4b** with TCO-modified antibodies, a TCO-anti-VEGFR2 conjugate was selected as the model compound. We have previously shown that (E)-cyclooct-4-enyl-2,5-dioxopyrrolidin-1-yl carbonate treated with anti-VEGFR2 antibody retained its affinity for VEGFR2 and was an effective agent for capturing tetrazine functionalized, ultrasound microbubbles.[32] Compound **4b** was incubated with the TCO-anti-VEGFR2 antibody and radioTLC confirmed conjugation (see Supporting Information, APPENDIX 2). The product, ^{125}I-labelled anti-VEGFR2, was isolated in 69% radiochemical yield, which is higher than previously reported for direct iodination of an anti-VEGFR2 antibody using iodogen.[33] To demonstrate the ^{125}I-labelled anti-VEGFR2 retained specificity for VEGFR2, western blots were performed on cell lysates from VEGFR2(+) H520 and VEGFR2(-) A431 cell lines. The positive control involved the use of an unmodified anti-VEGFR2 antibody, which identified the expected VEGFR2 protein band in the H520 lysate (but not the A431 lysate) when imaged using chemiluminecence. A similar molecular weight band was identified by autoradiography after incubation with ^{125}I-labelled anti-VEGFR2 construct, whereas no bands were identified using **4b** alone (see Supporting Information).

The tetrazine-TCO system can be used to assess binding to target molecules on cells using *in vitro* culture and conventional radioisotope assays. We have also developed a simple flow chamber system to screen compounds, taking advantage of the rapid kinetics of the TCO-tetrazine reaction (Figure 4-6). The flow system was designed for screening targeted ultrasound microbubbles,

but can also be used to test the binding of **4b** to TCO-functionalized biomolecules, under conditions that mimic fluid flow in blood vessels. Adherent cells were plated in a sealed chamber and incubated with the TCO-antibody construct of interest. The cells were washed with buffer, and then a solution of ^{125}I-labelled tetrazine **4b** was allowed to flow through the chamber, at a rate similar to that of capillary blood flow. After washing to remove excess and non-specifically bound reagents, the cells were lysed and the amount of radioactivity in the lysate determined relative to total cellular protein. In the case of TCO-anti-VEGFR2, there was nearly a 3-fold increase in ^{125}I-tetrazine binding to cells incubated with TCO-anti-VEGFR2, compared to with cells not incubated with that antibody (Figure 4-7). One could envisage expanding this approach to a parallel screening strategy where multiple wells of cells treated with different TCO-modified antibodies are exposed to **4b**, and the amount of binding determined by radioactivity bound to cells in each well.

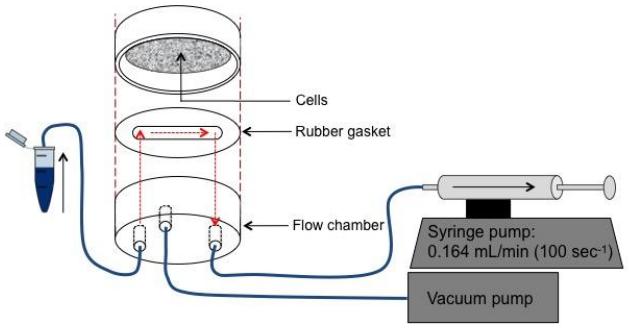

Figure 4-6. Schematic of the flow assay system.

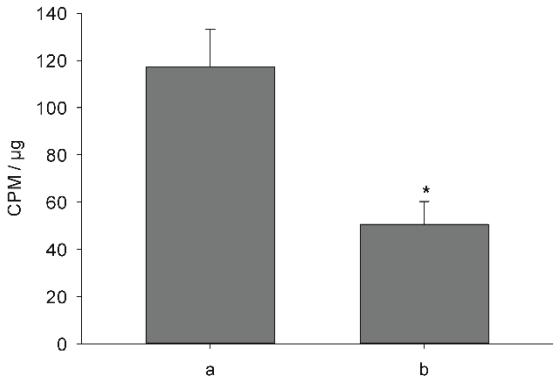

Figure 4-7. Data from flow chamber assay of **4b** binding to H520 cells previously incubated with (a) or without (b) TCO-anti-VEGFR2 antibody. The binding of **4b** was significantly higher in TCO-tagged cells compared to untreated H520 cells. Data is expressed as counts per minute (CPM) per µg of protein found in each sample (n= 5). Statistical analysis was done using a one-way ANOVA (* $p < 0.05$).

In addition to *in vitro* screening for antibody binding, **4b** can be used to assess the biodistribution of TCO-derived biomolecules. To demonstrate this, the biodistribution of the ^{125}I-labelled anti-VEGFR2 antibody was determined at 24, 48 and 72 hours post injection, in C57Bl/6 mice. There was significant initial uptake in the bladder, gall bladder, intestines, liver, spleen, and stomach, which eventually cleared, reaching less than 1% ID/g at 72 hours (Figure 4-8). The blood levels ranged from 0.43 ± 0.05 %ID/g at 24 hours to 0.17 ± 0.01 %ID/g at 72 hours. The thyroid uptake, which is the result of release of free I-125 *in vivo*, was 5.03 ± 0.38 %ID/g, 15.84 ± 0.60 %ID/g and 9.88 0.43 ± 5.94 %ID/g by 24, 48 and 72 h respectively, which are typical thyroid values, when using a radioiodinated antibody in a healthy mouse model. The distribution data is also in general agreement with a SPECT/CT study of directly iodinated, ^{123}I- anti-VEGFR2

antibody that was performed in a mouse arthritis model where rapid clearance was also observed by 24 hours.[33]

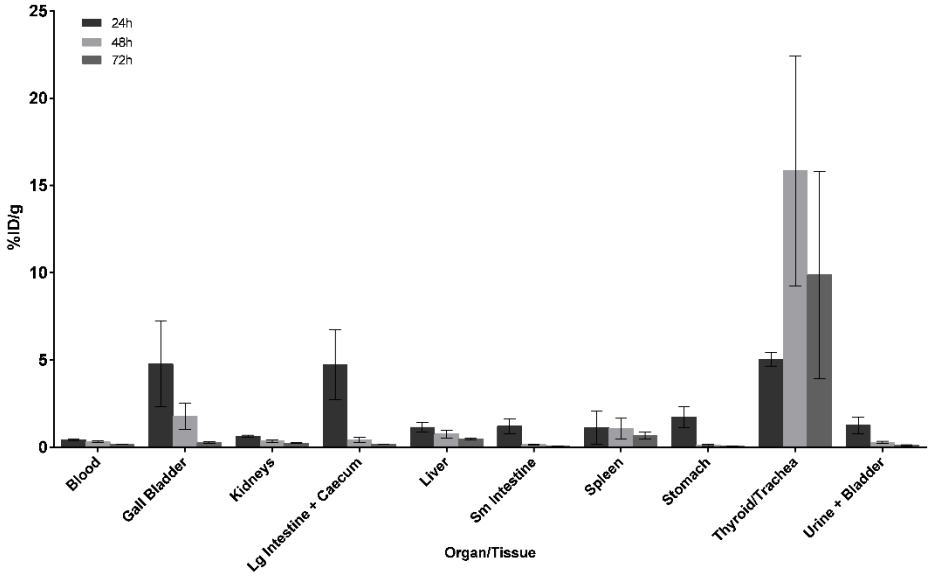

Figure 4-8. Biodistribution of ^{125}I-labelled, anti-VEGFR2 antibody, produced using **4b**, in female C57Bl/6 mice. Mice were injected with ~0.17 MBq and sacrificed at 24, 48 and 72 h post-injection. Data are expressed as percent injected dose per gram of tissue (%ID/g). Uptake levels in all tissues can be found in the Supporting Information.

It is important to note that the iodo-tetrazine can be used for labelling proteins other than antibodies. Smaller proteins are often difficult to iodinate, particularly if they have multiple tyrosine residues. In the case of insulin for example, preparation of ^{125}I-A14-insulin requires extensive HPLC purification of radioactive material to remove impurities that are associated with iodination at other tyrosine residues. As an alternative approach (Scheme 4-4), TCO was added to the ^{1}B-amine of insulin using a trifluoroacetyl-based protecting group strategy,[34] to produce the desired conjugate **12**. Derivatization at the ^{1}B site of

insulin, which is known to have negligible impact on IR binding,[35] was verified by enzyme digestion and LC-MS analysis. The IC_{50} value for **12** was also measured and was identical to that for native insulin determined using a competitive binding assay against ^{125}I-A14-insulin (see Supporting Information). TCO-insulin was subsequently treated with **4b**, which produced the desired product **13** in quantitative yield in under a minute. There was no evidence of any residual starting material in gamma trace and the product formed was again consistent with that observed when using the non-radioactive reference standard.

Scheme 4-4. Synthesis of TCO-insulin **12** and its reaction with ^{125}I-tetrazine **4b**.

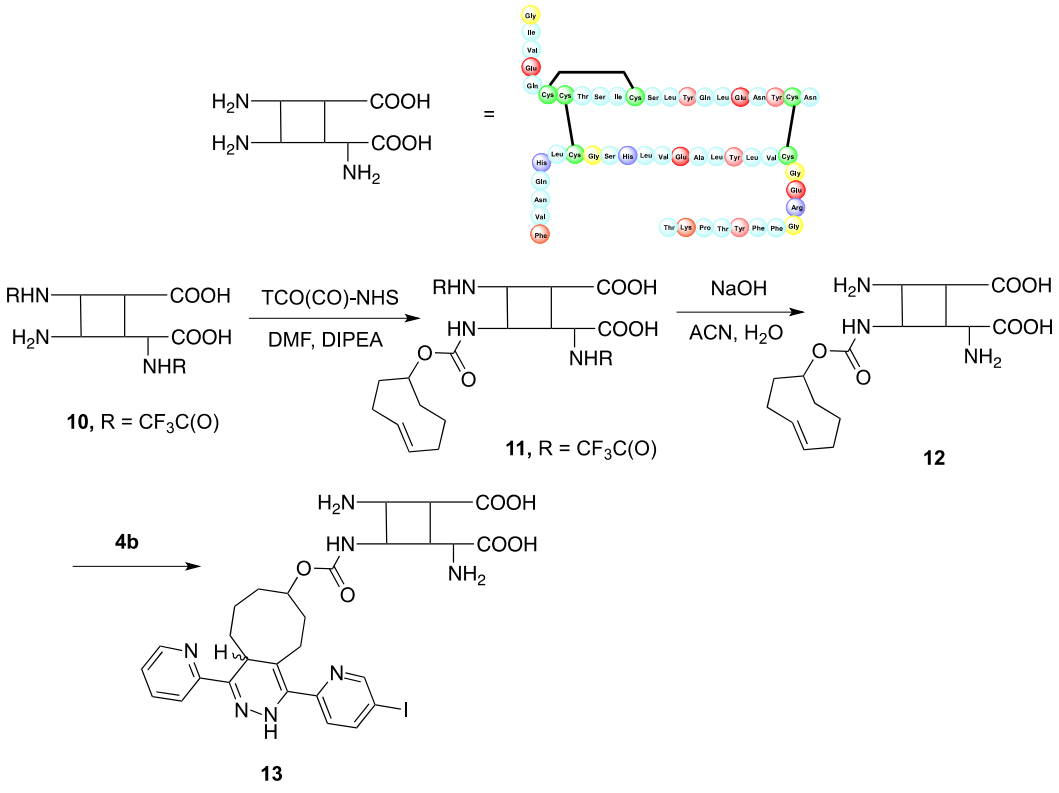

Further evaluation of **13**, a novel ^{125}I-labelled insulin derivative, is ongoing, but there were a number of additional benefits to the ^{125}I-tetrazine

approach to note. Firstly, it was far simpler to isolate the non-radioactive TCO-insulin conjugate **12** than it is to purify the complex mixture that forms during direct oxidative labelling of insulin, which requires extensive chromatography. Secondly, unlike other insulin labelling methods,[35-38] there was no need for additional protecting groups, because of the bioorthogonal nature of the labelling reaction. Furthermore, large quantities of the TCO-insulin precursor can be prepared and stored in a freezer for labelling, on an as needed basis, whereas with directly labelled material, radiolytic degradation results in the product having a limited shelf life.

4.4 Conclusions

A new methodology for labelling biomolecules with ^{125}I was developed using an iodinated tetrazine. The advantage for radiolabelling is provided by a convenient high yielding synthetic method that entails concomitant oxidation that generates the tetrazine and promotes an iododestannylation reaction from a precursor that can be stored for long periods of time. The iodotetrazine reacts rapidly and efficiently with TCO-functionalized proteins, and the products can be used for *in vitro* screening by conventional or flow-based assays, and *in vivo* to assess biodistribution, in preclinical models.

4.5 Experimental

4.5.1 Reagents and general procedure

Unless otherwise stated, all chemicals and reagents were purchased and used as received from Sigma-Aldrich without further purification. Solvents were

purchased from Caledon. 1,3,5,7-Tetramethyl-2,4,8-trioxa-6-phenyl-6-phospha-adamantane was purchased from Cytec Canada (CYTOP-292). Reaction products were monitored using Alugram Sil G/UV_{254} TLC plates and visualized under ultra-violet light. Column chromatography was performed using Silica Flash P60 purchased from Silicycle. ^{125}I was obtained from the McMaster University Nuclear reactor as a 0.1M NaOH solution, [^{125}I]NaI. For labelling experiments, radioactivity was measured using a dose calibrator (Capintec, Ramsey, NJ, USA).

Reactions requiring microwave irradiation were performed using a CEM Discover microwave at 150W. ^{1}H and ^{13}C NMR spectra were recorded on Bruker AV 700 spectrometer. ^{1}H Chemical shifts are reported in ppm relative to the residual proton signal of the NMR solvents. Coupling constants (*J*) are reported in Hertz (Hz). ^{13}C NMR chemical shifts are reported in ppm relative to the carbon signal of the NMR solvents. Mass spectra experiments were performed in a system consisting of a Waters 2695 HPLC coupled to a Water/Micromass Ultima mass spectrometer or a Water/Micromass QToF Global Ultima mass spectrometer for low and high resolution, respectively. For LCMS, a model 966 photodiode array multi-wavelength detector was also used. Reverse phase analytical HPLC was performed using a Varian Prostar instrument equipped with a 355 UV detector, or a Waters 2489 HPLC equipped with a Waters 2489 UV/Vis (λ = 254 nm) and a Bioscan glow count gamma detector (model 106). Elution protocols were as follows: Analytic Method A - Mobile phases composed of 0.08 % TFA in H_2O (A) and 0.08 % TFA in CH_3CN (B), using 0-30 min gradient from 5% B

to 95% B, with a Phenomenex, Gemini-NX column (C18, 110 Å, 4.6 × 250 mm) column, and a flow rate of 1 mL/min; Sem-preparative Method B – Mobile phases, time and gradient same as Method A, but with a Phenomenex, Gemini-C18 11A (250 × 10 mm, 5 micron) column, and a flow rate of 4 mL/min. Analytic Method C – Mobile phases composed of 0.1 % TFA in H_2O (A) and 0.1 % TFA in CH_3CN (B); using 0-25 min gradient from 20% B to 100% B, and a Phenomenex, Gemini-NX column (C18, 110 Å, 4.6 × 250 mm) column and a flow rate of 1 mL/min. Preparative Method D: - Using an Agilent 1200 series system equipped with a photodiode-array detector, an autosampler, a preparative fraction collector and a preparative reverse phase Phenomenex, Gemini-NX column (C18, 110 Å, 21.2 × 250 mm) and a flow rate of 20 mL/min. Mobile phases composed of 0.1 % TFA in H_2O (A) and 0.1 % TFA in CH_3CN (B); using gradient from 20% to 25% B: 0-30 min, then 25% to100% B: 30-40 min.

4.5.2 X-ray Crystallography

A clear purple plate-like sample of **4a**, approximate dimensions 0.029 mm × 0.099 mm × 0.297 mm, was used for the X-ray structure determination. The total exposure time was 3.40 hours. The frames were integrated with the Bruker SAINT software package, using a narrow-frame algorithm. Data were corrected for absorption effects using the numerical method (SADABS). The structure was solved and refined using the Bruker SHELXTL Software Package.

4.5.3 Cells and Culture Methods

H520 (ATCC® HTB-182) cells derived from human squamous cell carcinoma were cultured in RPMI-1640 media. A431 (ATCC® CRL-1555), human epithelial carcinoma cells and MCF-7 (ATCC HTB-22) human adenocarcinoma cells were cultured in DMEM media. All media were supplemented with 10% fetal bovine serum and 1% penicillin streptomycin (Invitrogen, Burlington, ON). The cell lines were maintained at 37 °C and 5% CO_2.

4.5.4 Synthesis of compounds

3-(5-Iodopyridin-2-yl)-6-(pyridin-2-yl)-1,2-dihydro-1,2,4,5-tetrazine (**3**). A vial was charged with picolinonitrile **1** (0.21 g, 2.02 mmol), 2-cyano-5-iodopyridine **2** (0.11 g, 0.48 mmol) and sulfur (0.03 g, 0.93 mmol) and purged with argon. A solution of 64% hydrazine monohydrate (600 µL, 7.89 mmol) and absolute ethanol (2 mL) were added to the vial which was then sealed and heated at 125 °C for 2 hours behind a blast shield. The reaction mixture was cooled to room temperature, the solvent evaporated and the mixture was suspended in water (10 mL) and extracted with dichloromethane (2 × 10 mL). The organic phase was dried over anhydrous magnesium sulfate, filtered and the desired product was isolated by silica gel flash chromatography (using 20% EtOAc in hexanes as the eluent) as an orange solid (0.064 g, 37%). Compound **3** showed: m.p 158-160 °C; R_f 0.38 (20% EtOAc/hexanes); ^{1}H NMR (700 MHz, $CDCl_3$) δ 8.79 (d, J = 1.40 Hz, 1 H), 8.59 (s, 1H), 8.59-8.56 (m, 1H), 8.39 (s, 1H), 8.07 (dd, J = 1.68 Hz, 7.63 Hz, 1H), 8.04 (d, J = 7.98 Hz, 1H), 7.83 (dd, J = 0.49 Hz, 8.40 Hz, 1H), 7.76 (dt,

J = 1.68 Hz, 7.63 Hz, 1H,), 7.36 (ddd, *J* = 0.98 Hz, 4.90 Hz, 7.42 Hz, 1H,); ^{13}C NMR (150 MHz, $CDCl_3$) δ 154.6, 148.5, 147.5, 146.7, 146.6, 146.3, 145.2, 136.9, 125.1, 122.9, 121.5, 95.0; HRMS (*m/z*-ESI$^+$) for $C_{12}H_{10}IN_6^+$ calculated: 365.0012, found: 365.0009.

3-(5-Iodopyridin-2-yl)-6-(pyridin-2-yl)-1,2,4,5-tetrazine (4a). Compound **3** (0.054 g, 0.15 mmol) was dissolved in glacial acetic acid (2 mL) and the solution was cooled to 0 °C. A solution of sodium nitrite (0.068 g, 0.98 mmol) in water (2 mL) was added drop-wise resulting in a colour change from orange to purple. The mixture was stirred for an additional 10 min at room temperature. The pH was adjusted to 11 via the addition of aqueous saturated sodium bicarbonate (10 mL) and the solution extracted with dichloromethane (2 × 15 mL). The organic layers were combined and dried over anhydrous magnesium sulphate and the solvent removed by rotary evaporation. The desired product was isolated by silica gel chromatography (using 65% EtOAc in hexanes as the eluent) and concentrated to afford a bright purple solid (0.049 g, 90%). Compound **4a** showed: m.p. 223-225 °C; R_f = 0.52 (5% MeOH/DCM); ^{1}H NMR (700 MHz, $CDCl_3$) δ 9.19 (dd, *J* = 0.35 Hz, 1.89 Hz, 1H,), 9.01-8.97 (m, 1H,) 8.75 (d, *J* = 7.91 Hz, 1H,), 8.52 (dd, *J* = 0.56 Hz, 8.26 Hz, 1H,), 8.35 (dd, *J* = 2.10 Hz, 8.26 Hz, 1H), 8.02 (dt, *J* = 1.68 Hz, 7.70 Hz, 1H), 7.59 (ddd, *J* = 1.05 Hz, 4.69 Hz, 7.56 Hz, 1 H); ^{13}C NMR (150 MHz, $CDCl_3$) δ 164.0, 163.9, 157.3, 151.3, 150.1, 149.0, 146.1, 137.7, 126.8, 125.8, 124.8, 98.3; HRMS (*m/z*-ESI$^+$) for $C_{12}H_8IN_6^+$ calculated: 362.9855, found: 362.9856.

3-(Pyridin-2-yl)-6-(5-(trimethylstannyl)pyridin-2-yl)-1,2-dihydro-1,2,4,5-tetrazine (5). A solution of 1,1,1,2,2,2-hexamethyldistannane (0.085 g, 0.26 mmol) in dry THF (1 mL) was added to a microwave vial which was evacuated and purged with argon. 1,3,5,7-Tetramethyl-2,4,8-trioxa-(2,4-dimethoxyphenyl)-6-phosphaadamantane (PA-Ph, 4.4 mg, 0.015 mmol) and palladium acetate (1.60 mg, 7.13 µmol) were added to the reaction vessel which was sealed and stirred at room temperature for 5 min. A solution of **3** (0.049 g 0.13 mmol) in THF (0.5 mL) was added under argon. The reaction vessel was heated in the microwave for 30 min at 70 °C. The vessel was cooled to room temperature and the solution treated with saturated aqueous potassium fluoride (1 mL) to quench the reaction. The mixture was extracted with dichloromethane (2 × 10 mL). The organic layers were combine, dried over anhydrous magnesium sulfate, filtered and the solvent removed by rotary evaporation. The desired product was obtained by silica gel chromatography (using 90% ether in pentane as the eluent) and concentrated to afford a yellow solid (0.039 g, 76%). Compound **5** showed: m.p. 73-75 °C; R_f = 0.50 (50% EtOAc/hexanes); ^{1}H NMR (700 MHz, $CDCl_3$) δ 8.56-8.60 (m, 2H), 8.57 (s, 1H), 8.54 (s, 1H), 8.05 (d, *J* = 7.98 Hz, 1H), 7.97 (dd, *J* = 0.91 Hz, 7.70 Hz, 1H), 7.84 (dd, *J* = 1.47 Hz, *J* = 7.70 Hz, 1H), 7.75 (dt, *J* = 1.68 Hz, 7.70 Hz, 1H), 7.34 (ddd, *J* = 1.05 Hz, 4.90 Hz, 7.42, 1H), 0.36 (s, 9H); ^{13}C NMR (150 MHz, $CDCl_3$) δ 154.4 (sat), 154.3, 154.1 (sat), 148.5, 147.7, 147.2, 147.1, 146.8, 144.3 (sat), 144.3, 144.2 (sat), 139.8, 136.9, 125.0, 121.4, 121.1 (sat), 121.0,

120.9 (sat), - 8.3 (sat), -8.4 (sat), -9.3, -10.3 (sat), -10.5 (sat); HRMS (*m/z*-ESI$^+$) for $C_{15}H_{19}N_6Sn^+$ calculated: 403.0693, found: 403.0696.

Reaction of 4a and *trans*-cyclooctene. Tetrazine **4a** (0.014 g, 0.04 mmol) was dissolved in 5% ethanol in 0.05 M PBS buffer (2 mL, pH 7.4) and added to a vial containing *trans*-cyclooctene (8.8 mg, 0.088 mmol) which brought about a colour change (from purple to colourless). The solution was extracted with ethyl acetate (2 × 5 mL) and the organic solvents combined and removed by rotary evaporation. The desired products were obtained by silica gel chromatography (using 10-15% pentane in EtOAc as the eluent) and concentrated to afford a mixture of **6a-9a**.

4-(5-Iodopyridin-2-yl)-1-(pyridin-2-yl)-2,4a,5,6,7,8,9,10-octahydrocycloocta[d]pyridazine (7a) showed: m.p 92-97 °C; R_f = 0.45 (20% EtOAc/hexanes); ^{1}H NMR (700 MHz, $CDCl_3$) δ 8.89 (s, 0.88H), 8.88 (d, *J* = 2.03 Hz, 0.12H), 8.80 (d, *J* = 1.47 Hz, 0.88 H), 8.73(s, 0.1H), 8.73 (s, 0.12H), 8.67-8.62 (m, 0.88H), 8.58-8.55 (m, 0.12 H), 8.17 (dd, *J* = 2.10, 8.26, 0.12 H), 8.05 (dd, *J* = 2.10 Hz, *J* = 8.47 Hz, 0.88 H), 8.05-8.01 (m, 0.12 H), 7.87 (dd, *J* = 0.49 Hz, 8.47 Hz, 0.88 H), 7.84 (dt, *J* = 1.82 Hz, 7.70 Hz, 0.88 H), 7.73 (dt, *J* = 1.61 Hz, 7.74 Hz, 0.12 H), 7.59 (d, *J*= 8.75, 0.88 H), 7.41 (d, *J* = 8.40 Hz, 0.12 H), 7.34, (ddd, *J* = 0.91 Hz, 4.83 Hz, 7.49 Hz, 0.88 H), 7.27 (ddd *J* = 0.84 Hz, 7.70 Hz, 5.11 Hz,7.28 Hz, 0.12 H), 4.43- 4.38 (m, 0.12 H), 4.26-4.36 (m, 0.88 H), 2.84 (ddd, *J* = 2.59 Hz, 8.89 Hz, 15.26 Hz, 0.88 H), 2.79 (ddd, *J* = 2.73 Hz, 9.03 Hz, 15.26 Hz, 0.12 H), 2.10-2.02 (m, 1H), 2.00-1.97 (m, 1H), 1.93-1.87 (m, 1H),

1.78-1.64 (m, 5H), 1.51-1.40 (m, 3H); ^{13}C NMR (150 MHz, CDCN) δ 155.5, 154.6, 153.2, 150.5, 145.4, 142.6, 137.8, 134.9, 125.3, 124.0, 123.4, 112.5, 92.6, 35.5, 31.9, 29.8, 28.2, 27.7, 25.4, 23.3; HRMS (*m/z*-ESI$^+$) for $C_{20}H_{22}IN_4^+$ calculated: 445.0889, found: 445.0904.

1-(5-Iodopyridin-2-yl)-4-(pyridin-2-yl)-2,4a,5,6,7,8,9,10-octahydrocycloocta[d]pyridazine (8a) showed: m.p 92-97 °C; R_f = 0.45 (20% EtOAc/hexanes);.^{1}H NMR (700 MHz, CD_3CN) δ 8.90 (s, 0.65H), 8.87 (d, *J* = 1.47 Hz, 0.35H), 8.79 (d, *J* = 1.47 Hz, 0.65 H), 8.74 (s, 0.35H), 8.67-8.60 (m, 0.65 H), 8.58-8.54 (m, 0.35 H), 8.16 (dd, *J* = 2.17 Hz, 8.33 Hz, 0.35H), 8.04 (dd, *J* = 2.17 Hz, 8.47 Hz, 0.65H), 8.03 (d, *J* = 7.91 Hz, 0.35 H), 7.86 (dd, *J* = 0.49 Hz, 8.54, 0.65 H), 7.84 (dt, *J* = 1.75 Hz, 0.65 H), 7.40 (dd, *J* = 0.28 Hz, 8.26 Hz, 0.35 H), 7.33 (ddd, *J* = 0.91 Hz, 4.83 Hz, 7.49 Hz, 0.65 H), 7.26 (ddd, *J* = 1.05 Hz, 4.90 Hz, 7.35 Hz, 0.35 H), 4.44-4.36 (m, 0.35 H), 4.34-4.27 (m, 0.65 H), 2.83 (ddd, *J* = 2.59 Hz, 8.89 Hz, 15.19 Hz, 0.65 H), 2.79 (ddd, *J* = 2.73 Hz, 8.96 Hz, 15.30 Hz, 0.35 H), 2.11-2.02 (m, 1H), 2.02-1.95 (m, 1H), 1.93-1.85 (m, 1H), 1.79-1.61 (m, 5H), 1.51-1.40 (m, 3H); ^{13}C NMR (150 MHz, CDCN) δ 156.4, 155.5, 155.4, 154.6, 153.2, 152.2, 150.5, 149.6, 146.0, 145.4, 143.7, 142.6, 137.8, 137.2, 134.9, 134.3, 126.9, 125.3, 124.0, 123.8, 123.4, 121.6, 113.5, 112.5, 92.6, 35.9, 35.5, 31.6, 31.9, 29.8, 29.7, 28.2, 28.2, 27.7, 25.3, 25.3, 23.4, 23.2; HRMS (*m/z*-ESI$^+$) for $C_{20}H_{22}IN_4^+$ calculated: 445.0889, found: 445.0904.

1-(5-Iodopyridin-2-yl)-4-(pyridin-2-yl)-5,6,7,8,9,10 hexahydrocycloocta[d]pyridazine (9a) showed: m.p 105-110 °C; R_f = 0.68

(EtOAc); ^{1}H NMR (700 MHz, CD_3CN) δ 8.96 (d, *J* = 2.12 Hz, 1H), 8.74-8.68 (m, 1H) 8.31 (dd, *J* = 2.17 Hz, 8.26 Hz, 1H), 7.95 (dt, *J* = 1.82 Hz, 7.77 Hz, 1H), 7.79 (d, *J* = 7.77 Hz, 1H), 7.67 (d, *J* = 8.19 Hz, 1H), 7.47 (ddd, *J* = 1.05 Hz, 4.83 Hz, 7.77 Hz, 1H), 3.01-2.94 (m, 4 H), 1.77-1.68 (m, 4H), 1.45-1.38 (m, 4H); ^{13}C NMR (150 MHz, CD_3CN) δ 160.4, 159.3, 158.0, 157.0, 155.6, 149.7, 146.4, 141.9, 141.9, 137.9, 127.6, 125.7, 124.5, 94.2, 31.2, 31.1, 27.3, 27.2, 26.8, 26.7; HRMS (*m/z*-ESI$^+$) for $C_{20}H_{19}IN_4^+$ calculated: 443.0733, found: 443.0745

4.5.5 Radiolabelling procedure for 5

A 5 mg/mL solution (5 µL) containing iodogen in 5% acetic acid/acetonitrile was added to a vial containing **5** (10 µL from a 10 mg/mL solution, in acetonitrile). The mixture was combined with aqueous [^{125}I]Na (7 µL, 12.6 MBq) that was obtained from a 0.1M NaOH solution. The mixture was agitated for several seconds by hand and allowed to stand for 5 min. To this was added an additional aliquot (28 µL) of the iodogen solution and left to stand for a further 15 min. The reaction mixture was quenched with aqueous sodium metabisulfite (100 µL, 0.1 M) and extracted with dichloromethane (100 µL). The organic solvent was separated and evaporated by purging the vessel with nitrogen. The resulting residue was dissolved in ethanol or acetonitrile for analysis and purification by HPLC. The desired product was isolated in 80% RCY (10 MBq).

Log P. A 100 µL of solution of **4b** (0.33 MBq) in 20 mM phosphate buffer (pH 7.4) was added to a mixture of n-octanol and phosphate buffer (100 µL of each). The mixture was vortexed for 30 min and centrifuged at 6000 rpm for 10 min.

The organic and aqueous phases were separated and 20 µL of each phase were pipetted into 12 × 75 mm RIA tubes. The counts per minute were determined using a Wallac Wizard 1470 automatic γ counter. The experiment was performed in triplicate giving an average log P of 1.29 ± 0.05

4.5.6 Reaction between 4b and TCO

3.7 MBq of **4b** was dissolved in a mixture of 95% ethanol (5 µL) and PBS buffer (85 µL, pH 7.4) in a micro-centrifuge tube. A freshly prepared solution of *trans*-cyclooctene (10 µL) in ethanol (2 µM) was added to the vial and the mixture agitated by hand for several seconds. The mixture was immediately analyzed by HPLC initially giving rise to three distinct peaks. After approximately 20 min HPLC analysis showed two major peaks corresponding to a mixture of isomers **7b** and **8b** and a peak associated with **9b**.

4.5.7 Kinetic study

The reaction between *trans*-cyclooct-4-enol (TCO-OH) and **4a** was conducted at 25 ± 0.5 °C in a 1-mL UV cuvette, and monitored by UV-Vis spectroscopy at 535 nm. The substrates were dissolved separately in MeOH, mixed together, and spectra acquired every 0.1 seconds over one minute. The kinetics were measured in triplicate for three different concentrations of TCO-OH (8.7×10^{-3}, 11.9×10^{-3}, 14.5×10^{-3} M) against 8.0×10^{-4} M **4a**. The K_{obs}, for each run was determined from a plot of absorbance versus time (Graphpad Prism 5). The average K_{obs} obtained from experiments was determined in triplicate and plotted against the

concentration of TCO-OH to determine the second order rate constant (k_2 = 229 ± 20 $M^{-1}s^{-1}$).

4.5.8 Preparation of TCO-modified anti-VEGFR2 antibody

Anti-VEGFR2 antibody (eBioscience, 14-5821) (1 mL, 500 µg, 3.34 nmol) was added to 6 µL of (E)-cyclooct-4-enyl-2,5-dioxopyrrolidin-1-yl carbonate (TCO(CO)-NHS), (17.8 µg, 66.6 nmol) in DMSO (18 µL). The pH of the solution was adjusted to 9-9.5 by adding Na_2CO_3 (10 µL, 1M). The solution was left on a shaker overnight at 4 °C. The desired product was isolated using an Amicon Ultra-0.5 Centrifugal filter (30 kDa) and washed with PBS three times. The molecular weight of the sample before and after the conjugation was determined by MALDI-TOF MS (MALDI Bruker UltrafleXtreme Spectrometer) indicating an average of 2.8 TCO groups per antibody molecule.

4.5.9 Antibody Labelling

TCO-anti-VEGFR2 (20µL, 10µg) was incubated with **4b** (10 µL, 1.48 MBq) for 20 min in the dark to generate ^{125}I-labelled anti-VEGFR2 antibody: iTLC (VARIAN, SGI0001) was run in a mixture of 75:25 (MeOH:HCl (0.1M)) and scanned on a BIOSCAN AR-2000. A solution containing **4b** (10 µL, 1.48 MBq) in PBS (20 µL) was used as a reference.

4.5.10 Western Blot analysis

20 µg of protein from H520 and A431 cell lysates were loaded on 10% Mini-PROTEAN TGX Precast gels along with molecular weight markers. The protein

extracts fractionated by SDS-PAGE and electro-transferred to polyvinylidene difluoride (PVDF) membranes. As a positive control, select samples were treated with rabbit anti-VEGFR2 primary antibody (Millipore 07-158) in a 1:250 dilution, overnight at 4 °C. After washing the membrane was incubated with goat anti-rabbit secondary antibody (Jackson ImmunoResearch, 111-055- 045) and then a chemiluminescent reagent (ECF substrate, GE RPN5785) was applied for 5 min, and an image collected using a STORM 840 imaging system. The test membrane samples were incubated with the ^{125}I-labelled anti-VEGFR2 construct (0.11 MBq/mL) and negative control membranes were incubated with ^{125}I-labelled tetrazine **4b**, overnight at 4 °C. After washing, the membrane was left to dry before radioactive imaging (Typhoon imaging system).

4.5.11 Flow Chamber Cell Adhesion Assay

8×10^5 of VEGFR2-expressing cells (H520) were plated on 30 mm Corning tissue culture dishes, 2 days prior to assay. They were pre-incubated with TCO-anti-VEGFR2 (30 μg) diluted in PBS (1 mL) for 30 min prior to assay. The parallel-plate flow chamber (Glycotech, Rockville, Md.) was mounted in the culture dish and then inverted to decrease any non-specific binding. Using a syringe pump (PhD 2000, Harvard Apparatus, Holliston, USA) cells were first rinsed with PBS (1 mL), followed by **4b** solution (0.07 MBq/mL) at a flow rate of 0.164 mL/min, which mimics flow conditions in tumor capillaries,[38] and finally washed with PBS (1 mL). Cells were subsequently lysed in 1% Triton-X100 (1 mL) at 37 °C for 30 min. A sample of each cell lysate was taken to measure the amount of activity

using a dose calibrator. Protein levels in cell lysates were determined using a Pierce BCA Protein assay kit (Thermo Scientific, 23225).

4.5.12 Synthesis of Insulin derivatives

Synthesis of $N^{\alpha A1}$,$N^{\varepsilon B29}$-di-*N*-trifluoroacetyl-$N^{\alpha B1}$-TCO-insulin carbamate (11). The protected insulin derivative **10** (100 mg, 17 μmol)[34] was dissolved in anhydrous DMF (2.0 mL). *N*,*N*-Diisopropylethylamine (20 μL) and TCO(CO)-NHS (10 mg, 37 μmol) were added to the solution and the reaction mixture was shaken gently and monitored by HPLC. After 3 h the reaction mixture was diluted with H_2O (15 mL) and purified by HPLC (method D). Lyophilization of the combined fraction gave **11** (49 mg) in 47% yield, 98% purity, and ESI-MS: 6153.0 (calculated: 6151.8). HPLC R_t (Method C) = 13.1 min.

Synthesis of $N^{\alpha B1}$-TCO-insulin carbamate (12). Compound **11** (49 mg, 8 μmol) was dissolved in an ice-cooled solution of 25 mM NaOH (10 mL, ACN/H_2O = 1:3). After 5 h the reaction mixture was diluted with H_2O (20 mL) and purified by HPLC (method D). Lyophilization of the combined fraction afforded the desired product (25 mg, 53% yield) in 98% purity. HRMS (*m/z*-ESI$^+$) $C_{26}6H_{395}N_{65}O_{79}S_6^+$ calculated: 5959.729, found 5959.724. HPLC R_t = 7.2 min (Method C).

Insulin Labelling. A solution of **12** (100 μL, 59 μg) in 6 mM HCl was combined with (0.59 MBq, 10 μL) of **4b** in 10% ethanol in PBS. The mixture was incubated at room temperature and monitored by HPLC (Method C).

4.5.13 Insulin Receptor Binding Assay

Competitive binding assays were conducted in triplicate for **12,** using recombinant human insulin (I2643, Sigma-Aldrich, Canada), as a positive control. MCF-7 cells were plated at a density of 1.0×10^5 or 1.5×10^5 cells per well in a 48 well plate 2 or 3 days (respectively) prior to the assay. At 20 to 24 h prior to start of assay, the wells were rinsed twice with warm PBS and replaced with fresh DMEM containing 10%, charcoal stripped fetal bovine serum (VWR, Mississauga, ON). Wells were rinsed once with warm PBS and the cells were then incubated for 4 hours at 4 °C with 150 µL of 1 nM ^{125}I-insulin (human recombinant (NEX420, PerkinElmer, Woodbridge ON) in the presence of 0 to 1000 nM cold competitor per well with each concentration tested in triplicate. To remove unbound ligand, wells were rinsed 3 times with ice-cold PBS and cells were solubilized with 600 µL of 1N NaOH at 37 °C for 30 min. A 500 µL sample from each well was collected in individual 12×55 mm Ria plastic test tubes (PerkinElmer, Woodbridge ON) and counted for 10 min each, using a Wizard 1470 Automatic Gamma Counter. The resulting CPM values were used to calculate the relative binding for each competition concentration, with respect to CPM obtained in the control run with no competitor. GraphPad Prism 5 software was used to analyse the data and determine the average IC_{50} values.

4.5.14 Biodistribution Studies

Biodistribution of ^{125}I-labelled anti-VEGFR2 antibody was performed using 4-5 week old female C57Bl/6 mice ordered from Charles River Laboratories

(Kingston, NY), (*n* = 3 per time point at t = 24 h, 48 h and 72 h). The mice were administered approximately 0.17 MBq of ^{125}I-labelled anti-VEGFR2 (100 μL in 10% EtOH/PBS) via tail vein injection. Animals were anesthetized with 3% isoflurane and euthanized by cervical dislocation. Blood, adipose, adrenals, bone (femur), brain, eyes, gall bladder, heart, kidneys, large intestine and caecum (with contents), liver, lungs, pancreas, skeletal muscle, small intestine (with contents), spleen, stomach (with contents), thyroid/trachea, urinary bladder with urine and tail were collected, weighed and counted in a Perkin Elmer Wizard 1470 Automatic Gamma Counter. Decay correction was used to normalize organ activity measurements to time of dose preparation for data calculations. Data was expressed as percent injected dose per gram (%ID/g) of tissue or organ.

4.6 Supporting Information

This material can be found in **APPENDIX 2**.

4.7 Acknowledgements

The authors acknowledge the Natural Sciences and Engineering Research Council (NSERC) of Canada and the Ontario Institute for Cancer Research (OICR), for financial support of this work. These funding sources were not directly involved in the research, writing, or submission of this manuscript. The authors also thank Dr. Denis Snider who provided medical/scientific proof-reading and editing in preparation of this manuscript.

Notes: The authors declare no competing financial interest.

Non-standard Abbreviations:

BCS: bioorthogonal coupling strategies; TCO: *trans*-cyclooctene; TCO-OH: *trans*-cyclooct-4-enol; ID: injected dose; PA-Ph: 1,3,5,7-tetramethyl-2,4,8-trioxa-6-phenyl-6-phospha-adamantane.

4.8 References

(1) Boado, R. J.; Hui, E. K.; Lu, J. Z.; Sumbria, R. K.; Pardridge, W. M. *Bioconjugate Chem.* **2013**, *24*, 1741-9.

(2) Fiechter, M.; Frey, K.; Fugmann, T.; Kaufmann, P. A.; Neri, D. *Atherosclerosis* **2011**, *214*, 325-30.

(3) Pruszynski, M.; Koumarianou, E.; Vaidyanathan, G.; Revets, H.; Devoogdt, N.; Lahoutte, T.; Zalutsky, M. R. *Nucl. Med. Biol.* **2013**, *40*, 52-9.

(4) Teghanemt, A.; Weiss, J. P.; Gioannini, T. L. *J. Innate Immun.* **2013**, *19*, 545-60.

(5) Vugmeyster, Y.; DeFranco, D.; Szklut, P.; Wang, Q.; Xu, X. *J. Pharm. Sci.* **2010**, *99*, 1028-45.

(6) Wall, J. S.; Richey, T.; Stuckey, A.; Donnell, R.; Oosterhof, A.; van Kuppevelt, T. H.; Smits, N. C.; Kennel, S. J. *Nucl. Med. Biol.* **2012**, *39*, 65-75.

(7) Chen, J.; Wang, M.; Joyce, A.; DeFranco, D.; Kavosi, M.; Xu, X.; O'Hara, D. M. *Pharm. Res.* **2014**, *31*, 2810-21.

(8) Bolton, A. E.; Hunter, W. M. *Biochem. J.* **1973**, *133*, 529-39.

(9) Lee, J.; Coleman, R. E.; Sherman, L. A. *J. Lab. Clin. Med.* **1977**, *89*, 836-44.

(10) Visser, G. W.; Klok, R. P.; Gebbinck, J. W.; ter Linden, T.; van Dongen, G. A.; Molthoff, C. F. *J. Nucl. Med.* **2001**, *42*, 509-19.

(11) Lang, K.; Chin, J. W. *ACS Chem. Biol.* **2014**, *9*, 16-20.

(12) Patterson, D. M.; Nazarova, L. A.; Prescher, J. A. *ACS Chem. Biol.* **2014**, *9*, 592-605.

(13) Rossin, R.; Robillard, M. S. *Curr. Opin. Chem. Biol.* **2014**, *21C*, 161-169.

(14) Rossin, R.; van Duijnhoven, S. M.; Lappchen, T.; van den Bosch, S. M.; Robillard, M. S. *Mol. Pharm.* **2014**, *11*, 3090-96.

(15) Denk, C.; Svatunek, D.; Filip, T.; Wanek, T.; Lumpi, D.; Frohlich, J.; Kuntner, C.; Mikula, H. *Angew. Chem. Int. Ed.* **2014**, *53*, 9655-9.

(16) Herth, M. M.; Andersen, V. L.; Lehel, S.; Madsen, J.; Knudsen, G. M.; Kristensen, J. L. *Chem. Commun.* **2013**, *49*, 3805-7.

(17) Li, Z.; Cai, H.; Hassink, M.; Blackman, M. L.; Brown, R. C.; Conti, P. S.; Fox, J. M. *Chem. Commun.* **2010**, *46*, 8043-5.

(18) Nichols, B.; Qin, Z.; Yang, J.; Vera, D. R.; Devaraj, N. K. *Chem. Commun.* **2014**, *50*, 5215-7.

(19) Rossin, R.; Verkerk, P. R.; van den Bosch, S. M.; Vulders, R. C.; Verel, I.; Lub, J.; Robillard, M. S. *Angew. Chem. Int. Ed.* **2010**, *49*, 3375-8.

(20) Sletten, E. M.; Bertozzi, C. R. *Acc. Chem. Res.* **2011**, *44*, 666-76.

(21) Zeglis, B. M.; Mohindra, P.; Weissmann, G. I.; Divilov, V.; Hilderbrand, S. A.; Weissleder, R.; Lewis, J. S. *Bioconjugate Chem.* **2011**, *22*, 2048-59.

(22) Zeglis, B. M.; Sevak, K. K.; Reiner, T.; Mohindra, P.; Carlin, S. D.; Zanzonico, P.; Weissleder, R.; Lewis, J. S. *J. Nucl. Med.* **2013**, *54*, 1389-96.

(23) Devaraj, N. K.; Weissleder, R. *Acc. Chem. Res.* **2011**, *44*, 816-27.

(24) Blackman, M. L.; Royzen, M.; Fox, J. M. *J. Am. Chem. Soc.* **2008**, *130*, 13518-9.

(25) Ahrens, B.; Jones, P. G. *Acta Crystallogr. Sect. C* **1999**, *55*, 1308-1310.

(26) Klein, A.; McInnes, E. J. L.; Scheiring, T.; Zalis, S. *J. Chem. Soc. Faraday T* **1998**, *94*, 2979-2984.

(27) Ahmed, N. A.; Jones, P. G. *Acta Crystallogr. Sect. B* **1972**, *28*, 739-742.

(28) Zhou, Q.; Audebert, P.; Clavier, G.; Meallet-Renault, R.; Miomandre, F.; Shaukat, Z.; Vu, T. T.; Tang, J. *J. Phys. Chem. C* **2011**, *115*, 21899-21906.

(29) McIntee, J. W.; Sundararajan, C.; Donovan, A. C.; Kovacs, M. S.; Capretta, A.; Valliant, J. F. *J. Org. Chem.* **2008**, *73*, 8236-43.

(30) Wilson, A. A.; Jin, L.; Garcia, A.; DaSilva, J. N.; Houle, S. *Appl. Radiat. Isot.* **2001**, *54*, 203-8.

(31) Karver, M. R.; Weissleder, R.; Hilderbrand, S. A. *Bioconjugate Chem.* **2011**, *22*, 2263-2270.

(32) Zlitni, A.; Janzen, N.; Foster, F. S.; Valliant, J. F. *Angew. Chem. Int. Ed.* **2014**,*53*, 6459-63.

(33) Kim, S. M.; Choi, N.; Song, Y.; Cho, G.; Bang, J.; Kim, S. M.; Lee, S. H.; Ryu, E. K. *B. Korean Chem. Soc.* **2012,** *33*, 1890-1894.

(34) Liu, F.; Kohn, W. D.; Mayer, J. P. *J. Pept. Sci.* **2012**, *18*, 336-341.

(35) Guenther, K. J.; Yoganathan, S.; Garofalo, R.; Kawabata, T.; Strack, T.; Labiris, R.; Dolovich, M.; Chirakal, R.; Valliant, J. F. *J. Med. Chem.* **2006**, *49*, 1466-1474.

(36) Iozzo, P.; Osman, S.; Glaser, M.; Knickmeier, M.; Ferrannini, E.; Pike, V. W.; Camici, P. G.; Law, M. P. *Nucl. Med. Biol.* **2002**, *29*, 73-82.

(37) Kim, D. H.; Blacker, M.; Valliant, J. F. *J. Med. Chem.* **2014**, *57*, 3678-86.

(38) Sundararajan, C.; Besanger, T. R.; Labiris, R.; Guenther, K. J.; Strack, T.; Garafalo, R.; Kawabata, T. T.; Finco-Kent, D.; Zubieta, J.; Babich, J. W.; Valliant, J. F. *J. Med. Chem.* **2010**, *53*, 2612-21.

(39) Jain, R. K. *Cancer Res.* **1988**, *48*, 2641-58.

Chapter 5 - A Second Fluorous Analogue of Chloramine-T: A Metal-Free and Recyclable Reagent for Recovering Sulfur from H_2S

5.1 Abstract

A new fluorous derivative of chloramine-T that is more soluble in perfluorinated solvents than our first generation agent FCAT (Chapter 3) has been prepared in 46% overall yield and fully characterized. This oxidant was employed successfully for a metal-free oxidation of bisulfide (HS^-) to elemental sulfur, and the sulfur recovered by centrifugation. The oxidant was easily regenerated with aqueous NaOCl in less than 15 min. The regenerated oxidant was reused and subsequently regenerated, where at least 95% of the oxidant was recovered after 12 cycles. The work reported demonstrates that the fluorous oxidants have utility beyond the field of radiochemistry.

5.2 Introduction

Hydrogen sulfide (H_2S) is a major contaminant of natural gas and oil deposits.[1,2] Methods for removing the highly toxic material include the Claus process, direct oxidation, and liquid-redox processes.[3–5] The latter are based on catalytic reactions which utilize transition metals. The Stretford process, for example, employs vanadium (V) to oxidize H_2S to sulfur where the resulting V^{4+} species is reoxidized using oxygen in the presence of anthraquinone-disulfonic

acid (ADA). The LO-CAT® technology, which remains in widespread use, utilizes chelated iron to promote the formation of sulfur where oxygen is also used to reoxidize the catalyst.[3,5]

There are a number of issues with using transition metal catalysts notably they are costly, have finite stability and they can contaminate product and waste streams. The latter increases the costs of disposal and requires the catalyst to be continually replaced. An additional concern is that the catalyst can contaminate the product sulfur reducing its quality.[6] While significant effort has been made to find the ideal metal catalyst for liquid desulfurization systems, attempts to develop transition metal-free liquid-redox systems for processing hydrogen sulfide have been limited.

Bendal *et al.* reported nearly 70 years ago that chloramine-T at alkaline pH efficiently converts H_2S to elemental sulfur.[7] Unfortunately, chloramine-T would be unsuitable for industrial processes since regenerating the oxidant would require treating solutions rich in sulfide with a chlorinating agent such as bleach, which would promote the formation of sulfate and thiosulfate. An alternative approach could be through the use of fluorous biphasic catalysis (FBC).[8–10] FBC takes advantage of the fact that fluorine rich compounds dissolve selectively in perfluorinated solvents, which are not miscible with water and most organic solvents. This feature makes it possible to separate a fluorous catalyst or reagent from non-fluorous reagents and products. As an example, FBC has been used to

promote trans-esterification through the use of fluoroalkyldistannoxane catalysts giving rise to nearly quantitative yields of product.[8]

We envisioned a biphasic system in which buffers used in conventional liquid-redox processes would be combined with perfluorinated solvents containing a fluorous analogue of chloramine-T (Figure 5-1). Upon formation of sulfur and the reduction of the oxidant, the fluorous layer would be collected, treated with inexpensive and readily available chlorinating agent such as bleach to regenerate the oxidant which would then be recombined with the sulfide-containing buffer. Herein we report the preparation and characterization of a new fluorous oxidant and an assessment of its potential utility in a fluorous biphasic metal-free liquid-redox desulfurization process.

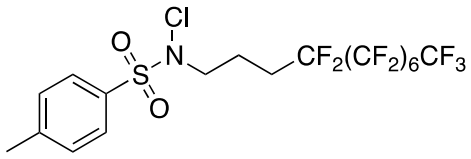

Figure 5-1. Fluorous chloramine-T, *N*-chloro-*N*-(4,4,5,5,6,6,7,7,8,8,9,9,10,10,11,11,11-heptadecafluoroundecyl)-4-methylbenzenesulfonamide (F-CAT).

5.3 Results and Discussion

In chapter 3 we reported the preparation of a fluorous analogue of chloramine-T (F-CAT, Figure 5-1) as an oxidant for radioiodination reactions.[11] Initial test reaction between F-CAT (0.75 mmol) and Na_2CO_3/$NaHCO_3$ buffer solution (pH = 9.5) containing sodium sulfide (0.71 mmol), resulted in immediate formation of a light yellow solid. The material that was thought to be sulfur was

collected by centrifugation. Analysis by Raman spectroscopy (Figure 5-2) showed the presence of peaks consistent with an authentic sample of elemental sulfur including 150 and 215 cm^{-1} which are the bending and stretching modes of the 8-membered ring, and a third strong peak at 470 cm^{-1} corresponding to the vibration of the S–S bond.[12] However the material was also contaminated with the reduced form of F-CAT.

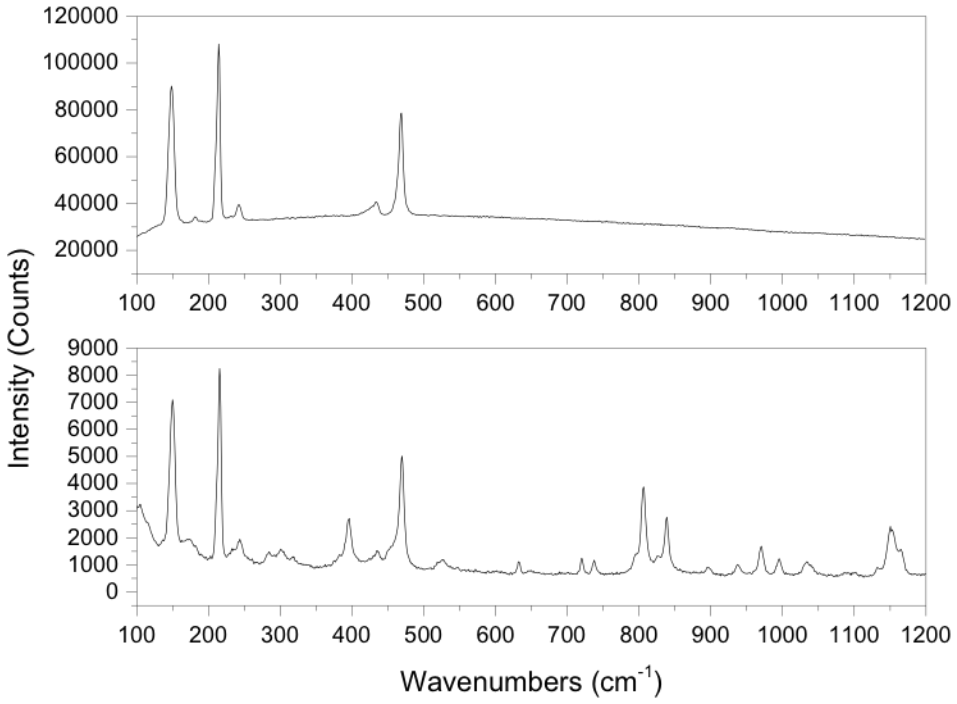

Figure 5-2. Raman spectrum of: (top) authentic elemental sulfur sample; (bottom) product produced from the F-CAT process. Peaks at 150, 215, and 470 cm^{-1} correspond to elemental sulfur vibrational modes. Peaks at 806, 838, 1148 and 1154 cm^{-1} correspond to F-CAT and its reduced form.

The presence of the reduced form of F-CAT was unexpected given the presence of FC-72. The solubility of F-CAT and the reduced form were tested where the maximum values in FC-72 were 0.6 mg/mL, and 0.1 mg/mL

respectively. The lower solubility of the reduced form was problematic in that it limited the maximum amount of oxidant that can be used for a given volume of solvent. The ability of compounds to dissolve in perfluorinated solvents is largely dictated by their fluorine content.[13–15] Consequently to address the issue, a more soluble second generation F-CAT, (referred to as F-CAT2), was developed.

To create a more fluorophilic reagent, a chloramine-T analogue with an additional fluorous chain attached to the aryl ring was prepared. Heptadecafluorooctylbenzene **3** was synthesized from commercially available iodobenzene **1** and perfluorooctyl iodide **2** in the presence of copper powder (Scheme 5-1).[16] The desired product **3** was isolated in 91% yield by silica gel chromatography. The ^{1}H NMR of the product showed two sets of multiplets; one at 7.58 ppm and the other at 7.50 ppm, which are consistent with the structure. ^{13}C NMR analysis revealed a triplet due to C-F coupling at 129.2 ppm, which was shown to be the ipso carbon atom of the aryl ring ($^{2}J_{CF}$ = 48 Hz). The *ortho* carbon atoms showed a similar splitting pattern, but with a smaller coupling constant ($^{3}J_{CF}$ = 12 Hz). The identity of compound **3** was further confirmed by HRMS (EI^{+}) with an observed *m/z* value of 496.0113 (calculated value = 496.0120).

Scheme 5-1. Scheme for preparation of **7**.

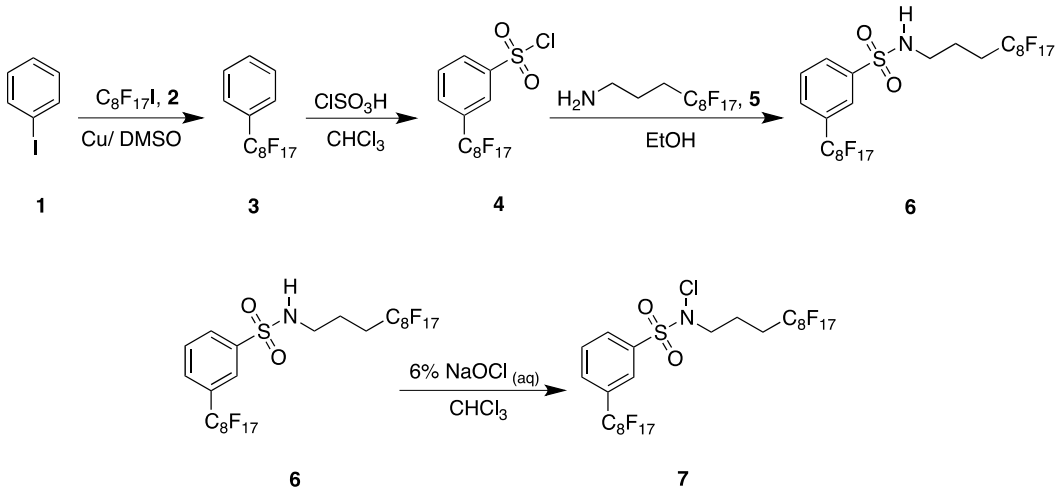

Preparation of the sulfonyl chloride **4** was accomplished by treating **3** dissolved in $CHCl_3$ with chlorosulfonic acid at 0 °C. After the initial evolution of gas ceased the reaction was warmed to RT and stirring continued overnight. The desired product was isolated by silica gel chromatography as a white crystalline solid in good yield (79%). ^{1}H NMR analysis showed that the substitution occurred exclusively at the *meta* position. Synthesis of the fluorous sulfonamide was accomplished by adding an excess of the fluorous amine **5** to a solution of **4** in EtOH.[11] After 30 min the desired sulfonamide, **6** was isolated by silica gel chromatography as a crystalline white compound in 59% yield. The ^{1}H NMR data was consistent with the desired product, where the chemical shift of the sulfonamide proton appears at 6.97 ppm as a triplet. In the IR spectrum, the N-H vibrational stretch occurred at 3276 cm^{-1} which is within the range of the N-H stretches observed for similarly reported *N*-alkyl sulfonamides.[11,17,18] HRMS (ESI^+) of **6** showed an *m/z* value of 1053.0317 where the calculated value was

1053.0311, further confirming the identity of the sulfonamide.

N-chlorination was performed following the method we used previously to generate F-CAT.[11] Compound **6** dissolved in chloroform was treated with an aqueous solution of 6% (w/v) NaOCl to yield the desired *N*-chlorosulfonamide **7** in quantitative yield. The signal corresponding to the sulfonamide proton in **6** (6.97 ppm) was absent in the product and there was a downfield shift of the adjacent methylene group signal upon conversion to **7**. In the ^{13}C NMR spectrum, the methylene carbon adjacent to the sufonamide similarly shifted downfield and the IR spectrum of **7** showed no peaks corresponding to the previously observed N-H stretch.

The solubility of **7** (oxidant) and **6** (reduced form) in FC-72 were evaluated and found to be 5 mg/mL and 1.2 mg/mL respectively. Though not ideal it was a marked improvement over FCAT consequently an evaluation of the ability of **7** to produce sulfur was assessed. Compound **7** was dissolved in FC-72 (0.200 g, 20 mL) and added to an excess (11 equivalences) of sodium bisulfide in $Na_2CO_3/NaHCO_3$ buffer (pH = 9.5) and the mixture stirred vigorously. After 5 min, an interfacial solid formed while the aqueous layer turned yellow in colour. The fluorous layer was subsequently separated and added to an aqueous NaOCl (6% w/v) and reoxidation of the sulfonamide **6** to **7** was monitored by TLC. The process was completed in less than 15 min. The formation of the recycled oxidant was confirmed by ^1H NMR and IR. The FC-72 layer was subsequently returned to the bicarbonate/carbonate buffer and the cycle repeated. Ultimately the yellowish

sulfide solution decolourized completely after 12 cycles which is evidence of consumption of all residual sulfide.

The amount of fluorous sulfonamide recovered after the last cycle was 95% with the loss due to the small amount of reagent used. ^{1}H NMR analysis of **7** after the 11 cycles showed no signs of oxidant degradation. One advantage of using fluorine substituted compounds is that they are known to be resistant to oxidation, and bacterial and radical degradation compared to hydrocarbon based analogues.[19–22] The amount of sulfur recovered from this process was 58 mg which was 89% of the expected amount of sulfur; with some of the sulfur lost in the various transfers between the reaction vessels. Raman spectroscopy of the product showed pure material which was confirmed by energy dispersive spectroscopy (EDS). EDS showed a dominant sulfur peak with additional solvent impurities non-of which were associated with the oxidant as there was no evidence of fluorine present.

To test the feasibility of establishing a continuous oxidation-FCAT-2-regeneration system, different reaction setups were evaluated. One simple approach that has been used with fluorous biphasic catalysis is to use a U-tube reaction vessel in which reagents dissolved in organic or aqueous solutions are separated by an FC-72 solution containing a fluorous reagent. To this end an analogous system was evaluated for sulfide processing where in one arm of a U-tube reactor, NaHS was dissolved in the $NaHCO_3/Na_2CO_3$ buffer and combined with the oxidant **7** dissolved in FC-72 (Figure 5-3). On the opposite side of the

vessel, aqueous NaOCl was added to provide a reagent to regenerate the oxidant once the reduced product is formed. A magnetic stirring bar was placed in the FC-72 layer to facilitate mixing at the interfaces.

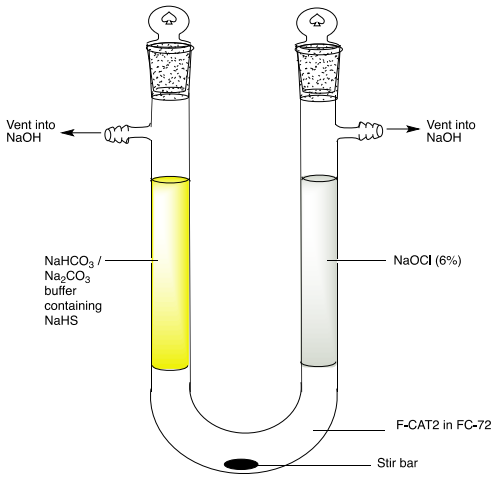

Figure 5-3. A system for continuous reduction of sulfide. The "left arm", which contains NaHS in aqueous buffer, is separated from the "right arm" of $NaOCl_{(aq.)}$ to regenerate the oxidant, by an FC-72 solution containing the fluorous oxidant.

Upon mixing, there was immediate evidence of the formation of an interfacial solid between the bicarbonate-carbonate solution and the FC-72 phase. The mixture was allowed to stir over the course of a week during which time the colour of the NaHS layer remained light yellow. The solid which had formed was collected (8 mg) and was identified as sulfur which was 53% of theoretical value. The amount of sulfur present represents more than one cycle which would have produced 1.5 mg of product. This suggests that a minimum number of 5 cycles had occurred during the week. The buffer was analyzed by UV-Vis spectrometry where there was an intense absorbance at 360 nm which indicated the presence of unreacted reduced sulfur in the form of polysulfide.[23,24] Polysulfides are produced

by partial oxidation of bisulfide[23] consequently their presence along with the low sulfur yield suggested that there was inefficient mixing of the reagents or ineffective recycling of the sulfonamide. ^{1}H NMR analysis of the FC-72 layer revealed that it was composed of 13% of **7** and 87% of the sulfonamide **6**. When this solution was treated with bleach and the mixture stirred vigorously the residual amount of **6** readily converted to **7** in quantitative yield. These results, along with the highly efficient conversion observed from the manual batch process suggests that if a more efficient system for mixing the FC-72 solution with bleach can be designed, a continuous process approach is feasible. [25–27]

The fluorous system reported here can efficiently convert hydrogen sulfide to sulfur and the oxidant regenerated with bleach. Interestingly the overall reaction produces HCl as the byproduct (Figure 5-4) which can be used to generate bleach through treatment with ozone.[28] In the Stretford process the byproduct of oxidation is water which must ultimately be disposed of and has no intrinsic value making the system one that can be regarded as being an atom inefficient process.

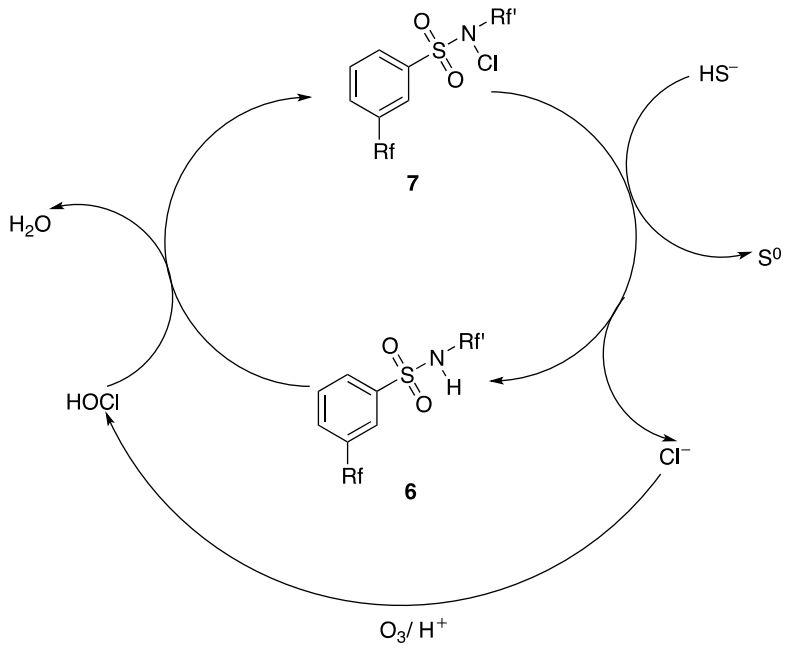

Figure 5-4. Potential mechanistic scheme for oxidation of HS^- to S^0 by **7** and subsequent regeneration of the fluorous oxidant from **6**. The HCl formed can be oxidized[28] to hypochlorite ions by ozone (O_3). Rf = C_8F_{17} and Rf′ = $CH_2CH_2C_8F_{17}$.

The potential limitation of the current system is the need to use fluorous solvents which are costly and potentially have environmental concerns. However, if the lifetime of the catalyst in FC-72 is long and its presence in the product sulfur stream minimized, the need to replenish the solvent can be minimized and additional cost savings found. It should also be noted that due to the increasing use and sources of fluorous solvents costs are decreasing.[29] The current focus is to construct a continuous operating system to assess the ability of the approach to generate larger quantities of sulfur and to evaluate the extent of formation of oxidized sulfur specifies over time.

5.4 Conclusion

A new fluorous oxidant was prepared and characterized and its use as an oxidant to convert bisulfide to sulfur assessed. In a batch biphasic process F-CAT2 was able to effectively convert all of the bisulfide present to sulfur and the catalyst was readily recovered and recycled through treatment with bleach. A "triphasic" system was explored which showed that it was possible to generate a continuous system though additional optimization is needed.

5.5 Experimental

5.5.1 Reagents and general procedures

Unless otherwise stated, all chemical reagents were purchased and used as received from Sigma-Aldrich, without further purification. FC-72 was purchased from 3M, while SiliaFlash® P60 Silica gel from SiliCycle was used for silica gel chromatography. Thin-layer chromatography plates (Merck F254 silica gel on aluminum) were visualized using ultraviolet (UV) light.

5.5.2 Instrumentation

Nuclear magnetic resonance (NMR) spectra were recorded using a Bruker DRX-600 spectrometer with chemical shifts reported as δ values in parts per million (ppm) relative to the residual proton signal of the deuterated solvent or the carbon signal of the solvent. ^{13}C NMR chemical shifts of perfluorinated carbon chains [$(CF_2)_n$] were not reported due to the J_{CF} of up to four bonds distances resulting in the signals appearing as a series of multiplets. Infrared (IR) spectra were acquired using a Nicolet 6700 FT-IR spectrometer. Low-resolution mass spectra were

obtained on an Agilent 630 ion trap electron spray ionization (ESI) instrument, using a Waters 1200 series LC system. High-resolution mass spectra (HRMS) were obtained using a Waters Micromass Global Ultima Q-TOF in ESI mode. Melting points were determined using a DigiMelt apparatus (Sanford Research Systems, USA). Raman spectroscopy was performed with a Renishaw Invia mapping Dispersive Raman system furnished with an argon ion laser (514 nm, green) and solid state laser (785 nm, red) and equipped with a Leica microscope, with 5, 20 and 50× objectives. Ultraviolet absorption spectra were recorded on a Varian Cary 50 UV-Visible spectrophotometer. Energy dispersive spectroscopy (EDS) was performed using a JEOL 700F Scanning Electron Microscope equipped with an OXFORD Instruments Aztec Energy Dispersive Spectroscope at the Canadian Centre for Electron Microscopy, McMaster University (Hamilton, ON).

5.5.3 Synthesis of primary compounds 3, 4, 6 and 7

Heptadecafluorooctylbenzene (3) Iodobenzene **1** (0.535 g, 2.62 mmol) was weighed into a flame dried round bottom flask equipped with a magnetic stir bar. Heptadecafluoro-1-iodooctane **2** (1.572 g, 2.88 mmol) was added followed by copper powder (0.399 g, 6.28 mmol) and the flask purged with argon for 5 min. Dry DMSO (3 mL) was added under argon and the reaction mixture heated to reflux overnight with stirring. On completion of the reaction, which was determined by TLC (n-hexane:EtOAc, 10:1 v/v), H_2O (20 mL) was added and the solution transferred to a separatory funnel. The solution was extracted with DCM

(3×15 mL) and the combined organic layers passed through a small plug of silica in a pasteur pipette to remove residual copper. The filtrate was then extracted with FC-72, and the FC-72 layer subsequently concentrated under reduced pressure. The product was isolated by silica gel column chromatography using a gradient of 0-5% n-hexane:EtOAc. The fractions containing the product were combined and the solvent was removed to afford **3** as a colourless oil. Yield (1.183 g, 91%); ^{1}H NMR (600 MHz, $CDCl_3$) δ 7.60-7.57 (m, 3H), 7.52-7.49 (m, 2H); ^{13}C NMR (150 MHz, $CDCl_3$) δ 132.1, 129.2 (t, $^{2}J_{CF}$ = 48 Hz), 128.8, 127.0 (t, $^{3}J_{CF}$ = 12 Hz); HRMS (ESI^+) *m/z* calcd. for $C_{14}H_5F_{17}$ $[M]^+$ 496.0120; found 496.0113.

3-Heptadecafluorooctylbenzenesulfonyl chloride (4)

Heptadecafluorooctylbenzene **3** (1.100 g, 2.22 mmol) was weighed into a flame dried round bottom flask equipped with a magnetic stir bar. $CHCl_3$ (3 mL) was added and the solution cooled to 0 °C in an ice-bath. Chlorosulfonic acid (2 mL) was added dropwise with stirring at 0 °C. After 30 min, the reaction was warmed to RT and allowed to stir overnight. On completion of the reaction which was determined by TLC (n-hexane:EtOAc, 10:1 v/v), the solution was diluted with $CHCl_3$ (10 mL) and added dropwise in to ice water in a separatory funnel. $CHCl_3$ (10 mL) was added, the organic layer collected and combined with two additional $CHCl_3$ extractions (2×15 mL). The combined organic layers were washed with brine, dried with $MgSO_4$ and concentrated under reduced pressure. The product was isolated by silica gel column chromatography using a gradient of 5-20% n-hexane:EtOAc. The fractions containing the product were combined and the

solvent was removed to afford **4** as a pale yellow crystalline solid. Yield (1.043 g, 79%); mp (61-63 °C); FTIR (KBr) 3085, 1381, 1147, cm^{-1}; ^{1}H NMR (600 MHz, $CDCl_3$) δ 8.29-8.27 (m, 2H), 7.98 (d, *J* = 7.9 Hz, 1H), 7.84 (t, *J* = 7.9 Hz, 1H); ^{13}C NMR (150 MHz, $CDCl_3$) δ 145.3, 133.5, 131.3 (t, $^{2}J_{CF}$ = 50 Hz), 130.7, 130.6, 125.8; HRMS (ESI^{+}) *m/z* calcd for $C_{14}H_4ClF_{17}O_2S$ $[M]^{+}$ 593.9349, found: 593.9375.

***N*-(4,4,5,5,6,6,7,7,8,8,9,9,10,10,11,11,11-heptadecafluoroundecyl)-3-(heptadecafluorooctyl)benzenesulfonamide (6)**

3-Heptadecafluorooctylbenzenesulfonyl chloride **4** (0.500 g, 0.84 mmol) was weighed into a 20 mL round bottom flask equipped with a magnetic stir bar. Ethanol (4 mL) was added and the suspension stirred until **4** was completely dissolved. A solution of 4,4,5,5,6,6,7,7,8,8,9,9,10,10,11,11,11-heptadecafluoroundecan-1-amine **5** (0.802 g, 1.68 mmol) in EtOH (1 mL) was added with stirring, followed by addition of TEA (0.5 mL). The initial colorless reaction mixture turned milky after a few minutes. Stirring was continued until the reaction was complete as determined by TLC (n-hexane:EtOAc, 3:1 v/v). The mixture was subsequently concentrated under reduced pressure and the desired product isolated by silica gel column chromatography using a gradient of 10-30% n-hexane:EtOAc. The fractions containing the product were combined and the solvent was removed to afford **6** as a white crystalline solid. Yield (0.565 g, 65%); mp 106-108 °C; FTIR (KBr) 3276, 1435, 1366, 1159 cm^{-1}; ^{1}H NMR (600 MHz, Acetone-d_6) δ 8.23 (d, *J* = 7.9 Hz, 1H), 8.14 (s, 1H), 8.02 (d, *J* = 7.9 Hz, 1H), 7.94

(t, J = 7.9 Hz, 1H), 6.97 (t, J = 6.0 Hz, 1H), 3.18 (q, J = 7.2 Hz, 2H), 2.32-2.22 (m, 2H), 1.82-1.77 (m, 2H); ^{13}C NMR (150 MHz, Acetone-d_6) δ 143.5, 131.9, 131.6, 131.5, 130.2 (t, $^{2}J_{CF}$ = 49 Hz), 125.9, 42.9, 28.6 (t, $^{2}J_{CF}$ = 44 Hz), 21.5; HRMS (ESI$^+$) *m/z* calcd for $C_{25}H_{15}N_2O_2SF_{34}$ $[M+NH_4]^+$ 1053.0311, found: 1053.0317.

***N*-Chloro-*N*-(4,4,5,5,6,6,7,7,8,8,9,9,10,10,11,11,11-heptadecafluoroundecyl)-3-heptadecafluorooctylbenzenesulfonamide (7)** The sulfonamide **6** (0.500 g, 0.48 mmol) was dissolved in $CHCl_3$ (10 mL) in a 50 mL round bottom flask equipped with a stir bar. Aqueous NaOCl (6% w/v, 10 mL) was added and the biphasic reaction mixture stirred vigorously at room temperature. Stirring was continued until the reaction was complete (monitored by TLC using 3:1 v/v hexane:EtOAc). The reaction mixture was transferred into a separatory funnel and the $CHCl_3$ layer separated and the aqueous layer extracted with $CHCl_3$ (3 × 5 mL). The combined organic layers were dried over anhydrous Na_2SO_4 and concentrated by rotary evaporation to afford a white solid. Yield (0.530 g, 98%); mp 87-89 °C; FTIR (KBr) 2923, 1595, 1364, 1148 cm^{-1}; ^{1}H NMR (600 MHz, $CDCl_3$) δ 8.18 (d, J = 7.9 Hz, 1H), 8.16 (s, 1H), 7.96 (d, J = 7.9 Hz, 1H), 7.81 (t, J = 7.9 Hz, 1H), 3.38 (t, J = 6.3 Hz, 2H), 2.26-2.17 (m, 2H), 2.05-2.01 (m, 2H); ^{13}C NMR (150 MHz, $CDCl_3$) δ 134.2, 133.0, 132.8, 130.8 (t, $^{2}J_{CF}$ = 50), 130.1, 128.1, 55.6, 27.8 (t, $^{2}J_{CF}$ = 44), 18.5; HRMS (ESI$^+$) *m/z* calcd for $C_{25}H_{14}N_2O_2SF_{34}Cl$ $[M+NH_4]^+$ 1086.9922, found: 1086.9946.

5.5.4 Oxidation of NaSH to Sulfur by F-CAT2

Sodium bisulfide (0.155 g, 2.09 mmol) was dissolved in a Na_2CO_3/$NaHCO_3$ buffer (20 mL, pH = 9.5) and added to F-CAT2 **7** (0.200 g, 0.19 mmol) dissolved in FC-72 (20 mL) in a Radleys Carousel reaction tube equipped with a stir bar. The biphasic reaction mixture was stirred vigorously to ensure optimum mixing of both phases. Stirring was stopped after 5 min, whereupon an interfacial solid was observed along with a yellow coloured aqueous layer. The fluorous layer was separated and added to an aqueous NaOCl (6%) solution (10 mL) in a separate reaction tube. After 15 min, the FC-72 layer was recombined with the bicarbonate/carbonate buffer and the cycle repeated. The process was repeated 12 times at which time the aqueous solution became colourless. The recovered sulfur was transferred to a centrifuge tube and water (10 mL) added and centrifuged at 3,000 rpm for 5 min. The water was decanted and the washing repeated twice. The recovered sulfur was dried and weighed. Yield (58 mg, 89%)

5.5.5 U-Tube Reaction

F-CAT2 **7** (0.050 g, 46 μmol) was dissolved in FC-72 (10 mL) and added to a U-tube equipped with a stir bar. Sodium bisulfide (0.034 g, 460 μmol) was dissolved in a Na_2CO_3/$NaHCO_3$ buffer (10 mL, pH = 9.5) and added to one arm of the tube while NaOCl (6%) solution (10 mL) was added to the other arm and both arms were closed with Teflon septum and vented into NaOH. The FC-72 layer was gently agitated over the period of the experiment. After a period of one week, all three phases were separated and the interfacial solid at the

buffer/fluorous layer isolated by centrifugation and the fluorous layer analyzed by ^{1}H NMR and FTIR spectroscopy, while the buffer layer was analyzed by UV-Vis spectroscopy (360 nm) using an aliquot of the original sodium bisulfide-buffer solution as a reference. The recovered sulfur was dried and weighed. Yield (8 mg, 53%).

5.6 Supporting Information

This material can be found in **APPENDIX 3**.

5.7 Acknowledgements

The authors gratefully acknowledge funding support from the Natural Science and Engineering Research Council (NSERC) of Canada. In addition, we wish to acknowledge Dr. Steve Kornic of the McMaster Combustion Analysis and Optical Spectroscopy (CAOS) facility (McMaster University, Hamilton, ON) for his support in obtaining the Raman spectroscopy data, and Dr. Denis Snider of the Centre for Probe Development and Commercialization, McMaster University, for scientific/medical document editing.

5.8 References

(1) Engineering Ltd, C. *A National Inventory of Greenhouse Gas (GHG), Criteria Air Contaminant (CAC) and Hydrogen Sulphide (H2S) Emissions by the Upstream Oil and Gas Industry*; 2004; Vol. 2.

(2) Ghosh, T. K.; Tollefson, E. L. *Can. J. Chem. Eng.* **1986**, *64*, 960–968.

(3) Vakili, M.; Gholami, Z.; Gholami, F. *World Appl. Sci. J.* **2012**, *19*, 241–245.

(4) Maat, H. ter; Hogendoorn, J. A.; Versteeg, G. F. *Sep. Purif. Technol.* **2005**, *43*, 199–213.

(5) Gendel, Y.; Levi, N.; Lahav, O. *Environ. Sci. Technol.* **2009**, *43*, 8315–8319.

(6) Son, H.-J.; Lee, J.-H. *Process Biochem.* **2005**, *40*, 2197–2203.

(7) Bendall, J. R.; Mann, F. G.; Purdie, D. *J. Chem. Soc.* **1942**, 157–163.

(8) Xiang, J.; Orita, A.; Otera, J. *Angew. Chem. Int. Ed.* **2002**, *41*, 4117–4119.

(9) Maayan, G.; Fish, R. H.; Neumann, R. *Org. Lett.* **2003**, *5*, 3547–3550.

(10) Hall, J. F. B.; Han, X.; Poliakoff, M.; Bourne, R. A.; George, M. W. *Chem. Commun.* **2012**, *48*, 3073–3075.

(11) Dzandzi, J. P. K.; Vera, D. R. B.; Genady, A. R.; Albu, S. A.; Eltringham-Smith, L. J.; Sheffield, W. P.; Valliant, J. F. *Submitted for publication in the Journal of Organic Chemistry*.

(12) Harvey, P. D.; Butler, I. S. *J. Raman Spectrosc.* **1986**, *17*, 329–334.

(13) Curran, D. P. *Angew. Chem. Int. Ed.* **1998**, *37*, 1174–1196.

(14) Curran, D.; Lee, Z. *Green Chem.* **2001**, *3*, G3–G7.

(15) Ubeda, M. A.; Dembinski, R. *J. Chem. Educ.* **2006**, *83*, 84–92.

(16) McLoughlin, V. C. R.; Thrower, J. *Tetrahedron* **1969**, *25*, 5921–5940.

(17) Topacli, C.; Topacli, A. *Spectrosc. Lett.* **2002**, *35*, 207–217.

(18) Aubineau, T.; Cossy, J. *Chem. Commun.* **2013**, *49*, 3303–3305.

(19) Böhm, H.-J.; Banner, D.; Bendels, S.; Kansy, M.; Kuhn, B.; Müller, K.; Obst-Sander, U.; Stahl, M. *ChemBioChem* **2004**, *5*, 637–643.

(20) Filler, R.; Saha, R. *Future Med. Chem.* **2009**, *1*, 777–791.

(21) Hagmann, W. K. *J. Med. Chem.* **2008**, *51*, 4359–4369.

(22) Müller, K.; Faeh, C.; Diederich, F. *Science* **2007**, *317*, 1881–1886.

(23) Kelsall, G. H.; Thompson, I. *J. Appl. Electrochem.* **1993**, *23*, 427–434.

(24) Kelsall, G. H.; Thompson, I. *J. Appl. Electrochem.* **1993**, *23*, 287–295.

(25) Nakamura, H.; Linclau, B.; Curran, D. P. *J. Am. Chem. Soc.* **2001**, *123*, 10119–10120.

(26) Luo, Z.; Swaleh, S. M.; Theil, F.; Curran, D. P. *Org. Lett.* **2002**, *4*, 2001–2003.

(27) Zhang, W. *Chem. Rev.* **2004**, *104*, 2531–2556.

(28) Levanov, A. V.; Antipenko, E. E.; Lunin, V. V. *Russ. J. Phys. Chem. A* **2012**, *86*, 2086–2086.

(29) Dobbs, A. P.; Kimberley, M. R. *J. Fluor. Chem.* **2002**, *4*, 3–17.

Chapter 6 - Summary and Future work

6.1 Summary

The overall objective was to develop a novel approach for HPLC-free preparation of high purity radioiodinated compounds. This was achieved using a single step approach employing perfluorostannyl precursors absorbed onto fluorous silica. The system developed is based on a hybrid platform in that it combines solid-phase and fluorous-phase chemistries. Initial success was achieved by treating fluorous silica coated with fluorous stannanes with iodine and chloramine-T (CAT) as the oxidant (Chapters 2). While excellent radiochemical purity was achieved, the limitation of this approach was the presence of CAT in the final product. Designing and synthesizing a fluorous derivative of CAT, F-CAT, resolved this issue (Chapter 3). Thus with the precursor and the oxidant being fluorous, treatment of fluorous arylstannanes coated on fluorous silica with [^{125}I]NaI made it possible to produce and selectively isolate the non-fluorous radiolabelled products in high radiochemical (>98%) and chemical (>99%) purity.

This platform was initially developed through a model system based on a fluorous benzoic acid derivative. The platform was then validated with simple aryl and heterocyclic derivatives, known radiopharmaceuticals including *meta*-iodobenzylguanidine (MIBG) and iododeoxyuridine (IUdR), and a new agent with high affinity for prostate-specific membrane antigen (PSMA). The coated fluorous silica 'kits' were simple to prepare, and reactions can be performed at

room temperature generating products in minutes in biocompatible solutions (Chapter 3). In all cases there was no evidence of residual starting materials in the product, which was verified by HPLC and ICP-MS analysis.

The fluorous oxidant developed during the course of this work, F-CAT, was further exploited to prepare a halogenated tetrazine (Chapter 4). This compound can be used to label biomolecules through bioorthogonal coupling reactions with prosthetic groups containing strained alkenes including norbornene and t*rans*-cyclooctene (TCO). This approach to labelling biomolecules has a number of advantages over conventional iodination methods and with the reported labelling method is readily accessible and requires minimal radiochemistry expertise and should therefore find widespread use. It is also noteworthy that a second generation of the fluorous oxidant, F-CAT2, was also prepared which has a higher solubility in perfluorinated solvents like FC-72 (Chapter 5). Application of F-CAT2 for oxidation of hydrogen sulfide to elemental sulphur in a fluorous-aqueous biphasic system was demonstrated. This metal-free process offers a new approach to scrubbing sour gas wells and demonstrates that the fluorous oxidants developed here have utility beyond radiochemistry.

6.2 Impact

The increasing demand for targeted radiotracers and therapeutics has created the need for expedient means of producing compounds in high effective specific activity. The described platform meets this need and its versatility has been demonstrated by producing a wide range of radiolabelled compounds.

Furthermore, the platform has been used to prepare a radioiodinated tetrazine which offers a means of labelling biomolecules and serves as a convenient tool for screening, pharmacokinetic and biodistribution studies. This method represents a new and general biomolecule radioiodination technique.

The oxidant, F-CAT, was shown to be versatile beyond simply the radioiodination of small molecules, and was also effective at promoting the labelling of proteins. F-CAT and its second-generation analogue, F-CAT2, have also been used for the oxidation of H_2S to elemental sulfur. As there are a limited number of fluorous oxidants that have been reported, F-CAT and F-CAT2 may become general purpose reagents for academic and industrial processes that require simple methods for removing or recycling oxidants.

6.3 Future work

6.3.1 Instant Kit Production and Automation of Radioiodination

The hybrid solid-fluorous phase platform developed here meets the goal of creating instant kits for producing radioiodinated compounds in high yield and purity. The ability to produce targeted radioiodinated agents in this manner is novel and should reduce the barriers to translation and dissemination of new iodine-based radiopharmaceuticals.

The obvious next step is to demonstrate this by employing the techniques developed here to create a kit for the production of a novel radiopharmaceutical and translate it into a phase I trial. In parallel, using the methodology and halogenated tetrazine to support preclinical drug development through

biomolecule labelling would also validate the utility of the approach. To achieve the clinical translation goal, a rigorous assessment of the platform around stability, sterility and pyrogenicity of the final drug product is needed. One additional component that would need to be explored is that the proof of concept work was done at a modest scale for safety and convenience reasons. The ability to scale to larger quantities of radioactivity, using other isotopes of iodine such as ^{131}I and ^{124}I needs to be undertaken. In the light of this (scale up) the stability of the precursor in the presence of larger quantities of radioactivity should also be evaluated.

The use of FSPE for retention of the fluorous-tin precursor and the fluorous oxidant thereby affording a facile purification approach makes the radioiodination process amenable to automation. Automation is used increasingly to produce PET agents where disposable cassettes are connected to an automated synthesis unit (ASU) which is programmed to produce and purify the tracer of interest. One can envisage a disposable kit containing the hybrid system here where the support is exposed to iodide and a fluorous oxidant and the product eluted into a multi-dose vial for administration to patients. The advantage of automation is that it reduces exposure and minimizes errors in production.

6.3.2 Adapting the hybrid solid-fluorous phase platform to radiobrominated and radioastatinated pharmaceuticals

The isotopes of bromine which have recently gained interest in nuclear medicine are ^{75}Br ($t_{1/2}$ = 72 min, β^+) and ^{76}Br ($t_{1/2}$ = 16.2 h, β^+) for PET imaging and ^{77}Br ($t_{1/2}$ = 57 h) for Auger electron, radiotherapy.[1] Fluorous-tin precursors could potentially be used to prepare radiobrominated agents where the labelling would proceed through electrophilic destannylation of fluorous-tin aryl precursors akin to the radioiodination methods reported in this thesis. Work would focus on optimizing the reaction conditions since rates of bromination and iodination are sufficiently different. The concern in using chlorine-based oxidants for radiobromination is the simultaneous formation chlorinated side products which could cause significant effects on the yield, chemical purity and ESA.[2], Suehiro and co-workers have reported that optimizing the balance between the precursor and oxidant prevented the formation of the chlorinated side product.[3] Once the most suitable conditions are identified the fluorous labeling strategy could be used to generate a range of novel radiobromine based radiopharmaceuticals..

α-Emitters have high linear energy transfer (LET) and higher radiobiological effectiveness than typical β-emitters. The alpha emitting halogen, ^{211}At ($t_{1/2}$ = 7.2 h) has been reported to have high tumor lethality and thus is of interest to create new cancer radiotherapies.[4,5] Labelling with ^{211}At generally follows an electrophilic demetallation strategy. However, the stability of astatine-carbon bonds is much lower than the corresponding iodine-carbon bonds making it difficult to generate labeled compounds using the same chemistry employed

with radioiodine.[1] Labelling biomolecules with ^{211}At has therefore often been accomplished using prosthetic groups such as *para*- and *meta*-astatobenzoate *N*-hydroxysuccinimidyl esters.[1] The adaptation of the hybrid platform for preparation of the radioastatinated prosthetic groups would offer a convenient and rapid method for producing these products in high purity. The ability to automate the approach would also ensure safety where hand doses from working with alpha emitters at production scales can be significant.

6.3.3 Adapting the hybrid solid-fluorous phase platform to drug discovery: An expedient tritiation strategy.

Radioisotope use in pharmaceutical research has been invaluable in definitively elucidating excretory and metabolic pathways in animal models.[6] The use of tritium (^{3}H) to obtain *in vitro* and *in vivo* biotransformation data has been widely reported.[7-10] Access to ^{3}H materials therefore plays an important role in the drug discovery process. Preparation of a wide range of tritium-labelled compounds, in support of pharmaceutical research, has extensively been accomplished by the use of metal-catalysed exchange with tritiated water or tritium gas.[11] The drawback to the metal-catalysed exchange approach is that the labelling is often not site-specific, hence the use of homogeneous and heterogeneous metal-catalysed exchanges have been employed to achieve diverse substitution products[11-12] Thus a generalized method that can be adapted to prepare a wide range of compounds has not been reported, to the best of our knowledge.

Seitz and coworkers[13] have demonstrated that in the presence of excess trifluoroacetic anhydride, trialkylstannyl compounds undergo regioselective tritiodestannylation upon the addition of tritiated water. The hybrid solid-fluorous phase radioiodination platform would offer a convenient strategy for producing tritiated analogues of new lead compounds free from the fluorous-stannyl derivatives. This strategy would prove to be an attractive alternative to introduction of tritium by tedious and time-consuming catalytic tritiation techniques, and can be used to produce agents in high purity for use in high-throughput screening[14,15] and low throughput *in vitro* assays. Comparable methods using ^{14}C are also conceivable.

6.3.4 Automation of H_2S oxidation to elemental sulfur

The development of cost effective, efficient and robust methods for H_2S removal from gaseous streams has been the focus of extensive research for decades. Liquid Redox Sulfur Recovery (LRSR) techniques are the most widely used methods, unfortunately they rely on metal-based catalyst which are costly and have detrimental environmental impact risk. Existing methods which are based on Fe, As, V, and Co complexes have high operational costs and require continual replacement of the catalysts.[16-18]

The development of F-CAT2 holds a key promise to overcoming these challenges and represents a metal-free strategy for scrubbing H_2S from sour gas.Our initial work has demonstrated the feasibility of oxidizing NaHS that is generated in the H_2S scrubbing process. Optimization of reaction conditions, and

'harvesting' of the recovered sulfur need further investigation. In particular, a goal should be to develop a continuous system that can test the durability of the catalyst and the extent of oxidized sulphur impurities that might be formed through this approach.

6.4 References

(1) Adam, M. J.; Wilbur, S. D. *Chem. Soc. Rev.* **2005**, *34*, 153–163.

(2) Moerlein, S. M. *J. Chem. Soc. Perk. T. 1* **1985**, 1687–1692.

(3) Suehiro, M.; Iwamoto, M.; Arai, I.; Nozaki, T. *Appl. Radiat. Isotopes* **1990**, *41*, 439–447.

(4) Garg, P. K.; John, C. S.; Zalutsky, M. R. *Nucl. Med. Biol.* **1995**, *22*, 467–473.

(5) Petrich, T.; Quintanilla-Martinez, L.; Korkmaz, Z.; Samson, E.; Helmeke, H. J.; Meyer, G. J.; Knaapp, W. H.; Potter, E. *Clin Cancer Res.* **2006**, *12*, 1342–1348.

(6) Shaffer, C. L.; Gunduz, M.; Thornburgh, B. A.; Fate, G. D. *Drug Metab. Dispos.* **2006**, *34*, 1615–1623.

(7) Linnet, K. *Hum. Psychopharmacol.* **2004**, *19*, 31–36.

(8) Gray, A.; Wilkinson, D. J.; Seddon, H. In *Synthesis and Applications of Isotopically Labelled Compounds. Volume 7*; Pleiss, U.; Voges, R., Eds.; John Wiley & Sons Ltd.: Chichester, UK, 2001; pp. 496–499.

(9) Rosenborg, J.; Larsson, P.; Tegner, K.; Hallstrom, G. *Drug Metab. Dispos.* **1999**, *27*, 1104–1116.

(10) Koller-Lucae, S. K. M.; Suter, M. J.; Rentsch, K. M.; Schott, H.; Schwendener, R. A. *Drug Metab. Dispos.* **1999**, *27*, 342–350.

(11) Hesk, D.; Lavey, C. F.; McNamara, P. *J. Labelled Compd. Rad.* **2010**, *53*, 722–730.

(12) Voges, R.; Heys, R. J.; Moenius, T. *Preparation of Compounds Labeled with Tritium and Carbon-14*; John Wiley & Sons, Ltd: Chichester, UK, 2009.

(13) Seitz, D. E.; Milius, R. A.; El-wakil, H. *Synth. Commun.* **1981**, *11*, 281–286.

(14) Warrior, U.; Chiou, G. X.; Sheets, M. P.; Sciotti, R. J.; Parry, J. M.; Simmer, R. L.; Surber, B. W.; Burns, D. J.; Beutel, B. A.; Mollison, K. W.; Djuric, S. W.; Trevillyan, J. M. *J. Biomol. Screen.* **1999**, *4*, 129–135.

(15) Carpenter, J. W.; Laethem, C.; Hubbard, F. R.; Eckols, T. K.; Baez, M.; McClure, D.; Nelson, D. L. G.; Johnston, P. A. In *High Throughput Screening: Methods and Protocols*; Jazen, W. P., Ed.; Humana Press Inc.: Totowa, New Jersey, 2002; Vol. 190, pp. 31–49.

(16) Dalrymple, D. A.; Trofe, T. W.; Corporation, R.; Evans, J. M. *Environ. Prog. Sustain. Energy* **1989**, *8*, 217–222.

(17) Son, H.-J.; Lee, J.-H. *Process Biochem.* **2005**, *40*, 2197–2203.

(18) Vakili, M.; Gholami, Z.; Gholami, F. *World Appl. Sci. J.* **2012**, *19*, 241–245.

APPENDIX 1

Supporting Information for Chapter 3

_N_-(4,4,5,5,6,6,7,7,8,8,9,9,10,10,11,11,11-heptadecafluoroundecyl)-4-methylbenzenesulfonamide (3)

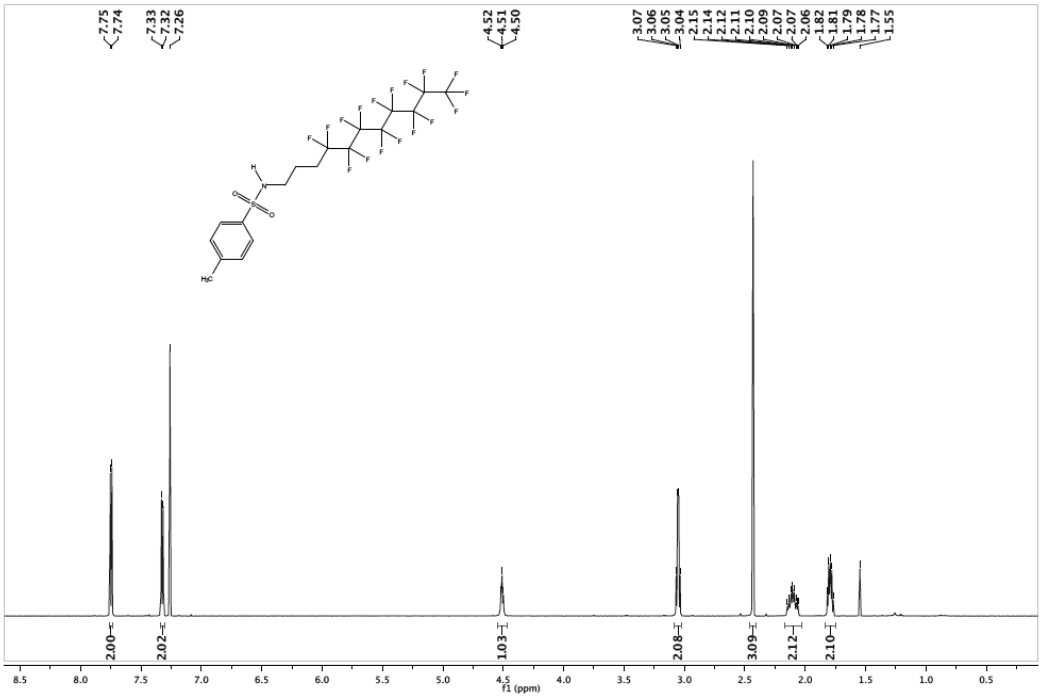

Figure S3-1. ^{1}H NMR (600 MHz, $CDCl_3$) of **3**.

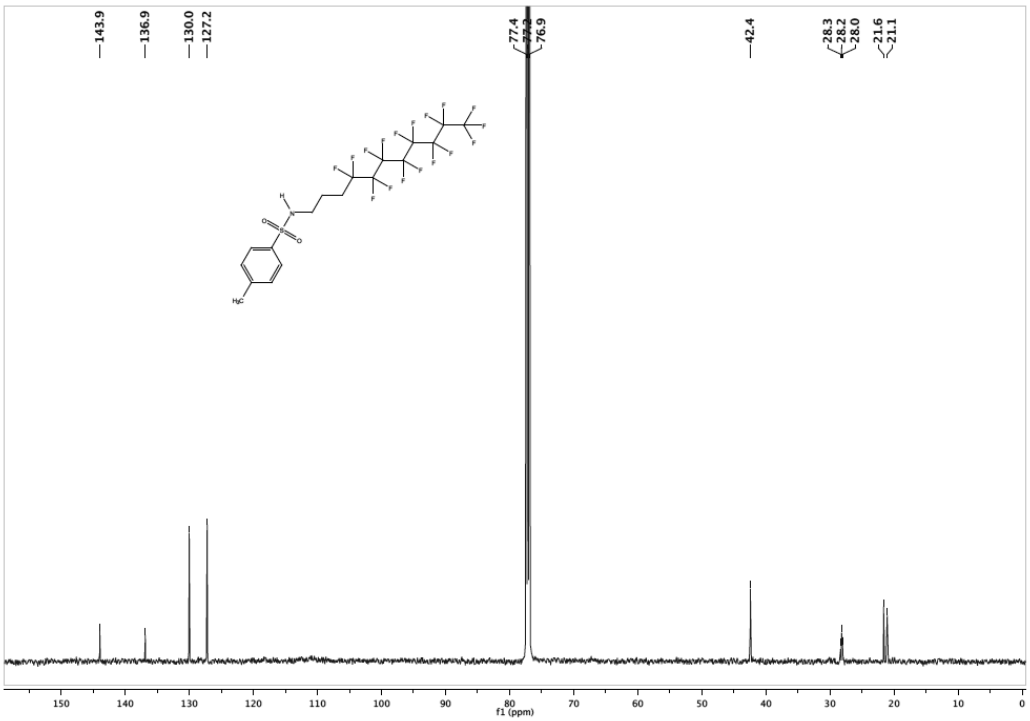

Figure S3-2. ^{13}C NMR (150 MHz, $CDCl_3$) of **3**.

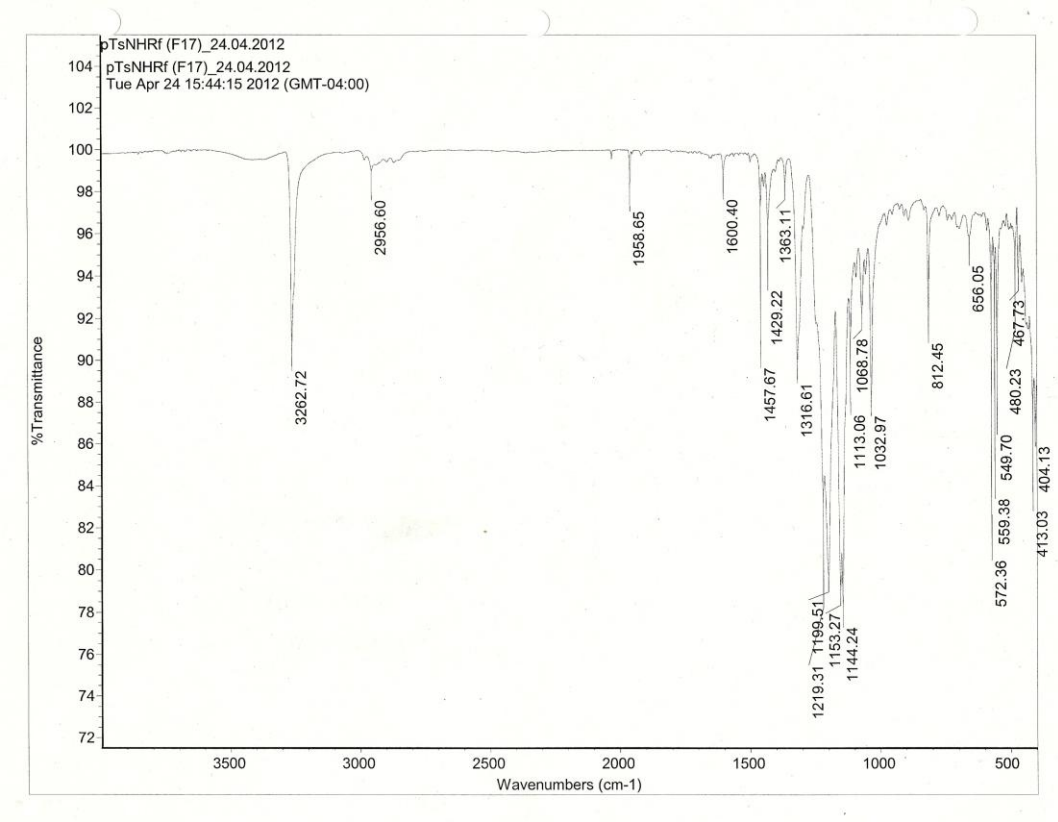

Figure S3-3. FTIR (KBr) spectrum of **3**.

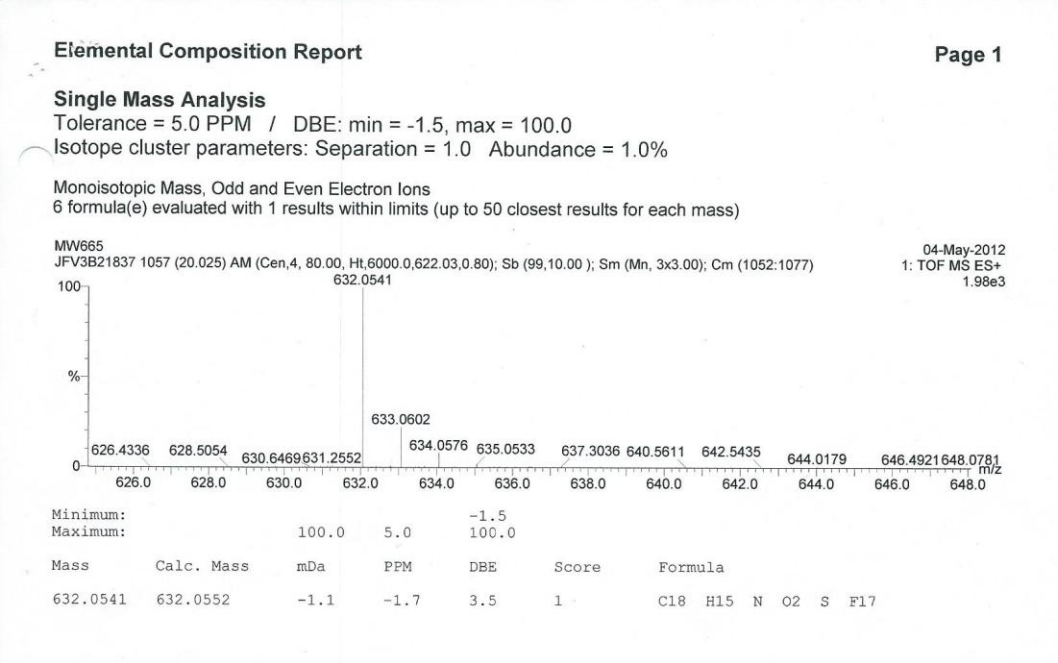

Figure S3-4. HRMS (ESI^+) of **3**.

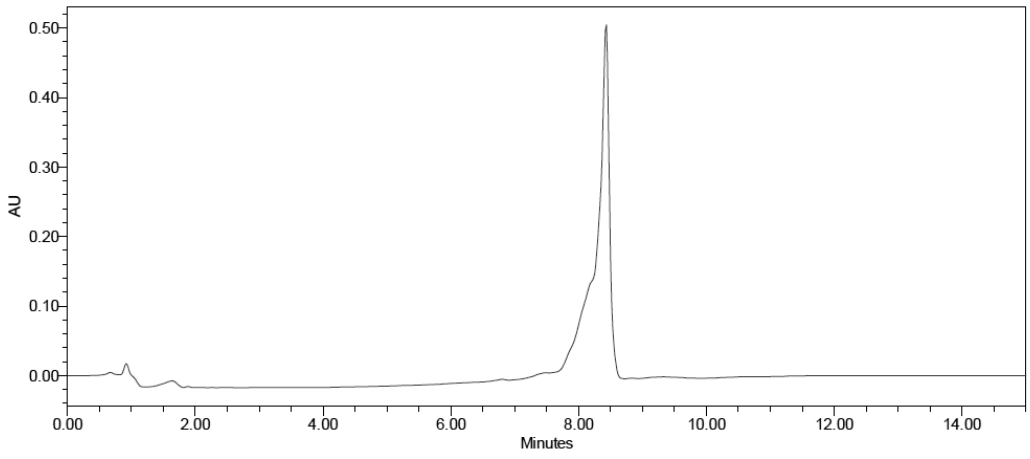

Figure S3-5. UV-HPLC chromatograms of a solution of compound **3** in ethanol (elution method B).

_N_-Chloro-_N_-(4,4,5,5,6,6,7,7,8,8,9,9,10,10,11,11,11-heptadecafluoroundecyl)-4-methylbenzenesulfonamide (4)

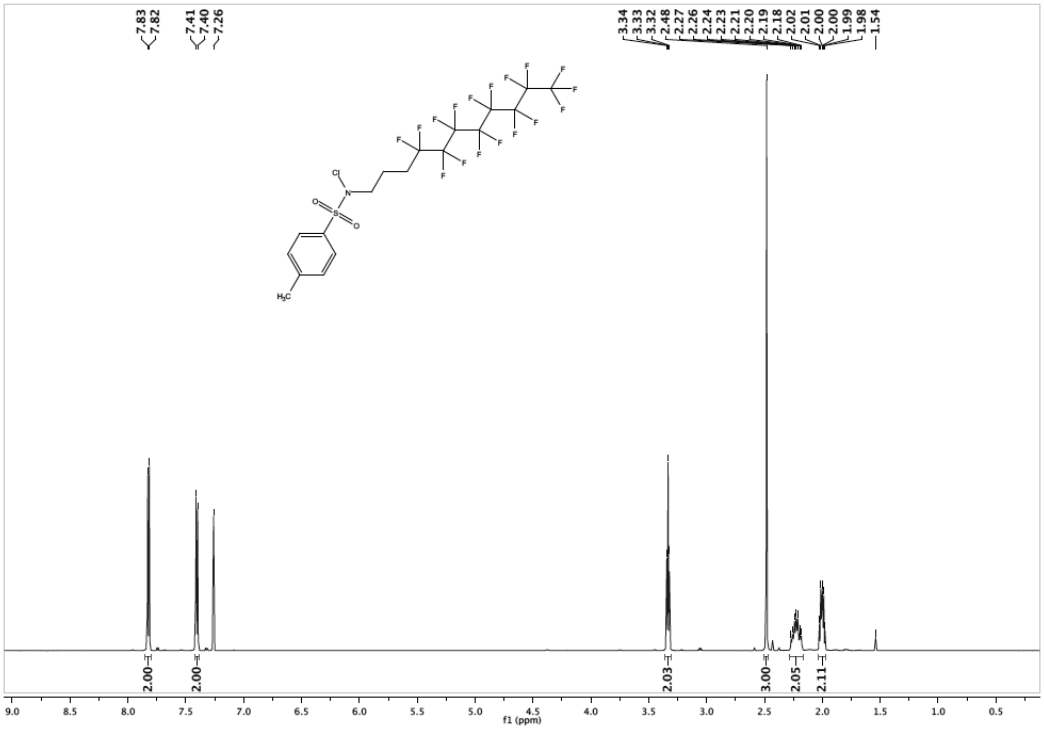

Figure S3-6. ^{1}H NMR (600 MHz, $CDCl_3$) of **4**.

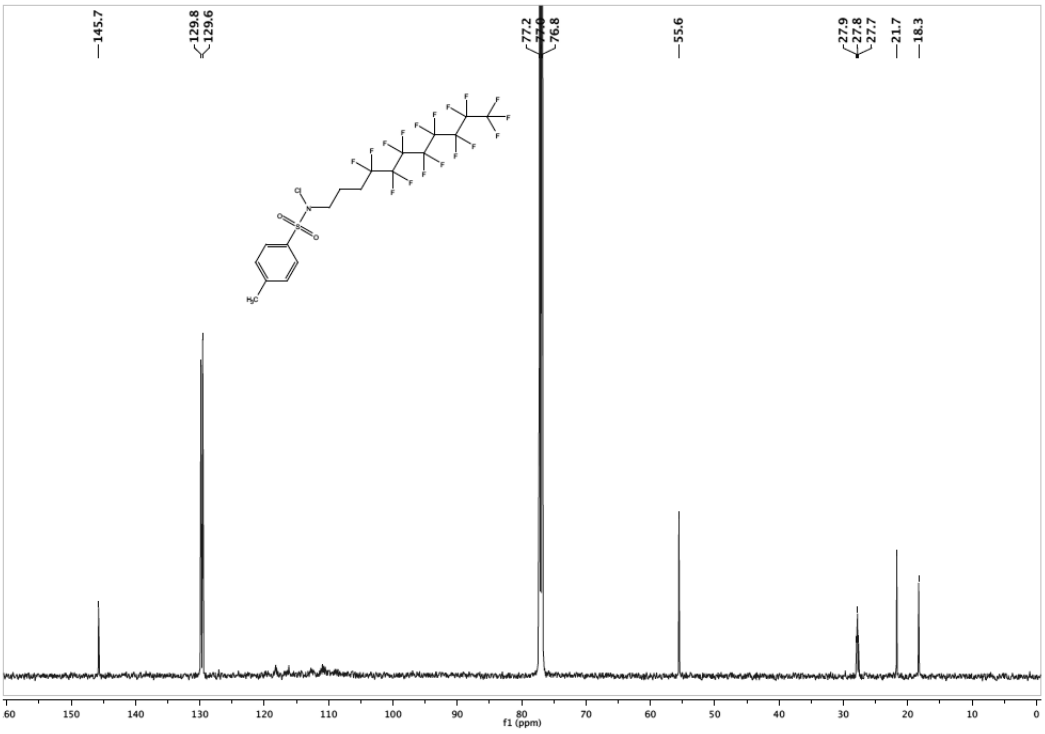

Figure S3-7. ^{13}C NMR (150 MHz, $CDCl_3$) of **4**.

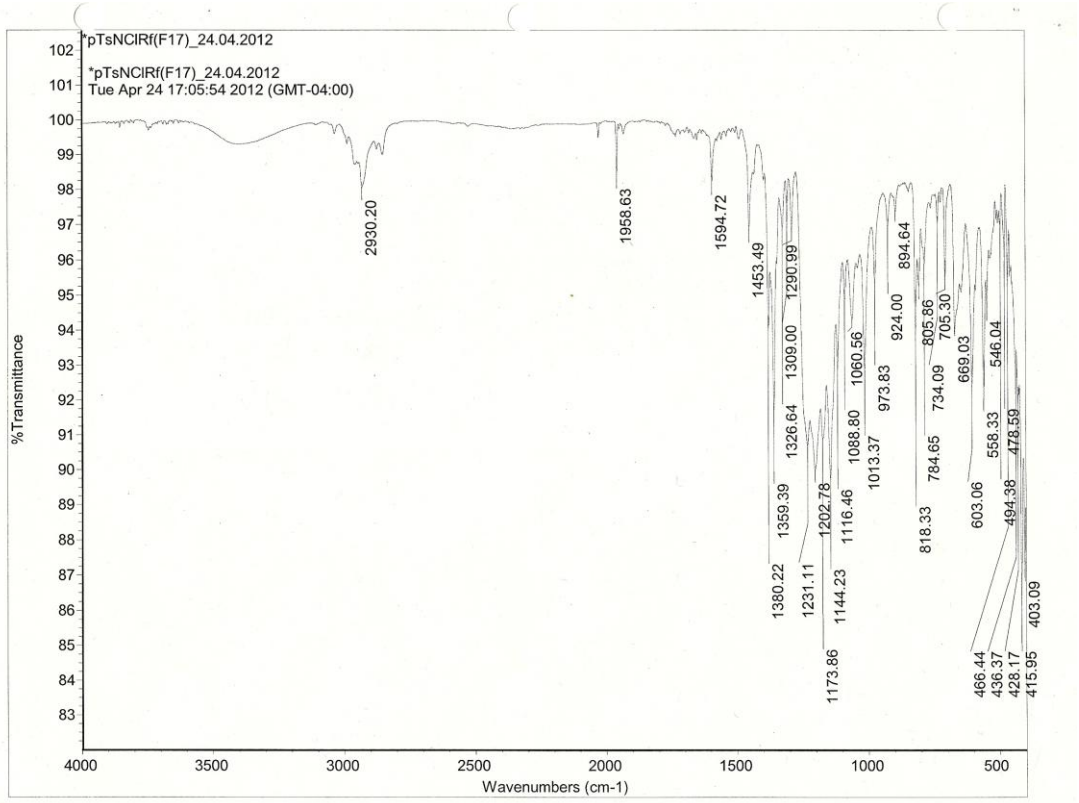

Figure S3-8. FTIR (KBr) spectrum of **4**.

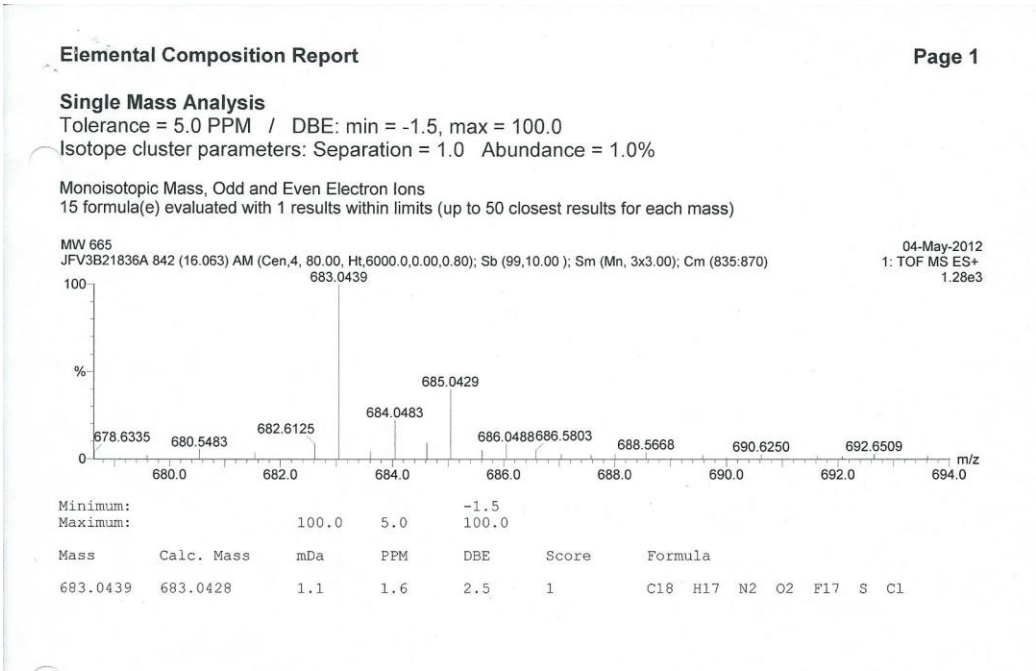

Elemental Composition Report **Page 1**

Single Mass Analysis
Tolerance = 5.0 PPM / DBE: min = -1.5, max = 100.0
Isotope cluster parameters: Separation = 1.0 Abundance = 1.0%

Monoisotopic Mass, Odd and Even Electron Ions
15 formula(e) evaluated with 1 results within limits (up to 50 closest results for each mass)

MW 665
JFV3B21836A 842 (16.063) AM (Cen,4, 80.00, Ht,6000.0,0.00,0.80); Sb (99,10.00); Sm (Mn, 3x3.00); Cm (835:870)
04-May-2012
1: TOF MS ES+
1.28e3

Minimum:				-1.5		
Maximum:		100.0	5.0	100.0		
Mass	Calc. Mass	mDa	PPM	DBE	Score	Formula
683.0439	683.0428	1.1	1.6	2.5	1	C18 H17 N2 O2 F17 S Cl

Figure S3-9. HRMS (ESI^+) of **4**.

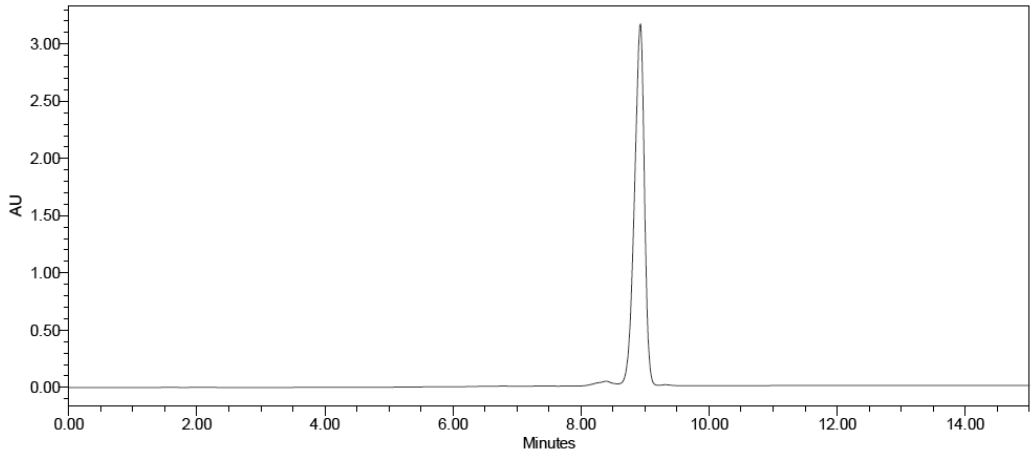

Figure S3-10. UV-HPLC chromatograms of a solution of compound **4** in ethanol (elution method B).

3-(5-Aminopyridin-2-yl)-6-(pyridin-2-yl)-1,2,4,5-tetrazine (16)

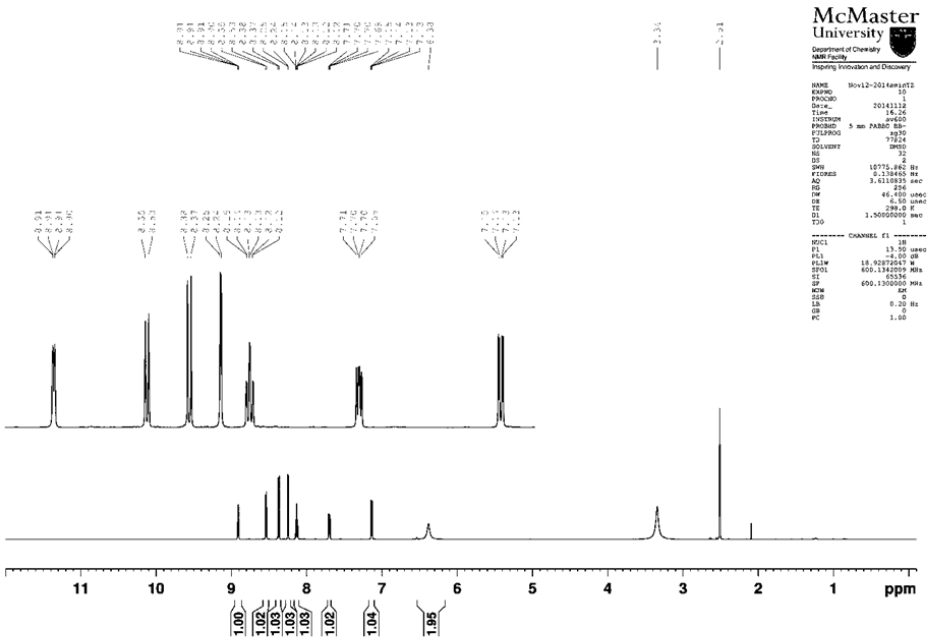

Figure S3-11. ^{1}H NMR (600 MHz, DMSO-d_6) of **16**.

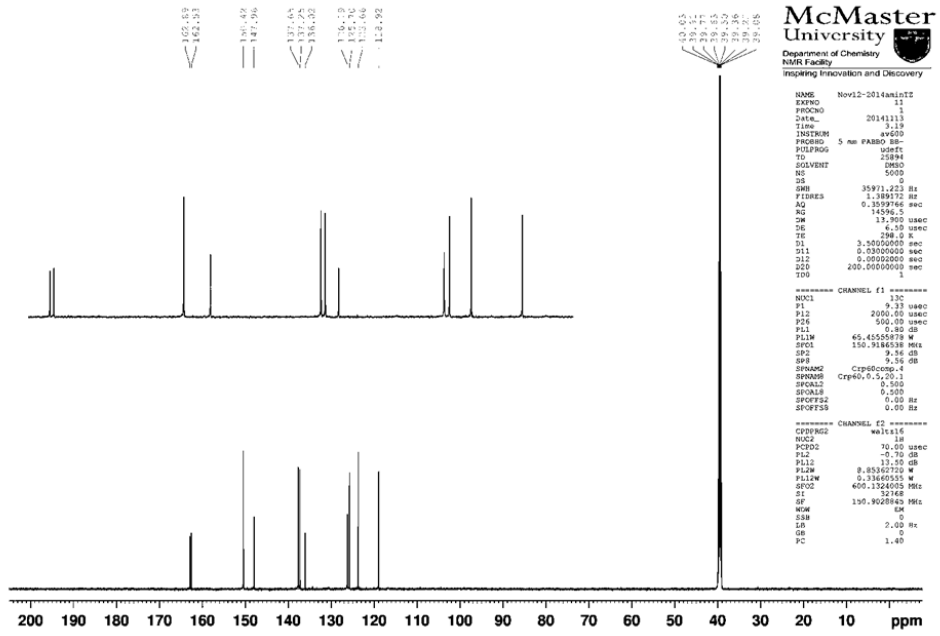

Figure S3-12. ^{13}C NMR (150 MHz, DMSO-d_6) of **16**.

HPLC chromatograms of radioiodinated compounds

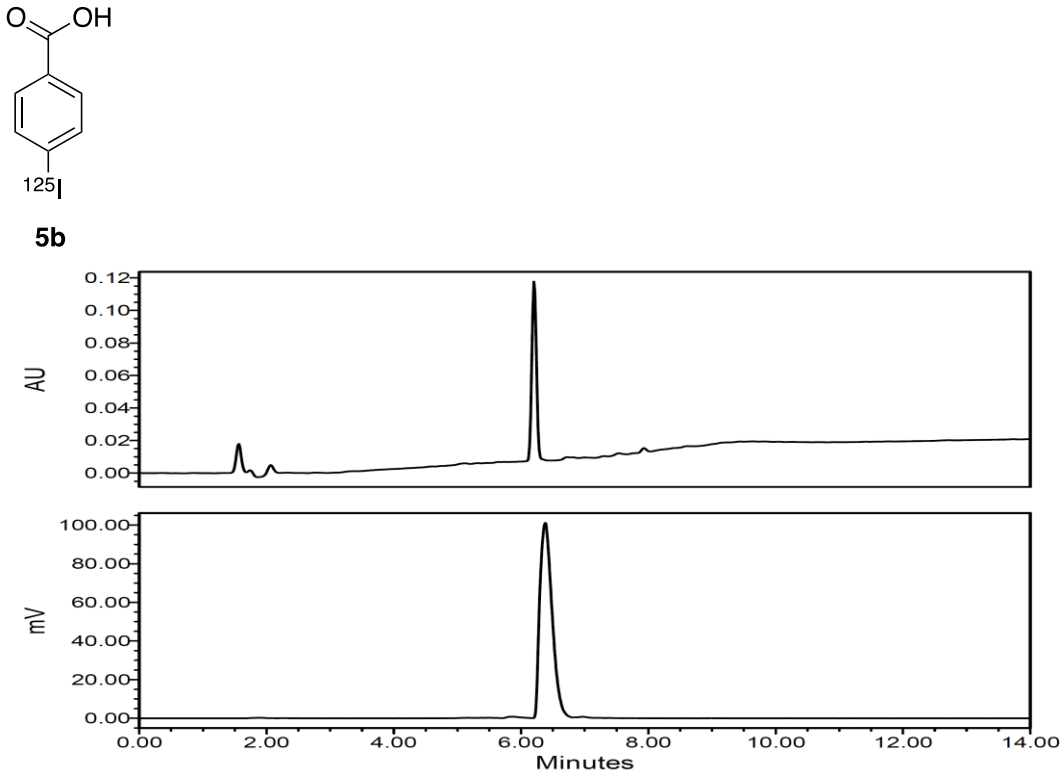

Figure S3-13. UV- (above) and γ-HPLC trace (below) of **5b** co-injected with its non-radioactive reference standard (elution method B).

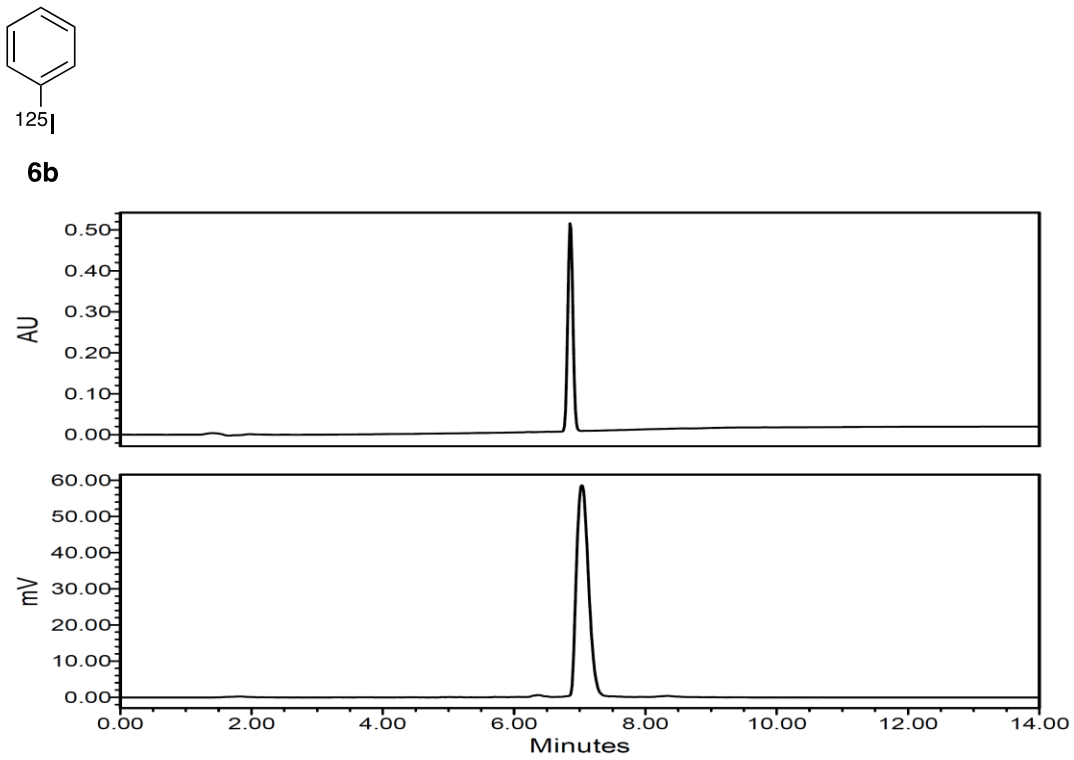

Figure S3-14. UV- (above) and γ-HPLC trace (below) of **6b** co-injected with its non-radioactive reference standard (elution method B).

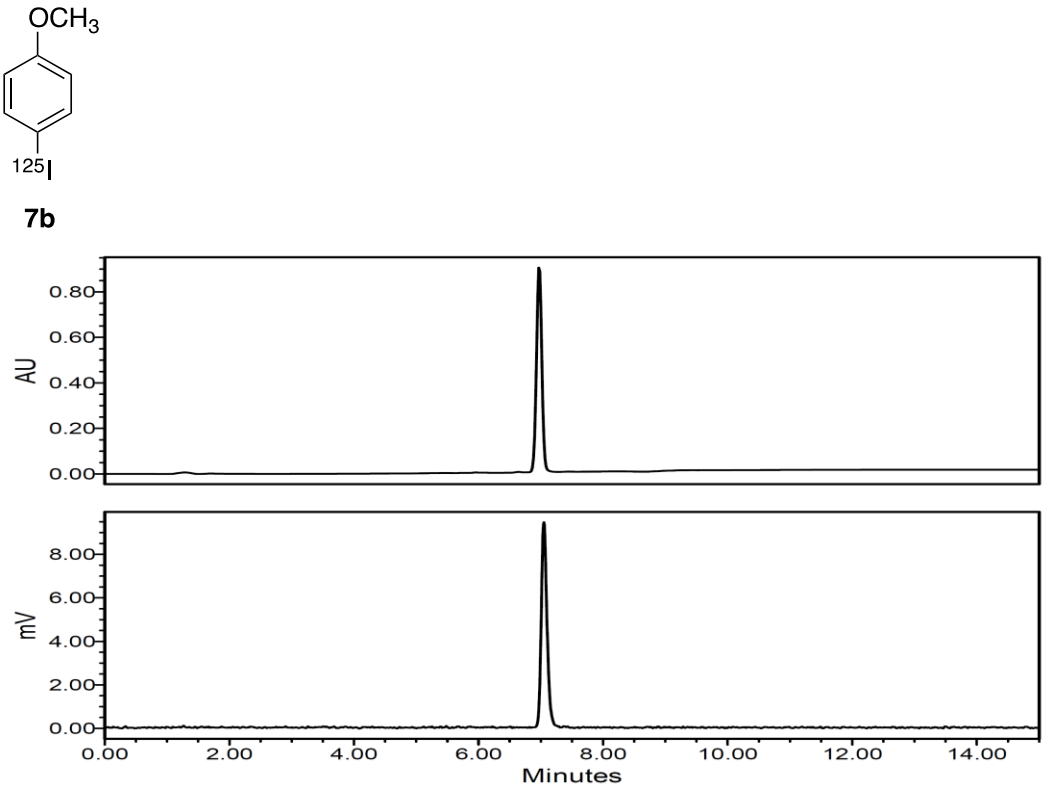

Figure S3-15. UV- (above) and γ-HPLC trace (below) of **7b** co-injected with its non-radioactive reference standard (elution method A).

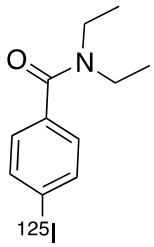

8b

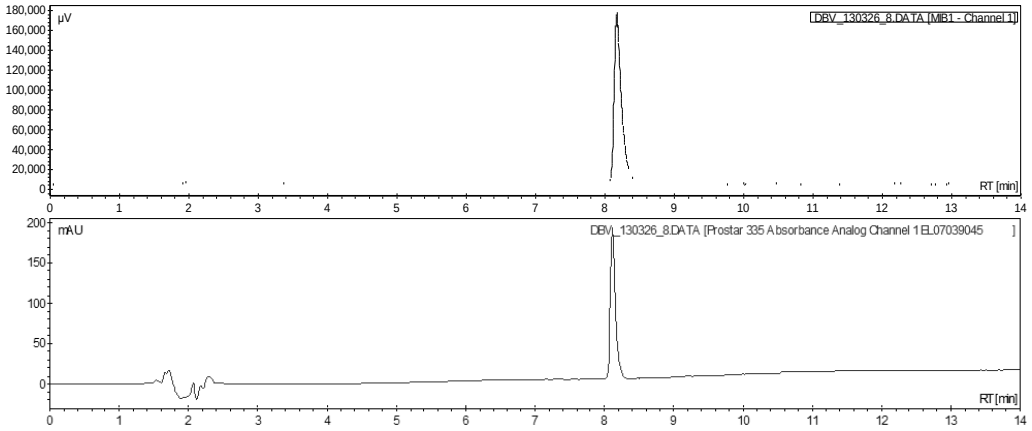

Figure S3-16. UV- (above) and γ-HPLC trace (below) of **8b** co-injected with its non-radioactive reference standard (elution method C).

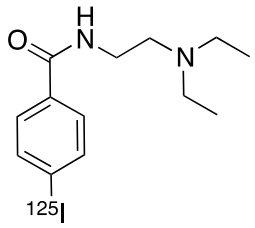

9b

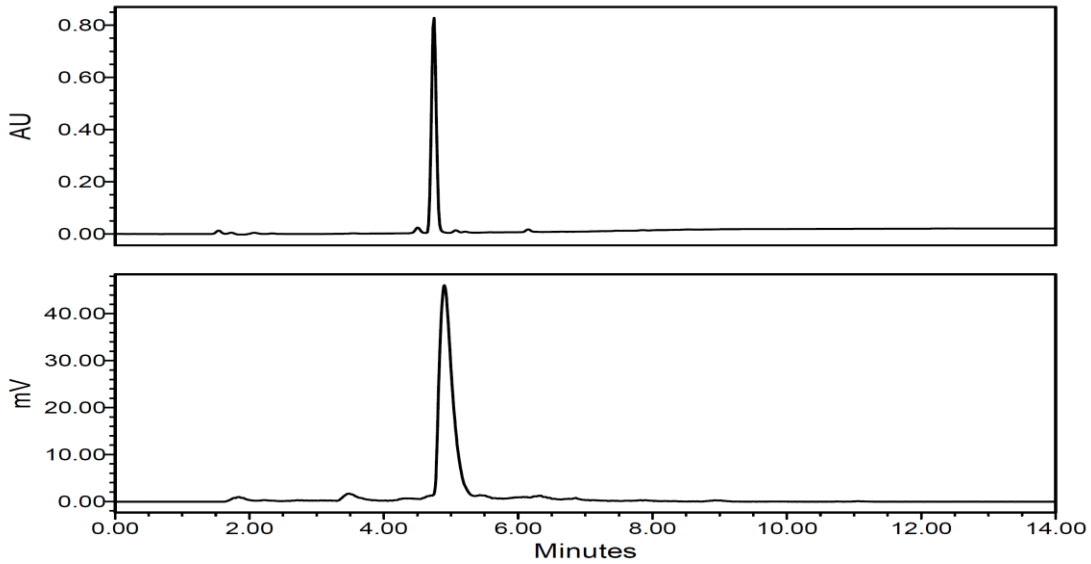

Figure S3-17. UV- trace (above) and γ-HPLC trace (below) of **9b** co-injected with its non-radioactive reference standard (elution method B).

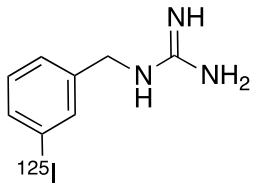

10b

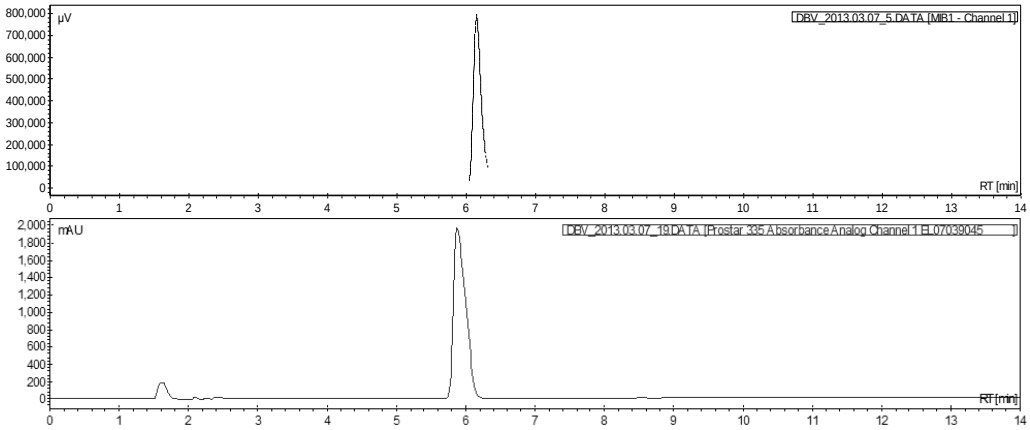

Figure S3-18. γ-HPLC trace (above) and UV-HPLC trace (below) of **10b** co-injected with its non-radioactive reference standard (elution method C).

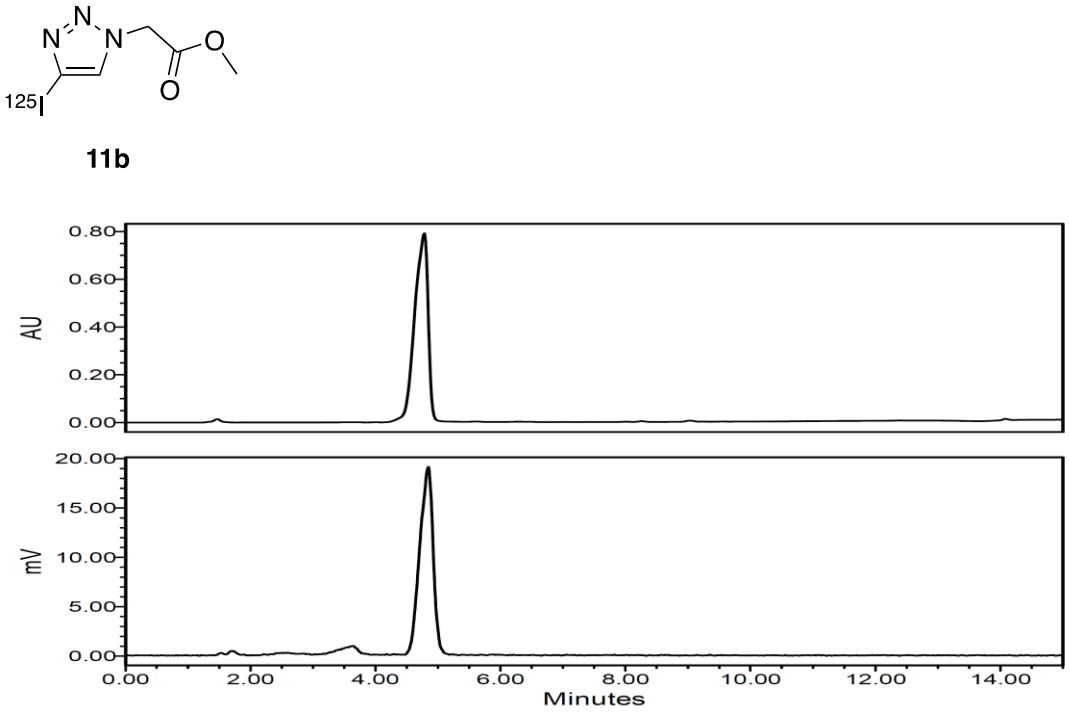

Figure S3-19. UV- (above) and γ-HPLC trace (below) of **11b** co-injected with its non-radioactive reference standard (elution method A).

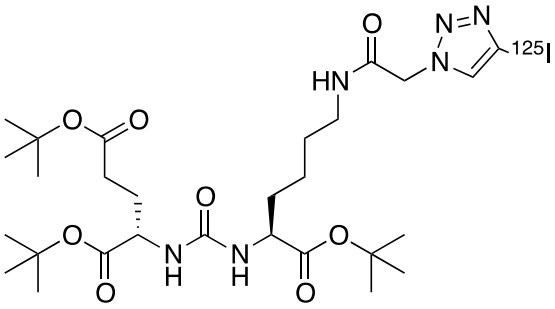

12b

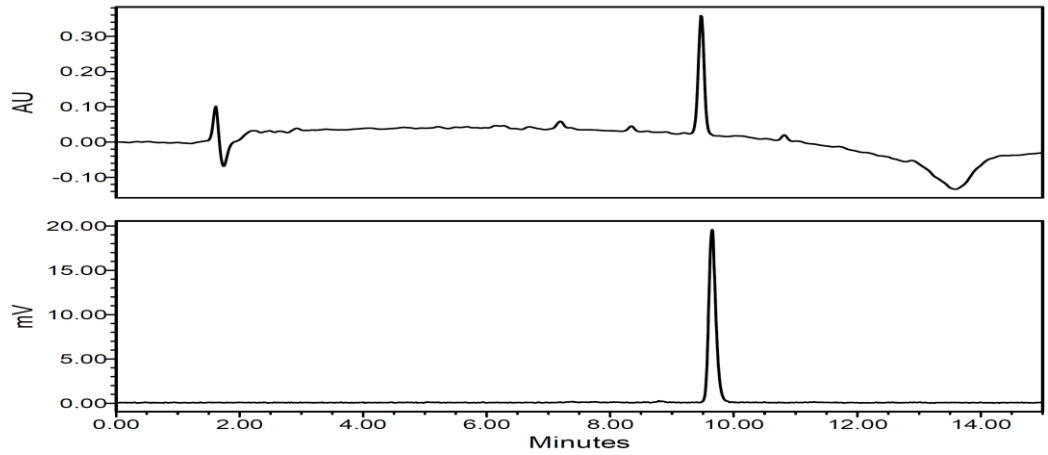

Figure S3-20. UV- (above) and γ-HPLC trace (below) of **12b** co-injected with its non-radioactive reference standard (elution method A).

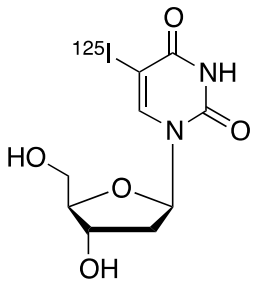

13b

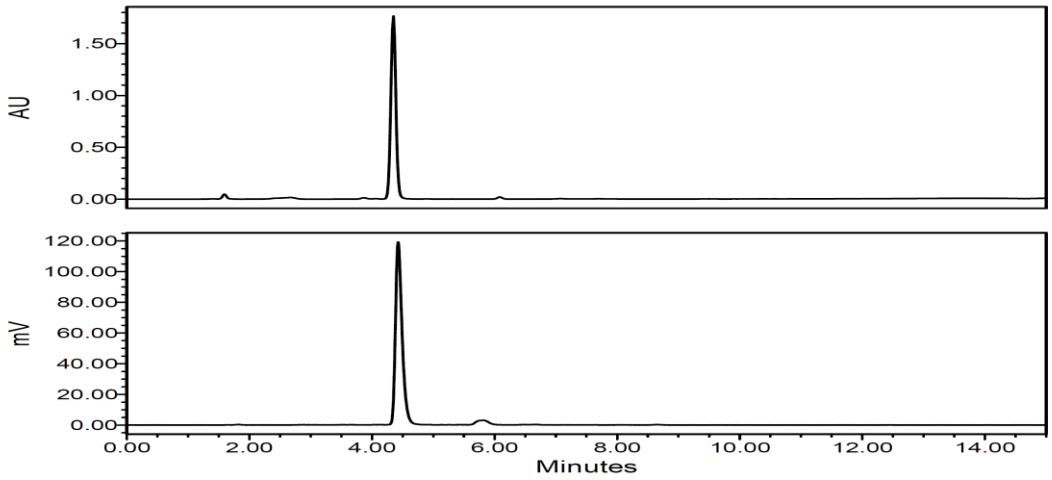

Figure S3-21. UV- (above) and γ-HPLC trace (below) of **13b** co-injected with its non-radioactive reference standard (elution method A).

Thrombin Assay

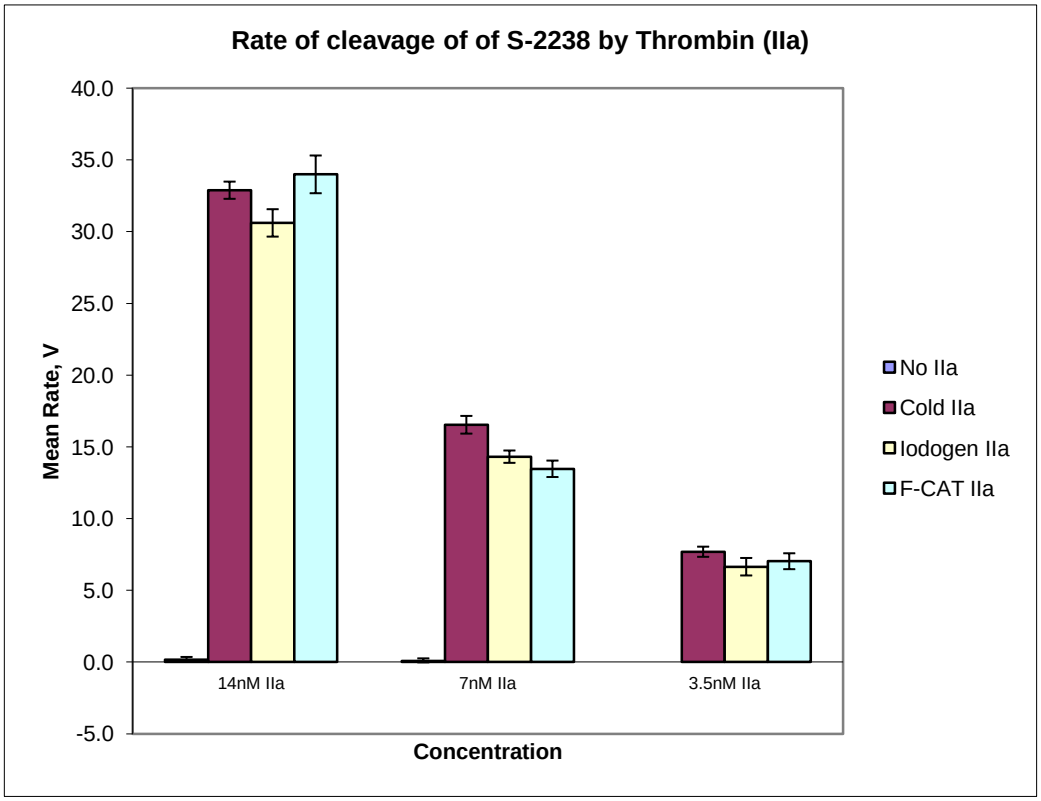

Figure S3-22. Rate of cleavage of the chromogenic substrate (S-2238) by labelled thrombin produced using both oxidants. Protein concentrations of 14 nM, 7 nM and 3.5 nM were analyzed, with unmodified thrombin (Cold IIa) as a positive control and buffer (No IIa) as the negative control.

Table S3-1. Crystal data and structure refinement for **3**.

Identification code	james3_0m
Empirical formula	$C_{18}H_{14}F_{17}NO_2S$
Formula weight	631.36
Temperature	173(2) K
Wavelength	1.54178 Å
Crystal system	Monoclinic
Space group	P2(1)/c
Unit cell dimensions	a = 21.9809(6) Å α = 90°
	b = 5.66540(10) Å β = 94.7170(10)°
	c = 18.7773(5) Å γ = 90°
Volume	2330.43(10) Å ^{3}
Z	4
Density (calculated)	1.800 Mg/m^3
Absorption coefficient	2.720 mm^{-1}
F(000)	1256
Crystal size	0.46 × 0.09 × 0.05 mm^3
θ range for data collection	4.04 to 68.35°.
Index ranges	$-26\leq h\leq 26$, $-6\leq k\leq 6$, $-22\leq l\leq 22$
Reflections collected	23861
Independent reflections	4258 [R(int) = 0.0369]
Completeness to θ = 68.35°	99.5 %
Absorption correction	Semi-empirical from equivalents
Max. and min. transmission	0.8760 and 0.3664
Refinement method	Full-matrix least-squares on F^2
Data / restraints / parameters	4258 / 6 / 366
Goodness-of-fit on F^2	1.094
Final R indices [I>2σ(I)]	R_1 = 0.0675, wR_2 = 0.2093
R indices (all data)	R_1 = 0.0774, wR_2 = 0.2187
Largest diff. peak and hole	0.722 and -0.340 eÅ^{-3}

Table S3-2. Atomic coordinates ($\times 10^4$) and equivalent isotropic displacement parameters ($Å^2 \times 10^3$) for **3**. U(eq) is defined as one third of the trace of the orthogonalized U^{ij} tensor.

	x	y	z	U(eq)
S(1)	4523(1)	10016(2)	1449(1)	49(1)
O(1)	4608(1)	11339(5)	2099(2)	62(1)
O(2)	4454(1)	11203(5)	783(2)	60(1)
N(1)	5128(1)	8346(6)	1451(2)	51(1)
F(1)	6979(1)	3744(4)	711(1)	62(1)
F(2)	6927(1)	5228(4)	1768(1)	63(1)
F(3)	7445(1)	9248(4)	1401(2)	65(1)
F(4)	7398(1)	8218(5)	278(1)	66(1)
F(5)	8173(1)	4831(5)	498(2)	74(1)
F(6)	8107(1)	4806(5)	1642(2)	73(1)
F(7)	8546(1)	9692(4)	694(2)	77(1)
F(8)	8650(1)	8858(5)	1823(2)	77(1)
F(9)	9290(1)	4727(4)	1404(2)	81(1)
F(10)	9316(1)	6460(6)	375(2)	86(1)
F(11)	9871(1)	8038(6)	2079(2)	86(1)
F(12)	9722(1)	10520(4)	1205(2)	90(1)
F(13)	10483(1)	5230(5)	1083(2)	81(1)
F(14)	10444(2)	8326(7)	417(2)	99(1)
C(18)	11007(2)	8570(9)	1513(3)	80(2)
F(15)	11487(1)	8184(7)	1161(2)	100(1)
F(16)	11100(2)	7433(8)	2138(2)	102(1)
F(17)	10950(2)	10820(6)	1644(3)	111(2)
C(18')	11007(2)	8570(9)	1513(3)	80(2)
F(15')	11563(7)	8150(80)	1789(19)	100(1)
F(16')	10709(18)	9600(80)	2024(15)	102(1)
F(17')	11015(18)	10040(70)	977(16)	111(2)
C(1)	3888(2)	8142(6)	1494(2)	45(1)

C(2)	3421(2)	8139(8)	962(2)	58(1)
C(3)	2937(2)	6605(9)	1009(2)	65(1)
C(4)	2917(2)	5038(7)	1569(2)	55(1)
C(5)	3388(2)	5085(8)	2098(3)	66(1)
C(6)	3876(2)	6616(8)	2072(2)	61(1)
C(7)	2393(2)	3328(9)	1603(3)	75(1)
C(8)	5153(2)	6621(7)	860(2)	53(1)
C(9)	5759(2)	5304(7)	953(2)	56(1)
C(10)	6298(2)	6927(7)	831(2)	56(1)
C(11)	6900(2)	5792(7)	1063(2)	51(1)
C(12)	7455(2)	7377(7)	953(2)	51(1)
C(13)	8091(2)	6203(7)	1073(2)	53(1)
C(14)	8636(2)	7926(7)	1161(2)	53(1)
C(15)	9268(2)	6805(7)	1075(3)	58(1)
C(16)	9818(2)	8268(7)	1369(2)	58(1)
C(17)	10435(2)	7559(8)	1092(3)	67(1)

Table S3-3. Bond lengths [Å] and angles [°] for **3**.

S(1)-O(2)	1.416(3)
S(1)-O(1)	1.432(3)
S(1)-N(1)	1.632(3)
S(1)-C(1)	1.762(4)
N(1)-C(8)	1.483(5)
N(1)-H(1A)	0.99(5)
F(1)-C(11)	1.354(5)
F(2)-C(11)	1.359(5)
F(3)-C(12)	1.355(5)
F(4)-C(12)	1.350(5)
F(5)-C(13)	1.354(5)
F(6)-C(13)	1.327(5)
F(7)-C(14)	1.334(5)
F(8)-C(14)	1.349(5)
F(9)-C(15)	1.329(5)
F(10)-C(15)	1.340(5)
F(11)-C(16)	1.335(5)
F(12)-C(16)	1.325(5)
F(13)-C(17)	1.324(5)
F(14)-C(17)	1.341(6)
C(18)-F(17)	1.306(6)
C(18)-F(15)	1.310(6)
C(18)-F(16)	1.339(7)
C(18)-C(17)	1.541(7)
C(1)-C(2)	1.372(5)
C(1)-C(6)	1.389(6)
C(2)-C(3)	1.382(6)
C(2)-H(2)	0.9500
C(3)-C(4)	1.379(6)
C(3)-H(3)	0.9500
C(4)-C(5)	1.376(6)
C(4)-C(7)	1.510(6)

C(5)-C(6)	1.383(6)
C(5)-H(5A)	0.9500
C(6)-H(6A)	0.9500
C(7)-H(7C)	0.9800
C(7)-H(7B)	0.9800
C(7)-H(7A)	0.9800
C(8)-C(9)	1.523(6)
C(8)-H(8B)	0.9900
C(8)-H(8A)	0.9900
C(9)-C(10)	1.533(6)
C(9)-H(9B)	0.9900
C(9)-H(9A)	0.9900
C(10)-C(11)	1.502(5)
C(10)-H(10B)	0.9900
C(10)-H(10A)	0.9900
C(11)-C(12)	1.543(6)
C(12)-C(13)	1.547(5)
C(13)-C(14)	1.543(5)
C(14)-C(15)	1.549(5)
C(15)-C(16)	1.531(6)
C(16)-C(17)	1.546(6)

O(2)-S(1)-O(1)	120.06(19)
O(2)-S(1)-N(1)	107.83(18)
O(1)-S(1)-N(1)	104.59(17)
O(2)-S(1)-C(1)	107.54(17)
O(1)-S(1)-C(1)	108.79(18)
N(1)-S(1)-C(1)	107.42(17)
C(8)-N(1)-S(1)	117.4(3)
C(8)-N(1)-H(1A)	120(3)
S(1)-N(1)-H(1A)	110(3)
F(17)-C(18)-F(15)	110.6(5)
F(17)-C(18)-F(16)	108.3(6)
F(15)-C(18)-F(16)	106.9(4)

F(17)-C(18)-C(17)	111.9(4)
F(15)-C(18)-C(17)	109.6(5)
F(16)-C(18)-C(17)	109.3(4)
C(2)-C(1)-C(6)	120.4(4)
C(2)-C(1)-S(1)	120.9(3)
C(6)-C(1)-S(1)	118.6(3)
C(1)-C(2)-C(3)	119.2(4)
C(1)-C(2)-H(2)	120.4
C(3)-C(2)-H(2)	120.4
C(4)-C(3)-C(2)	121.8(4)
C(4)-C(3)-H(3)	119.1
C(2)-C(3)-H(3)	119.1
C(5)-C(4)-C(3)	117.9(4)
C(5)-C(4)-C(7)	120.9(4)
C(3)-C(4)-C(7)	121.2(4)
C(4)-C(5)-C(6)	121.8(4)
C(4)-C(5)-H(5A)	119.1
C(6)-C(5)-H(5A)	119.1
C(5)-C(6)-C(1)	118.9(4)
C(5)-C(6)-H(6A)	120.6
C(1)-C(6)-H(6A)	120.6
C(4)-C(7)-H(7C)	109.5
C(4)-C(7)-H(7B)	109.5
H(7C)-C(7)-H(7B)	109.5
C(4)-C(7)-H(7A)	109.5
H(7C)-C(7)-H(7A)	109.5
H(7B)-C(7)-H(7A)	109.5
N(1)-C(8)-C(9)	108.8(3)
N(1)-C(8)-H(8B)	109.9
C(9)-C(8)-H(8B)	109.9
N(1)-C(8)-H(8A)	109.9
C(9)-C(8)-H(8A)	109.9
H(8B)-C(8)-H(8A)	108.3
C(8)-C(9)-C(10)	111.6(3)

C(8)-C(9)-H(9B)	109.3
C(10)-C(9)-H(9B)	109.3
C(8)-C(9)-H(9A)	109.3
C(10)-C(9)-H(9A)	109.3
H(9B)-C(9)-H(9A)	108.0
C(11)-C(10)-C(9)	111.9(3)
C(11)-C(10)-H(10B)	109.2
C(9)-C(10)-H(10B)	109.2
C(11)-C(10)-H(10A)	109.2
C(9)-C(10)-H(10A)	109.2
H(10B)-C(10)-H(10A)	107.9
F(1)-C(11)-F(2)	106.1(3)
F(1)-C(11)-C(10)	111.7(3)
F(2)-C(11)-C(10)	110.6(3)
F(1)-C(11)-C(12)	107.4(3)
F(2)-C(11)-C(12)	107.2(3)
C(10)-C(11)-C(12)	113.5(3)
F(4)-C(12)-F(3)	107.6(3)
F(4)-C(12)-C(11)	108.5(3)
F(3)-C(12)-C(11)	108.5(3)
F(4)-C(12)-C(13)	107.5(3)
F(3)-C(12)-C(13)	107.9(3)
C(11)-C(12)-C(13)	116.4(3)
F(6)-C(13)-F(5)	107.6(3)
F(6)-C(13)-C(14)	108.8(3)
F(5)-C(13)-C(14)	107.2(3)
F(6)-C(13)-C(12)	109.8(3)
F(5)-C(13)-C(12)	107.9(3)
C(14)-C(13)-C(12)	115.3(3)
F(7)-C(14)-F(8)	107.6(3)
F(7)-C(14)-C(13)	109.5(3)
F(8)-C(14)-C(13)	107.8(3)
F(7)-C(14)-C(15)	108.9(3)
F(8)-C(14)-C(15)	107.7(3)

C(13)-C(14)-C(15)	115.1(3)
F(9)-C(15)-F(10)	109.0(4)
F(9)-C(15)-C(16)	108.3(3)
F(10)-C(15)-C(16)	108.1(4)
F(9)-C(15)-C(14)	108.2(3)
F(10)-C(15)-C(14)	107.8(3)
C(16)-C(15)-C(14)	115.4(3)
F(12)-C(16)-F(11)	109.0(4)
F(12)-C(16)-C(15)	109.4(3)
F(11)-C(16)-C(15)	108.0(4)
F(12)-C(16)-C(17)	107.4(4)
F(11)-C(16)-C(17)	107.7(3)
C(15)-C(16)-C(17)	115.2(4)
F(13)-C(17)-F(14)	107.7(4)
F(13)-C(17)-C(18)	108.3(4)
F(14)-C(17)-C(18)	106.9(4)
F(13)-C(17)-C(16)	109.7(4)
F(14)-C(17)-C(16)	108.4(4)
C(18)-C(17)-C(16)	115.6(4)

Symmetry transformations used to generate equivalent atoms:

Table S3-4. Anisotropic displacement parameters ($Å^2 \times 10^3$) for **3**. The anisotropic displacement factor exponent takes the form: $-2\pi^2[h^2a^{*2}U^{11} + ... + 2hka^*b^*U^{12}]$

	U^{11}	U^{22}	U^{33}	U^{23}	U^{13}	U^{12}
S(1)	44(1)	39(1)	62(1)	0(1)	-6(1)	-3(1)
O(1)	57(2)	56(2)	72(2)	-15(1)	-10(1)	1(1)
O(2)	53(2)	51(2)	75(2)	9(1)	-9(1)	-8(1)
N(1)	41(2)	45(2)	65(2)	-3(2)	0(1)	-4(1)
F(1)	54(1)	48(1)	82(2)	-9(1)	4(1)	3(1)
F(2)	56(1)	67(2)	65(1)	9(1)	6(1)	3(1)
F(3)	51(1)	43(1)	100(2)	-11(1)	8(1)	4(1)
F(4)	48(1)	75(2)	75(2)	23(1)	-1(1)	1(1)
F(5)	52(1)	68(2)	101(2)	-32(1)	-2(1)	6(1)
F(6)	54(1)	64(2)	99(2)	27(1)	-5(1)	2(1)
F(7)	52(1)	54(1)	123(2)	29(2)	1(1)	6(1)
F(8)	54(1)	82(2)	96(2)	-36(2)	4(1)	0(1)
F(9)	54(1)	39(1)	148(3)	14(1)	4(2)	6(1)
F(10)	60(2)	115(3)	82(2)	-33(2)	6(1)	2(2)
F(11)	66(2)	114(3)	75(2)	-17(2)	1(1)	-6(2)
F(12)	57(2)	38(1)	174(3)	7(2)	-4(2)	2(1)
F(13)	62(2)	56(2)	126(2)	-10(2)	8(2)	12(1)
F(14)	75(2)	128(3)	96(2)	33(2)	18(2)	8(2)
C(18)	49(2)	61(3)	129(5)	10(3)	-1(3)	-1(2)
F(15)	49(2)	101(3)	152(3)	12(2)	18(2)	3(2)
F(16)	70(2)	122(3)	111(3)	14(2)	-20(2)	-2(2)
F(17)	61(2)	59(2)	211(5)	-15(2)	-3(2)	-13(2)
C(18')	49(2)	61(3)	129(5)	10(3)	-1(3)	-1(2)
F(15')	49(2)	101(3)	152(3)	12(2)	18(2)	3(2)
F(16')	70(2)	122(3)	111(3)	14(2)	-20(2)	-2(2)
F(17')	61(2)	59(2)	211(5)	-15(2)	-3(2)	-13(2)
C(1)	38(2)	40(2)	56(2)	0(2)	1(1)	0(1)

C(2)	50(2)	64(3)	58(2)	9(2)	-10(2)	-6(2)
C(3)	48(2)	82(3)	63(2)	5(2)	-7(2)	-16(2)
C(4)	44(2)	51(2)	70(2)	-6(2)	11(2)	-2(2)
C(5)	52(2)	70(3)	76(3)	24(2)	5(2)	-6(2)
C(6)	47(2)	69(3)	66(2)	14(2)	-4(2)	-4(2)
C(7)	55(2)	70(3)	101(4)	1(3)	17(2)	-16(2)
C(8)	47(2)	46(2)	64(2)	-6(2)	4(2)	-9(2)
C(9)	51(2)	45(2)	74(3)	0(2)	3(2)	-1(2)
C(10)	47(2)	48(2)	72(2)	6(2)	3(2)	2(2)
C(11)	50(2)	42(2)	62(2)	1(2)	2(2)	3(2)
C(12)	48(2)	41(2)	64(2)	1(2)	1(2)	6(2)
C(13)	46(2)	39(2)	73(3)	1(2)	1(2)	5(2)
C(14)	51(2)	36(2)	70(2)	-3(2)	1(2)	5(2)
C(15)	51(2)	40(2)	84(3)	-4(2)	4(2)	5(2)
C(16)	49(2)	41(2)	81(3)	0(2)	-3(2)	4(2)
C(17)	53(2)	53(2)	94(3)	13(2)	5(2)	4(2)

Table S3-5. Hydrogen coordinates ($\times 10^4$) and isotropic displacement parameters ($Å^2 \times 10^3$) for **3**.

	x	y	z	U(eq)
H(1A)	5260(20)	7860(80)	1950(20)	61
H(2)	3430	9179	566	70
H(3)	2610	6630	646	78
H(5A)	3378	4037	2492	79
H(6A)	4197	6624	2443	74
H(7C)	2117	3898	1950	112
H(7B)	2552	1773	1752	112
H(7A)	2170	3205	1131	112
H(8B)	5117	7454	395	63
H(8A)	4810	5491	867	63
H(9B)	5751	3975	611	68
H(9A)	5813	4641	1442	68
H(10B)	6289	7328	317	67
H(10A)	6258	8412	1100	67

Table S3-6. Torsion angles [°] for **3**.

O(2)-S(1)-N(1)-C(8)	-55.4(3)
O(1)-S(1)-N(1)-C(8)	175.8(3)
C(1)-S(1)-N(1)-C(8)	60.3(3)
O(2)-S(1)-C(1)-C(2)	-4.1(4)
O(1)-S(1)-C(1)-C(2)	127.4(3)
N(1)-S(1)-C(1)-C(2)	-119.9(4)
O(2)-S(1)-C(1)-C(6)	174.3(3)
O(1)-S(1)-C(1)-C(6)	-54.3(4)
N(1)-S(1)-C(1)-C(6)	58.4(4)
C(6)-C(1)-C(2)-C(3)	0.2(7)
S(1)-C(1)-C(2)-C(3)	178.5(4)
C(1)-C(2)-C(3)-C(4)	-1.4(7)
C(2)-C(3)-C(4)-C(5)	1.8(7)
C(2)-C(3)-C(4)-C(7)	-178.4(4)
C(3)-C(4)-C(5)-C(6)	-1.0(7)
C(7)-C(4)-C(5)-C(6)	179.2(5)
C(4)-C(5)-C(6)-C(1)	-0.1(7)
C(2)-C(1)-C(6)-C(5)	0.5(7)
S(1)-C(1)-C(6)-C(5)	-177.8(4)
S(1)-N(1)-C(8)-C(9)	178.4(3)
N(1)-C(8)-C(9)-C(10)	-68.3(4)
C(8)-C(9)-C(10)-C(11)	168.5(4)
C(9)-C(10)-C(11)-F(1)	58.8(5)
C(9)-C(10)-C(11)-F(2)	-59.1(5)
C(9)-C(10)-C(11)-C(12)	-179.6(3)
F(1)-C(11)-C(12)-F(4)	74.3(4)
F(2)-C(11)-C(12)-F(4)	-172.1(3)
C(10)-C(11)-C(12)-F(4)	-49.7(4)
F(1)-C(11)-C(12)-F(3)	-169.1(3)
F(2)-C(11)-C(12)-F(3)	-55.5(4)
C(10)-C(11)-C(12)-F(3)	66.9(4)
F(1)-C(11)-C(12)-C(13)	-47.2(4)

F(2)-C(11)-C(12)-C(13)	66.4(4)
C(10)-C(11)-C(12)-C(13)	-171.2(4)
F(4)-C(12)-C(13)-F(6)	-163.0(3)
F(3)-C(12)-C(13)-F(6)	81.2(4)
C(11)-C(12)-C(13)-F(6)	-41.0(5)
F(4)-C(12)-C(13)-F(5)	-46.0(4)
F(3)-C(12)-C(13)-F(5)	-161.7(3)
C(11)-C(12)-C(13)-F(5)	76.0(4)
F(4)-C(12)-C(13)-C(14)	73.8(4)
F(3)-C(12)-C(13)-C(14)	-42.0(5)
C(11)-C(12)-C(13)-C(14)	-164.3(3)
F(6)-C(13)-C(14)-F(7)	-164.8(3)
F(5)-C(13)-C(14)-F(7)	79.1(4)
C(12)-C(13)-C(14)-F(7)	-41.0(5)
F(6)-C(13)-C(14)-F(8)	-48.0(4)
F(5)-C(13)-C(14)-F(8)	-164.1(3)
C(12)-C(13)-C(14)-F(8)	75.8(4)
F(6)-C(13)-C(14)-C(15)	72.2(4)
F(5)-C(13)-C(14)-C(15)	-43.9(5)
C(12)-C(13)-C(14)-C(15)	-164.1(4)
F(7)-C(14)-C(15)-F(9)	-164.7(3)
F(8)-C(14)-C(15)-F(9)	78.8(4)
C(13)-C(14)-C(15)-F(9)	-41.4(5)
F(7)-C(14)-C(15)-F(10)	-47.1(4)
F(8)-C(14)-C(15)-F(10)	-163.5(3)
C(13)-C(14)-C(15)-F(10)	76.3(4)
F(7)-C(14)-C(15)-C(16)	73.8(5)
F(8)-C(14)-C(15)-C(16)	-42.6(5)
C(13)-C(14)-C(15)-C(16)	-162.8(4)
F(9)-C(15)-C(16)-F(12)	-162.8(4)
F(10)-C(15)-C(16)-F(12)	79.3(4)
C(14)-C(15)-C(16)-F(12)	-41.3(5)
F(9)-C(15)-C(16)-F(11)	-44.3(4)
F(10)-C(15)-C(16)-F(11)	-162.2(3)

C(14)-C(15)-C(16)-F(11)	77.1(4)
F(9)-C(15)-C(16)-C(17)	76.1(5)
F(10)-C(15)-C(16)-C(17)	-41.8(5)
C(14)-C(15)-C(16)-C(17)	-162.4(4)
F(17)-C(18)-C(17)-F(13)	-169.7(5)
F(15)-C(18)-C(17)-F(13)	67.2(6)
F(16)-C(18)-C(17)-F(13)	-49.7(6)
F(17)-C(18)-C(17)-F(14)	74.5(6)
F(15)-C(18)-C(17)-F(14)	-48.6(5)
F(16)-C(18)-C(17)-F(14)	-165.5(4)
F(17)-C(18)-C(17)-C(16)	-46.2(7)
F(15)-C(18)-C(17)-C(16)	-169.3(4)
F(16)-C(18)-C(17)-C(16)	73.8(5)
F(12)-C(16)-C(17)-F(13)	-164.9(4)
F(11)-C(16)-C(17)-F(13)	77.9(5)
C(15)-C(16)-C(17)-F(13)	-42.7(6)
F(12)-C(16)-C(17)-F(14)	-47.5(5)
F(11)-C(16)-C(17)-F(14)	-164.8(4)
C(15)-C(16)-C(17)-F(14)	74.6(5)
F(12)-C(16)-C(17)-C(18)	72.4(5)
F(11)-C(16)-C(17)-C(18)	-44.9(5)
C(15)-C(16)-C(17)-C(18)	-165.5(4)

Symmetry transformations used to generate equivalent atoms:

Table S3-7. Crystal data and structure refinement for **4**

Identification code	james4_0m
Empirical formula	$C_{18}H_{13}ClF_{17}NO_2S$
Formula weight	665.80
Temperature	173(2) K
Wavelength	1.54178 Å
Crystal system	Monoclinic
Space group	P2(1)/n
Unit cell dimensions	a = 5.92980(10) Å α = 90°
	b = 9.0060(2) Å β = 90.1160(10)°
	c = 44.0769(11) Å γ = 90°
Volume	2353.87(9) $Å^3$
Z	4
Density (calculated)	1.879 Mg/m^3
Absorption coefficient	3.753 mm^{-1}
F(000)	1320
Crystal size	0.50 × 0.42 × 0.03 mm^3
θ range for data collection	4.01 to 68.04°.
Index ranges	-6≤h≤7, -10≤k≤10, -52≤l≤50
Reflections collected	17085
Independent reflections	4091 [R(int) = 0.0547]
Completeness to θ = 68.04°	96.0 %
Absorption correction	Semi-empirical from equivalents
Max. and min. transmission	0.7530 and 0.4942
Refinement method	Full-matrix least-squares on F^2
Data / restraints / parameters	4091 / 0 / 361
Goodness-of-fit on F^2	1.054
Final R indices [I>2σ(I)]	R_1 = 0.0613, wR_2 = 0.1548
R indices (all data)	R_1 = 0.0729, wR_2 = 0.1621
Largest diff. peak and hole	0.458 and -0.382 $eÅ^{-3}$

Table S3-8. Atomic coordinates ($\times 10^4$) and equivalent isotropic displacement parameters ($Å^2 \times 10^3$) for **4**. U(eq) is defined as one third of the trace of the orthogonalized U^{ij} tensor.

	x	y	z	U(eq)
S(1)	11759(2)	2653(1)	1928(1)	38(1)
Cl(1)	12210(2)	5735(1)	1824(1)	51(1)
O(1)	10677(5)	1408(3)	1790(1)	47(1)
O(2)	14156(4)	2732(3)	1941(1)	50(1)
N(1)	10903(5)	4096(4)	1717(1)	37(1)
F(1)	5067(4)	3996(3)	848(1)	60(1)
F(2)	7836(5)	5458(3)	741(1)	60(1)
F(3)	10334(4)	3089(3)	553(1)	58(1)
F(4)	7575(5)	1602(3)	664(1)	58(1)
F(5)	4830(3)	3031(3)	272(1)	54(1)
F(6)	7444(5)	4636(2)	169(1)	54(1)
F(7)	7634(5)	783(3)	88(1)	62(1)
F(8)	10219(4)	2406(4)	-15(1)	63(1)
F(9)	7366(5)	3805(3)	-407(1)	59(1)
F(10)	4737(4)	2212(3)	-302(1)	60(1)
F(11)	7344(5)	-47(3)	-491(1)	63(1)
F(12)	10161(4)	1440(3)	-566(1)	57(1)
F(13)	7779(7)	2990(3)	-978(1)	82(1)
F(14)	4846(4)	1634(5)	-897(1)	88(1)
F(15)	7131(9)	-770(4)	-1085(1)	115(2)
F(16)	10088(6)	463(5)	-1138(1)	104(1)
F(17)	7236(5)	999(3)	-1401(1)	71(1)
C(1)	10655(6)	2882(4)	2296(1)	35(1)
C(2)	8599(6)	2251(5)	2366(1)	40(1)
C(3)	7707(6)	2469(5)	2651(1)	41(1)
C(4)	8838(7)	3301(5)	2870(1)	42(1)
C(5)	10921(7)	3906(4)	2793(1)	43(1)

C(6)	11856(6)	3708(5)	2510(1)	42(1)
C(7)	7841(8)	3552(5)	3179(1)	52(1)
C(8)	8411(6)	4275(5)	1688(1)	40(1)
C(9)	7785(7)	4843(5)	1373(1)	41(1)
C(10)	8377(7)	3714(5)	1130(1)	43(1)
C(11)	7344(6)	4053(4)	828(1)	35(1)
C(12)	8086(6)	2985(4)	574(1)	35(1)
C(13)	7057(6)	3231(4)	254(1)	32(1)
C(14)	7993(6)	2190(4)	4(1)	34(1)
C(15)	6972(6)	2411(4)	-316(1)	34(1)
C(16)	7900(6)	1343(4)	-563(1)	35(1)
C(17)	7097(7)	1660(5)	-890(1)	41(1)
C(18)	7880(8)	552(5)	-1131(1)	49(1)

Table S3-9. Bond lengths [Å] and angles [°] for **4**.

S(1)-O(2)	1.424(3)
S(1)-O(1)	1.428(3)
S(1)-N(1)	1.677(3)
S(1)-C(1)	1.761(4)
Cl(1)-N(1)	1.733(3)
N(1)-C(8)	1.492(5)
F(1)-C(11)	1.354(4)
F(2)-C(11)	1.354(4)
F(3)-C(12)	1.340(4)
F(4)-C(12)	1.343(4)
F(5)-C(13)	1.335(4)
F(6)-C(13)	1.340(4)
F(7)-C(14)	1.338(4)
F(8)-C(14)	1.337(4)
F(9)-C(15)	1.338(4)
F(10)-C(15)	1.339(4)
F(11)-C(16)	1.333(4)
F(12)-C(16)	1.344(4)
F(13)-C(17)	1.322(5)
F(14)-C(17)	1.335(5)
F(15)-C(18)	1.287(5)
F(16)-C(18)	1.312(5)
F(17)-C(18)	1.311(5)
C(1)-C(2)	1.381(5)
C(1)-C(6)	1.396(5)
C(2)-C(3)	1.376(6)
C(2)-H(2B)	0.9500
C(3)-C(4)	1.393(6)
C(3)-H(3A)	0.9500
C(4)-C(5)	1.393(6)
C(4)-C(7)	1.504(6)
C(5)-C(6)	1.378(6)

C(5)-H(5A)	0.9500
C(6)-H(6A)	0.9500
C(7)-H(7A)	0.9800
C(7)-H(7B)	0.9800
C(7)-H(7C)	0.9800
C(8)-C(9)	1.524(5)
C(8)-H(8A)	0.9900
C(8)-H(8B)	0.9900
C(9)-C(10)	1.520(5)
C(9)-H(9A)	0.9900
C(9)-H(9B)	0.9900
C(10)-C(11)	1.495(5)
C(10)-H(10A)	0.9900
C(10)-H(10B)	0.9900
C(11)-C(12)	1.542(5)
C(12)-C(13)	1.550(5)
C(13)-C(14)	1.551(5)
C(14)-C(15)	1.546(5)
C(15)-C(16)	1.554(5)
C(16)-C(17)	1.541(5)
C(17)-C(18)	1.532(6)

O(2)-S(1)-O(1)	120.23(18)
O(2)-S(1)-N(1)	106.48(17)
O(1)-S(1)-N(1)	103.62(17)
O(2)-S(1)-C(1)	109.36(18)
O(1)-S(1)-C(1)	108.50(18)
N(1)-S(1)-C(1)	107.94(17)
C(8)-N(1)-S(1)	115.4(2)
C(8)-N(1)-Cl(1)	111.9(3)
S(1)-N(1)-Cl(1)	111.93(18)
C(2)-C(1)-C(6)	121.1(4)
C(2)-C(1)-S(1)	119.3(3)
C(6)-C(1)-S(1)	119.6(3)

C(3)-C(2)-C(1)	119.2(4)
C(3)-C(2)-H(2B)	120.4
C(1)-C(2)-H(2B)	120.4
C(2)-C(3)-C(4)	121.5(4)
C(2)-C(3)-H(3A)	119.2
C(4)-C(3)-H(3A)	119.2
C(5)-C(4)-C(3)	117.9(4)
C(5)-C(4)-C(7)	120.8(4)
C(3)-C(4)-C(7)	121.3(4)
C(6)-C(5)-C(4)	121.9(4)
C(6)-C(5)-H(5A)	119.0
C(4)-C(5)-H(5A)	119.0
C(5)-C(6)-C(1)	118.4(4)
C(5)-C(6)-H(6A)	120.8
C(1)-C(6)-H(6A)	120.8
C(4)-C(7)-H(7A)	109.5
C(4)-C(7)-H(7B)	109.5
H(7A)-C(7)-H(7B)	109.5
C(4)-C(7)-H(7C)	109.5
H(7A)-C(7)-H(7C)	109.5
H(7B)-C(7)-H(7C)	109.5
N(1)-C(8)-C(9)	110.7(3)
N(1)-C(8)-H(8A)	109.5
C(9)-C(8)-H(8A)	109.5
N(1)-C(8)-H(8B)	109.5
C(9)-C(8)-H(8B)	109.5
H(8A)-C(8)-H(8B)	108.1
C(10)-C(9)-C(8)	111.2(3)
C(10)-C(9)-H(9A)	109.4
C(8)-C(9)-H(9A)	109.4
C(10)-C(9)-H(9B)	109.4
C(8)-C(9)-H(9B)	109.4
H(9A)-C(9)-H(9B)	108.0
C(11)-C(10)-C(9)	113.4(3)

C(11)-C(10)-H(10A)	108.9
C(9)-C(10)-H(10A)	108.9
C(11)-C(10)-H(10B)	108.9
C(9)-C(10)-H(10B)	108.9
H(10A)-C(10)-H(10B)	107.7
F(2)-C(11)-F(1)	105.6(3)
F(2)-C(11)-C(10)	110.7(3)
F(1)-C(11)-C(10)	110.0(3)
F(2)-C(11)-C(12)	108.4(3)
F(1)-C(11)-C(12)	108.0(3)
C(10)-C(11)-C(12)	113.7(3)
F(3)-C(12)-F(4)	108.1(3)
F(3)-C(12)-C(11)	106.9(3)
F(4)-C(12)-C(11)	107.3(3)
F(3)-C(12)-C(13)	108.6(3)
F(4)-C(12)-C(13)	108.3(3)
C(11)-C(12)-C(13)	117.3(3)
F(5)-C(13)-F(6)	108.3(3)
F(5)-C(13)-C(12)	108.3(3)
F(6)-C(13)-C(12)	108.8(3)
F(5)-C(13)-C(14)	108.4(3)
F(6)-C(13)-C(14)	108.0(3)
C(12)-C(13)-C(14)	114.8(3)
F(8)-C(14)-F(7)	108.2(3)
F(8)-C(14)-C(15)	108.0(3)
F(7)-C(14)-C(15)	108.2(3)
F(8)-C(14)-C(13)	108.2(3)
F(7)-C(14)-C(13)	108.5(3)
C(15)-C(14)-C(13)	115.6(3)
F(9)-C(15)-F(10)	108.3(3)
F(9)-C(15)-C(14)	108.9(3)
F(10)-C(15)-C(14)	108.9(3)
F(9)-C(15)-C(16)	108.0(3)
F(10)-C(15)-C(16)	107.7(3)

C(14)-C(15)-C(16)	114.9(3)
F(11)-C(16)-F(12)	108.1(3)
F(11)-C(16)-C(17)	108.7(3)
F(12)-C(16)-C(17)	106.6(3)
F(11)-C(16)-C(15)	109.0(3)
F(12)-C(16)-C(15)	108.7(3)
C(17)-C(16)-C(15)	115.5(3)
F(13)-C(17)-F(14)	108.4(4)
F(13)-C(17)-C(18)	107.1(3)
F(14)-C(17)-C(18)	106.0(3)
F(13)-C(17)-C(16)	110.3(3)
F(14)-C(17)-C(16)	109.0(3)
C(18)-C(17)-C(16)	115.7(3)
F(15)-C(18)-F(17)	109.1(4)
F(15)-C(18)-F(16)	106.9(4)
F(17)-C(18)-F(16)	106.6(4)
F(15)-C(18)-C(17)	112.8(4)
F(17)-C(18)-C(17)	110.0(4)
F(16)-C(18)-C(17)	111.1(4)

Symmetry transformations used to generate equivalent atoms:

Table S3-10. Anisotropic displacement parameters ($Å^2 \times 10^3$) for **4**. The anisotropic displacement factor exponent takes the form:
$-2\pi^2[h^2a^{*2}U^{11} + ... + 2hka^*b^*U^{12}]$

	U^{11}	U^{22}	U^{33}	U^{23}	U^{13}	U^{12}
S(1)	30(1)	40(1)	45(1)	0(1)	1(1)	2(1)
Cl(1)	43(1)	44(1)	65(1)	2(1)	6(1)	-7(1)
O(1)	46(2)	43(2)	53(2)	-9(1)	2(1)	-1(1)
O(2)	32(1)	58(2)	61(2)	4(2)	2(1)	7(1)
N(1)	30(2)	42(2)	39(2)	2(1)	3(1)	-2(1)
F(1)	34(1)	93(2)	51(2)	-16(1)	0(1)	14(1)
F(2)	103(2)	34(1)	44(1)	0(1)	-1(1)	0(1)
F(3)	29(1)	98(2)	49(1)	-17(1)	-2(1)	15(1)
F(4)	99(2)	32(1)	42(1)	4(1)	-7(1)	5(1)
F(5)	26(1)	90(2)	45(1)	-9(1)	3(1)	8(1)
F(6)	90(2)	28(1)	44(1)	2(1)	-2(1)	6(1)
F(7)	110(2)	31(1)	44(1)	3(1)	-2(1)	10(1)
F(8)	26(1)	112(2)	51(1)	-23(2)	1(1)	10(1)
F(9)	101(2)	31(1)	45(1)	4(1)	2(1)	9(1)
F(10)	27(1)	106(2)	48(1)	-16(1)	0(1)	9(1)
F(11)	108(2)	31(1)	51(2)	-1(1)	10(1)	-3(1)
F(12)	33(1)	90(2)	50(1)	-15(1)	2(1)	16(1)
F(13)	158(3)	42(2)	45(2)	5(1)	-7(2)	-1(2)
F(14)	46(2)	157(3)	59(2)	-33(2)	-13(1)	34(2)
F(15)	224(5)	56(2)	66(2)	-19(2)	35(3)	-27(2)
F(16)	67(2)	183(4)	61(2)	-36(2)	0(2)	47(2)
F(17)	93(2)	77(2)	42(1)	-10(1)	-14(1)	31(2)
C(1)	28(2)	37(2)	41(2)	4(2)	-5(2)	0(2)
C(2)	32(2)	44(2)	44(2)	5(2)	-9(2)	-6(2)
C(3)	29(2)	48(2)	47(2)	8(2)	-3(2)	-3(2)
C(4)	40(2)	42(2)	44(2)	8(2)	-3(2)	9(2)
C(5)	44(2)	38(2)	46(2)	0(2)	-11(2)	-3(2)

C(6)	31(2)	45(2)	48(2)	2(2)	-4(2)	-6(2)
C(7)	53(3)	52(3)	51(3)	4(2)	-3(2)	6(2)
C(8)	29(2)	54(2)	38(2)	1(2)	5(2)	3(2)
C(9)	39(2)	47(2)	36(2)	-2(2)	0(2)	9(2)
C(10)	43(2)	44(2)	40(2)	1(2)	-5(2)	10(2)
C(11)	31(2)	33(2)	40(2)	0(2)	2(2)	4(2)
C(12)	29(2)	33(2)	41(2)	2(2)	-2(2)	5(2)
C(13)	29(2)	26(2)	40(2)	1(2)	-1(2)	6(2)
C(14)	31(2)	29(2)	42(2)	0(2)	-2(2)	6(2)
C(15)	29(2)	31(2)	42(2)	2(2)	0(2)	5(2)
C(16)	33(2)	31(2)	41(2)	0(2)	1(2)	8(2)
C(17)	42(2)	40(2)	41(2)	-1(2)	-1(2)	10(2)
C(18)	57(3)	46(3)	44(2)	-4(2)	-5(2)	8(2)

Table S3-11. Hydrogen coordinates ($\times 10^4$) and isotropic displacement parameters ($Å^2 \times 10^3$) for **4**.

	x	y	z	U(eq)
H(2B)	7809	1674	2220	48
H(3A)	6287	2042	2699	49
H(5A)	11721	4472	2940	52
H(6A)	13284	4124	2462	50
H(7A)	6374	3055	3192	78
H(7B)	7644	4619	3213	78
H(7C)	8855	3144	3334	78
H(8A)	7869	4984	1843	48
H(8B)	7665	3308	1724	48
H(9A)	6147	5053	1366	49
H(9B)	8598	5783	1333	49
H(10A)	10037	3677	1107	51
H(10B)	7865	2720	1196	51

Table S3-12. Torsion angles [°] for **4**.

O(2)-S(1)-N(1)-C(8)	-176.8(3)
O(1)-S(1)-N(1)-C(8)	55.5(3)
C(1)-S(1)-N(1)-C(8)	-59.4(3)
O(2)-S(1)-N(1)-Cl(1)	-47.2(2)
O(1)-S(1)-N(1)-Cl(1)	-174.90(18)
C(1)-S(1)-N(1)-Cl(1)	70.2(2)
O(2)-S(1)-C(1)-C(2)	-152.7(3)
O(1)-S(1)-C(1)-C(2)	-19.9(4)
N(1)-S(1)-C(1)-C(2)	91.8(3)
O(2)-S(1)-C(1)-C(6)	28.0(4)
O(1)-S(1)-C(1)-C(6)	160.8(3)
N(1)-S(1)-C(1)-C(6)	-87.5(3)
C(6)-C(1)-C(2)-C(3)	1.2(6)
S(1)-C(1)-C(2)-C(3)	-178.0(3)
C(1)-C(2)-C(3)-C(4)	-0.5(6)
C(2)-C(3)-C(4)-C(5)	-0.3(6)
C(2)-C(3)-C(4)-C(7)	179.2(4)
C(3)-C(4)-C(5)-C(6)	0.3(6)
C(7)-C(4)-C(5)-C(6)	-179.2(4)
C(4)-C(5)-C(6)-C(1)	0.4(6)
C(2)-C(1)-C(6)-C(5)	-1.2(6)
S(1)-C(1)-C(6)-C(5)	178.1(3)
S(1)-N(1)-C(8)-C(9)	-144.4(3)
Cl(1)-N(1)-C(8)-C(9)	86.0(4)
N(1)-C(8)-C(9)-C(10)	64.9(5)
C(8)-C(9)-C(10)-C(11)	167.0(3)
C(9)-C(10)-C(11)-F(2)	53.0(5)
C(9)-C(10)-C(11)-F(1)	-63.3(4)
C(9)-C(10)-C(11)-C(12)	175.4(3)
F(2)-C(11)-C(12)-F(3)	64.5(4)
F(1)-C(11)-C(12)-F(3)	178.5(3)
C(10)-C(11)-C(12)-F(3)	-59.2(4)

F(2)-C(11)-C(12)-F(4)	-179.8(3)
F(1)-C(11)-C(12)-F(4)	-65.8(4)
C(10)-C(11)-C(12)-F(4)	56.5(4)
F(2)-C(11)-C(12)-C(13)	-57.7(4)
F(1)-C(11)-C(12)-C(13)	56.3(4)
C(10)-C(11)-C(12)-C(13)	178.7(3)
F(3)-C(12)-C(13)-F(5)	176.1(3)
F(4)-C(12)-C(13)-F(5)	58.9(4)
C(11)-C(12)-C(13)-F(5)	-62.7(4)
F(3)-C(12)-C(13)-F(6)	-66.4(4)
F(4)-C(12)-C(13)-F(6)	176.5(3)
C(11)-C(12)-C(13)-F(6)	54.8(4)
F(3)-C(12)-C(13)-C(14)	54.8(4)
F(4)-C(12)-C(13)-C(14)	-62.4(4)
C(11)-C(12)-C(13)-C(14)	176.0(3)
F(5)-C(13)-C(14)-F(8)	179.4(3)
F(6)-C(13)-C(14)-F(8)	62.2(4)
C(12)-C(13)-C(14)-F(8)	-59.3(4)
F(5)-C(13)-C(14)-F(7)	-63.4(4)
F(6)-C(13)-C(14)-F(7)	179.4(3)
C(12)-C(13)-C(14)-F(7)	57.8(4)
F(5)-C(13)-C(14)-C(15)	58.3(4)
F(6)-C(13)-C(14)-C(15)	-58.9(4)
C(12)-C(13)-C(14)-C(15)	179.5(3)
F(8)-C(14)-C(15)-F(9)	-61.6(4)
F(7)-C(14)-C(15)-F(9)	-178.5(3)
C(13)-C(14)-C(15)-F(9)	59.6(4)
F(8)-C(14)-C(15)-F(10)	-179.5(3)
F(7)-C(14)-C(15)-F(10)	63.6(4)
C(13)-C(14)-C(15)-F(10)	-58.2(4)
F(8)-C(14)-C(15)-C(16)	59.7(4)
F(7)-C(14)-C(15)-C(16)	-57.2(4)
C(13)-C(14)-C(15)-C(16)	-179.1(3)
F(9)-C(15)-C(16)-F(11)	-174.4(3)

F(10)-C(15)-C(16)-F(11)	-57.7(4)
C(14)-C(15)-C(16)-F(11)	63.8(4)
F(9)-C(15)-C(16)-F(12)	68.0(4)
F(10)-C(15)-C(16)-F(12)	-175.3(3)
C(14)-C(15)-C(16)-F(12)	-53.8(4)
F(9)-C(15)-C(16)-C(17)	-51.8(4)
F(10)-C(15)-C(16)-C(17)	64.9(4)
C(14)-C(15)-C(16)-C(17)	-173.5(3)
F(11)-C(16)-C(17)-F(13)	-175.0(3)
F(12)-C(16)-C(17)-F(13)	-58.7(4)
C(15)-C(16)-C(17)-F(13)	62.2(4)
F(11)-C(16)-C(17)-F(14)	66.1(4)
F(12)-C(16)-C(17)-F(14)	-177.6(3)
C(15)-C(16)-C(17)-F(14)	-56.7(5)
F(11)-C(16)-C(17)-C(18)	-53.3(5)
F(12)-C(16)-C(17)-C(18)	63.0(4)
C(15)-C(16)-C(17)-C(18)	-176.1(3)
F(13)-C(17)-C(18)-F(15)	-173.9(4)
F(14)-C(17)-C(18)-F(15)	-58.4(5)
C(16)-C(17)-C(18)-F(15)	62.6(5)
F(13)-C(17)-C(18)-F(17)	-51.8(5)
F(14)-C(17)-C(18)-F(17)	63.7(5)
C(16)-C(17)-C(18)-F(17)	-175.3(4)
F(13)-C(17)-C(18)-F(16)	66.0(5)
F(14)-C(17)-C(18)-F(16)	-178.5(4)
C(16)-C(17)-C(18)-F(16)	-57.5(5)

Symmetry transformations used to generate equivalent atoms:

APPENDIX 2

Supporting Information for Chapter 4

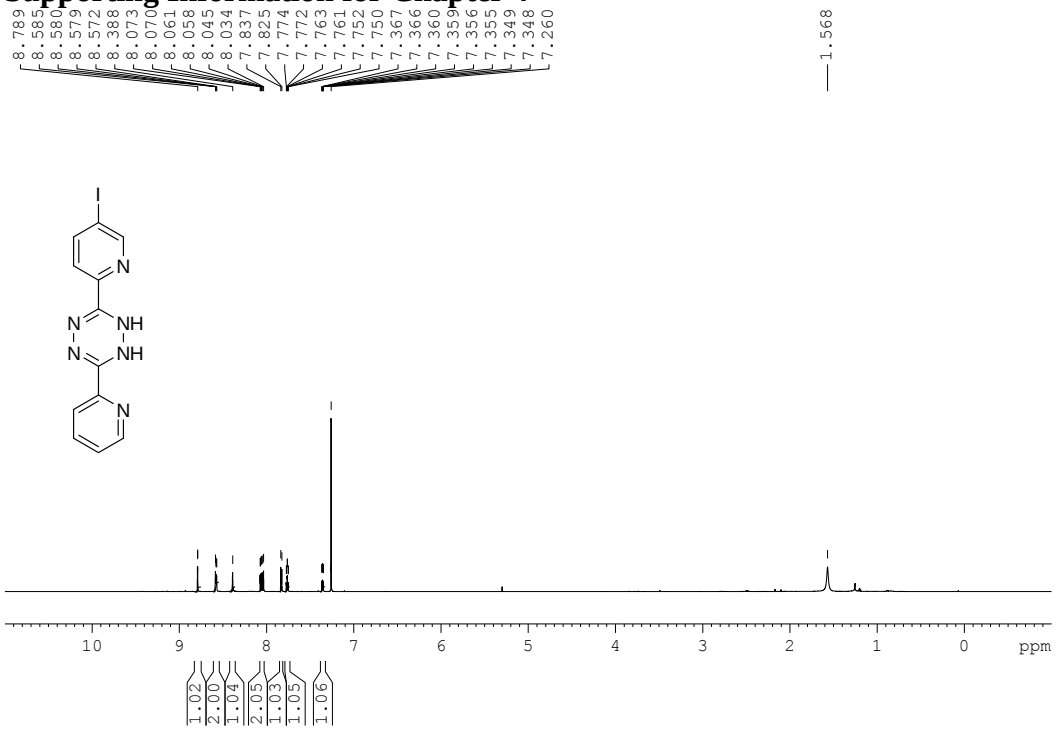

Figure S4-1. ^{1}H NMR (700 MHz, $CDCl_3$) spectrum of **3**.

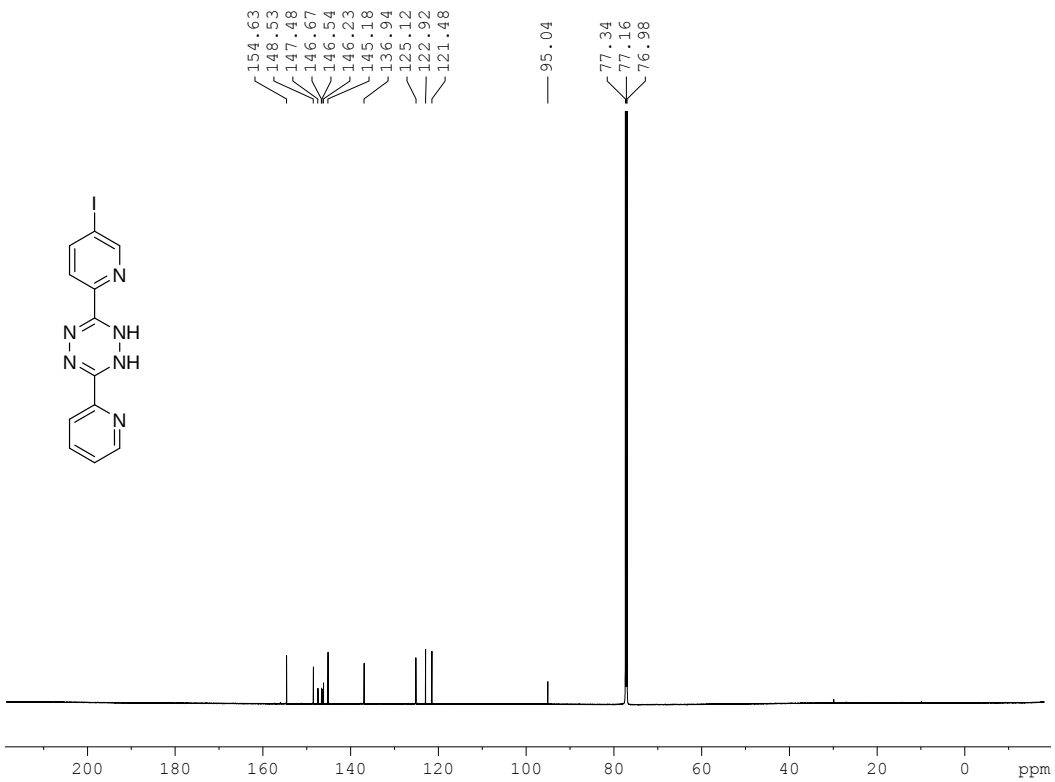

Figure S4-2. ^{13}C NMR (150 MHz, $CDCl_3$) spectrum of **3**.

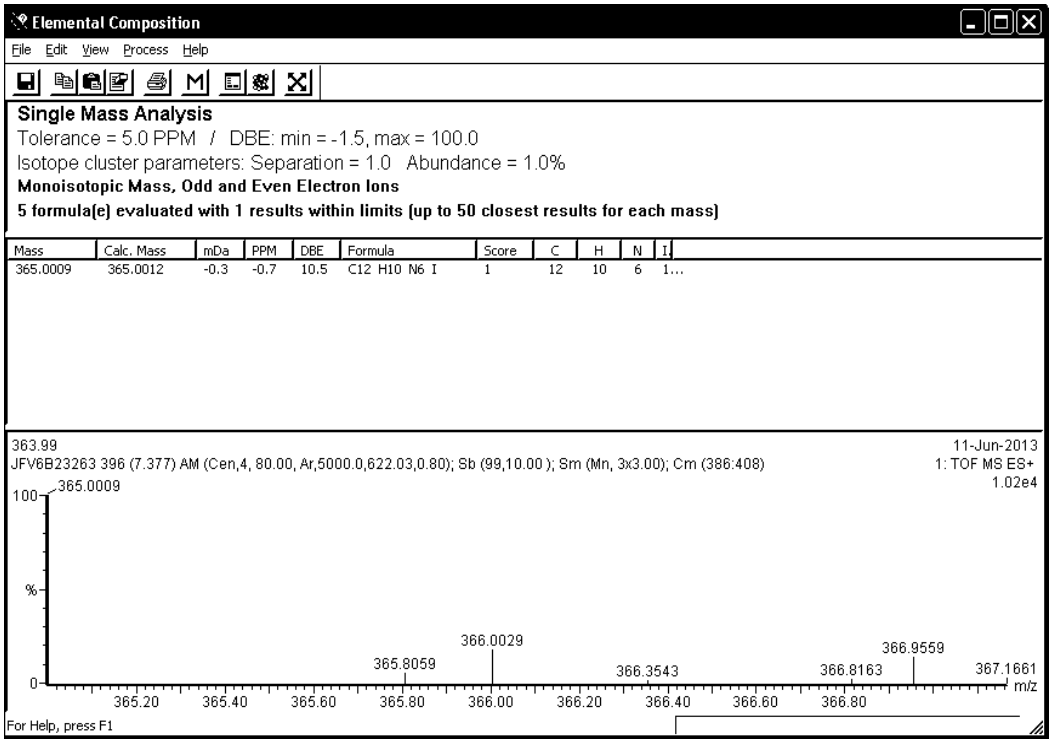

Figure S4-3. HRMS (TOF ESI$^+$) spectrum of **3**.

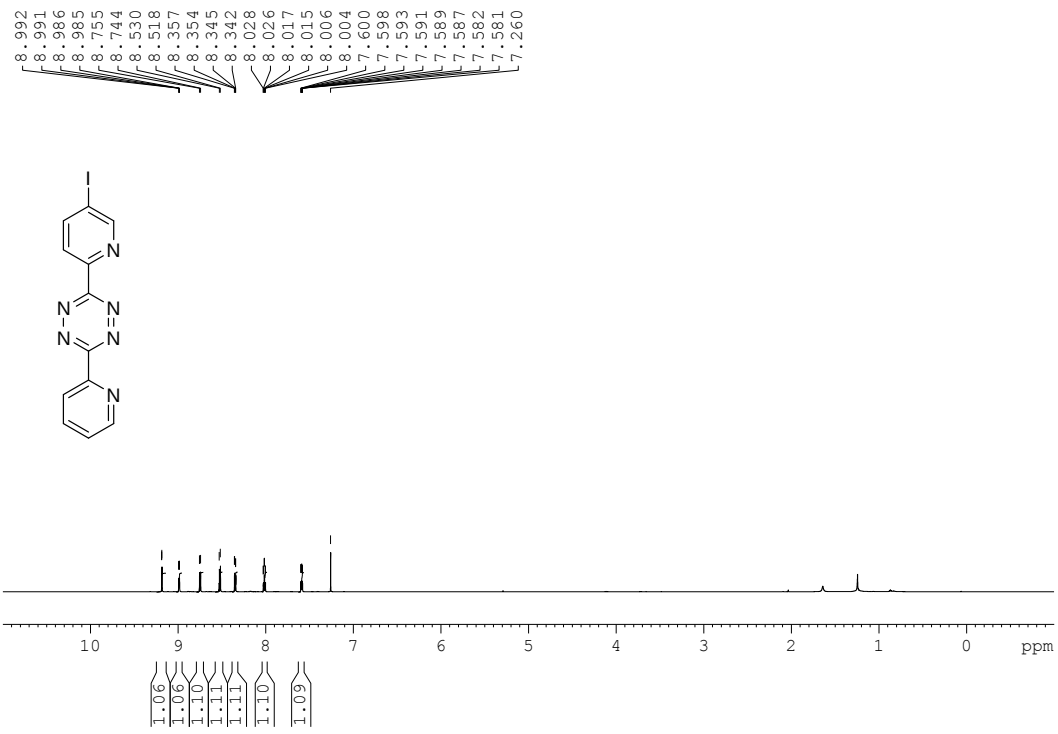

Figure S4-4. ^{1}H NMR ($CDCl_3$, 700 MHz) spectrum of **4a**.

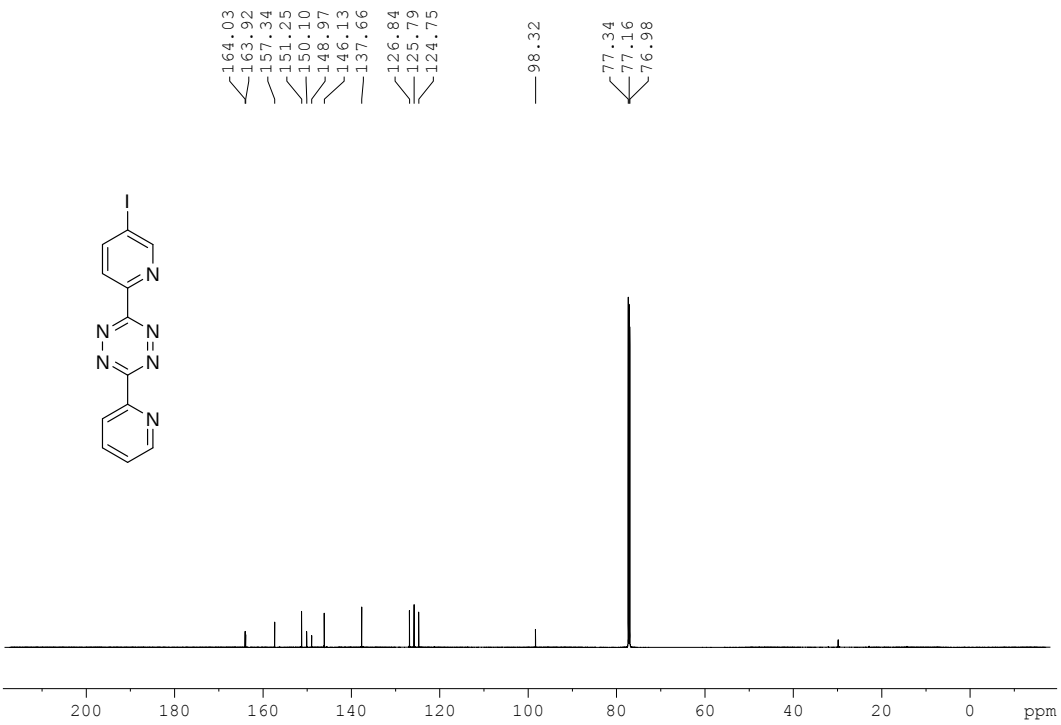

Figure S4-5. ^{13}C NMR ($CDCl_3$, 150 MHz) spectrum of **4a**.

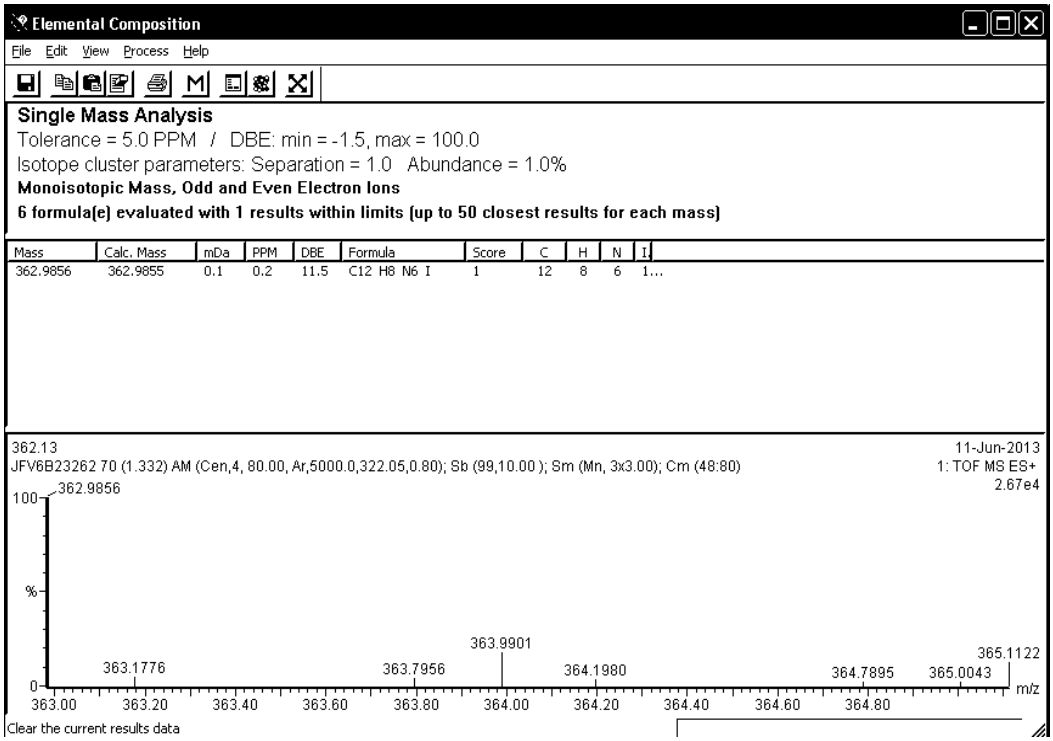

Figure S4-6. HRMS (TOF ESI$^+$) spectrum of **4a**.

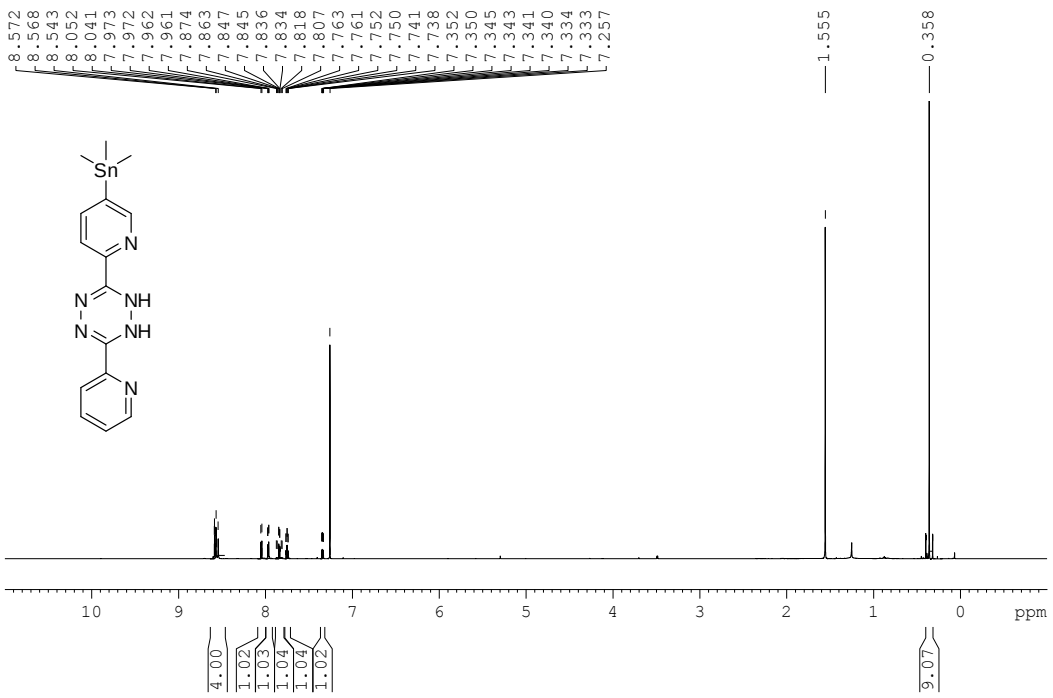

Figure S4-7. ^{1}H NMR (700 MHz, $CDCl_3$) spectrum of **5**.

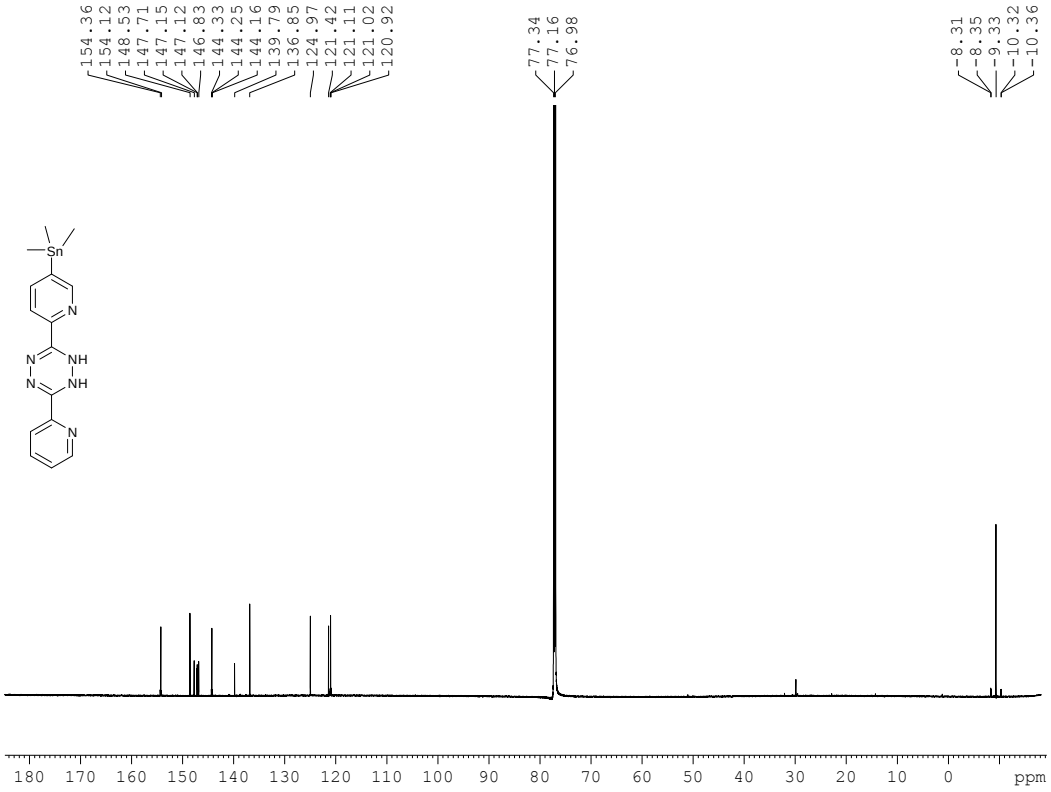

Figure S4-8. ^{13}C NMR (150 MHz, $CDCl_3$) spectrum of **5**.

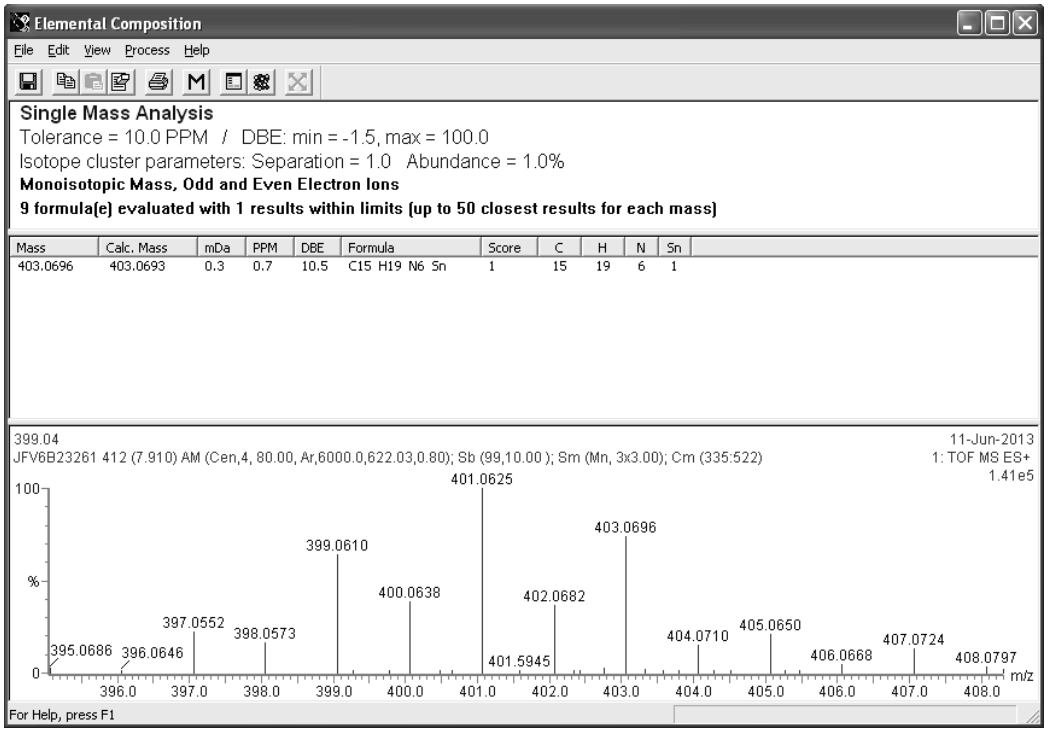

Figure S4-9. HRMS (TOF ESI$^+$) spectrum of **5**.

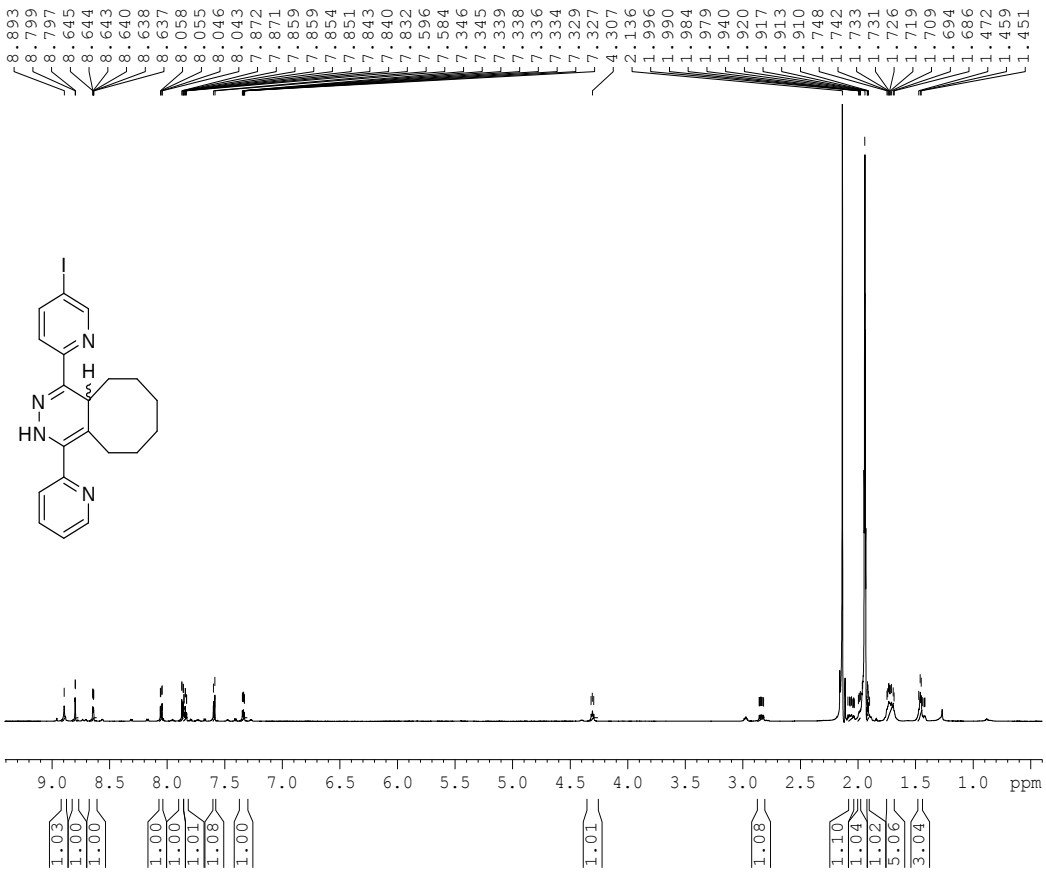

Figure S4-10. ^{1}H NMR (700 MHz, CD_3CN) spectrum **7a**.

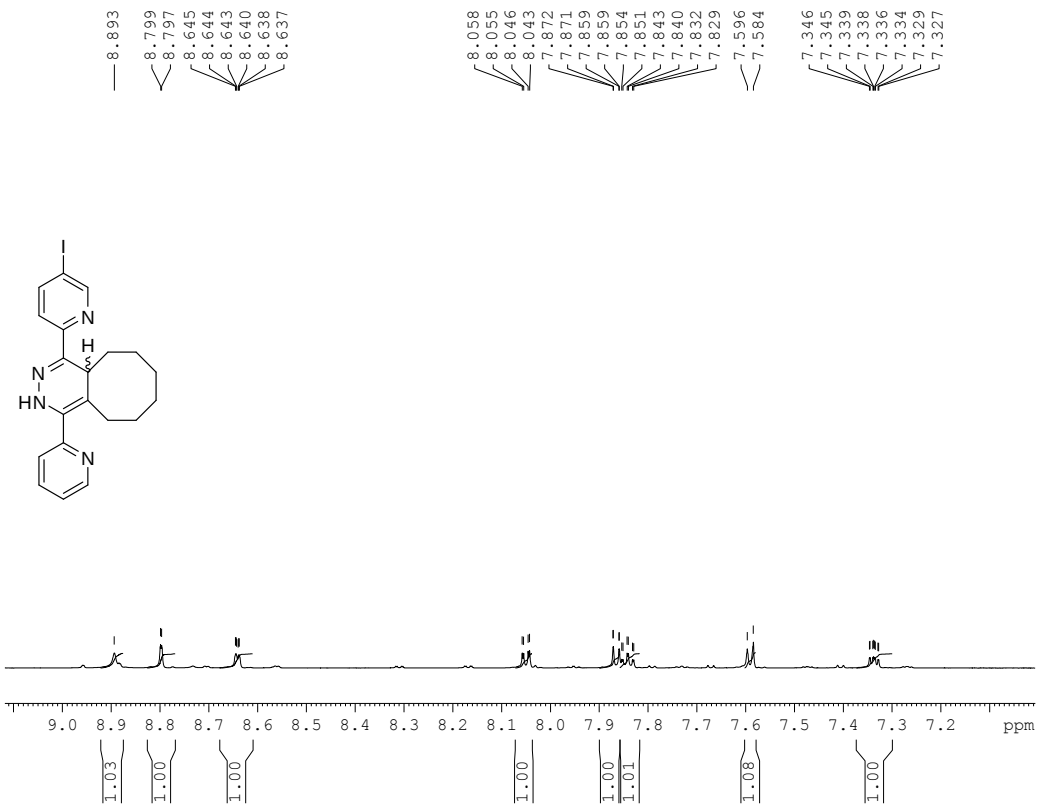

Figure S4-11. Expansion of the ^{1}H NMR (700 MHz, CD_3CN) spectrum of **7a** showing the aromatic region.

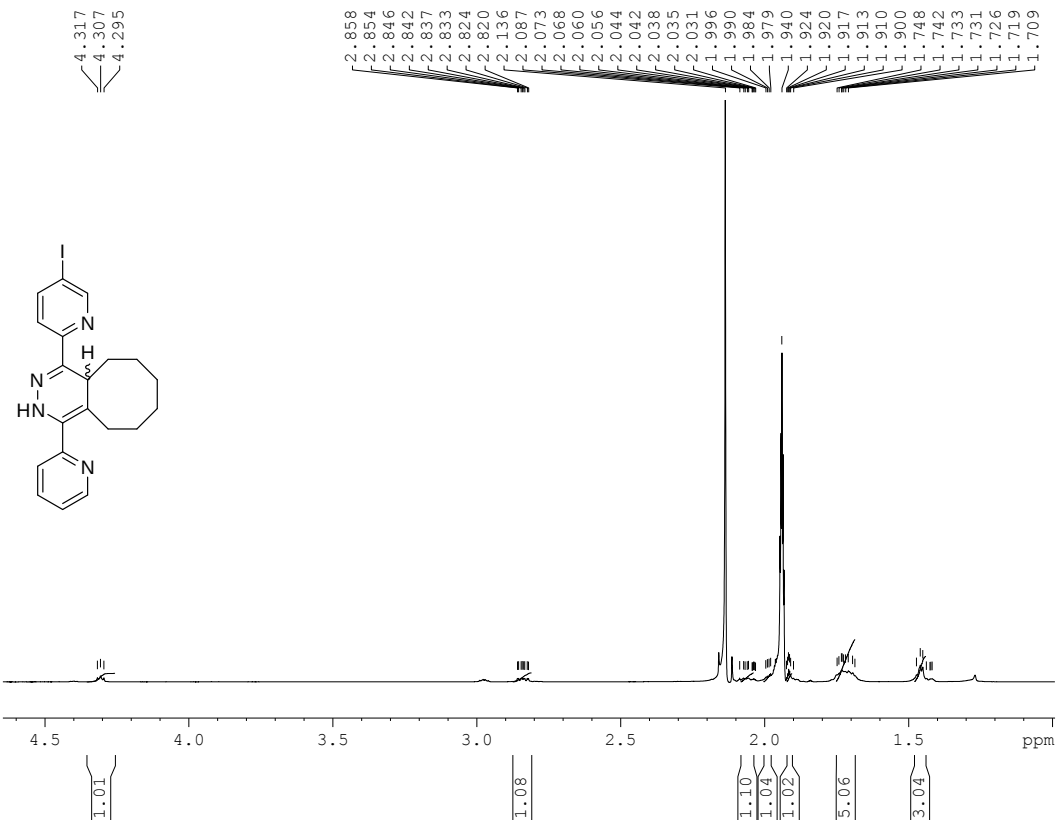

Figure S4-12. Expansion of the ^{1}H NMR (700 MHz, CD_3CN) spectrum of **7a** showing the aliphatic region.

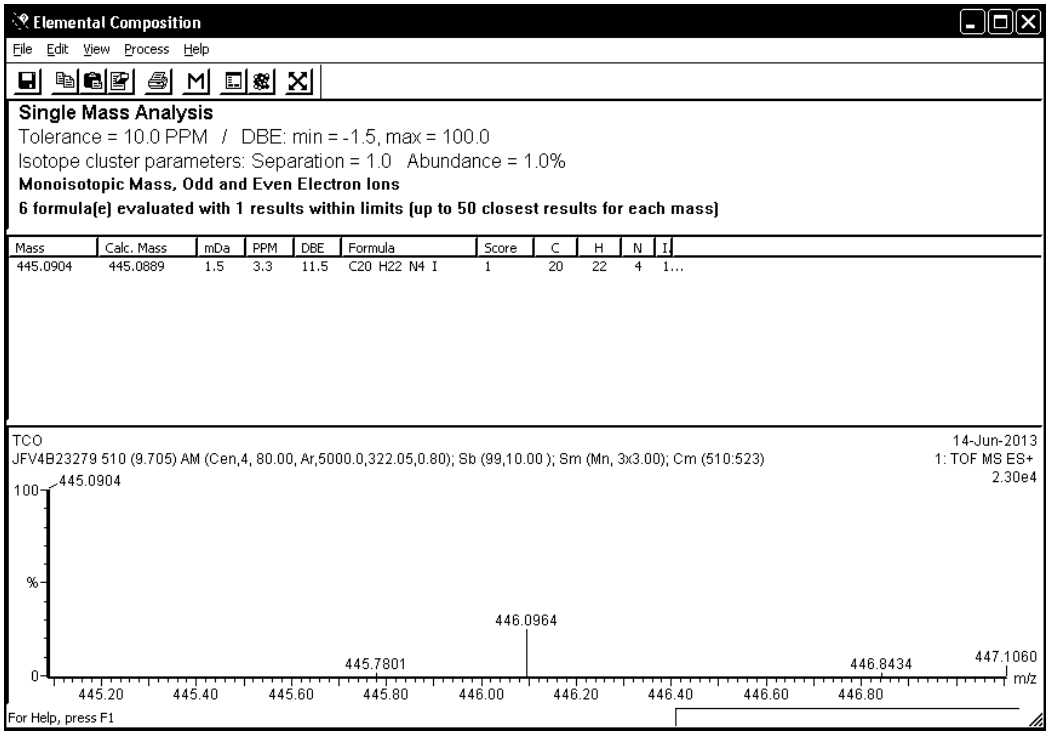

Figure S4-13. HRMS (TOF ESI$^+$) spectrum of **7a**.

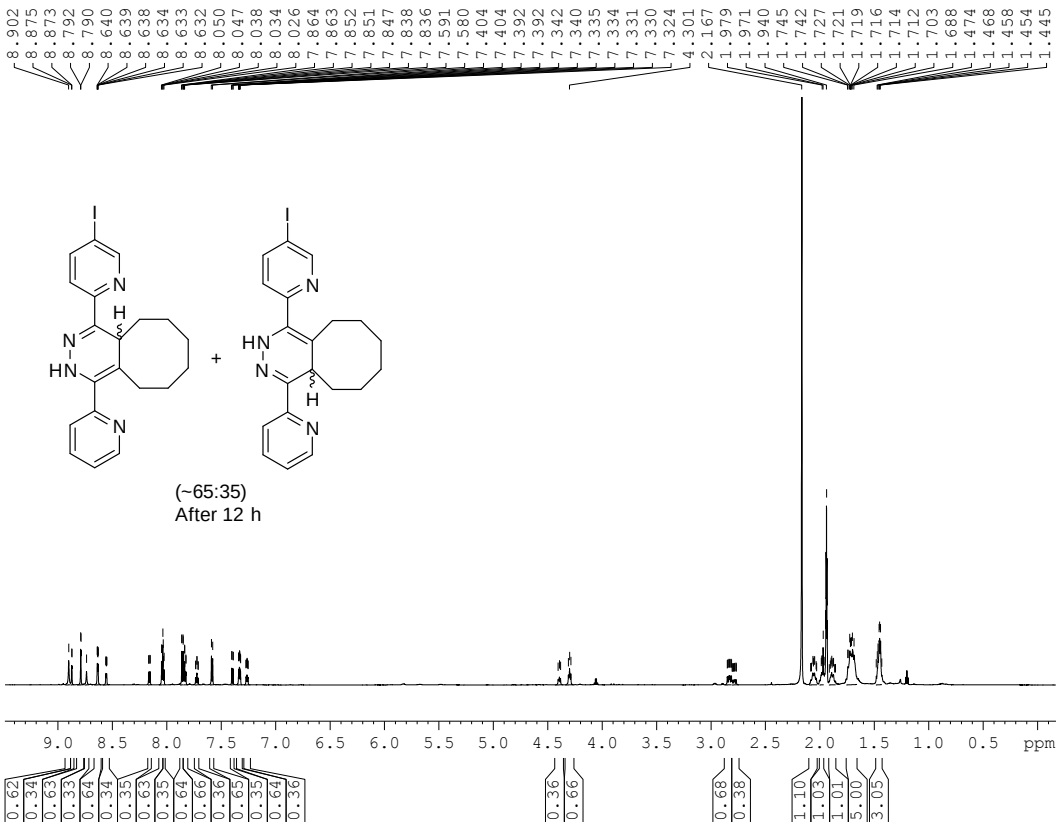

Figure S4-14. ^{1}H NMR (700 MHz, CD_3CN) spectrum of isomeric mixture **7a** and **8a** 12 hours after ligation.

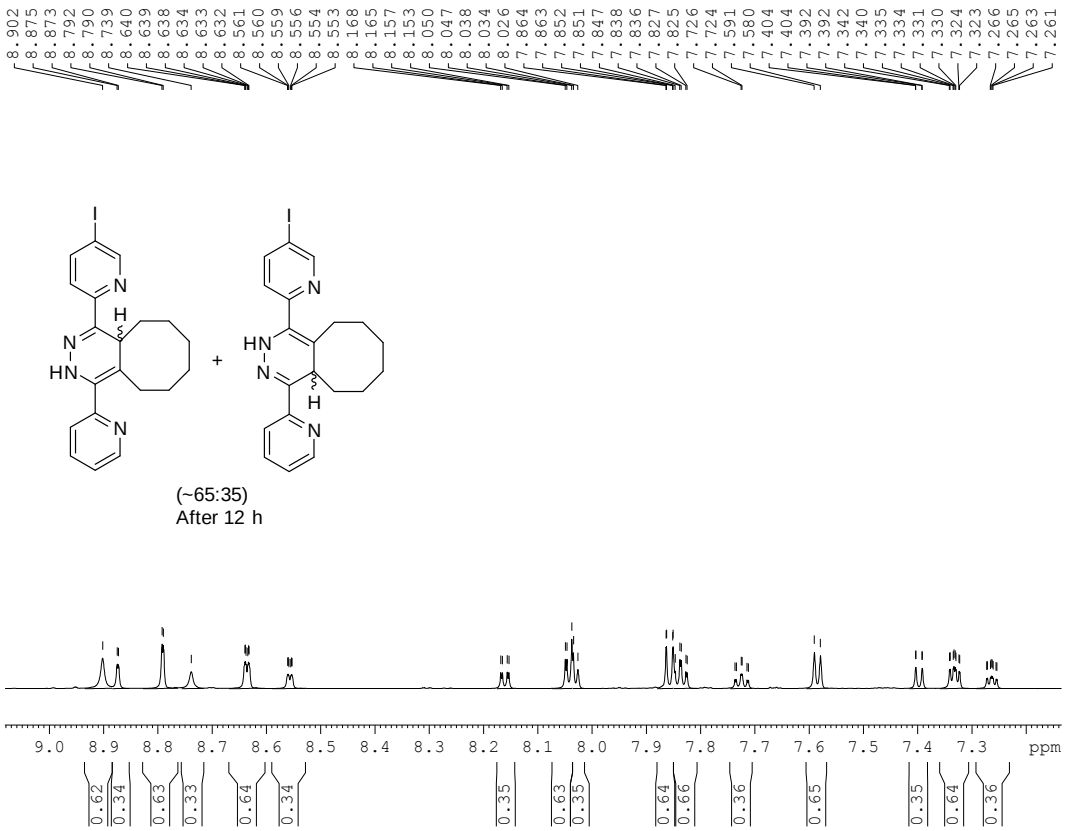

Figure S4-15. Expansion of ^{1}H NMR spectrum (700 MHz, CD_3CN) showing aromatic protons corresponding to isomers **7a** and **8a** 12 hours after ligation.

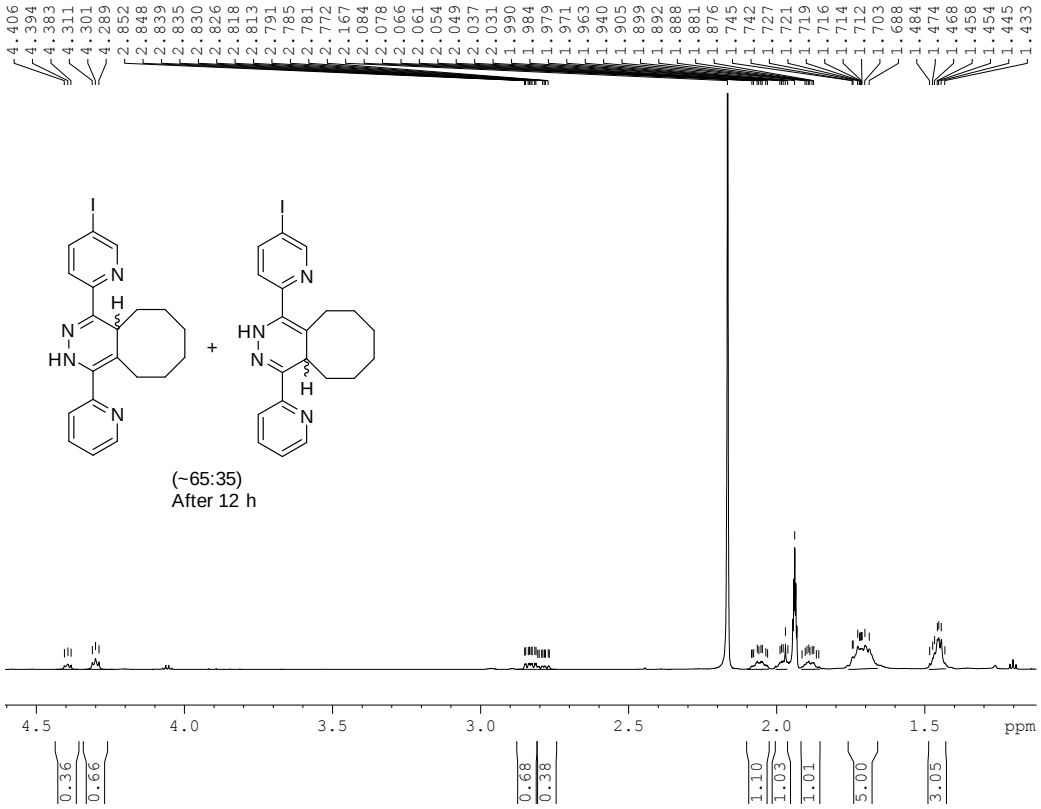

Figure S4-16. Expansion of ^{1}H NMR (700 MHz, CD_3CN) spectrum showing aliphatic protons corresponding to isomers **7a** and **8a** 12 hours after ligation.

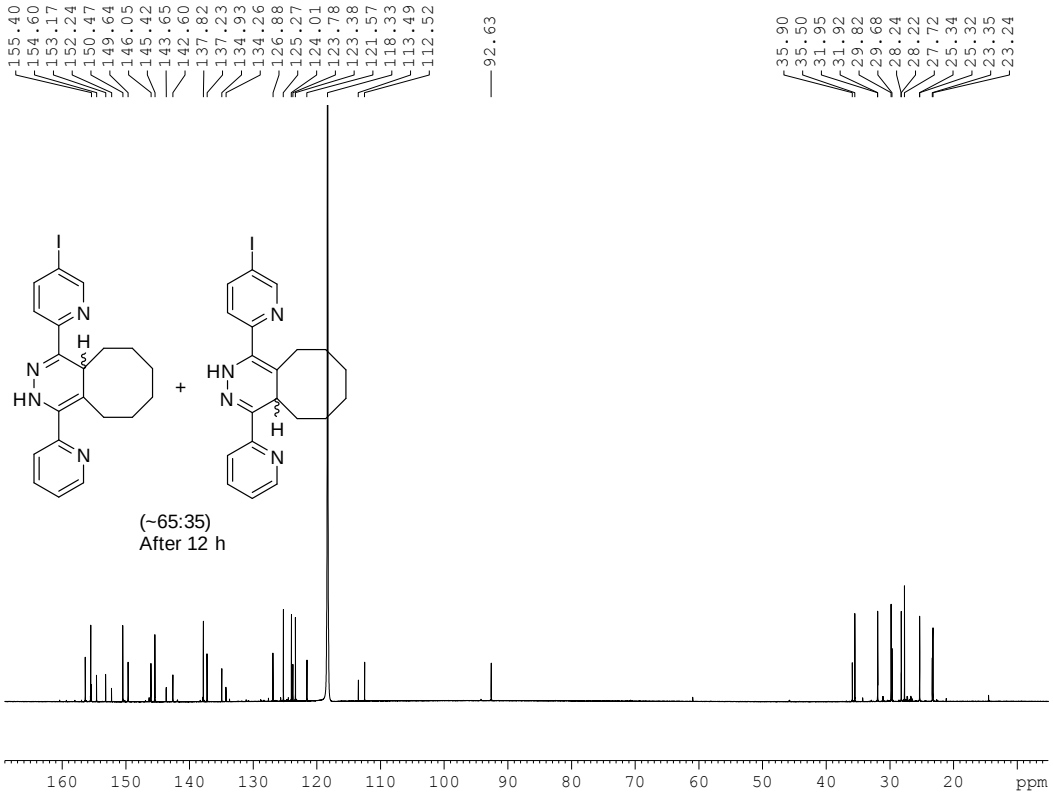

Figure S4-17. ^{13}C NMR (150 MHz, CD_3CN) spectrum of isomeric mixture **7a** and **8a** 12 hours after ligation.

Figure S4-18. ^{1}H NMR (700 MHz, CD_3CN) spectrum of isomeric mixture **7a** and **8a** 2 hours after ligation.

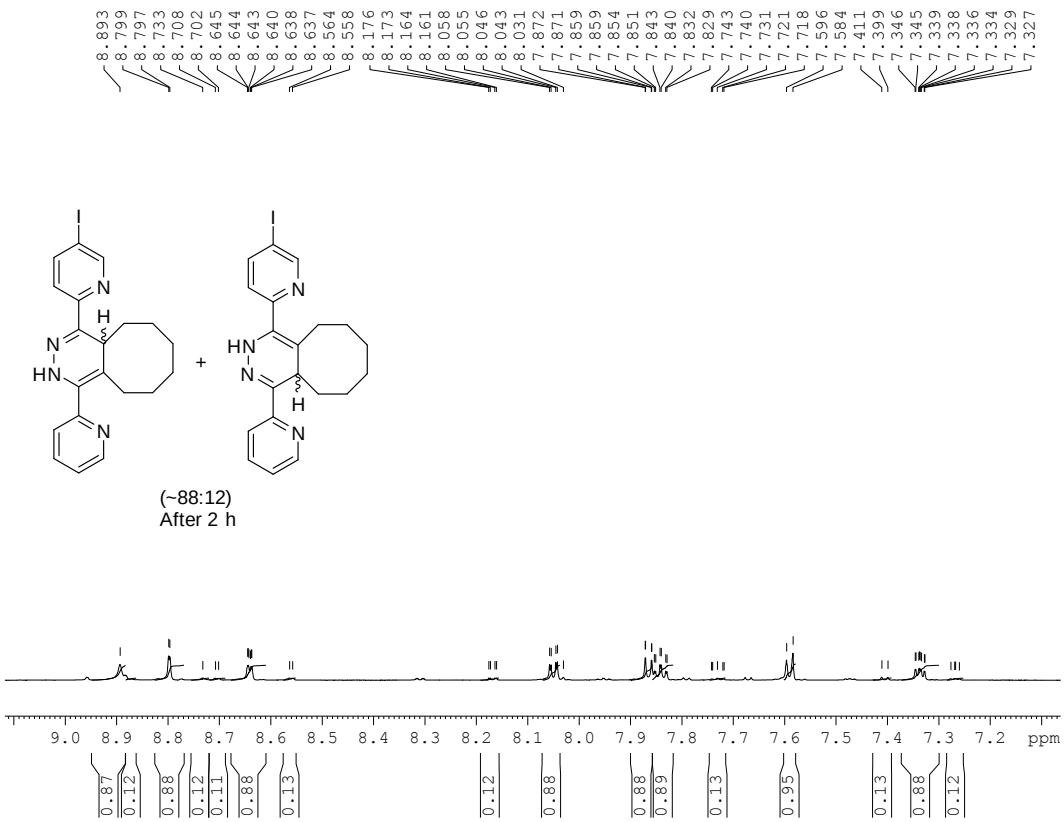

Figure S4-19. Expansion of ^{1}H NMR (700 MHz, CD_3CN) spectrum showing aromatic protons corresponding to isomers **7a** and **8a** 2 hours after ligation.

Figure S4-20. Expansion of ^{1}H NMR (700 MHz, CD_3CN) spectrum showing aliphatic protons corresponding to isomers **7a** and **8a** 2 hours after ligation.

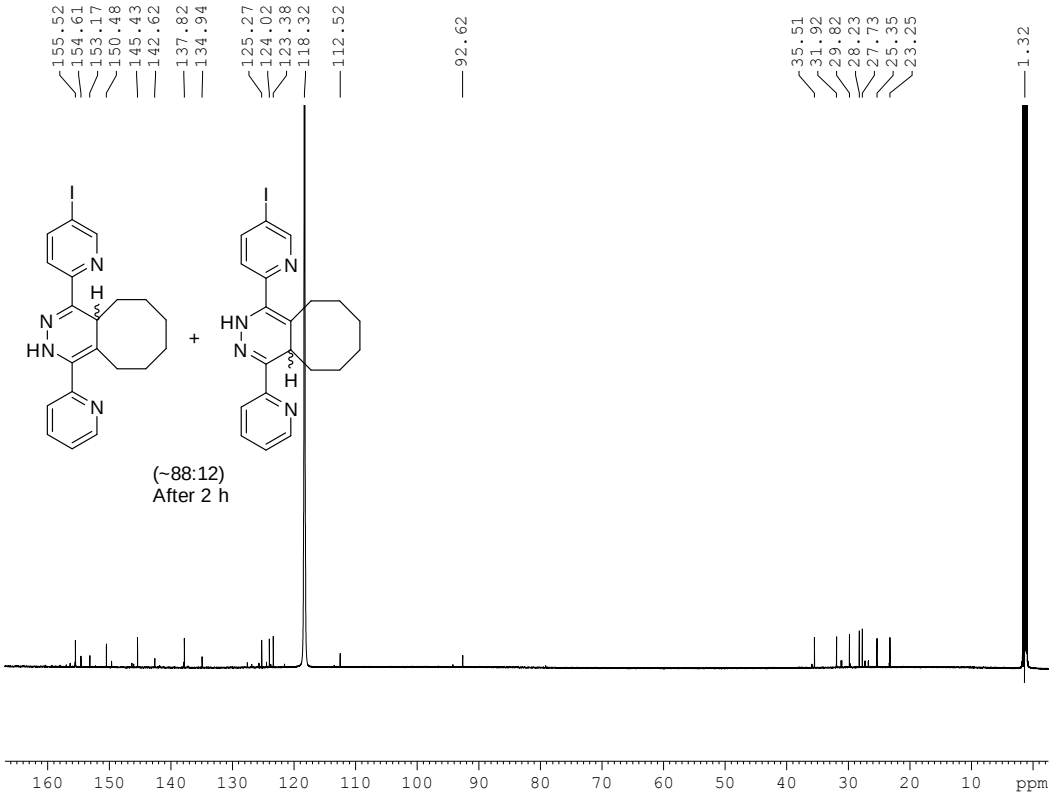

Figure S4-21. ^{13}C NMR (150 MHz, CD_3CN) spectrum of isomeric mixture **7a** and **8a** 2 hours after ligation.

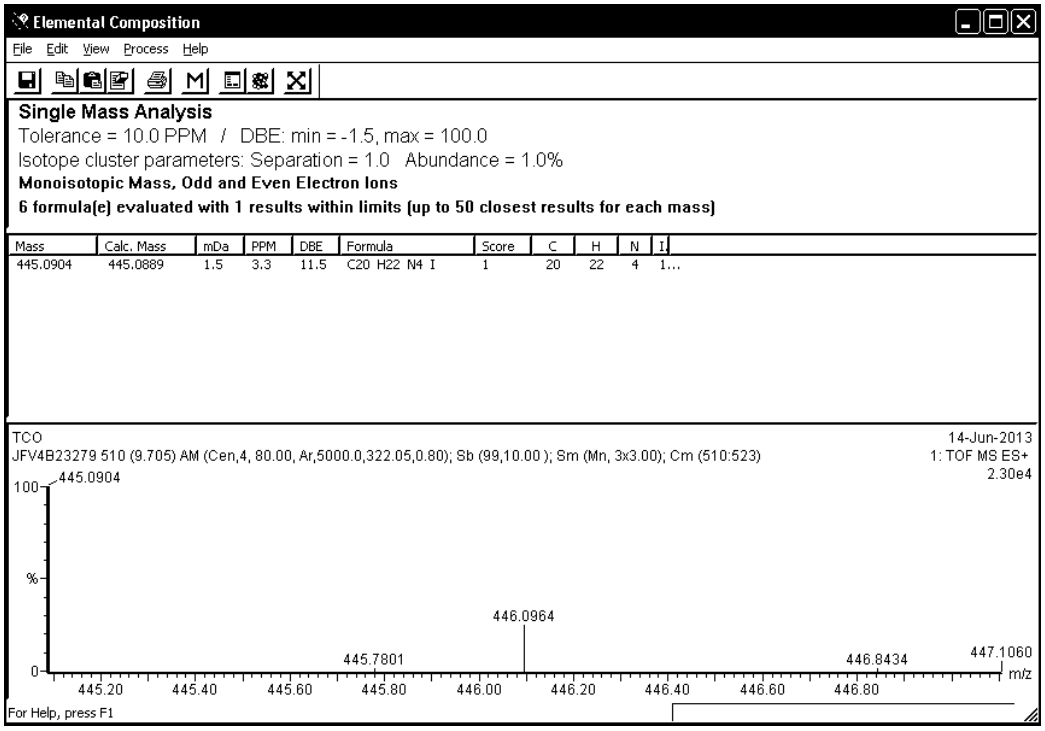

Figure S4-22. HRMS (TOF ESI$^+$) spectrum of a mixture **7a** and **8a**.

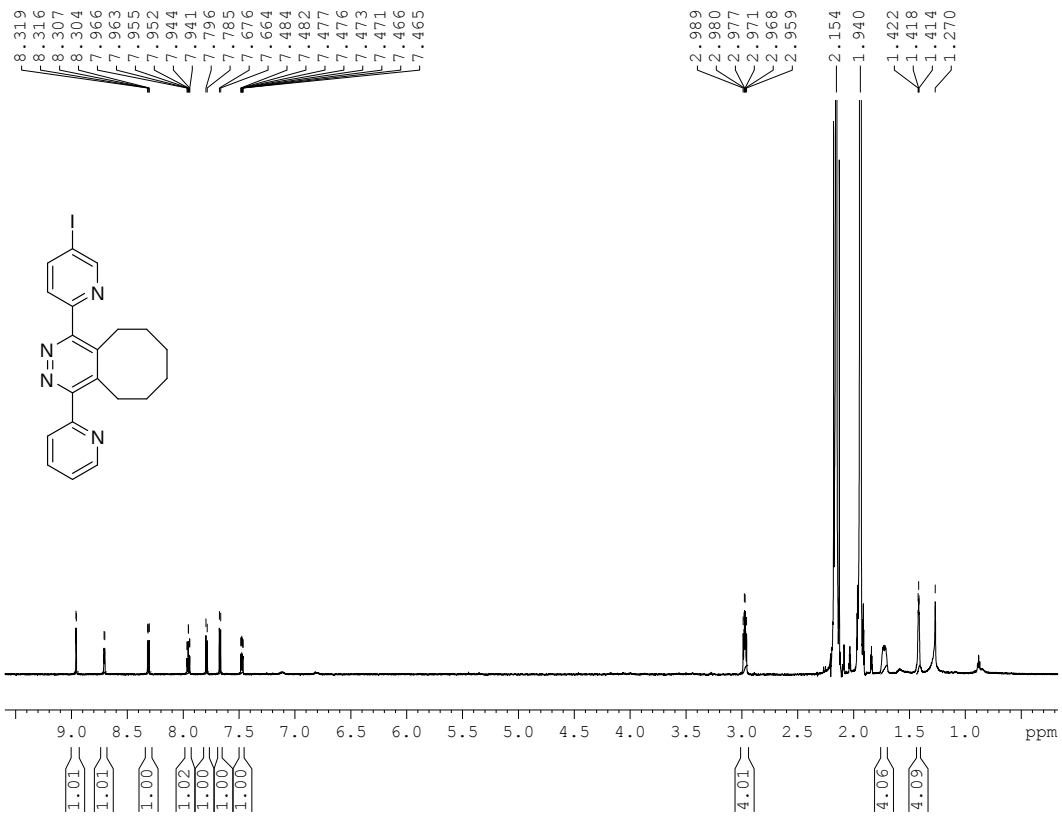

Figure S4-23. ^{1}H NMR (700 MHz, CD_3CN) spectrum of **9a**.

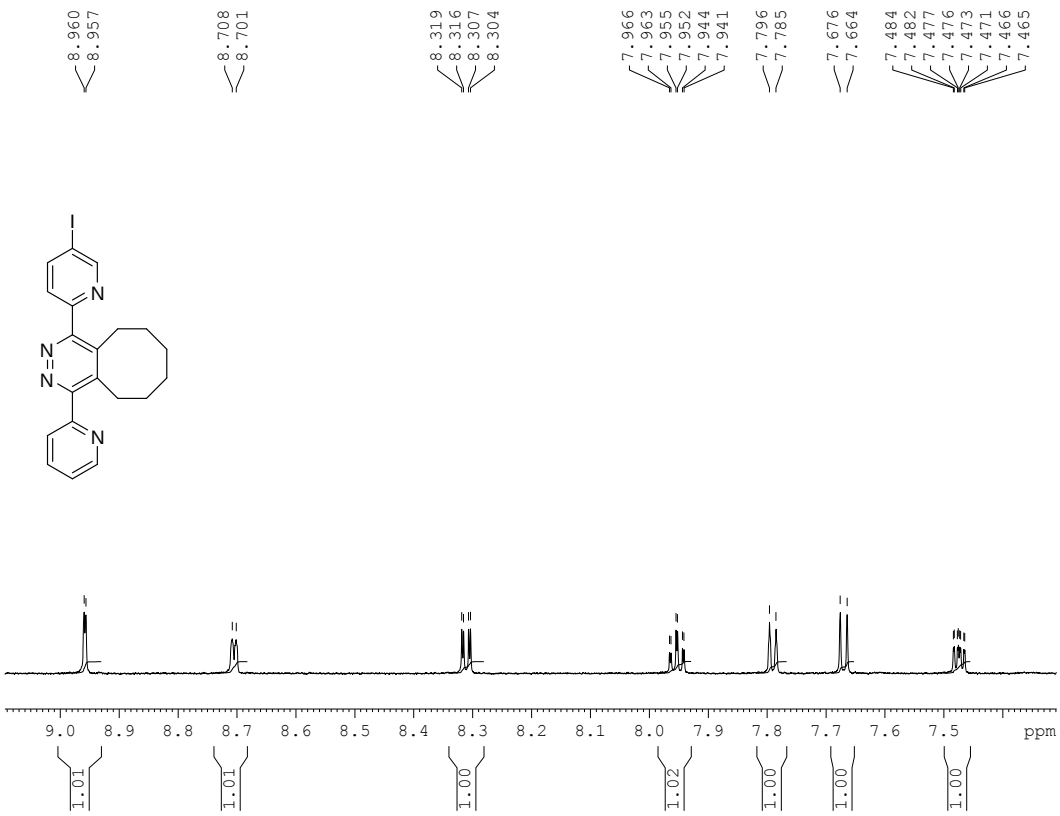

Figure S4-24. Expansion of ^{1}H NMR (700 MHz, CD_3CN) spectrum showing aromatic protons corresponding to **9a**.

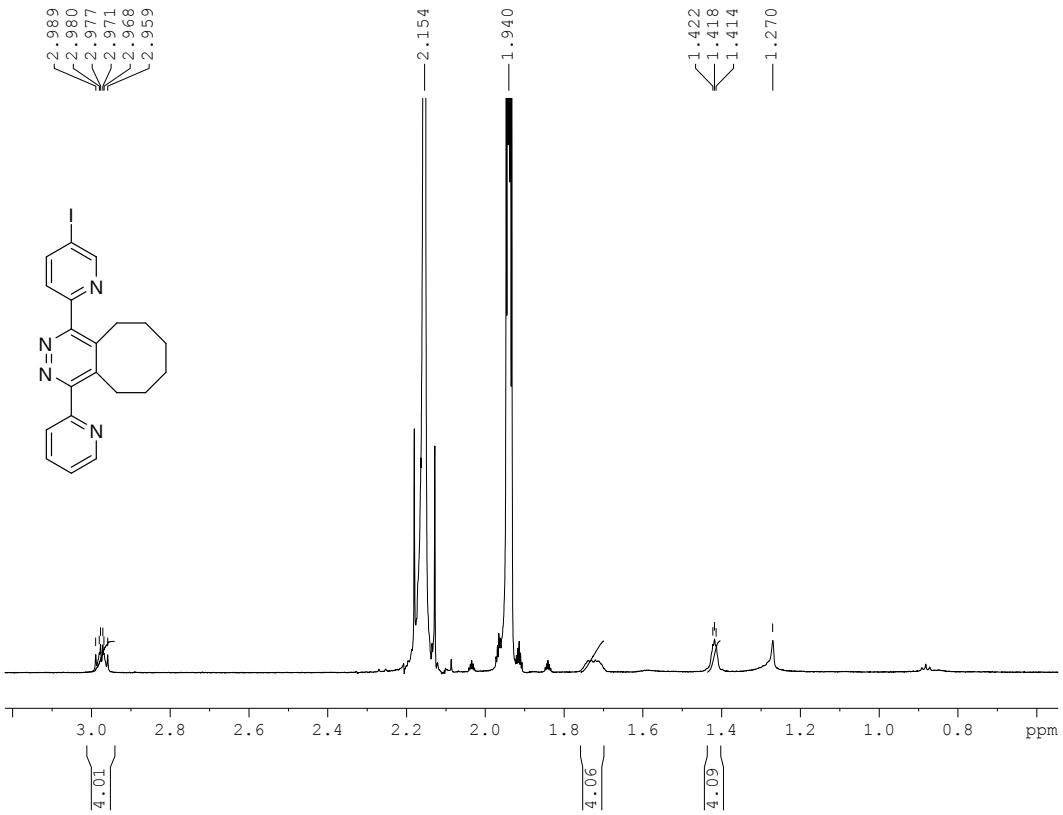

Figure S4-25. Expansion of ^{1}H NMR (700 MHz, CD_3CN) spectrum showing aliphatic protons corresponding to **9a**.

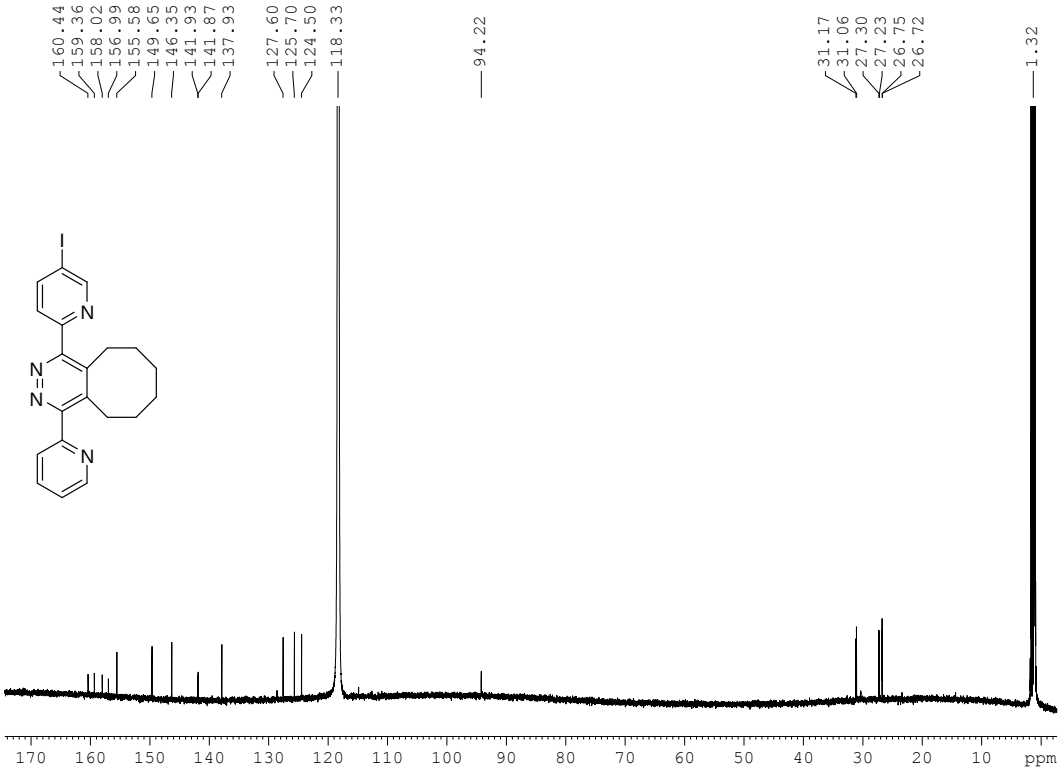

Figure S4-26. ^{13}C NMR (150 MHz, CD_3CN) spectrum of **9a**.

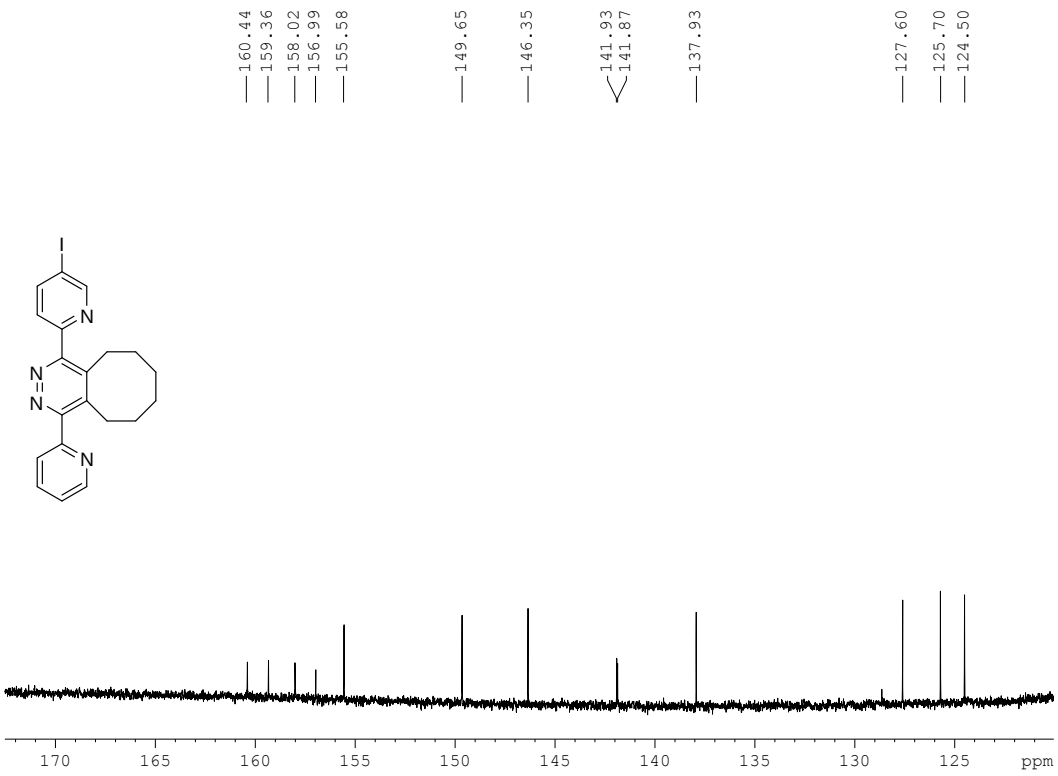

Figure S4-27. Expansion of the aromatic region in the ^{13}C NMR (150 MHz, CD_3CN) spectrum of **9a**.

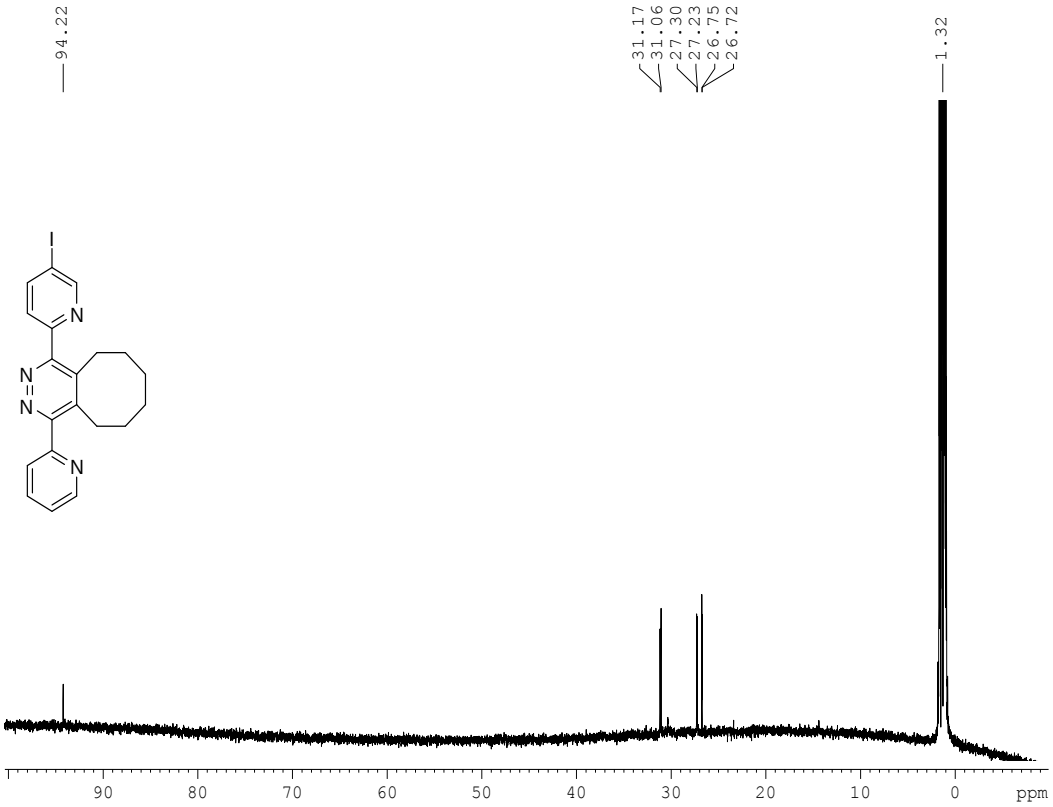

Figure S4-28. Expansion of the aliphatic region in the ^{13}C NMR (150 MHz, CD_3CN) spectrum of **9a**.

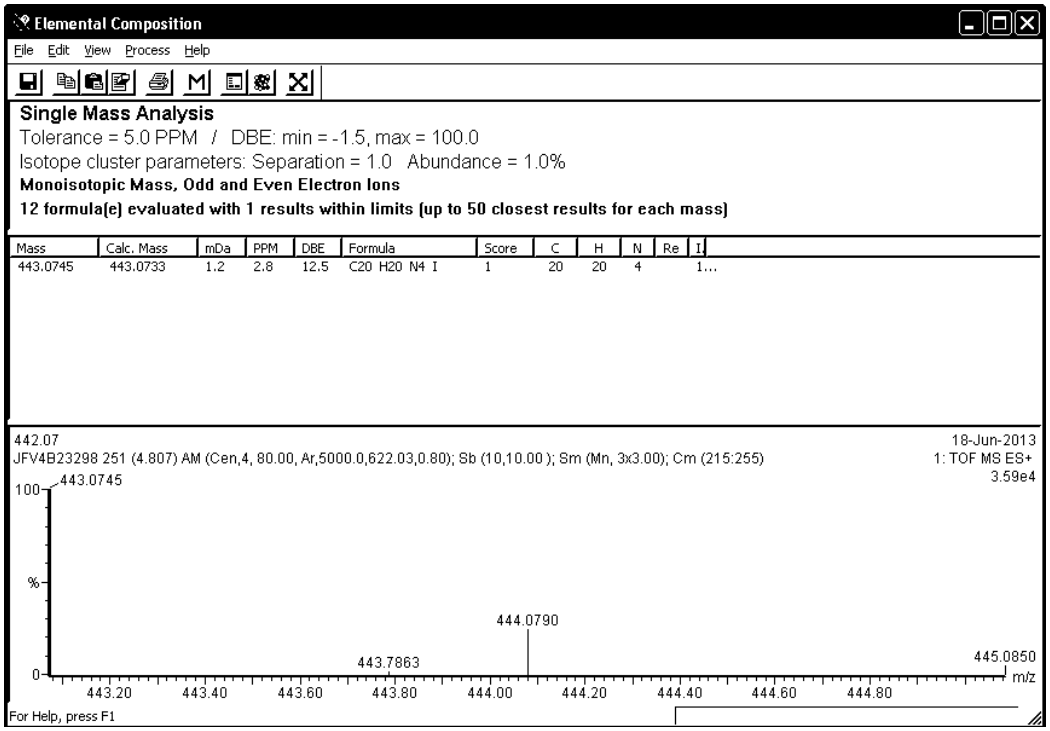

Figure S4-29. HRMS (TOF ESI$^+$) spectrum of **9a**.

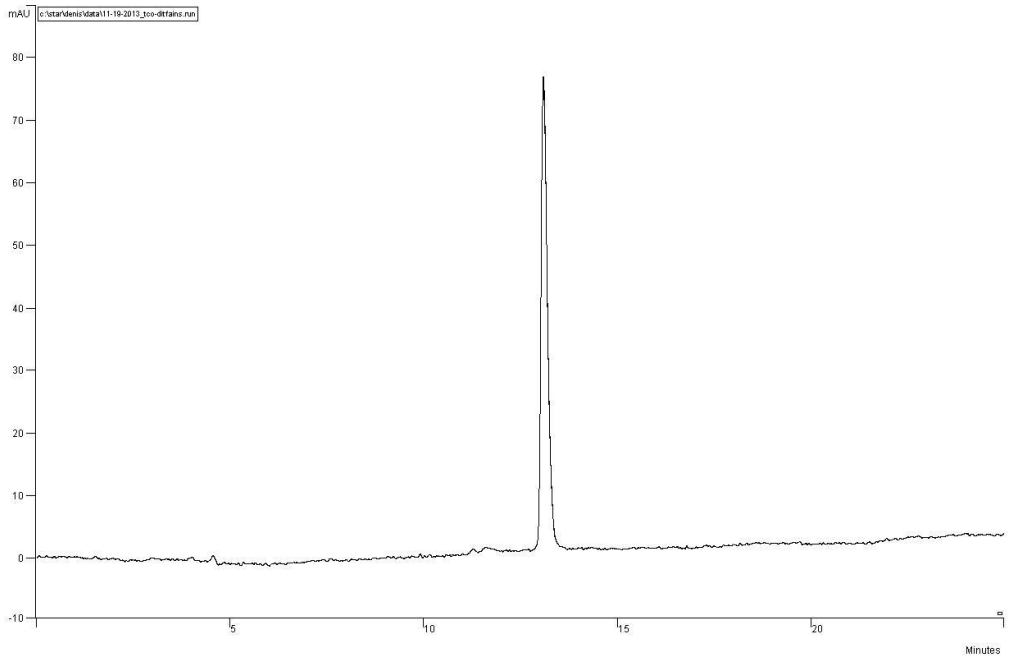

Figure S4-30. UV-HPLC chromatogram of **11** showing an R_t = 13.1 min (method

D).

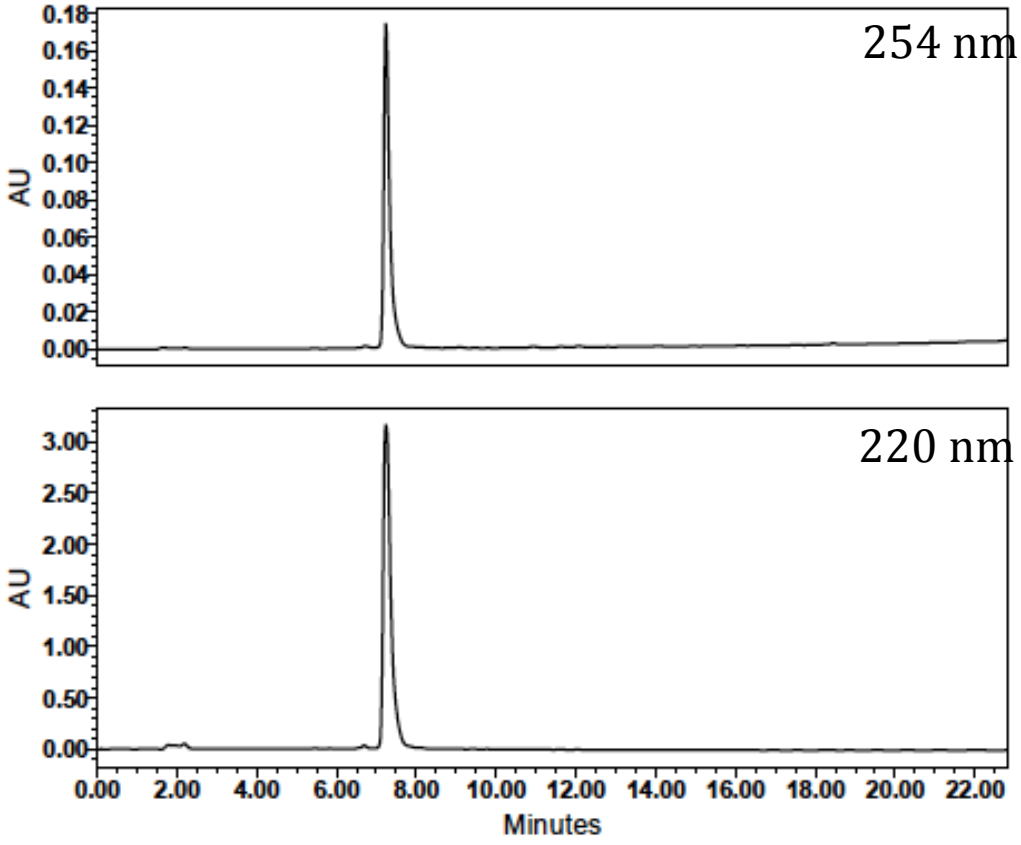

Figure S4-31. UV-HPLC chromatogram of **12** showing an R_t = 7.2 min (method D).

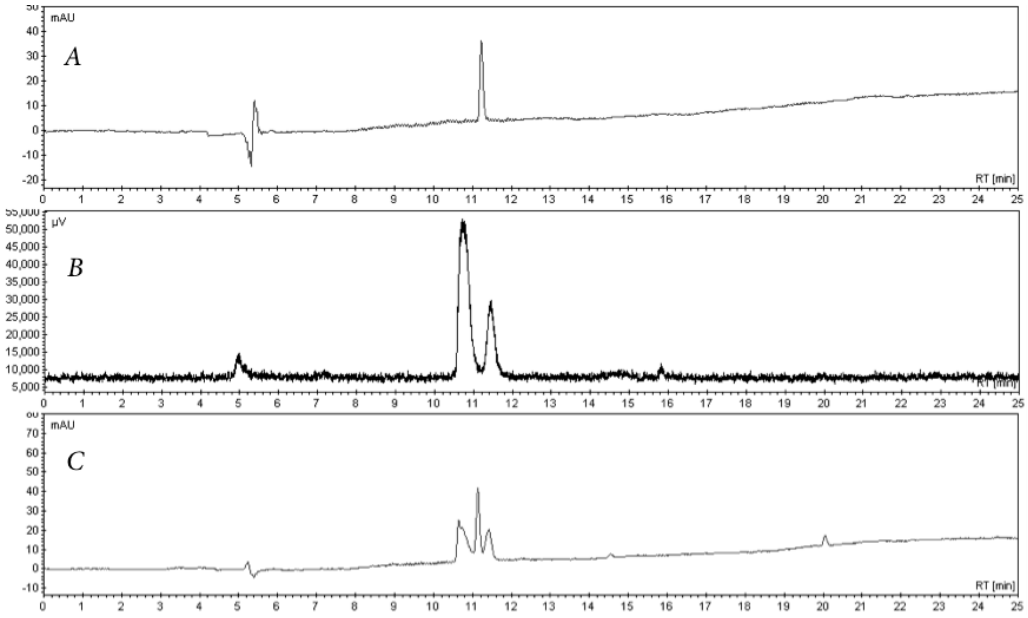

Figure S4-32. A) UV-HPLC chromatogram of insulin-TCO **12**, R_t = 11.2 min (method D). B) γ-HPLC chromatogram of the reaction mixture of **4b** and insulin-TCO spiked with non-radioactive iodotetrazine. C) UV-HPLC chromatogram of the same spiked reaction mixture (as in D).

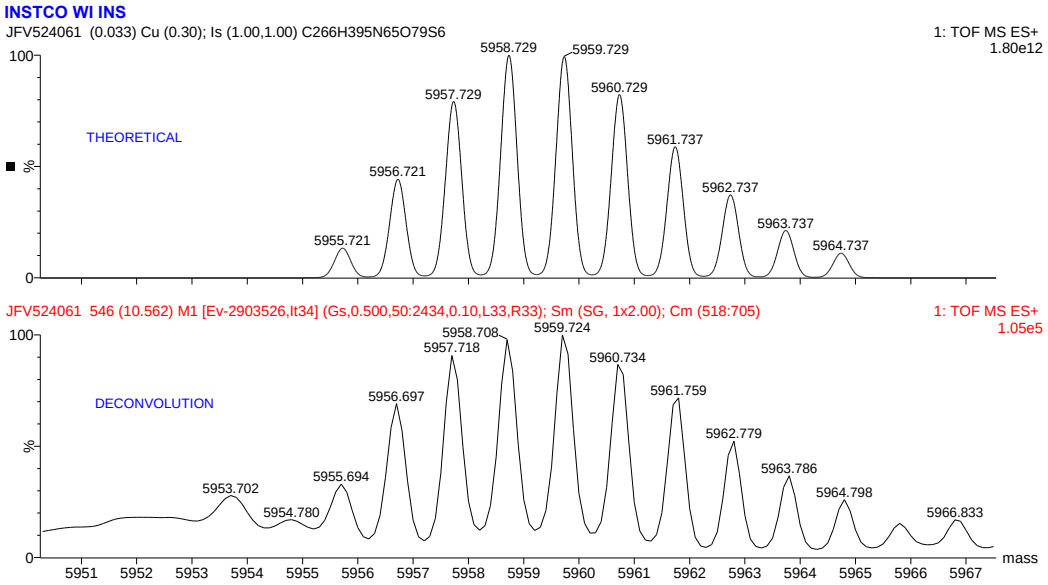

Figure S4-33. HRMS (TOF ESI$^+$) spectrum of **12**.

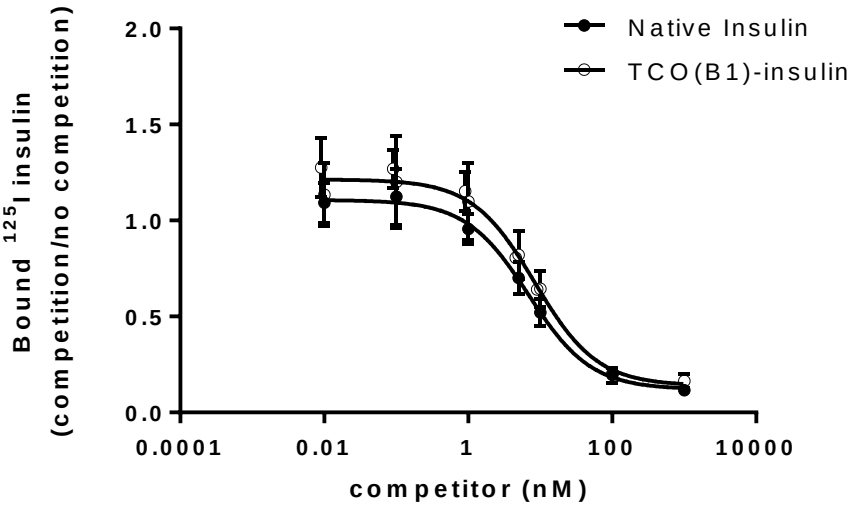

Figure S4-34. Competition binding curve for native insulin and **13**.

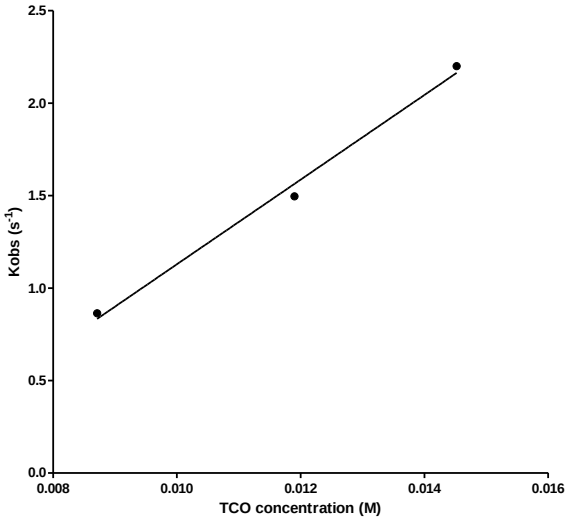

Best-fit values		
Slope	228.9 ± 20.07	
Y-intercept when X=0.0	-1.160 ± 0.2398	
X-intercept when Y=0.0		0.005068
1/slope		0.004369
95% Confidence Intervals		
Slope	-26.07 to 483.9	
Y-intercept when X=0.0	-4.207 to 1.886	
X-intercept when Y=0.0	-infinity to 0.009045	
Goodness of Fit		
R square		0.9924
Sy.x		0.08257
Is slope significantly non-zero?		
F		130.1
DFn, DFd	1.000, 1.000	
P value		0.0557
Deviation from zero?	Not Significant	
Data		
Number of X values		3
Maximum number of Y replicates		1
Total number of values		3
Number of missing values		0

Figure S4-35. Kinetic Data for Reaction of **4a** with TCO-OH.

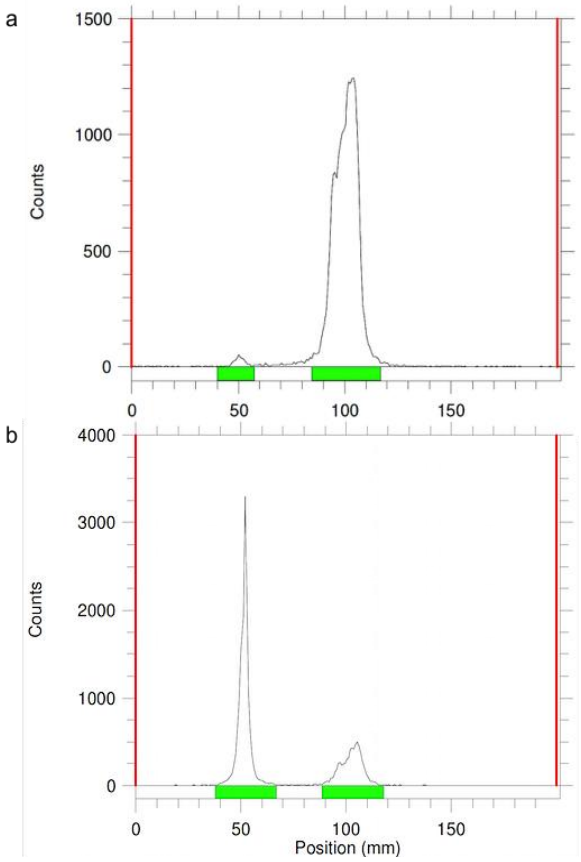

Figure S4-36. Radioactive iTLC analysis of **4b** before (a) and after (b) incubation with TCO-anti-VEGFR2 for 20 min.

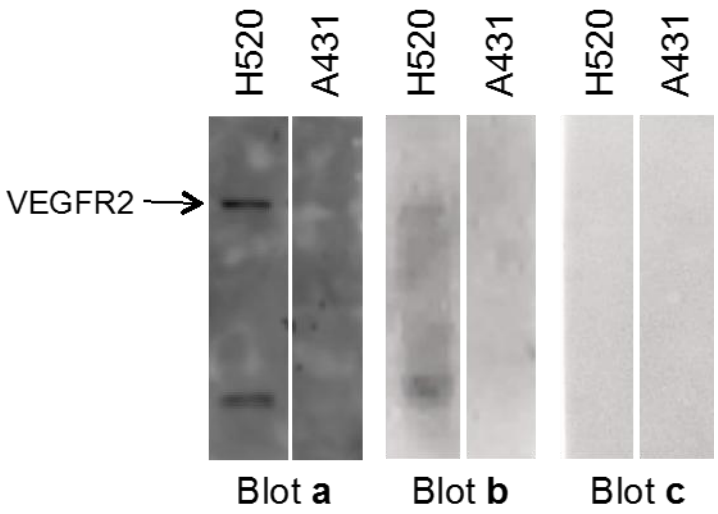

Figure S4-37. Western blot analysis of SDS-Page gel electrophoresed lysates from VEGFR2(+)H520 and control VEGFR2(-) A431 cells. For positive control (Blot **a**), rabbit anti-VEGFR2 primary antibody was followed by goat anti-rabbit secondary antibody and visualized using chemiluminescence. Test sample blots were incubated with ^{125}I-labelled anti-VEGFR2 construct (Blot **b**). As negative control, compound **4b** alone was incubated with electrophoresed cellular lysates (Blot **c**).

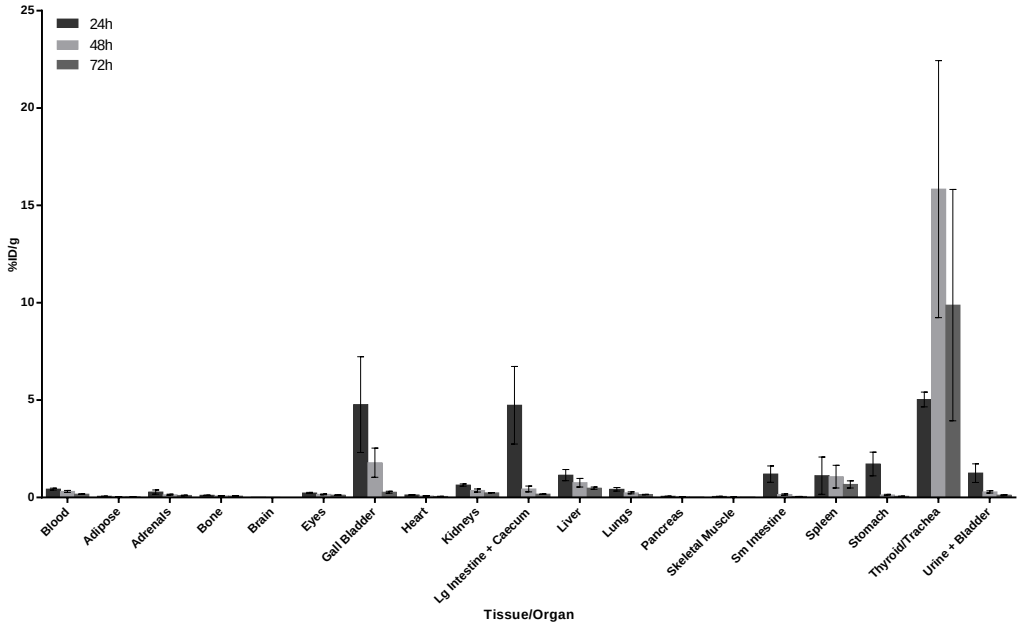

Figure S4-38. *In vivo* biodistribution of ^{125}I-labelled anti-VEGFR2 antibody in female C57Bl/6 mice. Mice were injected with 0.17 MBq of ^{125}I-labelled anti-VEGFR2 and sacrificed at 24h, 48h and 72h post-injection. Data expressed as %ID/g. (For values, see Table of data, Table S4-1).

Table S4-1: Distribution of radioactivity for injected ^{125}I-labelled anti-VEGFR2 in female C57Bl/6 mice.

Organs	24h	48h	72h
Blood	0.43 ± 0.05	0.31 ± 0.05	0.17 ± 0.01
Adipose	0.06 ± 0.01	0.04 ± 0.01	0.03 ± 0.01
Adrenals	0.28 ± 0.11	0.14 ± 0.03	0.10 ± 0.02
Bone	0.11 ± 0.01	0.08 ± 0.02	0.07 ± 0.01
Brain	0.01 ± 0.001	0.01 ± 0.001	0.004 ± 0.001
Eyes	0.23 ± 0.03	0.16 ± 0.02	0.12 ± 0.01
Gall Bladder	4.77 ± 2.46	1.79 ± 0.75	0.27 ± 0.05
Heart	0.13 ± 0.02	0.08 ± 0.01	0.05 ± 0.01
Kidneys	0.64 ± 0.06	0.36 ± 0.08	0.24 ± 0.01
Lg Intestine + Caecum	4.74 ± 1.99	0.44 ± 0.15	0.17 ± 0.02
Liver	1.15 ± 0.29	0.76 ± 0.22	0.48 ± 0.06
Lungs	0.42 ± 0.09	0.24 ± 0.05	0.15 ± 0.01
Pancreas	0.06 ± 0.01	0.04 ± 0.01	0.02 ± 0.001
Skeletal Muscle	0.05 ± 0.01	0.02 ± 0.005	0.02 ± 0.003
Sm Intestine	1.20 ± 0.42	0.15 ± 0.04	0.05 ± 0.001
Spleen	1.12 ± 0.96	1.07 ± 0.58	0.67 ± 0.18
Stomach	1.72 ± 0.61	0.13 ± 0.03	0.06 ± 0.01
Thyroid/Trachea	5.03 ± 0.38	15.84 ± 6.60	9.88 ± 5.94
Urine + Bladder	1.25 ± 0.48	0.29 ± 0.06	0.12 ± 0.03

Table S4-2. Crystal data for **4a.**

Identification code	JD4	
Chemical formula	$C_{12}H_7IN_6$	
Formula weight	362.14 g/mol	
Temperature	173(2) K	
Wavelength	0.71073 Å	
Crystal size	0.029 × 0.099 × 0.297 mm	
Crystal habit	clear purple plate	
Crystal system	Monoclinic	
Space group	P 1 21/n 1	
Unit cell dimensions	a = 6.5050(13) Å	α = 90°
	b = 25.321(5) Å	β = 107.026(3)°
	c = 7.8405(16) Å	γ = 90°
Volume	1234.8(4) $Å^3$	
Z	4	
Density (calculated)	1.948 g/cm^3	
Absorption coefficient	2.588 mm^{-1}	
F(000)	696	

Table S4-3. Data collection and structure refinement for **4a.**

Theta range for data collection	1.61 to 27.49°
Index ranges	$-8\leq h\leq 8$, $-32\leq k\leq 32$, $-10\leq l\leq 10$
Reflections collected	13693
Independent reflections	2824 [R(int) = 0.0346]
Coverage of independent reflections	99.9%
Absorption correction	numerical
Max. and min. transmission	0.9751 and 0.7134
Structure solution technique	direct methods
Structure solution program	SHELXT (Sheldrick 2014)
Refinement method	Full-matrix least-squares on F^2
Refinement program	SHELXL-2014/6 (Sheldrick, 2014)
Function minimized	$\Sigma\, w(F_o^2 - F_c^2)^2$
Data / restraints / parameters	2824 / 0 / 172
Goodness-of-fit on F^2	1.033
Δ/σ_{max}	0.001
Final R indices	2306 data; $I>2\sigma(I)$ R1 = 0.0355, wR2 = 0.0816
	all data R1 = 0.0479, wR2 = 0.0854
Weighting scheme	$w=1/[\sigma^2(F_o^2)+(0.0371P)^2+3.7453P]$ where $P=(F_o^2+2F_c^2)/3$
Largest diff. peak and hole	1.864 and -0.924 $eÅ^{-3}$
R.M.S. deviation from mean	0.119 $eÅ^{-3}$

Table S4-4. Atomic coordinates and equivalent isotropic atomic displacement parameters ($Å^2$) for **4a.**

U(eq) is defined as one third of the trace of the orthogonalized U_{ij} tensor.

	x/a	y/b	z/c	U(eq)
I1	0.23725(5)	0.23880(2)	0.77114(4)	0.02912(11)
N1	0.6125(6)	0.34366(14)	0.5490(5)	0.0267(8)
N2	0.7571(6)	0.42303(15)	0.3787(5)	0.0298(8)
N3	0.4241(5)	0.46763(14)	0.3296(5)	0.0247(8)
N4	0.4927(6)	0.50659(13)	0.2494(5)	0.0245(8)
N5	0.8282(6)	0.46254(15)	0.3009(5)	0.0309(8)
N6	0.6333(5)	0.58399(14)	0.0668(5)	0.0232(7)
C1	0.5376(7)	0.30465(17)	0.6301(6)	0.0271(9)
C2	0.3287(7)	0.30265(16)	0.6409(5)	0.0221(8)
C3	0.1861(6)	0.34243(16)	0.5650(5)	0.0218(8)
C4	0.2611(7)	0.38367(16)	0.4822(5)	0.0223(8)
C5	0.4735(6)	0.38294(15)	0.4771(5)	0.0191(8)
C6	0.5568(6)	0.42646(16)	0.3909(5)	0.0208(8)
C7	0.6946(6)	0.50291(16)	0.2360(5)	0.0200(8)
C8	0.7772(7)	0.54673(16)	0.1487(5)	0.0213(8)
C9	0.9931(7)	0.54822(16)	0.1566(5)	0.0225(8)
C10	0.0659(7)	0.59050(17)	0.0765(6)	0.0284(9)
C11	0.9234(8)	0.62996(19)	0.9917(6)	0.0315(10)
C12	0.7093(7)	0.62408(17)	0.9924(6)	0.0278(9)

Table S4-5. Bond lengths (Å) for **4a.**

I1-C2	2.089(4)	N1-C1	1.341(5)
N1-C5	1.351(5)	N2-N5	1.324(5)
N2-C6	1.337(5)	N3-N4	1.316(5)
N3-C6	1.349(5)	N4-C7	1.351(5)
N5-C7	1.341(6)	N6-C12	1.336(5)
N6-C8	1.352(5)	C1-C2	1.387(6)
C1-H1	0.95	C2-C3	1.381(6)
C3-C4	1.391(6)	C3-H2	0.95
C4-C5	1.394(6)	C4-H3	0.95
C5-C6	1.476(5)	C7-C8	1.485(6)
C8-C9	1.388(6)	C9-C10	1.393(6)
C9-H4	0.95	C10-C11	1.392(6)
C10-H5	0.95	C11-C12	1.402(7)
C11-H6	0.95	C12-H7	0.95

Table S4-6. Bond angles (°) for **4a.**

C1-N1-C5	116.6(3)	N5-N2-C6	117.6(4)
N4-N3-C6	118.6(3)	N3-N4-C7	117.3(3)
N2-N5-C7	118.4(4)	C12-N6-C8	116.4(4)
N1-C1-C2	123.7(4)	N1-C1-H1	118.2
C2-C1-H1	118.2	C3-C2-C1	119.6(4)
C3-C2-I1	121.6(3)	C1-C2-I1	118.8(3)
C2-C3-C4	117.7(4)	C2-C3-H2	121.1
C4-C3-H2	121.1	C3-C4-C5	119.3(4)
C3-C4-H3	120.3	C5-C4-H3	120.3
N1-C5-C4	123.1(4)	N1-C5-C6	116.8(3)
C4-C5-C6	120.2(3)	N2-C6-N3	124.1(4)
N2-C6-C5	118.7(4)	N3-C6-C5	117.2(3)
N5-C7-N4	124.0(4)	N5-C7-C8	117.6(4)
N4-C7-C8	118.4(4)	N6-C8-C9	123.6(4)
N6-C8-C7	116.6(4)	C9-C8-C7	119.8(4)
C8-C9-C10	118.3(4)	C8-C9-H4	120.9
C10-C9-H4	120.9	C11-C10-C9	120.0(4)
C11-C10-H5	120.0	C9-C10-H5	120.0
C10-C11-C12	116.4(4)	C10-C11-H6	121.8
C12-C11-H6	121.8	N6-C12-C11	125.3(4)
N6-C12-H7	117.4	C11-C12-H7	117.4

Table S4-7. Torsion angles (°) for **4a.**

C6-N3-N4-C7	-0.9(6)	C6-N2-N5-C7	-1.3(6)
C5-N1-C1-C2	0.8(6)	N1-C1-C2-C3	0.1(7)
N1-C1-C2-I1	179.7(3)	C1-C2-C3-C4	-0.9(6)
I1-C2-C3-C4	179.5(3)	C2-C3-C4-C5	0.8(6)
C1-N1-C5-C4	-0.9(6)	C1-N1-C5-C6	178.8(4)
C3-C4-C5-N1	0.1(6)	C3-C4-C5-C6	-179.6(4)
N5-N2-C6-N3	-0.3(7)	N5-N2-C6-C5	180.0(4)
N4-N3-C6-N2	1.4(6)	N4-N3-C6-C5	-178.9(4)
N1-C5-C6-N2	4.2(6)	C4-C5-C6-N2	-176.0(4)
N1-C5-C6-N3	-175.5(4)	C4-C5-C6-N3	4.2(6)
N2-N5-C7-N4	1.9(7)	N2-N5-C7-C8	-179.8(4)
N3-N4-C7-N5	-0.7(6)	N3-N4-C7-C8	-179.1(4)
C12-N6-C8-C9	-0.6(6)	C12-N6-C8-C7	178.3(4)
N5-C7-C8-N6	172.8(4)	N4-C7-C8-N6	-8.8(5)
N5-C7-C8-C9	-8.2(6)	N4-C7-C8-C9	170.2(4)
N6-C8-C9-C10	0.3(6)	C7-C8-C9-C10	-178.6(4)
C8-C9-C10-C11	0.2(6)	C9-C10-C11-C12	-0.2(6)
C8-N6-C12-C11	0.6(6)	C10-C11-C12-N6	-0.2(7)

Table S4-8. Anisotropic atomic displacement parameters ($Å^2$) for **4a**.
The anisotropic atomic displacement factor exponent takes the form:
$-2\pi^2[h^2 a^{*2} U_{11} + ... + 2 h k a^* b^* U_{12}]$

	U_{11}	U_{22}	U_{33}	U_{23}	U_{13}	U_{12}
I1	0.03137(17)	0.02386(16)	0.03042(16)	0.00556(12)	0.00637(11)	-0.00497(13)
N1	0.0206(18)	0.0257(19)	0.033(2)	0.0060(15)	0.0073(16)	0.0052(15)
N2	0.0207(18)	0.026(2)	0.043(2)	0.0144(17)	0.0112(17)	0.0078(15)
N3	0.0179(17)	0.0223(18)	0.034(2)	0.0034(15)	0.0079(15)	0.0035(14)
N4	0.0209(18)	0.0205(18)	0.034(2)	0.0040(15)	0.0102(16)	0.0039(14)
N5	0.0213(18)	0.028(2)	0.044(2)	0.0149(17)	0.0117(16)	0.0066(16)
N6	0.0216(17)	0.0217(18)	0.0235(17)	-0.0008(14)	0.0025(14)	0.0033(14)
C1	0.026(2)	0.024(2)	0.030(2)	0.0060(18)	0.0057(18)	0.0061(18)
C2	0.028(2)	0.019(2)	0.0199(19)	-0.0002(15)	0.0074(16)	-0.0018(17)
C3	0.020(2)	0.023(2)	0.0213(19)	-0.0021(16)	0.0047(16)	-0.0005(16)
C4	0.023(2)	0.019(2)	0.024(2)	0.0000(16)	0.0042(17)	0.0021(16)
C5	0.020(2)	0.0163(18)	0.0188(18)	-0.0009(15)	0.0016(16)	0.0027(15)
C6	0.021(2)	0.020(2)	0.0205(19)	0.0007(15)	0.0040(16)	0.0026(16)
C7	0.018(2)	0.0197(19)	0.021(2)	-0.0012(15)	0.0038(17)	0.0033(15)
C8	0.023(2)	0.019(2)	0.021(2)	-0.0011(15)	0.0069(17)	0.0007(16)
C9	0.021(2)	0.020(2)	0.026(2)	0.0014(16)	0.0064(17)	0.0035(16)
C10	0.028(2)	0.028(2)	0.032(2)	-0.0018(18)	0.0125(19)	-0.0037(18)
C11	0.034(3)	0.036(3)	0.021(2)	-0.0063(19)	0.0043(19)	0.003(2)
C12	0.034(2)	0.023(2)	0.024(2)	0.0038(17)	0.0054(19)	0.0034(18)

Table S4-9. Hydrogen atomic coordinates and isotropic atomic displacement parameters ($Å^2$) for **4a**.

	x/a	y/b	z/c	U(eq)
H1	0.6329	0.2768	0.6831	0.033
H2	0.0416	0.3417	0.5692	0.026
H3	0.1685	0.4120	0.4297	0.027
H4	1.0887	0.5211	0.2152	0.027
H5	1.2128	0.5924	0.0797	0.034
H6	0.9688	0.6593	-0.0636	0.038
H7	0.6103	0.6508	-0.0648	0.033

APPENDIX 3

Supporting Information for Chapter 5

Heptadecafluorooctylbenzene (3)

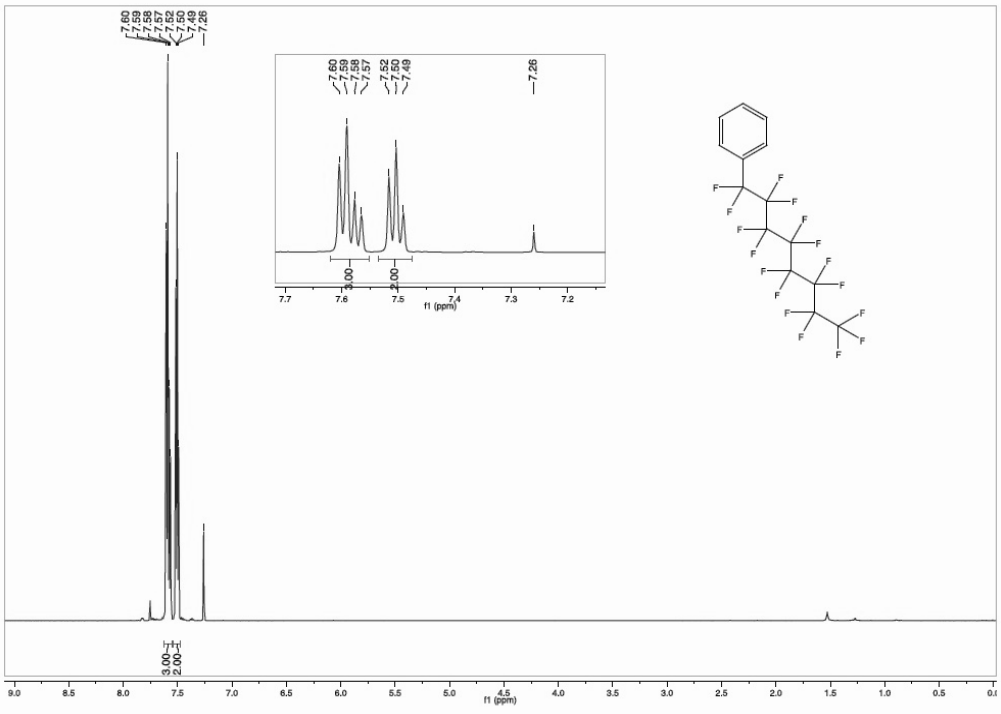

Figure S5-1. ^{1}H NMR (600 MHz, $CDCl_3$) spectrum of **3**, with expanded aromatic region (inset).

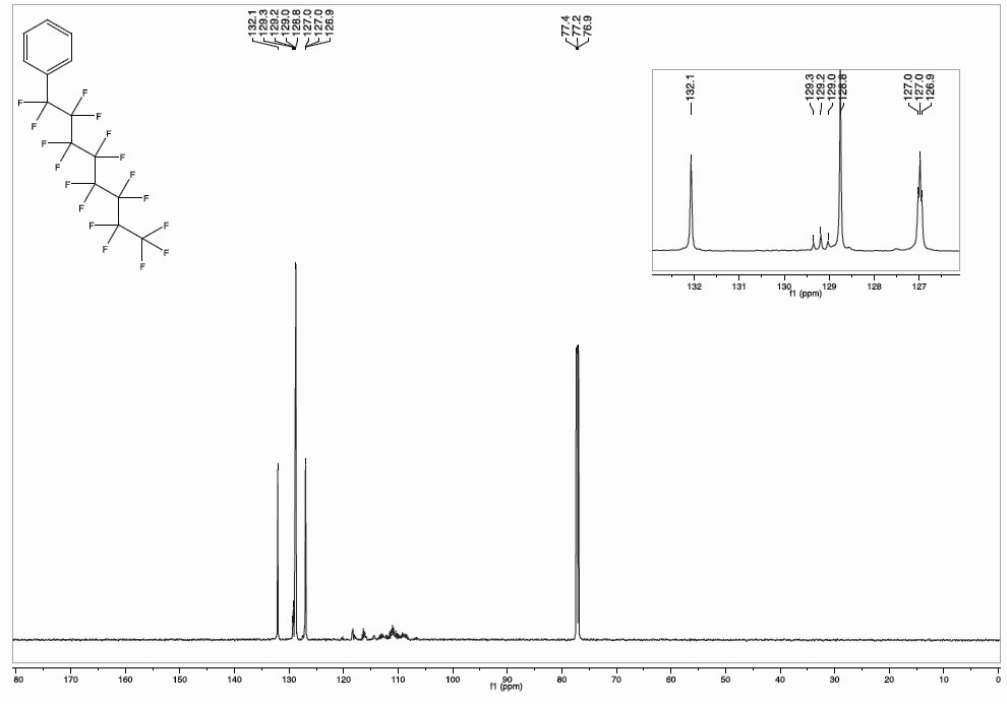

Figure S5-2. ^{13}C NMR (150 MHz, $CDCl_3$) spectrum of **3**, showing multiplets due to $^{2}J_{CF}$ and $^{3}J_{CF}$ coupling (inset), and between 106-119 ppm due to C-F coupling in $(CF_2)_7CF_3$.

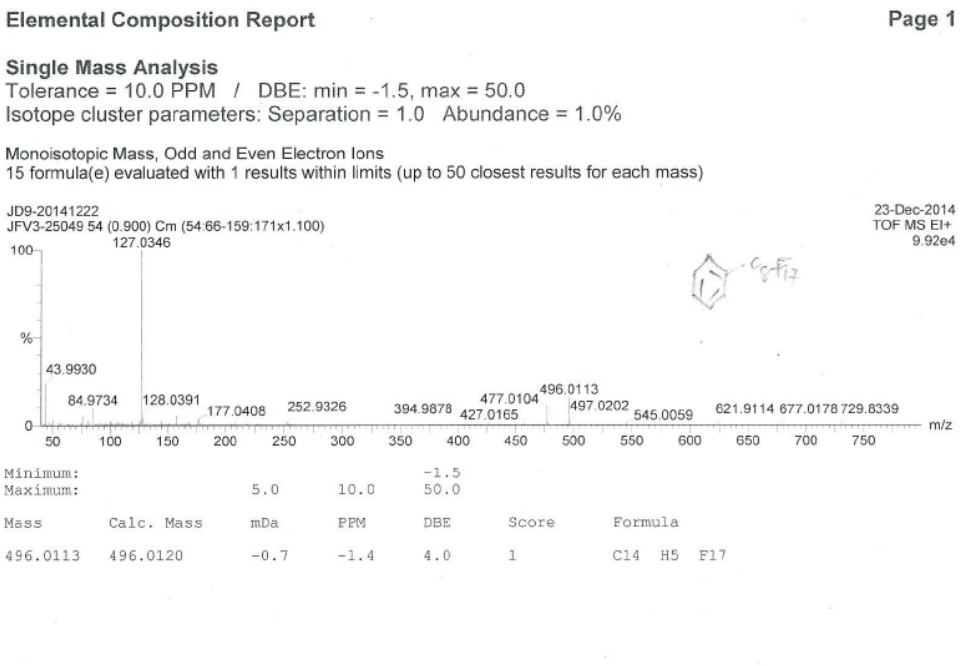

Figure S5-3. HRMS (TOF MS ESI$^+$) of **3**.

3-Heptadecafluorooctylbenzenesulfonyl chloride (4)

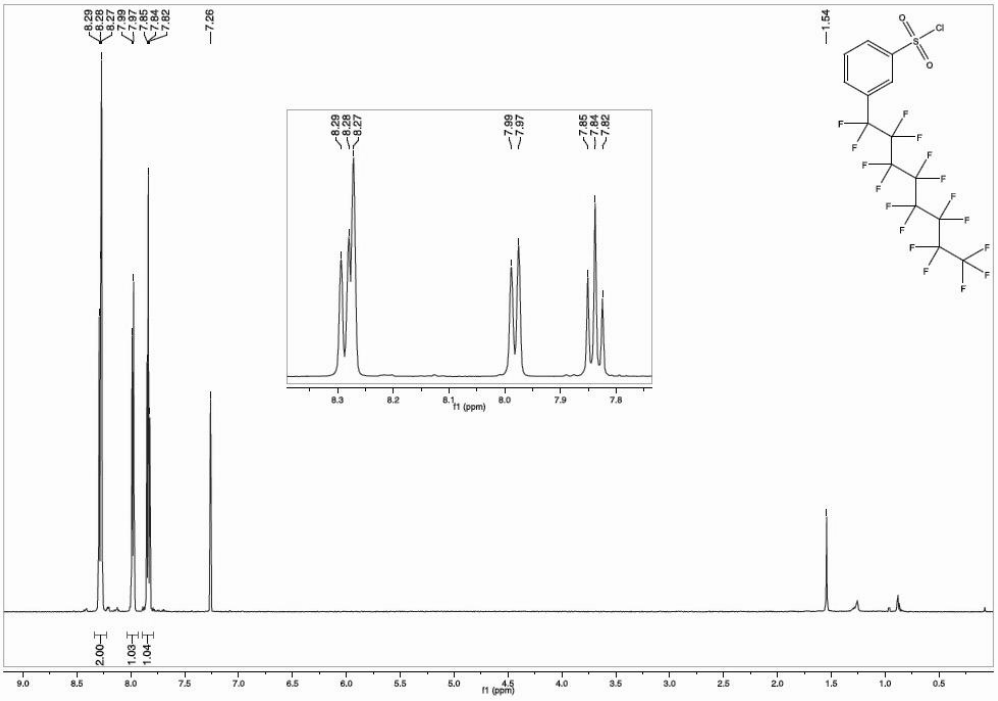

Figure S5-4. ^{1}H NMR (600 MHz, $CDCl_3$) spectrum of **4**, with expanded aromatic region (inset).

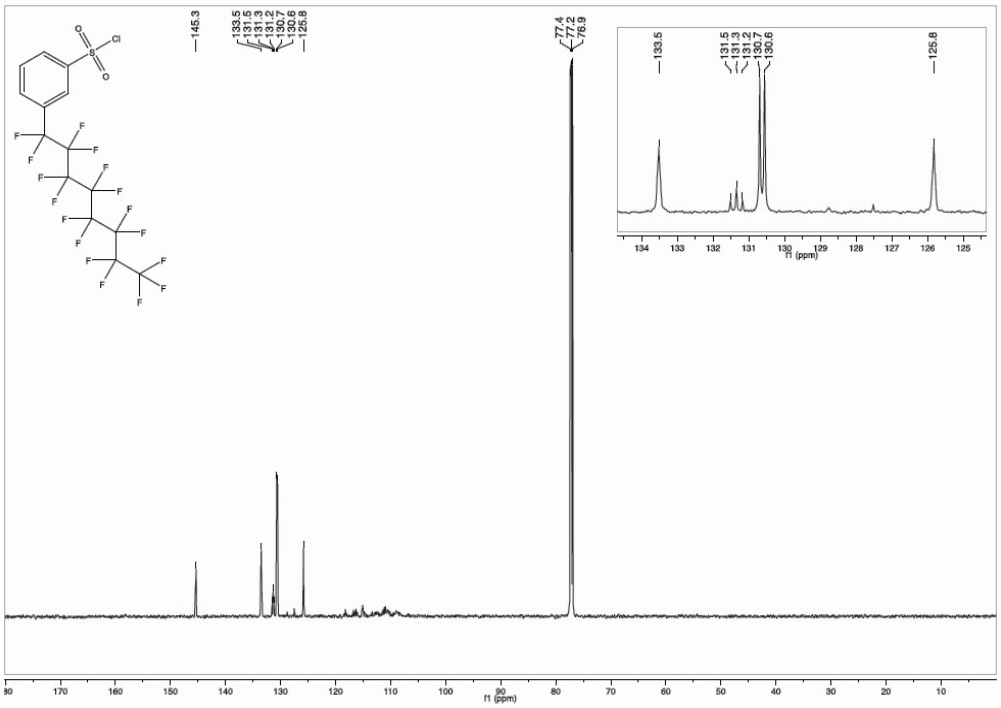

Figure S5-5. ^{13}C NMR (150 MHz, $CDCl_3$) spectrum of **4**, showing multiplets due to $^{2}J_{CF}$ at 131.3 ppm (inset).

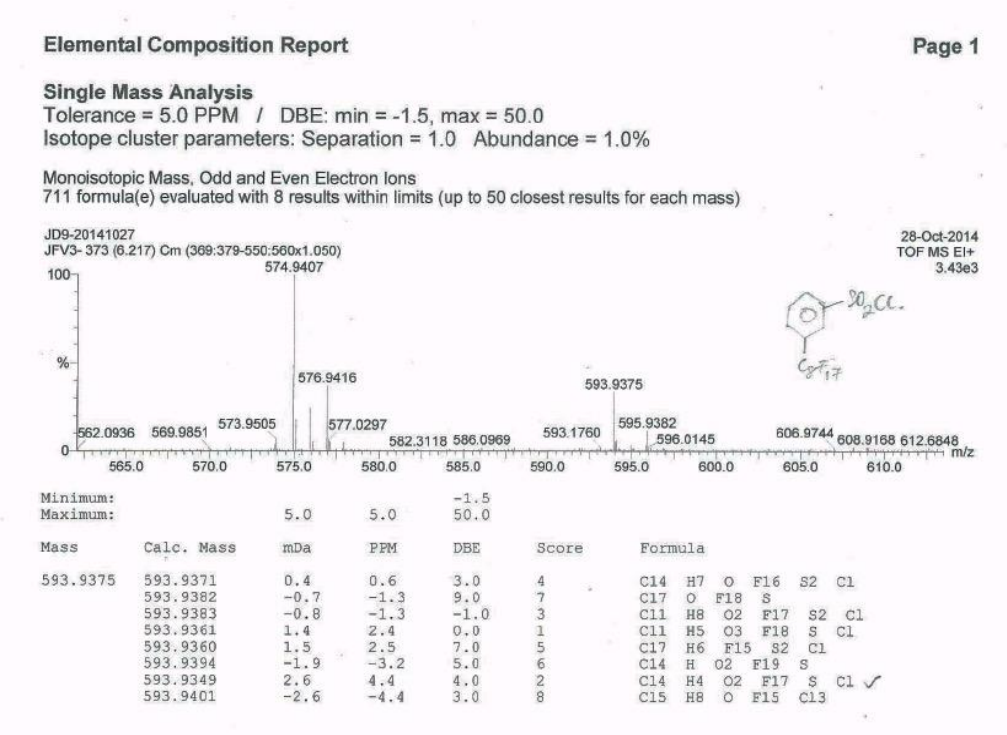

Elemental Composition Report **Page 1**

Single Mass Analysis
Tolerance = 5.0 PPM / DBE: min = -1.5, max = 50.0
Isotope cluster parameters: Separation = 1.0 Abundance = 1.0%

Monoisotopic Mass, Odd and Even Electron Ions
711 formula(e) evaluated with 8 results within limits (up to 50 closest results for each mass)

JD9-20141027
JFV3- 373 (6.217) Cm (369:379-550:560x1.050)
28-Oct-2014
TOF MS EI+
3.43e3

Mass	Calc. Mass	mDa	PPM	DBE	Score	Formula
Minimum:				-1.5		
Maximum:		5.0	5.0	50.0		
593.9375	593.9371	0.4	0.6	3.0	4	C14 H7 O F16 S2 Cl
	593.9382	-0.7	-1.3	9.0	7	C17 O F18 S
	593.9383	-0.8	-1.3	-1.0	3	C11 H8 O2 F17 S2 Cl
	593.9361	1.4	2.4	0.0	1	C11 H5 O3 F18 S Cl
	593.9360	1.5	2.5	7.0	5	C17 H6 F15 S2 Cl
	593.9394	-1.9	-3.2	5.0	6	C14 H O2 F19 S
	593.9349	2.6	4.4	4.0	2	C14 H4 O2 F17 S Cl ✓
	593.9401	-2.6	-4.4	3.0	8	C15 H8 O F15 Cl3

Figure S5-6. HRMS (TOF MS ESI$^+$) of **4**.

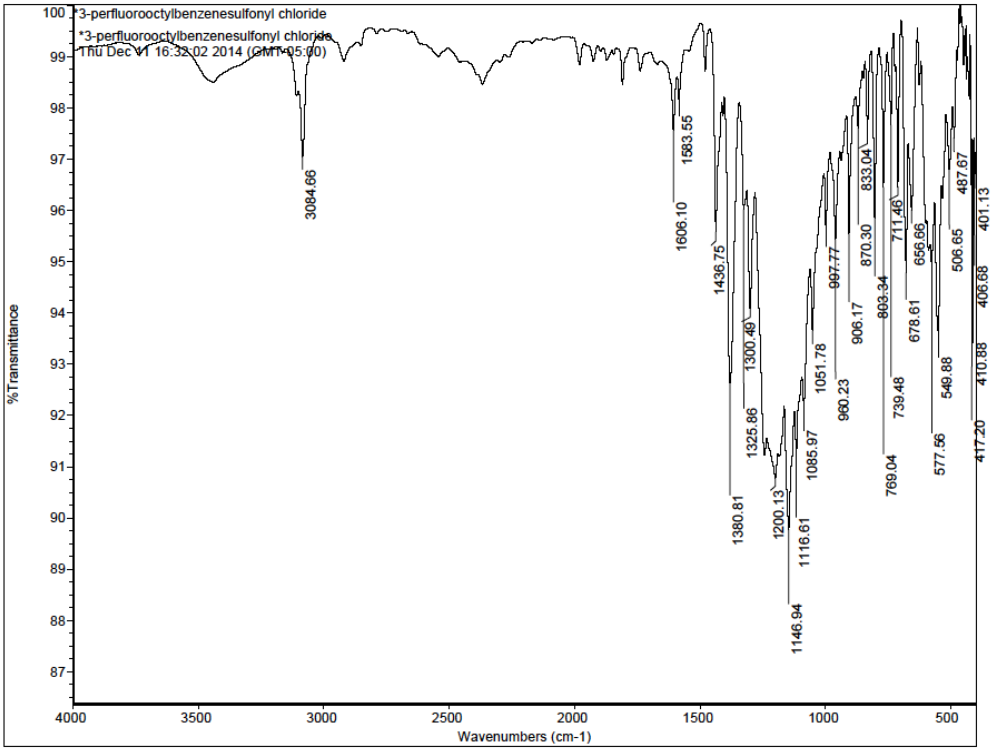

Figure S5-7. FTIR (KBr) spectrum of **4**.

_N_-(4,4,5,5,6,6,7,7,8,8,9,9,10,10,11,11,11-heptadecafluoroundecyl)-3-(heptadecafluorooctyl)benzenesulfonamide (6)

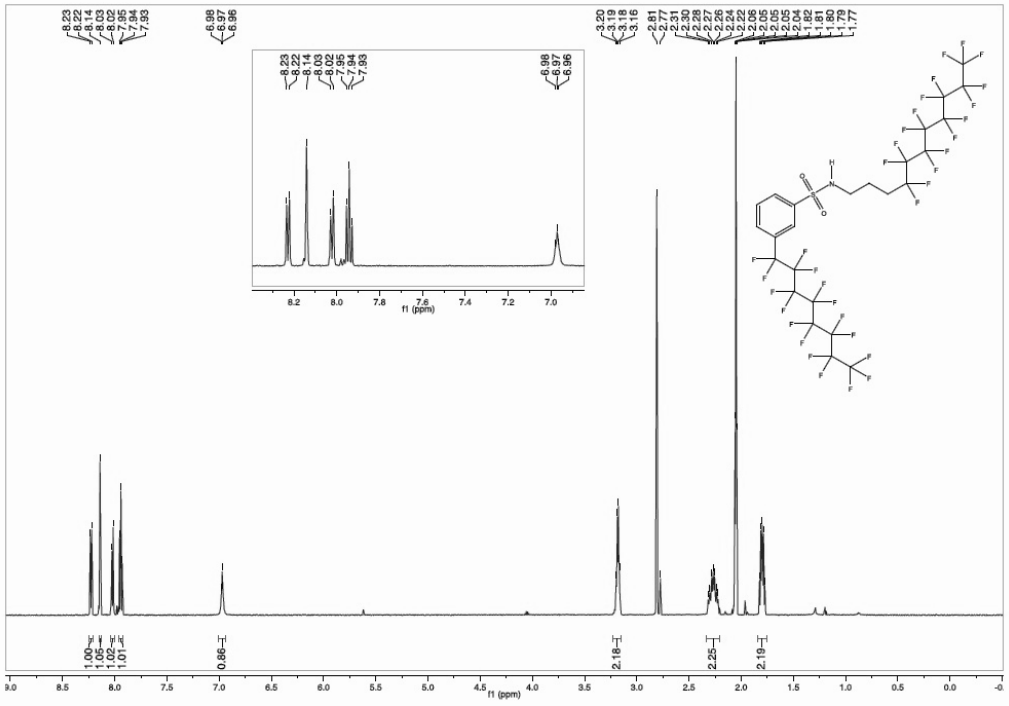

Figure S5-8. ^{1}H NMR (600 MHz, Acetone-d_6) spectrum of **6**, with expanded aromatic region (inset).

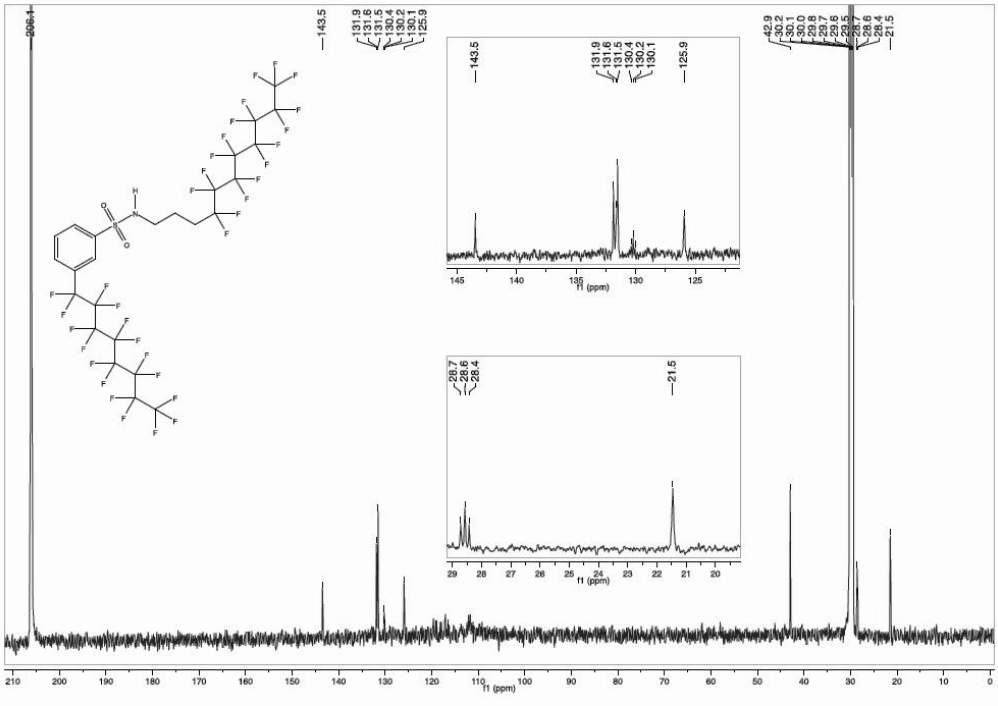

Figure S5-9. ^{13}C NMR (150 MHz, Acetone-d_6) spectrum of **6**, showing multiplets due to $^{2}J_{CF}$ at 130.2 and 28.6 ppm (insets).

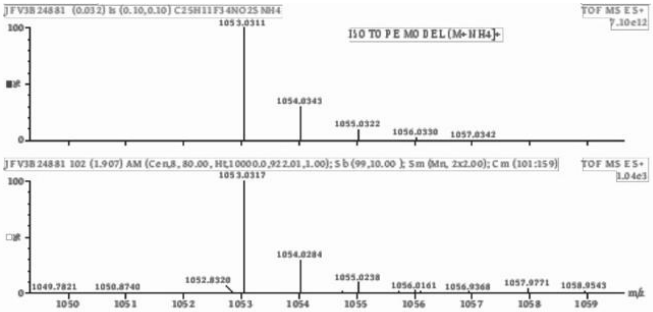

Elemental Composition Report

Single Mass Analysis
Tolerance = 5.0 PPM / DBE: min = -1.5, max = 300.0
Isotope cluster parameters: Separation = 1.0 Abundance = 1.0%

Monoisotopic Mass, Odd and Even Electron Ions
495 formula(e) evaluated with 22 results within limits (up to 50 closest results for each mass)

Minimum:				-1.5		
Maximum:		5.0	5.0	300.0		
Mass	Calc. Mass	mDa	PPM	DBE	Score	Formula
1053.0317	1053.0316	0.1	0.1	0.5	18	C25 H12 F39
	1053.0316	0.1	0.1	8.0	15	C28 H10 N3 F35
	1053.0311	**0.6**	**0.5**	**2.5**	**1**	**C25 H15 N2 O2 F34 S**
	1053.0323	-0.6	-0.5	-1.5	6	C22 H16 N2 O3 F35 S
	1053.0324	-0.7	-0.7	9.5	14	C30 H15 N2 O3 F30 S
	1053.0327	-1.0	-1.0	4.0	13	C25 H11 N3 O F36
	1053.0329	-1.2	-1.2	7.5	19	C30 H12 O F35
	1053.0300	1.7	1.6	6.5	7	C28 H14 N2 O F33 S
	1053.0339	-2.2	-2.1	0.0	22	C22 H12 N3 O2 F37
	1053.0340	-2.3	-2.2	11.0	20	C30 H11 N3 O2 F32
	1053.0341	-2.4	-2.3	3.5	10	C27 H13 O2 F36
	1053.0289	2.8	2.7	3.5	11	C25 H12 N2 O3 F35
	1053.0287	3.0	2.9	-0.5	4	C23 H14 N2 F37 S
	1053.0350	-3.3	-3.1	3.0	2	C25 H14 N3 F35 S
	1053.0352	-3.5	-3.3	6.5	8	C30 H15 F34 S
	1053.0352	-3.5	-3.3	7.0	9	C27 H12 N3 O3 F33
	1053.0352	-3.5	-3.3	-0.5	16	C24 H14 O3 F37
	1053.0278	3.9	3.7	7.5	12	C28 H11 N2 O2 F34
	1053.0361	-4.4	-4.2	-1.0	5	C22 H15 N3 O F36 S
	1053.0363	-4.6	-4.3	10.0	17	C30 H14 N3 O F31 S
	1053.0363	-4.6	-4.4	2.5	3	C27 H16 O F35 S
	1053.0265	5.2	5.0	0.5	21	C23 H11 N2 O F38

Figure S5-10. HRMS (TOF MS ESI$^+$) of **6**.

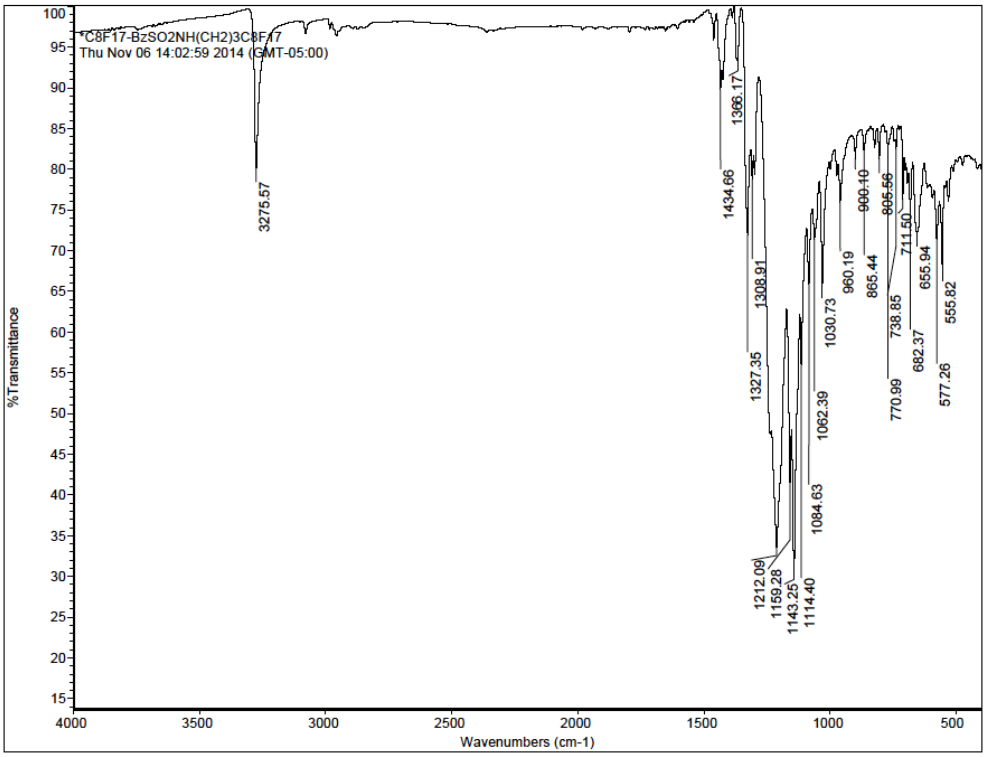

Figure S5-11. FTIR (KBr) spectrum of **6**.

_N_-Chloro-_N_-(4,4,5,5,6,6,7,7,8,8,9,9,10,10,11,11,11-heptadecafluoroundecyl)-3-heptadecafluorooctylbenzenesulfonamide (7)

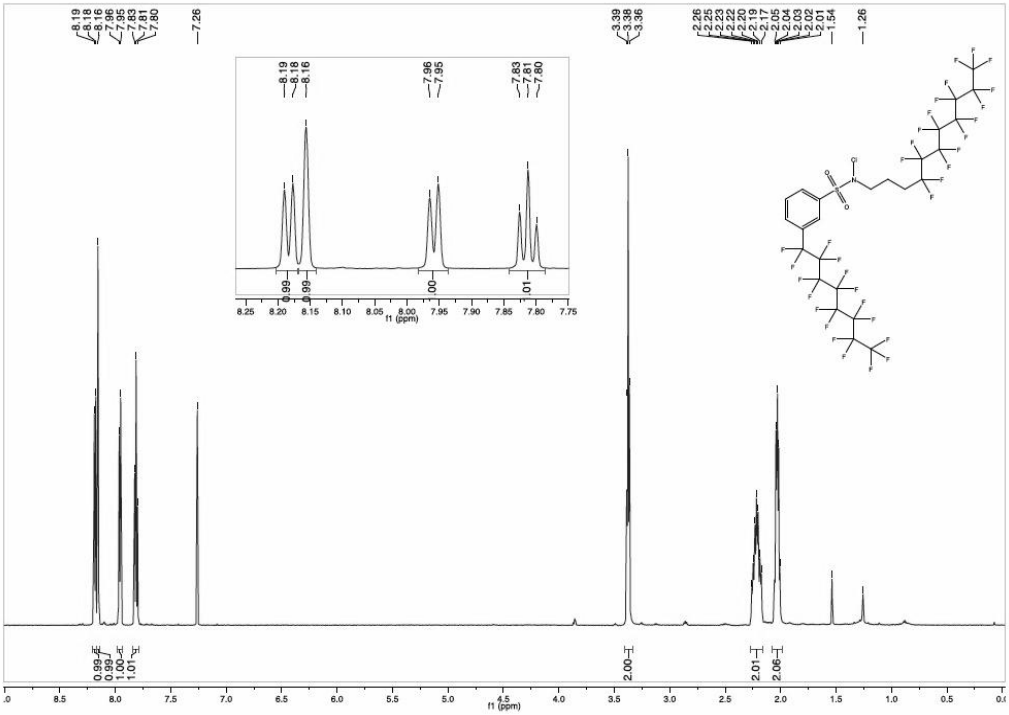

Figure S5-12. ^{1}H NMR (600 MHz, $CDCl_3$) spectrum of **7,** with expanded aromatic region (inset).

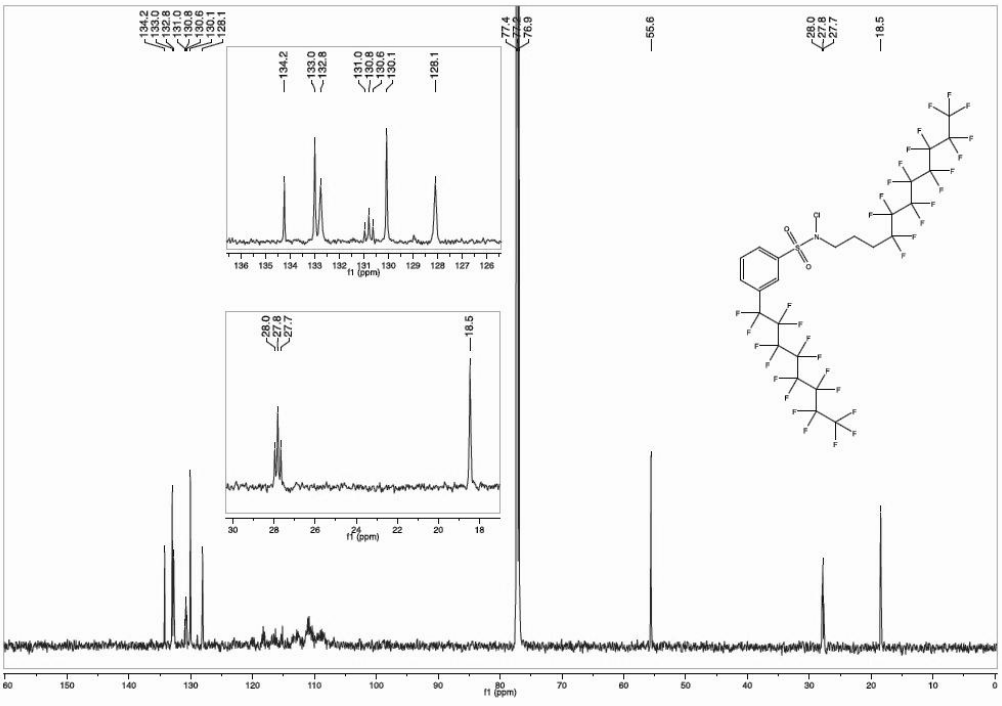

Figure S5-13. ^{13}C NMR (150 MHz, $CDCl_3$) spectrum of **7**, showing multiplets due to $^{2}J_{CF}$ (inset), showing multiplets due to $^{2}J_{CF}$ at 130.8 and 27.8 ppm (insets).

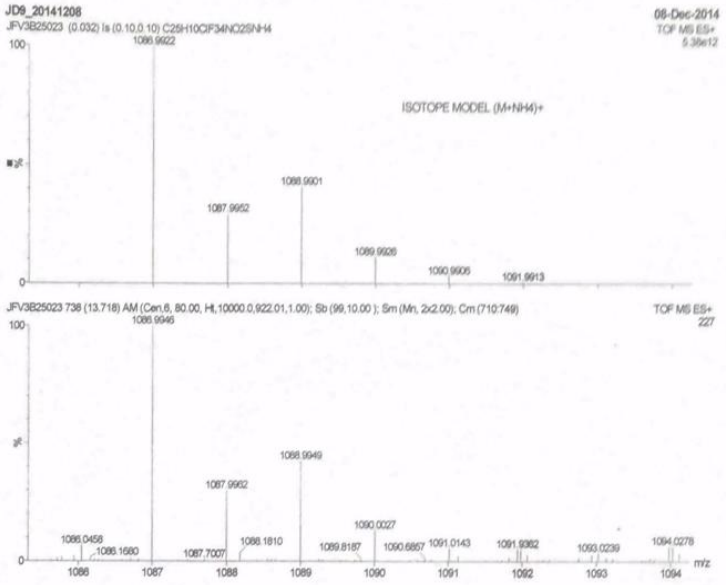

Elemental Composition Report

Single Mass Analysis
Tolerance = 5.0 PPM / DBE: min = -1.5, max = 300.0
Isotope cluster parameters: Separation = 1.0 Abundance = 1.0%

Monoisotopic Mass, Odd and Even Electron Ions
86 formula(e) evaluated with 11 results within limits (up to 50 closest results for each mass)

Minimum:				-1.5		
Maximum:		5.0	5.0	300.0		
Mass	Calc. Mass	mDa	PPM	DBE	Score	Formula
1086.9946	1086.9944	0.2	0.2	1.5	1	C25 H17 N2 O Cl S2 F33
	1086.9935	1.1	1.0	9.5	9	C30 H14 N2 O3 Cl S F30
	1086.9933	1.3	1.2	-1.5	11	C22 H15 N2 O3 Cl S F35
	1086.9968	-2.2	-2.1	4.5	7	C27 H18 N2 O3 Cl S2 F30
	1086.9922	**2.4**	**2.2**	**2.5**	**4**	**C25 H14 N2 O2 Cl S F34**
	1086.9973	-2.7	-2.5	10.0	10	C30 H13 N3 O Cl S F31
	1086.9910	3.6	3.3	6.5	6	C28 H13 N2 O Cl S F33
	1086.9984	-3.8	-3.5	6.0	2	C27 H14 N3 O2 Cl S F32
	1086.9906	4.0	3.7	1.0	3	C25 H18 N O3 Cl S2 F32
	1086.9996	-5.0	-4.6	2.0	5	C24 H15 N3 O3 Cl S F33
	1086.9894	5.2	4.8	5.0	8	C28 H17 N O2 Cl S2 F31

Figure S5-14. HRMS (TOF MS ESI$^+$) of **7**.

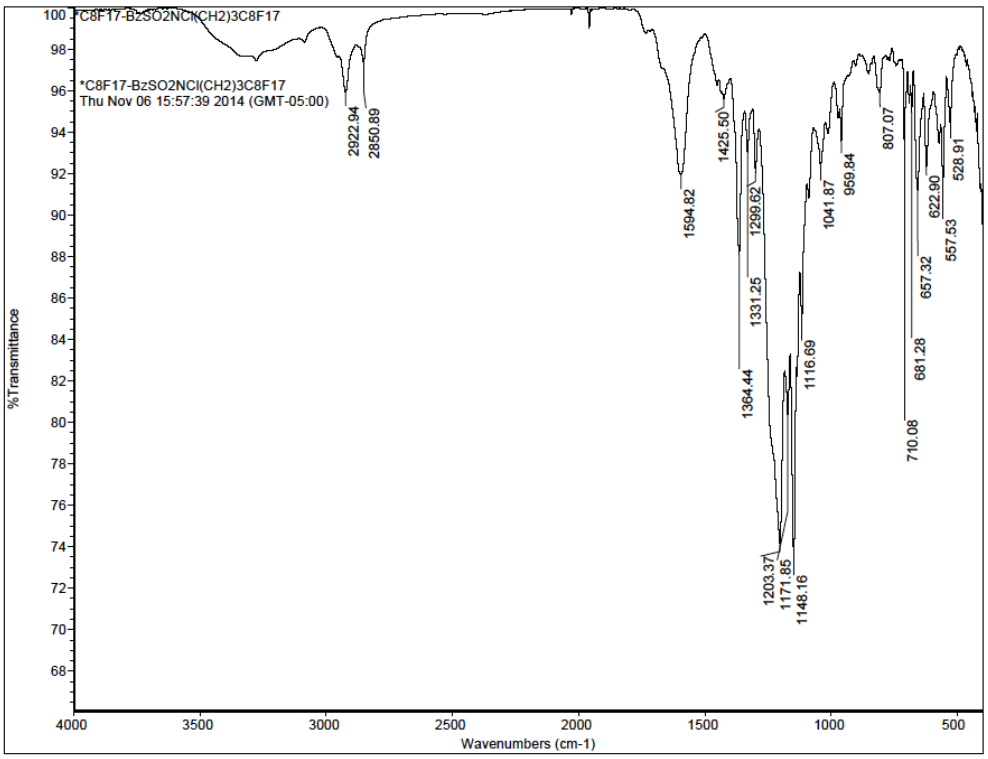

Figure S5-15. FTIR (KBr) spectrum of **7**.